The Dissertation Committee for David Michael Wald
Certifies that this is the approved version of the following dissertation:

ASR Expansion Behavior in Reinforced Concrete – Experimentation and Numerical Modeling for Practical Application

Committee:

Oguzhan Bayrak, Supervisor

Trevor Hrynyk, Co-Supervisor

James O. Jirsa

Eric Williamson

Harovel Wheat

ASR Expansion Behavior in Reinforced Concrete – Experimentation and Numerical Modeling for Practical Application

by

David Michael Wald

Dissertation

Presented to the Faculty of the Graduate School of
The University of Texas at Austin
in Partial Fulfillment
of the Requirements
for the Degree of

Doctor of Philosophy

The University of Texas at Austin
August 2017

Dedication

To my family for their love and support.

Acknowledgements

Firstly, and most importantly, to my parents and sister, I cannot express how deeply your undying love, support, and commitment to me have truly meant, not only during my time performing research, but all of the time. I could not be where I am today without you.

To my supervisors, Dr. Oguzhan Bayrak and Dr. Trevor Hrynyk, I extend my sincerest gratitude for their feedback and guidance in completing my work. I also offer my thanks for advice given from the rest of my dissertation committee: Dr. James Jirsa, Dr. Eric Williamson, and Dr. Harovel Wheat.

To the student researchers and technical staff at Ferguson Lab who made this research possible, your contributions are greatly appreciated. I particularly could not have succeeded without the assistance of Gloriana Arrieta Martinez, Morgan Allford, and Melvin Goh.

Special thanks is also extended to MPR Associates, Inc. whose financial support made the experimental work conducted possible.

ASR Expansion Behavior in Reinforced Concrete – Experimentation and Numerical Modeling for Practical Application

David Michael Wald, Ph.D.
The University of Texas at Austin, 2017
SUPERVISOR: Oguzhan Bayrak
CO-SUPERVISOR: Trevor Hrynyk

Most practicing structural engineers are not well-equipped with the knowledge or tools necessary to adequately address the problem of alkali-silica reaction (ASR). While the mechanisms and consequences of ASR in plain, unloaded concrete are fairly well-understood, such a statement cannot be made about ASR-affected reinforced concrete (RC). Central to the problem is that the expansion behavior of ASR-affected RC behavior as influenced by restraint in the form of embedded reinforcing bars and sustained applied loads is unclear. It is these ASR-induced expansions in concrete that lead to cracking, possible strength and stiffness degradation of the material, and the introduction of unanticipated material stresses that may impair the durability, serviceability, functionality, and integrity of affected structures.

In an effort to transition from a materials science perspective on ASR toward a practical structural engineering approach for addressing ASR in RC, experimental and analytical research was conducted with the goals of: 1) generating more insight into the mechanism of ASR expansion in RC and better assessing how a variety of structural details influence expansion behavior, 2) enlarging the database of information on ASR expansion behavior in RC within the literature, and 3) developing a new tool that could be used to reliably estimate life-cycle expansions for subsequent use in quantifying current and future load-carrying response of existing ASR-affected structures.

Expansion monitoring studies were carried out at the Ferguson Structural Engineering Laboratory on a large-scale, biaxially reinforced concrete beam and large-scale, multi-axially reinforced concrete cubes affected by ASR. The multi-directional expansion behaviors of these elements were measured over time and with volumetric expansion development to evaluate the influences of different reinforcing schemes (e.g., amounts, directions, and layouts of reinforcement) on overall behavior.

Using principles of mechanics, a new ASR expansion model, the Distributed Volumetric Expansion Pressure (DVEP) model, was developed to estimate the multi-directional distribution of volumetric expansions developing in RC structures. The DVEP model was designed as a non-incremental analysis tool accounting for constitutive relationships and utilizing simple, structural detailing inputs (e.g., reinforcement ratios and material properties) for rapid and accurate assessment of global RC expansion behavior by hand or within the framework of finite element analysis programs employing secant stiffness solution algorithms. The modeling approach was extensively validated and shown to be robust and capable of being implemented with limited subjective application.

The results obtained from the numerical modeling of expansion behavior were used to preliminarily examine the consequences of expansion on RC load-deformation behavior. Finally, several recommendations for future work were provided.

Table of Contents

List of Tables

List of Figures

CHAPTER 1: INTRODUCTION

1.1 MOTIVATION

Durability-related distress in concrete has long been a topic of interest to structural engineers and materials scientists. As our buildings and infrastructure age, the need to evaluate the civil infrastructure rises given heavy usage, long-term exposure to the elements, and a gradual onset of internal degradation mechanisms. In recent decades, these issues have attracted the attention of structural engineers who have begun to focus on identifying how structural performance (e.g., load-carrying resistance and ductility) may be impacted by physical and chemical changes to hardened concrete.

Alkali-silica reaction (ASR) represents one very common distress mechanism which results in the bulk expansion of concrete and a subsequent introduction of unanticipated stresses locally within the concrete material itself, in bonded reinforcement, and globally within differentially expanding components of a structural assembly. These expansions result in widespread cracking of the concrete material which in turn may lead to worsened durability, degradation of material strength and stiffness, and impairment of load transfer throughout a structure.

Ultimately, the integrity of structures afflicted by ASR may or may not be compromised. In order to appropriately assess current and future performance of an ASR-affected structure, it is imperative for engineers to develop a practical understanding of the phenomenon of ASR and be able to characterize deleterious behavior of the concrete material within the context of structural applications (i.e., in the presence of reinforcement and applied loads). ASR-affected, reinforced concrete (RC) does not behave the same way as ASR-affected, plain concrete. Restraint to expansion provided by reinforcement and/or applied loads alters the development and distribution of expansions and related damage in concrete. Thus, as the structural engineering profession moves forward attempting to comprehensively address the issue of ASR, it is critical that

ongoing experimental, field, and analytical assessment approaches begin to focus more on the role structural detailing plays in influencing ASR behavior. Plain concrete material behavior alone is invaluable; however, practical engineering requires a big-picture, global perspective on structural behavior when developing and implementing the tools needed to make rational and confident assessments and conclusions.

1.2 OBJECTIVES AND SCOPE

Successfully identifying and addressing the impact of ASR on the behavior of RC structures necessitates an initial exploration of expansion behavior in concrete as influenced by design details such as reinforcement amounts and layouts and loading conditions. Expansion behavior must be understood and evaluated first, as expansions represent the immediate physical consequence of the chemical reaction which lead to cracking as well as changes in the mechanical response of the concrete material and structures as a whole.

This dissertation primarily focuses on the identification of RC expansion behavior. The influences of applied loading, reinforcement, and other structural details are covered; however, emphasis is specifically placed on behavior in the presence of reinforcement, a topic which has received limited attention through prior experimental and analytical research. Associated cracking behavior and structural response to expansions and cracking are secondarily addressed to contextualize how expansion information can and should be used in future evaluations.

The main objectives of the research conducted were to: 1) utilize experimentation and numerical modeling to enhance understanding of the influence of reinforcement on ASR expansion behavior, and 2) develop and implement a new, practical analytical tool with which to evaluate current and future expansion behavior in RC and be able to subsequently assess structural response.

A comprehensive literature review on past experimentation and existing analytical techniques was conducted to examine the state-of-the-art in ASR expansion research and identify deficiencies in knowledge and available data. Two new experimental studies

were conducted on large-scale, RC elements at the Ferguson Structural Engineering Laboratory in an effort to significantly expand the database of available information on multi-directional expansion behavior in structures with varying amounts and layouts of multi-directional reinforcement. These studies were particularly aimed at overcoming inadequacies of past research which included monitoring only uniaxially reinforced elements in a limited number of directions. Using principles of structural mechanics, along with limited empirical observation, a new modeling technique to reliably estimate the multi-directional distribution of ASR-induced expansions in RC was formulated and subsequently implemented, validated, and compared to pre-existing expansion models. This model was designed as a robust alternative to incremental finite element analysis approaches relying upon time-dependent stress-strain history and uncertain concrete material reactivity and environmental conditioning history. Instead, the model uses a non-incremental formulation to evaluate the multi-directional distribution of threshold-level volumetric expansions for a structure. This is done by hand or with limited finite element analysis using simple inputs of concrete and steel material properties, sustained loads, and reinforcement amounts and layout parameters. Finally, the modeling technique was used to provide a preliminary investigation of the influence of ASR expansion-induced prestressing and material property degradation on the strength, stiffness, and deformation capacity of elements subjected to post-ASR loading.

1.3 DISSERTATION ORGANIZATION

The experimental and analytical research conducted on ASR expansion behavior is outlined in the following eight chapters of this dissertation:

- Chapter 2: Background on ASR and ASR Expansion Behavior
- Chapter 3: Experimental Investigations
- Chapter 4: Introduction to Numerical Modeling of ASR Expansion Behavior
- Chapter 5: Distributed Volumetric Expansion Pressure Model – Background and Development

- Chapter 6: Distributed Volumetric Expansion Pressure Model – Implementation and Validation
- Chapter 7: Expansion Distribution Model Application and Results
- Chapter 8: Influence of ASR Expansions on Structural Response
- Chapter 9: Summary, Conclusions, and Future Work

Chapter 2 presents a structural engineer's practical introduction to the phenomenon of ASR and the expansion and cracking behaviors that result. Topics covered in this chapter include the mechanisms of expansions and cracking, factors which influence the development and distribution of expansions in RC, techniques for physically measuring or monitoring expansions, and the consequences of expansions and associated cracking with regard to the durability, functionality, and integrity of afflicted structures.

Chapter 3 provides an overview of prominent, past experimental studies on ASR expansion behavior in RC and an in-depth presentation of the experimental programs, results, results discussions, and conclusions for the two new studies conducted as part of the current research.

Chapter 4 introduces the topic of numerical modeling of ASR expansion behavior. Included in this chapter are discussions of the benefits and uses of modeling, a brief overview of different types of modeling, and a more thorough presentation of the typical characteristics and specific details of notable modeling approaches currently found in the literature.

Chapters 5 and 6 present the background, development, implementation, and validation of the Distributed Volumetric Expansion Pressure model, the newly developed mechanics-based approach for quickly and reliably estimating ASR expansion behavior in RC.

Chapter 7 provides comparisons of the existing numerical modeling approaches covered in Chapter 4 and the Distributed Volumetric Expansion Pressure model. Differences in the application of these techniques and their results highlight the advantages of the new model.

Chapter 8 presents a brief illustration of the potential consequences of ASR expansions on the load-deformation response of RC structures via simple analyses using traditional RC finite element programs paired with the Distributed Volumetric Expansion Pressure model.

Chapter 9 summarizes the research conducted and the principal conclusions and findings obtained from experimentation and numerical modeling. Additionally, recommendations for future experimentation and analysis work to be conducted on the topic of ASR expansion behavior in RC are outlined.

CHAPTER 2: BACKGROUND ON ASR AND ASR EXPANSION BEHAVIOR

2.1 OVERVIEW

This chapter introduces material regarding alkali-silica reaction (ASR) and ASR expansion behavior in reinforced concrete (RC) pertinent to structural engineers. As such, focus is not largely placed on the processes that cause expansion – a topic better suited to the field of materials science – but rather on factors that influence the amounts and locations of, means of measuring, and global implications of distress. First, background information on expansion behavior is presented, with emphasis placed on bridging the disconnect between the perspectives on ASR from materials scientists and structural engineers. Then, the primary features of ASR-related distress in concrete – expansions and cracking – are discussed. Conditions that control expansion behavior – the makeup of concrete, environmental exposure conditions, and structural details – are described at length. In particular, an examination of the influence of structural details helps push the discussion of distress in plain concrete toward a discussion of distress in RC structures. Common methods used to document and evaluate expansion behavior in research and field settings are covered. Finally, broad implications of ASR expansion behavior on the durability, functionality, and integrity of RC structures are outlined. The topics covered in this chapter provide fundamental information on ASR and elaborate on the challenges facing ASR investigators of which experimentation and numerical modeling, described throughout Chapters 3 and 4, aim to overcome.

2.2 ASR EXPANSION BEHAVIOR

In the most basic terms, ASR is a chemical reaction in hardened concrete in which alkalis present in the pore solution of the material react with siliceous minerals found in coarse and/or fine aggregates to produce a gel product that swells in the presence of an

adequate supply of moisture (Bauer et al. 2006). It is this swelling of ASR gel which serves as the mechanism of bulk expansion of the hardened concrete and mechanical deterioration (i.e., cracking), leading to much concern. In totality, ASR is an extremely complex and variable chemo-mechanical process. There exist many highly variable conditions and parameters that control initiation of the reaction and the manifestation of expansions and cracking. It is arguably less important for structural engineers to understand how the chemical reaction works and the source of the constituent components required for the reaction. While these topics are covered elsewhere in the literature, it is necessary for engineers to familiarize themselves with the development process and consequences of distress in order to ensure the safety, functionality, and integrity of ASR-affected structures. As will be made clear throughout this dissertation, assessment of these structures should begin with and center on a comprehensive understanding of ASR expansion behavior. Ultimately, expansions in the solid concrete material are the direct physical product of a chemical reaction which, when paired with cracking, serves as the instigator of a wide array of problems that can plague structures, including degradation of concrete material properties (strength and stiffness) and the induction of unanticipated stresses.

To avoid confusion, note that "expansions" of the concrete material can have one of two interpretations, both of which are considered throughout this dissertation without much distinction. For one, concrete expansions may refer only to the chemically-imposed expansions of the solid material owing to the swelling of reaction product. These expansions are distinct from cracks that develop and widen due to differences in localized reaction behavior. The majority of this chapter addresses "expansions" with this definition. In much of the rest of this document, ASR-induced expansions are taken as a combination of the chemically-imposed expansions throughout the bulk volume of the solid material and concurrent mechanical effects (i.e., cracks) that develop. The term "expansion" in this case simply refers to a physical increase or enlargement of length. As such, the development and growth (i.e., widening) of a crack qualifies as a form of expansion – a rigid separation of hardened concrete parts that once comprised a

continuum. Experimental studies and many numerical models, discussed in Chapters 3 and 4, aim to measure or estimate these global expansions without differentiating expansions of the solid material and cracks.

The need to either distinguish between chemical and mechanical expansions or lump them together is largely related to the underlying approach used to describe and analyze ASR-affected elements. ASR may be viewed as either a materials science problem or as a structural engineering problem. Both perspectives are equally valid and share a number of common concerns, including cracking behavior, durability, and material property degradation. Structural engineering, however, focuses more on global behavior of the material in the context of the components for which it is used whereas materials science explores local behavior of the material and the interaction of its chemical and physical components. As such, structural engineers are likely to be less interested in how much or where ASR cracking occurs and simply focus on the fact that ASR-affected concrete cracks. For practical application, the second of the aforementioned definitions of "expansion" is more useful to structural engineers.

In traditional engineering mechanics, RC is treated as a two-phase composite material with concrete and steel responding individually to structural effects according to unique constitutive laws but with the two materials remaining kinematically compatible. Baseline material strengths or stress-strain curves for concrete are often assumed to be well-represented by the response of plain concrete materials samples (e.g., cylinders) under load that are cast with and conditioned similarly to in-situ concrete. The load response of in-situ concrete will be a function of active or passive loading conditions in the presence of applied loads or reinforcement, influenced by effects associated with confinement, compression softening, and tension stiffening. Ultimately, the key to successfully adapting material sample behavior to in-situ behavior of actual structures is ensuring that the concrete material in question is the same for both the samples and structures.

With ASR, plain concrete and concrete within a reinforced structure are two completely dissimilar materials. As will be discussed in further detail in this dissertation,

the expansion behavior and cracking associated with ASR are highly dependent on load and reinforcement conditions, element or member size and shape, and environmental conditioning. As such, the expansion and cracking patterns that develop in plain concrete, and notably small-scale materials samples, which poorly reflect ASR-related distress that occurs in actual structures.

Perhaps one of the greatest challenges standing in the way of practicality or comprehension of ASR is ascribing how much of a role ASR materials science plays in influencing structural response. Structural engineers working with normal concrete typically need to know little more than basic mixture design and the bulk properties of the hardened material – compressive strength, tensile strength, and stiffness. Concepts like hydration processes, particle distribution, and the mechanisms of strength and stiffness development are beyond the scope of necessary knowledge. Ultimately, there is a very clear demarcation of the responsibilities and knowledge required of traditional concrete materials scientists and structural engineers. In other words, a significant overlap of knowledge is not required between the two groups of individuals. Such is not the case when working with ASR-affected concrete. ASR-affected concrete is a multi-phase material comprised of solids and ASR gel. Further, a structural engineer cannot begin to address the problem of ASR without a foundational understanding of the mechanisms of expansion and cracking and acknowledgement of the role stochastic reactivity, heterogeneity, porosity, and environmental conditions play in influencing concrete behavior. In other words, while concrete can be idealized as a single-phase, homogenous material for many structural applications, such an idealization for ASR-affected concrete should not be blindly accepted; the natural heterogeneity of concrete – a mixture of water, cement, and aggregates – is exponentially compounded given ASR.

2.3 FACTORS INFLUENCING ASR EXPANSION BEHAVIOR

The following sections summarize the process of ASR and expansion development in more detail, with particular emphasis placed on outlining the primary factors which influence expansion development.

ASR expansion behavior in concrete, which comprises rates, amounts, and multi-directional distributions of expansions, is influenced by three broad sets of factors described herein: 1) the chemical and physical makeup of the concrete, 2) environmental conditions, and 3) structural details. It should be noted that these sets are not mutually exclusive; factors from each group are inter-related.

The first set of factors largely controls the development and expansion-readiness of the chemical reaction product – the ASR gel. The second set of factors mainly influences the speed of the reaction and resulting expansions. The third set of factors affects numerous aspects of expansion behavior including expansion distribution patterns, expansion rates, and the ultimate amounts of expansion that can be generated.

2.3.1 Chemical and Physical Makeup of Concrete

Regardless of environmental conditions, loading conditions, and/or the presence of reinforcement, concrete is not subject to expansion without the formation of ASR gel. As explained by Fournier et al. (2006), ASR gel is a product of the dissolution of unstable siliceous minerals found in coarse and fine aggregates via the highly alkaline fluid within the micropores of hardened concrete. As the pH of the pore solution rises above 12.5 due to a high hydroxyl ion (OH^-) concentration in equilibrium with a high sodium and potassium ion (Na^+ and K^+) concentration, silicon-oxygen bonds within the microstructure of aggregate particles break down and dissolved silica combines with alkalis to form the ASR gel. These alkalis are primarily sourced from Portland cement but are also found in other concrete materials like aggregates, admixtures, and mixing water (Bauer et al. 2006).

The chemical reactivity of ASR-affected concrete (i.e., the amount and rate of gel formation) is highly dependent on the amounts of alkalis and silica present, the crystalline structure or solubility of the silica, and the sizes of the aggregate particles used (Institution of Structural Engineers (ISE) 1992). With an increasing amount of alkalis, more stable forms of silica are prone to dissolve in an increasingly basic pore solution (Bauer et al. 2006). As more alkalis and dissolved silica are made available, the potential

for ASR gel formation increases. Also, smaller aggregate particles can provide increased surface area for dissolution to take place, thus prompting higher rates and maximum levels of expansion (Wigum et al. 2006).

Chemical reactivity and developing expansions are not perfectly uniform, largely due to the natural heterogeneity of concrete, aggregate gradation, and concrete permeability. Aggregate particles, providing the source of silica to the reaction, serve as local reaction sites for gel formation but are both randomly distributed throughout the hardened concrete and generally non-uniformly graded. Not only does the concrete consist of aggregates of multiple sizes (e.g., coarse versus fine, coarse aggregate gradation), but the amounts and gradation of these aggregates can influence local packing density and exposed surface area to high-alkaline cement paste (Wigum et al. 2006). Meanwhile, the permeability of concrete, which can be affected in part by the presence of supplementary cementitious materials like fly ash and silica fume, can influence the migration and thus distribution of alkalis or moisture within concrete (Bauer et al. 2006). Cyclic wetting and drying can result in an elevated near-surface concentration of alkalis due to evaporation, potentially promoting increased gel formation. At the same time, the near-surface alkali concentration may decrease due to leaching, especially in elements with large surface area-to-volume ratios (Courtier 1990).

It is also critical to note that not all ASR gel behaves the same way. As shown by Struble and Diamond (1982), the swelling characteristics of alkali-silica gels are a function of their chemical compositions. More importantly, expansion and cracking in concrete only occur when an ASR gel swells within a sufficiently moist environment; the presence of ASR gel alone does not necessarily represent an active concern (Bauer et al. 2006).

Ultimately, the aforementioned chemical and physical parameters of ASR-affected concrete collectively describe the material and its propensity to exhibit deleterious behavior. It is important to acknowledge each of these individual parameters in appreciation of the complexity of the problem of ASR and to temper expectations of our ability to achieve consistency and repeatability through ASR experimentation or to

computationally estimate ASR behavior with a high degree of precision. The reality is that, given such a wide range of materials science variables, it is often easier to explain possible sources of inconsistency or error than it is to reliably explain causation of behavior. This is especially true with regard to the time it takes for the entire ASR deterioration process to manifest as a function of chemical reactivity and the environmental and structural conditions described in the following sections. In fact, guidelines on ASR by the ISE (1992) warn against making "generalized statements on the time scale" of ASR, particularly as it pertains to concrete mixtures with varying amounts and types of reactive silica.

As will be highlighted and encouraged throughout this dissertation, a shift toward practicality in the study of ASR should focus less on when the effects of ASR manifest and more on what those effects are, when and if they happen. For example, consider two concrete mixtures, one more reactive than the other. We can devote much experimental or computational effort to determine how quickly each concrete will expand as a function of the many aforementioned variables. However, if we anticipate that, over the course of time, each mixture will eventually reach a common level of bulk expansion and we assume that, on average, the multi-directional distribution of that expansion and any cracking-induced material property degradation are similar, the need to establish the timeframe of expansion behavior becomes far less relevant. These ideas have helped guide the development of new analytical tools for quantifying ASR expansion behavior.

2.3.2 Environmental Conditions

The amount and rate of expansion due to ASR is significantly influenced by exposed temperature and humidity. These conditions generally go hand-in-hand with the discussion of chemical reactivity. Initial internal conditions, external ambient conditions, and heat and moisture transfer through the concrete material describe the environment in which ASR may occur. Physical characteristics of the concrete material and structural elements including permeability, element size and shape, and exposed surface area to high temperature or moisture are relevant. Temperature and humidity differentials can

lead to differential expansion behavior between multiple ASR-affected elements or even within the same element, such as for mass structures like dams. It must be noted, however, that ASR occurs over a very long timescale, typically on the order of years or even decades. Transient fluctuations in temperature and humidity, such as those that occur over the course of a single day or even week, are likely not relevant for practical consideration. Generally, it may be more appropriate to describe environmental conditions for ASR development with long-term, steady-state values.

As stated previously, the mechanism of expansion in concrete due to ASR is the swelling of the ASR gel. Appreciable expansions will only occur where the internal relative humidity of the concrete exceeds approximately 75-80 % (ISE 1992). Available moisture is provided via the internal free water content within concrete and external sources including atmospheric moisture, dam water, groundwater, and pooled precipitation. The water-to-cement ratio for the concrete is a key factor influencing the free water content and permeability (Fournier et al. 2000). As the internal relative humidity of the concrete rises, the rate of expansion increases (ISE 1992). All sources of moisture, however, do not necessarily affect expansion behavior the same way. Constant exposure to water is highly favorable for expansion; however submersion of concrete in water can accelerate the leaching of alkalis from the surface of the concrete and thus limit ASR gel formation and ultimate expansion potential (ISE 1992). Meanwhile, cyclic wetting and drying can promote elevated alkali migration toward the surface of concrete elements, thus increasing ASR gel formation and expansion potential at these locations (Fournier et al. 2000). According to the ISE Guidelines (1992), extended periods of low external moisture may slow or even stop expansions, especially in comparison to periods of constant moisture exposure; however, such behavior is only temporary as concrete can continue to expand after being re-exposed to an appropriate level of moisture. It is not quite clear in the literature, though, whether the maximum expansion potential is inhibited due to delayed moisture exposure. This topic is considered further in later parts of this dissertation.

Temperature is also an important consideration. As summarized by Wigum et al. (2006), temperature plays two key roles in influencing ASR expansion behavior: 1) controlling the rate of the reaction (i.e., ASR gel formation), and 2) controlling the maximum expansion potential. With increasing temperatures, the rate of ASR (i.e., gel formation), like many chemical reactions, increases, but the rate of expansion and/or maximum expansion can actually decrease. The net effect of these counteracting behaviors is that concrete will often expand more quickly at first given a higher temperature but expand a greater total amount at a later age given a lower temperature. Often, the possibility of different maximum expansions for varied temperatures is neglected in analytical models (Ulm et al. 2000; Saouma and Perotti 2006). One of the greatest detriments to the practical usage of ASR knowledge may be determining how to appropriately account for thermal effects or whether to account for them at all. Real-world structures typically do not experience the constant temperatures that are often considered in experimental programs, nor are they exposed to uniform temperatures, especially in the case of mass concrete structures. Wigum et al. (2006) noted that differential expansion and cracking behavior has been evidenced within separate elements of a structure (e.g., multiple bridge girders) and within the cross-sections of individual elements (e.g., single girders) due to variations in sun exposure and shading alone. It is important to acknowledge that local expansion behavior is justifiably influenced by these temperature differentials within a single element, if for no other reason than to help explain surface cracking. However, one must recognize that there are significant practical advantages of focusing on global expansion behavior under averaged thermal conditions as opposed to using complicated thermo-mechanical and heat transfer formulations to ascertain local behavior with complex temperature profiles.

2.3.3 Structural Details

Within a volume of concrete, ASR expansion behavior is heavily influenced by design and construction details that must be considered. These include reinforcement conditions, loading conditions, member size and shape, and component assemblies. Like

factors pertaining to the chemical and physical makeup of concrete and environmental conditions, certain structural details may influence the time development of ASR-induced expansions within different portions of a structure. Perhaps more importantly, structural details will influence the multidirectional distribution of volumetric expansions of concrete.

2.3.3.1 Restraint to Expansions

The majority of this dissertation focuses on the effects of reinforcement, and, to a lesser but still high degree, applied loading on ASR expansion behavior. Applied loading and reinforcement serve as sources of active and passive "restraint" to expansions, respectively. The term "restraint" generally implies a reduction of expansion in an individual direction of restraint with respect to time or, as will be discussed later, volumetric expansion development. It must be noted, however, that the presence of restraint against ASR, as well as increasing amounts of restraint, may not necessarily alleviate durability and structural issues in ASR-affected concrete or create a more favorable material. Restraint can cause a redistribution of expansions amongst different directions of an element, potentially promoting increased distress in transverse directions not otherwise anticipated (Multon and Toutlemonde 2006). In other words, discretely oriented restraint may not only influence expansion behavior in the direction of restraint. Expansions in different directions of an element may be nonuniform or anisotropic, but these expansions may not be independent of one another (Multon and Toutlemonde 2006). Thus, ASR-affected RC may behave as a continuum material, with respect to expansions, during ASR generation. Also, and importantly, any interaction between expanding directions would signify that the expansions in the unrestrained directions of a restrained element are not necessarily equal to "free" expansions (i.e., those in completely unrestrained elements). This implied distinction between unrestrained and free expansions is carried out throughout this dissertation.

Ultimately, the challenge facing most ASR researchers is determining how different types and amounts of restraint influence expansion behavior not only in the

direction of restraint but in other directions at the same time. For example, if an increased amount of applied load or reinforcement for an element were shown to result in a reduced expansion in the direction of restraint, the overall expansion behavior would be very different if expansions in other directions remained constant compared to if such expansions changed given directional interaction. As will be seen more in Chapters 3 and 4, many experimental research studies and analytical models fail to address this fundamental problem, which can severely limit their practicality and usefulness.

The discussion of restraint is further complicated by attempts to comprehend the mechanism by which different forms of restraint influence expansion behavior. Restraint against expansion is most commonly quantified as a function of the stresses that exist in the concrete material during ASR generation (Charlwood et al. 1992; Cope et al. 1994; Saouma and Perotti 2006). Some stresses are actively produced in concrete through external applied loading. Other stresses are passively induced in concrete via equilibrium as internally bonded or externally anchored reinforcement prevents concrete from expanding as much as it would otherwise do so in a "free" state. Similarly, stresses can be passively induced in individual members at the joints or connections of a structural assembly where adjacent components expand differentially. While a dependency on stresses can be simple to quantify and universally links different forms of restraint, alternatives to stress-dependency may also be suitable parameters with which to gauge expansion behavior.

In the discussion of restraint against ASR, it is easy to misinterpret what "restraint" means in the context of engineering mechanics. For a plain, ASR-affected concrete element under load, the total strain of the element relative to its unloaded, unaffected state will include the initial elastic lengthening/shortening of the element due to load and expansion of the concrete material due to ASR. For the sake of discussion, other strain components associated with loading like those related to creep or ASR-induced stiffness degradation will be ignored. Any variation of the loading will result in a corresponding change to the elastic lengthening/shortening of the element as well as a change in the amount of expansion in the concrete material. This change in material

expansion is what load-related "restraint" against ASR controls. For an unloaded, ASR-affected RC element, the total strain of the element relative to its unaffected state will include any expansion of the concrete material due to ASR and the strain variation due to the compatibility between the expanding concrete and bonded steel reinforcement. In accordance with fundamental mechanics of perfectly bonded composite systems, the overall lengthening of such an element will be reduced (i.e., the total strain will be less than the concrete material expansion) due to resistance provided by the compatible reinforcement. For reference, this is exactly the opposite effect of an RC element experiencing shrinkage in which shortening of the element is partly prevented by resistance from the compatible reinforcement. In the case of shrinkage, however, the presence of reinforcement does not influence the amount the concrete material alone would want to shrink. In ASR-affected concrete, the presence of reinforcement changes the amount that the concrete material alone would want to expand. It is this effect which reinforcement-related "restraint" against ASR refers to. Thus, overall, "restraint" is more of a constitutive type of response in which the nature of the expanding material (i.e., the amount the concrete material alone wants to expand) changes in the presence of applied loads or reinforcement.

2.3.3.1.1 Characteristics of Applied Loading

The amounts and type of loading on a structure, both in individual and multiple directions, can influence ASR expansion behavior. In the presence of sustained, externally applied loads on an ASR-affected structure, individual portions of the structure may be under states of compression and/or tension due to direct load application or indirectly via bending or shear. As discussed in greater detail in Chapter 3, increasing amounts of direct compression, at least up to some limit, have been shown to reduce expansions in the direction of loading by Le Roux et al. (1992), Larive (1997), and Dunant and Scrivener (2012). It is somewhat unclear, experimentally, whether shear- and bending-induced compression or passively induced compression from internal and external forms of restraint to expansion have the same impact. Existing expansion

models, described in Chapter 4, consider that all forms of compression influence expansion behavior in the same way, while the newly developed expansion model described in Chapter 5, argues that such may not be the case. Meanwhile, increasing amounts of direct tension have been shown by Jones and Clark (1996) to increase expansions in the direction of loading. As with compression, however, it is unclear if shear- and bending-induced tension have the same impact. Regardless, largely in part from a lack of widespread experimentation on ASR elements under tension, all expansion models described in this dissertation ignore the influence of tension on expansion behavior.

2.3.3.1.2 Characteristics of Reinforcement

The amount of reinforcement, size of reinforcing bars, distribution of reinforcement, and types of reinforcement, both in individual and multiple directions, may influence ASR expansion behavior. The amount and distribution of reinforcement are topics covered in significant depth later in this dissertation. Limited testing performed by Mohammed et al. (2013), which is discussed in Chapter 3, indicated that expansion behavior can differ where individual bars are deformed, nondeformed, and/or externally anchored.

2.3.3.2 Component Size and Shape

Impacts associated with the size and shape of a structural component are largely related to environmental conditions, as they can influence sensitivity to changes in ambient temperatures and moisture content. Massive structures may maintain higher constant humidity while smaller structures with a higher surface area to volume ratio may be very sensitive to external moisture. Small structures may have a more uniform thermal profile whereas mass structures may not. Also, the size of structure can influence the likelihood of alkalis leaching, the amount of alkalis available for the reaction to occur, and the potential for heightened expansion differentials between cover and core concretes.

2.3.3.3 Casting Direction

As reported by Jones and Clark (1996) and Larive (1997), concrete may expand more in the casting direction of a structural component due to the introduction of perpendicular weakened planes. This may contribute to differences in the directional expansions of plain concrete elements without high aspect ratios (e.g., a cube with an aspect ratio of 1:1). The extent to which casting direction influences expansions in RC, especially where reinforcement exists in the direction of casting, is unclear.

2.4 EXPANSION-INDUCED CRACKING

The primary source of physical deterioration of concrete due to ASR is cracking. Cracking is the first and often only readily apparent sign that a structure is affected by ASR. ASR can result in two forms of cracking: microcracking and macrocracking. All cracking is the result of some form of differential expansion due to ASR. As discussed further in Section 2.6, ASR-induced cracking can correlate to durability concerns, potential material property degradation, ineffective transfer of compressive or tensile loads, and complications with bond between concrete and steel.

Cracks at the microstructure level form in and around aggregate particles (i.e., at reaction sites) and propagate through the cement paste in hardened concrete (Figure 2-1). These cracks can be detected through petrographic examination. As explained by Courtier (1990), microcracking occurs as local expansions induce tension within the surrounding paste matrix. According to Le Roux et al. (1992), the pressures introduced locally by swelling of ASR gel have been shown to reach as high as 3 to 10 MPa, well in excess of the tensile strength of most concretes. Additionally, local expansion can also exacerbate pre-existing microcracking (Courtier 1990). Ultimately, microcracking is largely responsible for any reduction in the strength (compressive and/or tensile) and stiffness (i.e., elastic modulus) of concrete, which is discussed in more detail in Section 2.6.7. Microcracking, however, can be somewhat beneficial as these cracks can absorb

ASR gel under compressive loads, thus limiting the amount of gel available to expand and curtailing volumetric expansion development (Saouma 2014).

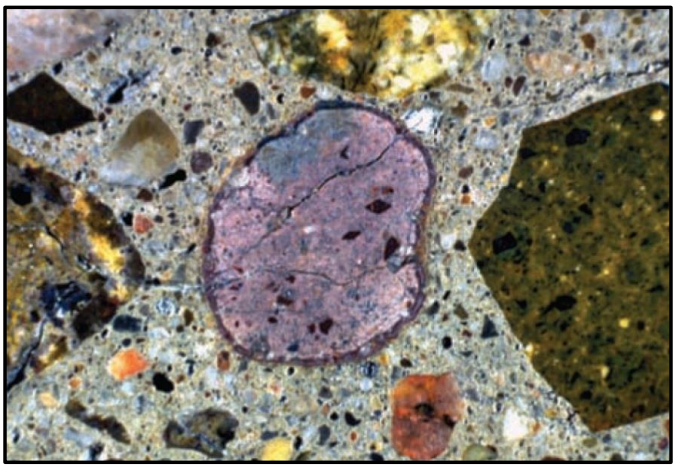

Figure 2-1: Cracking of aggregates and cement paste (Farny and Kerkhoff 2007)

Macroscopic cracks due to ASR generally form at the surface of hardened concrete elements. These cracks are large, visible to the naked eye, and serve as the primary indicator of ASR distress. Engineers and materials scientists commonly attempt to quantify overall expansions or distress as a function of the development of macrocracks at the surface. As explained by Courtier (1990), macrocracking occurs due to differentials or gradients of bulk chemical expansion throughout the volume of a concrete element. Most commonly, concrete deep within the core of an element expands a greater amount than concrete nearer the surface at the same time, resulting in the outer skin or membrane of the element being placed into tension. This may be caused by a reduction in ASR gel formation near porous, evaporative surfaces due to leaching of alkalis and the propensity of interior concrete to maintain a higher relative humidity. Such behavior is depicted in Figure 2-2. Other sources of nonuniform bulk expansion development, such as thermal gradients and nonuniform restraint conditions, can also result in crack development. Ultimately, macrocracking that occurs at the surface of concrete elements may contribute to material property degradation but can raise a more serious concern, discussed further in Section 2.6.4 – whether or not to rely upon cover

concrete to contribute to the shear and flexural capacities of concrete members. At the same time, macrocracking can help to mitigate volumetric expansion development as macrocracks forming under tension can absorb ASR gel and thus limit the amount of gel available to expand in a moist environment (Saouma 2014).

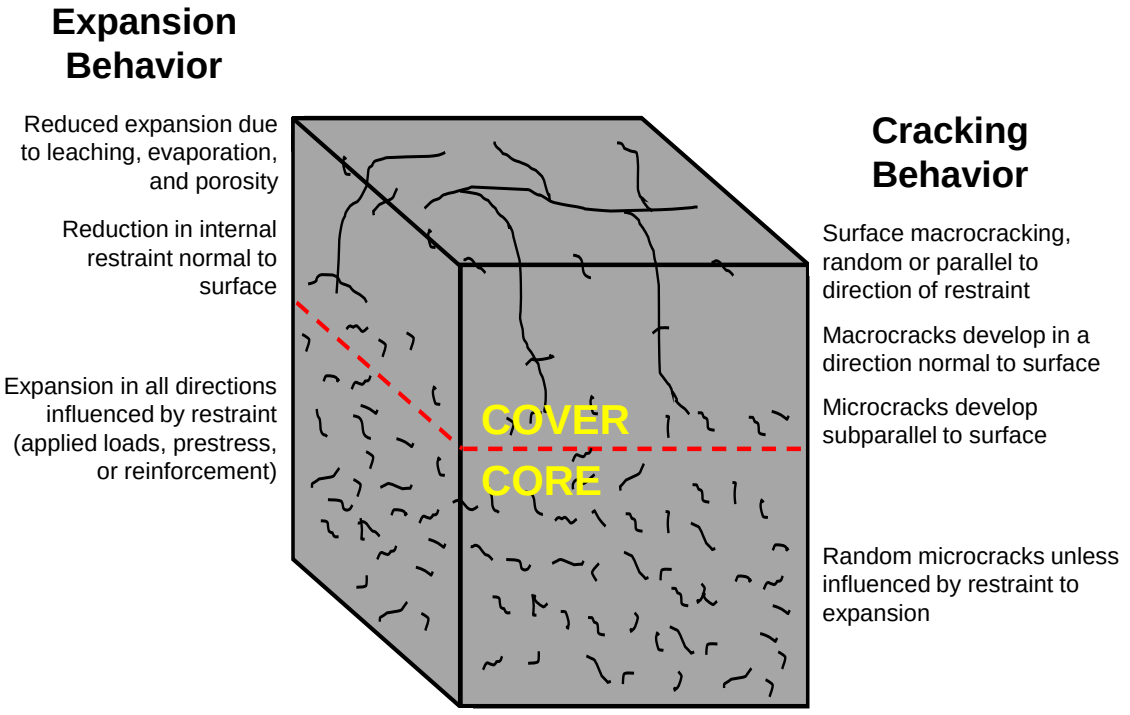

Figure 2-2: Macroscopic cracking behavior (adapted from Courtier 1990)

It is reiterated that macrocracking represents a mechanical form of expansion. Overall interior expansions of concrete are primarily comprised of large chemical expansions whereas overall exterior expansions of concrete, which are most commonly measured in the field or through experimentation, are a combination of significant macrocracking and reduced chemical expansions. Ultimately, when considering both chemical and mechanical forms of expansion, the distribution of overall expansions may be more uniform than the distribution of chemical expansions alone. This is important to keep in mind for computational analysis where the interior-exterior chemical expansion

differential and associated cracking are not explicitly modeled, but overall expansions are approximated to be uniform.

The distribution and orientation of ASR surface cracking can help identify distressed regions or a structure's expansion response under various restraint conditions as well as influence direction-dependent material properties. Cracking pattern phenomena are well explained by ISE Guidelines (1992). Plain, unrestrained concrete typically exhibits surface crack patterns consisting of randomly oriented, intersecting cracks. This form of cracking is often referred to as "map cracking." Concrete which is restrained by either reinforcement and/or loading will often crack parallel to the direction of restraint. This occurs where concrete tends to expand a greater amount perpendicular to the direction of restraint. As such, concrete that is uniaxially loaded or reinforced may exhibit more prominent restraint-oriented cracking than concrete that is restrained in more than one direction. Ultimately, restrained concrete may exhibit a combination of restraint-oriented cracking and map cracking. Figure 2-3 illustrates the forms of surface cracking that may manifest.

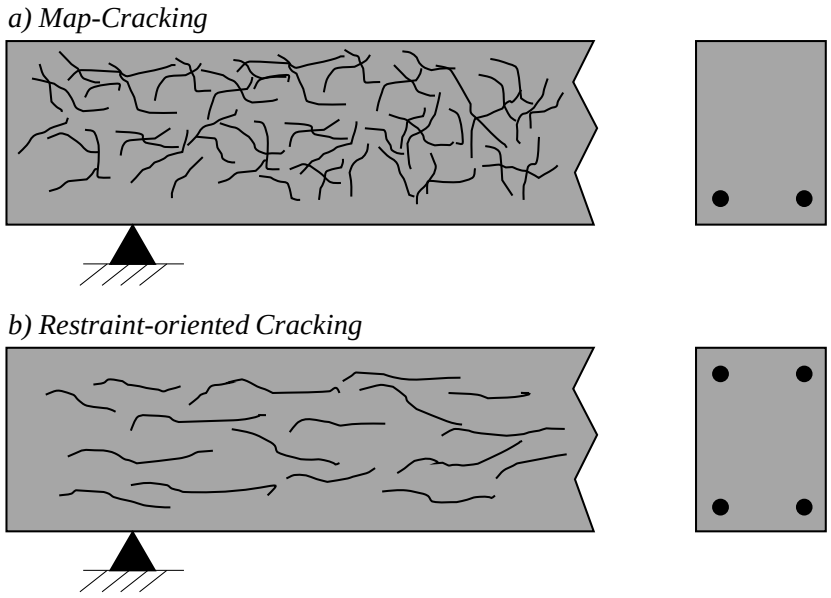

Figure 2-3: Surface cracking (adapted from ISE 1992)

In addition to influencing the orientation of cracks, it is possible that restraint may impact the amount and sizes of the cracks that form. For one, cracking behavior should be tied to expansion levels, both locally (i.e., directionally) and volumetrically. If restraint alters the directional distribution of expansions, or curtails total expansion development via the aforementioned gel absorption under load or some other means, the increase or decrease of cracking and crack widths will likely match the increase or decrease of associated expansions. It is also reasonable to expect that there may be a relationship between the amount of ASR cracking and crack widths themselves when in the presence of restraint or not. For unaffected concrete elements under any type of loading condition, engineers may identify an increased number of smaller, load-induced cracks at reinforced locations and fewer wider cracks in unreinforced regions. In essence, cracking concentrates at unreinforced "weak" points. In ASR-affected concrete, it is probable that one might observe a greater number of smaller, expansion-induced cracks near restrained locations and fewer wider cracks at unrestrained locations. On a related note, nonuniform restraint conditions may result in differentials of restrained expansion that can promote increased potential for crack development, widening, and propagation, namely at any unreinforced locations. Such behavior is documented through experimentation in Section 3.3. Ultimately, the amounts and sizes of cracks will have a large influence on material property degradation and the ability to effectively transmit loads in highly cracked regions of a structure.

Lastly, the amount and distribution of cracking and the subsequent effects of cracking on the response of a structural component may be largely related to its size. In particular, there will be more macrocracking in smaller elements relative to their volumes than in larger elements. As a result, smaller elements may be more prone to increased durability issues and heightened material property degradation.

2.5 COMMON METHODS OF MEASURING EXPANSIONS

Measuring ASR-induced expansions in both laboratory and field structures is critical toward assessing the amount of ASR progress or damage that is present, gauging

future expansion behavior, and obtaining data needed to advance our knowledge and to develop analytical tools geared toward examining the influences of ASR. Various methods are used experimentally and/or in-situ to measure ASR expansions. These include devices directly attached to the concrete or reinforcement. Regarding the former, it may be argued that measured surface expansions in RC elements are either expansions for the concrete material alone or the entire RC element. As previously discussed, these two types of expansions slightly differ due to the compatibility between the concrete and steel. For general assessment, these expansions might be approximated as being equal, but the distinction is important to recognize. Throughout the remainder of this dissertation, measured expansions in RC elements from devices attached to the concrete are considered to be the expansions for the entire RC element. As such, this would imply that the strain in the reinforcement is equal to the measured strain, provided that the steel and concrete remain perfectly bonded. Lastly, stresses in reinforcement may be directly evaluated from these RC strains or with devices directly attached to the steel. With knowledge of, or an assumption of, bond conditions and given reinforcement percentages, one could estimate compressive stresses that are passively induced in the concrete.

Note that the following sections briefly summarize details pertaining to different expansion measurement techniques that can be used and outline important advantages and disadvantages regarding utilization of such techniques. The content presented is for information purposes only; the amount and order in which information is provided are not meant to represent an evaluation of which technique is "best" or "worst." More extensive information (e.g., a greater number of advantages or disadvantages) is simply provided for the more widely used and well-researched techniques, including those utilized in experimental studies covered in Chapter 3.

2.5.1 Internal Mechanical Devices

Expansions can be measured using a variety of strain gages embedded in concrete elements. Types of gages used include foil gages attached to reinforcing bars, vibrating

wire gages, and fiber optic gages. Foil strain gages provide direct measure of the strains developed in reinforcement due to tensioning whereas vibrating wire and fiber optic gages are attached to concrete and can provide a measure of overall expansions in reinforced or plain concrete. When using both foil gages and one of the concrete gages in the same specimen, one might be able to assess if there is any degradation of bond between the concrete and steel. When working properly, strain gages provide the most objective measure of expansions of all measurement approaches. Strain gages are not difficult to install and can be connected to data acquisition systems for continuous measurement. These gages, however, must be placed during casting. This makes them suitable for use in laboratory specimens, in which ASR-affected concrete is purposely employed, but not as a measure of in-situ behavior in field structures, which would not be instrumented prior to casting.

There exist a number of concerns and disadvantages of using strain gages:

- Gages are expensive, especially compared to other expansion measurement techniques. This can limit the number of gages that may be placed in an element. Notably, fewer vibrating wire and fiber optic gages are likely to be used as they are significantly more expensive than foil gages. Without a suitable number and distribution of measurement devices, particularly in larger specimens, it may be difficult to fully trust results or obtain a complete picture of overall expansion behavior.
- Results may be skewed by the locations where gages are placed. Apart from inherent variability, measurements can be influenced by expansion gradients between cover and core concrete, proximity to reinforcement, directionality, and strain variations along individual reinforcing bars or between different bars.
- The gages themselves may possibly influence expansion behavior. Foil gages attached to reinforcement may locally impair bond between the concrete and steel, thus reducing the effective amount of restraint provided against expansion. This issue is mainly related to the method of waterproofing of the gages, which often can involve wrapping reinforcing bars with some form of tape. Meanwhile,

vibrating wire gages are relatively large and could hypothetically provide an increase in local restraint against expansion. In either case, more of each of these devices and/or placement of these devices in smaller specimens could exacerbate concerns.

- The durability and longevity of the different gages may counteract their usefulness. All gages are electrical and are thus sensitive to moisture. Humid conditioning provides an abundant source of moisture, and ASR-induced cracking increases moisture transport. Thus, wiring and the gages themselves must be adequately waterproofed. This is especially true of foil gages. Because foil gages are small and bonded to reinforcing bars with adhesive, they may be damaged as concrete expands around the bars. Also, different gages have a limited working range. In other words, the gages may not be able to measure expansions beyond certain amounts. Foil gages particularly suffer from this problem as the gages cannot measure strains in bars after yielding.

2.5.2 Exterior Mechanical Measurement Techniques

Expansions in both laboratory and field structures can be measured in a variety of ways using, for example, calipers or extensometers to measure element surface deformations. These deformations can then be compared to original element dimensions or gauge lengths between measurement points to obtain strains/expansions. Measurement techniques include directly measuring changes in element dimensions with calipers and measuring deformations in reinforcement or RC between surface-mounted or embedded targets. These techniques are very cost-efficient and can be widely used to gather expansion data at many locations, generally without any concern of providing additional restraint against expansion. They can, however, be time-consuming, as measurements, often large in number, must be frequently taken and are done manually.

The most commonly used and practical of all measurement techniques is measuring deformations between targets. For one, in a laboratory specimen, pairs of target points can be secured to individual reinforcing bars prior to casting, ultimately

extending through cover concrete to the specimen surface where deformations between those points can be measured. Researchers like Smaoui et al. (2007) and Deschenes et al. (2009) have done so with target points attached to studs that were welded to reinforcing bars as shown in Figure 2-4. Such a method is a cheaper and possibly more reliable method than using foil gages susceptible to the aforementioned durability and longevity concerns. More commonly, targets are attached to or embedded directly in concrete, as illustrated in Figure 2-5. This technique is suitable for both laboratory and field structures, and it may be done alone or in combination with targets attached to reinforcing bars. Embedded targets can be cast-in-place or post-installed in elements while surface-mounted target points, like Demec studs, can be placed with adhesive. Expansions between target points may be determined from surface measurements on individual element faces or from through-dimension measurements between opposite faces. As an alternative to using targets, calipers can be used to directly measure changes in dimensions of a structure, but only if those dimensions are short where the extension of the calipers is long enough to perform such measurements.

Figure 2-4: Welded, reinforcement stud measurement targets (Smaoui et al. 2007)

Figure 2-5: Examples of concrete measurement targets

As with strain gages, a number of concerns exist when using exterior mechanical measurement techniques:

- Expansion measurements may be sensitive to the locations of measurement points and the particular exterior measurement approach used. Expansions obtained with surface-mounted target points or embeds bonded with cover concrete may reflect the influence of expansion gradients, surface cracking, leaching of alkalis, increased surface porosity/permeability, and exposure to external environmental conditions on near-surface expansions. Consequently, these expansions may not be indicative of expansions in element cores. An example of how this issue may be counteracted, at least in laboratory specimens, is by extending embeds to the core and physically separating any embeds from the cover concrete. For instance, Deschenes et al. (2009) did so using specially designed PVC and foam blockouts. This is, however, an issue that arises only for surface measurements on individual element faces in which only cover behavior can be reliably identified. In measuring across opposite faces instead, one can capture the combined behaviors of cover and core concrete. Otherwise, interior measurement devices like vibrating wire gages would be necessary to determine core behavior. Unfortunately, standard calipers and extensometers cannot extend far enough to

span between opposite faces of larger elements, nor are the jaws of such devices typically long enough to capture mid-depth, through-dimension deformations.

- The distance between target points for measuring surface expansions, often limited by the extendibility of the calipers or extensometer used, may not be appropriate. Short gauge lengths may result in inaccurate average measurements of expansion. This may be especially true if the gauge length crosses significant surface cracks caused by expansion gradients and/or nonuniform restraint conditions. This issue is confirmed and discussed further in Section 2.5.3.
- Some faces of field structures may be inaccessible for instrumenting, thus limiting the number of locations in which target points can be placed for in-situ expansion measurements and precluding the collection of through-dimension measurements between opposite element faces.
- In a high temperature and humidity conditioning environment, surface-mounted target points may become detached, especially if a weak adhesive is used. Reattaching these targets at their pre-detachment locations is challenging. For this reason, embeds may be more suitable.
- If calipers are used to directly measure specimen dimensions, the precision of results might be questioned. For example, to effectively use jaw calipers for any prismatic object, the jaws must be flush with the surfaces of the object and should be parallel to the appropriate axis of that object. Often, the surfaces of ASR-affected elements, even if originally cast with perfectly flat surfaces, do not remain flat upon expansion. Additionally, the element may also not remain prismatic thus changing the orientation of the element's axis. These effects can skew measured results.

2.5.3 Visual Inspection

Various attempts have been made to correlate certain physical features of ASR-affected concrete, sometimes detected with microscopy, to levels of expansion. These include the Damage Rating Index (DRI) and Cracking Index (CI) techniques. With the

DRI method (Grattan-Bellew and Danay 1992), free expansions are related to petrographic features of ASR-affected concrete found on polished sections taken from cores extracted from a structure. With the CI method, expansions are related to the amount of surface cracking detected on a structure. Due to its widespread use, especially in comparison to the DRI method, the CI method is discussed here in greater detail. More information about the DRI method can be found elsewhere (Smaoui et al. 2004).

When using the CI method, often referred to as "crack summation," the expansion in a given direction of a structure is measured by comparing the sum of the widths of all cracks across a particular gauge length to that of the gauge length. Commonly, cracks are monitored along multiple gridlines drawn on the surface of a structure at locations of interest. At a location of interest, a CI value (i.e., an expansion) for a particular direction is mathematically taken as the sum of the cracks across all gridlines in that direction divided by the sum of the original lengths of the gridlines. In order to obtain an appropriate measure of expansions, various sources encourage that cracks be monitored over multiple, long gridlines to capture a representative distribution of cracks. The ISE Guidelines (1992) recommend taking measurements for five, one-meter-long lines separated by at least 250 mm. Fournier et al. (2010) recommend taking measurements using two sets of rectangular reference grids per monitored surface of a structure, with each grid comprised of half-meter-long lines. Ultimately, the CI method is advantageous in that it: 1) is relatively simple to use, 2) is cost-efficient, 3) is an in-situ technique requiring no removal of material from a structure, and 4) requires no embedment of internal devices or external measurement points.

Unfortunately, there are several disadvantages to using the CI method, namely those related to the precision and accuracy of the results:

- The CI method is highly subjective. Measurement of cracks requires human interpretation of the widths of cracks barely visible to the naked eye. The devices used to measure crack widths, especially crack comparators, may not be accurate, and individual users may be left attempting to distinguish cracks that differ by less than 0.05 mm with much uncertainty. In fact, the ISE Guidelines (1992)

encourage the use of magnifying devices for crack widths below 0.20 mm. It can be especially difficult to identify how to account for cracks that run near-parallel to gridlines and cross the lines at multiple points. Additionally, cracks can easily be overlooked, especially given that the entire indexing process is exceptionally time-consuming.

- Values obtained with the CI method may poorly reflect the actual amount of expansion in the structure. If gridlines are not drawn and measured prior to the onset of ASR expansion (i.e., where no initial datum exists), CI values obtained will not be measures of the true total amount of ASR expansion that has occurred (ISE 1992). Further, expansions evaluated directly from crack widths do not take into account the fact that the concrete in-between cracks can still exhibit expansive strains. As such, actual expansions are likely greater than CI values, and CI values should be taken as a lower bound. Ultimately, the ISE Guidelines (1992) indicate that the error associated with the CI method can be as much as 50 %.
- The CI method, whether accurate or not, only gives a measure of expansions at the surface of an element. As discussed previously in Section 2.5.2 on mechanical surface measurements, surface expansions may not be the same as those in the interior of the element. Similarly, the expansions measured at one location of the surface may be different than at another location depending on any local differences in restraint or environmental exposure conditions.
- CI measurements are not necessarily indicative of ASR expansions alone. Measurements can capture other strain effects, such as shrinkage or thermal expansion/contraction as well. As such, the ISE Guidelines (1992) recommend that appropriate adjustments be made in order to isolate ASR-only strains.

In an effort overcome some of the problems or limitations of the CI method, numerous researchers have proposed modifications to the technique itself or the way in which crack measurements are correlated to expansions of ASR-affected concrete or mortar. Studies by McGowan et al. (1952), Kobayashi et al. (1987), Nishibayashi et al.

(1989), Chana and Korobokis (1991), Ng (1991), and Jones and Clark (1994) have generated different multiplication factors (generally greater than 1.0) that can be applied to crack summation values to obtain a truer measure of ASR-induced expansions. Jones and Clark (1994) also suggested that crack widths should be measured perpendicular to the angle of cracking rather than perpendicular to CI gridlines in order to give improved results.

2.5.4 Other Expansion Measurement Techniques

While the aforementioned expansion measurement techniques are the most commonly used, they do not represent an exhaustive list of all possibilities. Some other measurement methods that have been utilized include:

- Use of the Stiffness Damage Test (SDT), developed by Chrisp et al. (1989, 1993), which relates in-situ expansions to the cyclic compressive behavior of concrete cores. Although simple to perform and closely related to elastic modulus testing of concrete, the SDT method notably requires removal of material from structures and generates estimates of free expansion rather than restrained expansion in an in-situ condition.
- Nondestructive testing methods, many of which were investigated by Kreitman (2011). Using these techniques, ASR behavior can often be investigated for a structure in an in-situ condition without removal of material or alteration of restraint conditions. However, use of these techniques is not yet standardized, and results have not accurately reflected actual behavior at high expansion levels.

2.6 IMPLICATIONS OF ASR

ASR may result in changes to the durability, functionality, and integrity of affected structures. The expansion and cracking in concrete due to ASR may have a detrimental effect on a structure's ability to perform as intended. It is, however, also possible for some deleterious behavior to be counteracted by unique mechanical effects that manifest in affected concrete that is reinforced and thus restrained against expansion.

Notably, with regard to a structure's ability to carry and transfer loads, ASR may ultimately have a positive, negative, or neutral impact. In order to assess this structural response, as well as nonstructural response, all issues related to the expansion and cracking in concrete due to ASR must be acknowledged and thoughtfully considered. The following sections detail many of the implications of ASR.

2.6.1 Impairment of Concrete Durability

Cracking associated with ASR can increase the permeability of concrete by creating new paths through which water can penetrate and migrate through a structure. This is especially true of concrete near the surface of structures which experiences macrocracking due to expansion gradients throughout the bulk volume of the material. Increased access to water can expedite ASR-related damage. Additionally, ASR-affected structures like dams, bridge piers, and retaining walls are commonly found in extreme exposure environments with water that may contain constituents like chlorides or sulfates which can be deleterious to concrete. Given direct exposure to large quantities of liquid water and an increased propensity for water to easily transmit through cracks, such structures may be more susceptible to other mechanisms of deterioration like sulfate attack, corrosion, and freeze-thaw attack (Fournier et al. 2000). In effect, any additional damage to a structure that occurs secondary to the ASR-induced cracking can hinder a structure's ability to function effectively. Of special concern is an increased potential for corrosion in pre-tensioned concrete structures which can threaten the integrity of the prestressing strands under very high tension.

2.6.2 Impairment of Functionality

Dams, other retaining structures, containment structures, and subgrade walls are intended to separate interior spaces and housed contents from exposure to exterior elements and/or prevent the transmission of water, gases, or other fluids or contents from penetrating through the structural components in question. Ultimately, cracking associated with ASR can undermine the intended role of these structures, creating more

permeable concrete and enhancing the risk of catastrophic damage to equipment or contents within structures and/or danger to the general public who rely upon a structure's retaining or encapsulating functionality.

Equipment within structures can also be interfered with simply by way of ASR-induced expansions. For example, expanding concrete could potentially interfere with turbines operating within a dam. To mitigate detrimental expansions in hydraulic structures, relief slots have commonly been cut to provide open space for expansion without continued interference with turbines. Such a procedure has been utilized numerous times for the Mactaquac Generating Station in Canada (Curtis 2000).

2.6.3 Bond Degradation

The bond between concrete and steel reinforcement in RC structures may be degraded due to ASR. Bond degradation may be the result of either cracking of concrete from ASR near the interface with steel reinforcement and/or due to the physical expansion of concrete away from the embedded reinforcement. Reduced bond may impair a structure's ability to effectively transmit forces from concrete to reinforcement, a requirement of well-designed RC structures. Similarly, tension stiffening of concrete – the ability of cracked concrete to continue carrying tension in the presence of reinforcement – may be negatively impacted. Bond degradation may result in anchorage distress or bar development problems for both individual and spliced bars. Ultimately, the load-carrying capacity and ductility of an RC structure may be reduced.

Bond degradation due to ASR is a topic that requires more attention by researchers. Chana (1989) showed that bond may be reduced by up to 40 % for near-surface reinforcing bars in small-scale specimens without transverse reinforcement and a small cover. The likelihood or extent of bond degradation in large-scale RC structures, however, is not clear. Understanding bond behavior is a critical requirement to fully and effectively assess or model how a structure will behave due to ASR. It is worth noting here that the analysis of experimental results on expansion behavior in RC elements (described in Chapter 3) and the use and formulation of existing and newly developed

analytical ASR models (described in Chapters 4 and 5) often rely upon the assumption of perfect bond between concrete and steel reinforcement. That is not to say that bond degradation cannot or should not be considered in experimental analysis or model development and usage, but simply that the phenomenon is not yet well understood. Work on bond degradation was beyond the scope of the work in this dissertation but should be addressed in the future.

2.6.4 Ineffective Load Transfer

Pre-cracked, ASR-affected concrete may be unable to transmit loads as effectively as unaffected concrete. Notably, macrocracking at the surface of structural members due to ASR expansion gradients and/or due to nonuniformity of restraint (e.g., given discretely placed reinforcement) may hinder a structure's ability to carry load within cover concrete. Loads may not be transmitted well across these wide and deeply penetrating cracks at the surface where expansions can concentrate. An example of where such behavior might be observed is in a component like the ASR-affected, biaxially reinforced concrete beam discussed in detail in Section 3.3 in which wide, mid-depth cracks formed at the surface of the member between discretely placed mats of reinforcement. Further, the existence of these cracks may disrupt the mechanism of aggregate interlock and thus hinder shear transfer. Ultimately, it may be conservative to evaluate an ASR-affected structure's load-carrying capacity, at least for shear, based on member cross-sections neglecting contributions of surface layers of concrete where large cracks are generally observed or likely to exist. The distribution and depth of surface cracking would certainly influence such decision-making.

2.6.5 Chemical Prestressing

ASR produces a chemical prestressing effect in RC in which bonded reinforcement is tensioned by expanding concrete which in turn is subjected to compression to balance the induced tension via equilibrium. Conceptually, this is the opposite of shrinkage behavior in RC. The prestressing effect is illustrated in Figure 2-6.

Consider an RC element free of externally applied load in which the concrete and steel reinforcing bars are assumed to be perfectly bonded and behavior in a single reinforced direction is being considered. Given a total expansion (or strain), ε, for the RC element in the direction considered, the average tensile stress in the reinforcement, f_s, will be equal to the product of the elastic modulus of steel, E_s, and the total strain in the material. To satisfy equilibrium, the compressive stress introduced in the concrete, f_c, will be equated to the smeared reinforcement stress (i.e., the product of the average tensile stress in the reinforcement and the reinforcement ratio, ρ). This is the approach generally taken by researchers when evaluating the level of ASR prestress during post-experimentation analysis of ASR expansion behavior.

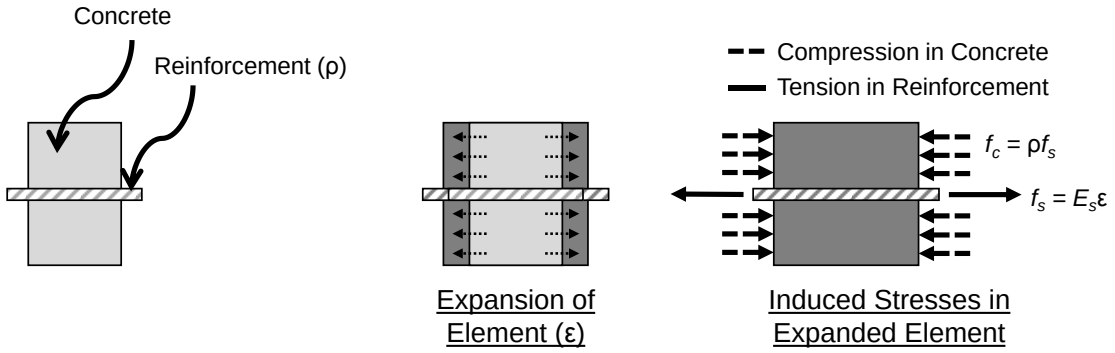

(a) Prior to ASR Distress *(b) During ASR Distress*

Figure 2-6: Chemical prestressing effect due to ASR

In normal prestressed concrete design applications, engineers prestress concrete to counteract induced tension due to loading, delay initial cracking, improve service-level stiffness of structures, and construct members with longer spans. The ultimate flexural capacity of a prestressed member, which may be evaluated using traditional sectional analysis with useful limiting strains in concrete and considering yielding of reinforcement, should not differ from the flexural capacity of a nonprestressed member. Meanwhile, the evaluation of shear behavior and capacity of prestressed concrete often differs from ordinary reinforced concrete. The ACI 318 Building Code (2014) uses

separate shear design equations to evaluate cracking loads (in excess of those for nonprestressed concrete) and the contribution of concrete to shear capacity, V_c, for prestressed flexural members, slabs, and footings. The value of V_c for prestressed concrete can often exceed values determined for nonprestressed concrete. Increased cracking loads can be especially beneficial for prestressed members lacking transverse reinforcement which are expected to fail in shear upon first cracking. In both the ACI 318 Building Code (2014) and the AASHTO LRFD Bridge Design Specifications (2014), any vertical component of prestressing force introduced in a member by harping prestressing strands or tendons can contribute to an increased total concrete contribution to shear capacity. On a related note, code equations also exist to capture increased shear capacity in the presence of combined shear and axial compression.

Ultimately, any of the aforementioned benefits of prestressing may also be observed in ASR-affected RC, however, it is certainly not recommended to computationally rely upon any improvement to structural behavior, capacity, or ductility provided through the chemical prestressing process. ASR-induced prestressing is not designed for; it is an unintended and unanticipated phenomenon. Given concerns about the effectiveness of bond between concrete and steel, and uncertainties regarding the accuracy or applicability of expansion measurements which are used to quantify induced stresses, there may be doubts about the true measure of prestress introduced in these structures. At worst, the effects of bond degradation and/or concrete material property degradation may outweigh any potential benefits provided by the prestressing effect, thus leading to a possible net reduction in capacity or ductility. The induced prestress may be conservatively neglected, accepting that overall structural response may otherwise be impaired; however, the prestressing effect should not be wholly discounted in the overall assessment of afflicted structures and in the determination of their safe, continued use. Ultimately, the prestressing may sufficiently counteract issues of bond degradation and material property degradation, the net result of which may lead to the conclusion that a structure's overall response may not be negatively impacted.

Perhaps where ASR-induced prestressing can offer the greatest benefit to ensure that a structure is sound lies in the fact that RC elements should be prestressed in all reinforced directions undergoing expansion. This differs from many ordinary prestressed concrete members, such as pre-tensioned bridge girders, which are prestressed in only one direction (i.e., longitudinally). As a result of this multi-directional prestressing, states of biaxial or triaxial compression are introduced in concrete which can serve to confine the material and enhance the peak compressive stresses and strains that the material can attain. This can consequently serve to elevate the load-carrying capacity and/or ductility of a structure. Further, prestressing in directions of transverse shear reinforcement may contribute to increased shear capacity in the same manner as the vertical component of prestressing force in members with harped strands or tendons. As one example, triaxially reinforced beams tested in shear by Deschenes et al. (2009) experienced capacity increases of up to 15 % or more when affected by ASR. As another example, Ng and Clark (1992) found that the ductility of two-way slabs under punching shear increased in the presence of ASR. At the same time however, the punching shear capacity remained unchanged at low levels of expansion and reduced due to ASR-induced delamination at expansions above 0.6 %.

2.6.6 Yielding of Reinforcement

As a consequence of the tensioning of reinforcement due to ASR-induced expansion in concrete, the reinforcement may be strained to the point of yielding. Unlike prestressed concrete, which utilizes high-yield strands designed to develop large strain levels while still remaining elastic, conventional RC structures typically utilize ordinary deformed reinforcement with low yield strengths. This deformed reinforcement is not intended to be used in prestressed applications. For example, ASTM A615 (2016) Grade 60 reinforcement yields at a strain of approximately 2.0 mε, or 0.2 %. It is a strong possibility for concrete to expand more than 0.2 %, especially where light amounts of reinforcement are used. Assuming that the concrete and reinforcement are perfectly compatible such that the total strains in both materials are equivalent, the reinforcement is

likely to yield at such levels of expansion. Ultimately, the resistance provided by reinforcement against pre- and post-yield expansions may differ. Existing expansion distribution models, which are covered in Chapter 4, capture this response – when steel stresses plateau upon yielding, the otherwise increasing concrete material stresses, which are defined to curb expansion development under restraint, plateau as well according to equilibrium. With no further increase in concrete material stress, yielded reinforcement is said to offer no additional resistance against additional expansion after yielding.

Apart from changes in restraint to expansion, yielding of reinforcement may have undesirable consequences. At a minimum, yielding may result in:

- Reduced member stiffness
- Permanent deformations
- Reduced structural stability
- Reduced tension stiffening
- Reduced energy dissipation in seismic events

These are concerns that have not been widely addressed and should be researched in more depth in the future.

2.6.7 Concrete Material Property Degradation

As mentioned previously, the strength and stiffness of ASR-affected concrete in both compression and tension may be reduced due to microcracking and macrocracking produced as expansions develop. The amount of material property degradation is undoubtedly related to the amount, distribution, and size of the cracks that form. However, such cracking parameters can be difficult to quantify, both experimentally and analytically. Instead, attempts are generally made to link material property degradation to the amount of expansion that exists in concrete. Expansions are more readily quantifiable than cracks and can be a more objective measure of ASR distress analytically, experimentally, and in field structures. The expansions in question include either expansions in individual directions of concrete elements or volumetric expansions for those elements. The main thought process behind correlating material property

degradation to expansions is as follows: if strength and stiffness degrade more so with increased cracking, and if greater expansions induce more cracking, then the properties should decrease in value with increasing expansions. Two major sources of guidance in the literature on quantifying material property degradation as a function of expansions are the 1992 ASR guidelines recommended by the ISE and the analytical work performed by Huang and Pietruszczak (1999).

2.6.7.1 Analytical Recommendations

The ISE Guidelines (1992) consider degradation of both uniaxial cylinder and cube compressive strengths, uniaxial tensile strength (either splitting or torsional), and modulus of elasticity. Lower-bound, expansion-dependent estimates of the retained percentage of each property relative to 28-day values are provided and listed in Table 2-1. At 28 days, concrete is assumed to have not yet experienced any appreciable amount of expansion and thus will not have experienced any property degradation. Property degradation for expansions between the values listed can be determined using linear interpolation. The tabulated values are graphically depicted in Figure 2-7. Each material property degrades at a decreasing rate with increasing expansion. In other words, properties degrade quickly at initial levels of expansion and more slowly at higher levels of expansion, evidently approaching nonzero terminal values. In comparing the influence of ASR on different properties, the ISE Guidelines imply that: 1) the cylinder compressive strength degrades more quickly than the cube compressive strength, 2) the tensile strength degrades more quickly than either type of compressive strength, and 3) the elastic modulus degrades more quickly than the compressive or tensile strengths. It must be noted that the tabulated values were determined based on expansions of unrestrained, small-scale materials samples (e.g., cylinders or cubes). As such, it is not clear whether these values apply to equal amounts of restrained expansion or even in larger structures. However, if material property degradation does correlate to expansions in general, it is still likely that different amounts of restrained expansion will result in different amounts of property degradation. Perhaps more importantly, the expansions

given in the table appear to refer to individual directional expansions. If this is correct, and given that restrained expansions in RC structures are not uniform in all directions, application of the ISE Guidelines would imply anisotropy of ASR-affected concrete material properties.

Table 2-1: ISE (1992) material property degradation

		Property retention relative to non-ASR-affected 28-day values (%)				
	Free Expansion (%)	0.05	0.1	0.25	0.5	1.0
Property	*Compressive Strength (Cube)*	100	85	80	75	70
	Compressive Strength (Cylinder)	95	80	60	60	---
	Tensile Strength (Splitting)	85	75	55	40	---
	Elastic Modulus	100	70	50	35	30

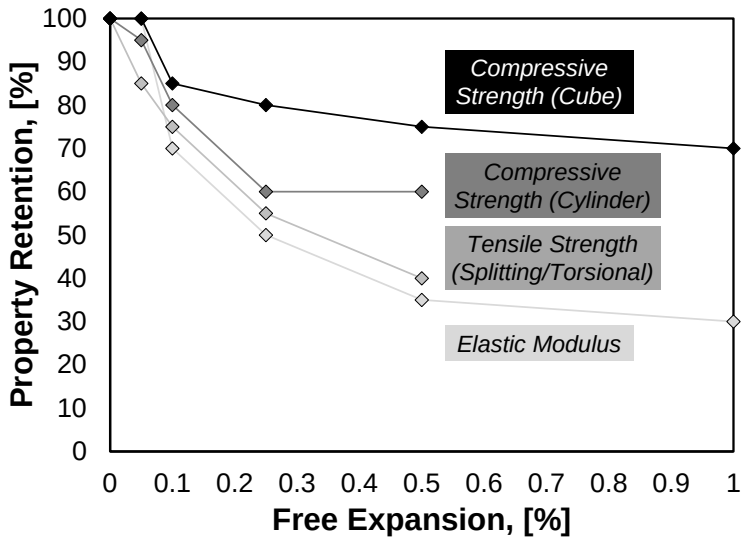

Figure 2-7: ISE (1992) material property degradation

Huang and Pietruszczak (1992) suggested that the degradation of material properties is a function of the overall progress of ASR, ξ, from the start of the reaction (at $\xi = 0$) to the end of the reaction (at $\xi = 1$). In terms of expansions, the progress of ASR is

taken as the amount of volumetric expansion occurring in an element at a given point in time relative to the terminal amount of volumetric expansion that can develop. Because material property degradation is linked to volumetric expansion in this case, it is implied that the ASR-affected material properties are isotropic (i.e., the same in all directions of an element). The lack of consensus as to whether properties are isotropic or anisotropic is an issue that has not yet been resolved. According to the researchers, all material properties degrade linearly with increasing reaction progress/expansion. The relationship between the retained percentage of each property relative to nondegraded values may be given in the following general form:

$$\frac{A}{A_o} = 1 - (1 - \beta) \cdot \xi \qquad \textit{Equation 2-1}$$

where: A = value of property at a given level of reaction progress

A_o = value of property at $\xi = 0$ (i.e., nondegraded property value)

A/A_o = retained fraction of property at a given level of reaction progress

β = material constant

Nondegraded properties and properties at 28 days may be assumed to be equivalent. In terms of volumetric expansions, Equation 2-1 may be rewritten as:

$$\frac{A}{A_o} = 1 - (1 - \beta) \cdot \frac{\varepsilon_{vol}}{\varepsilon_{vol}^{max}} \qquad \textit{Equation 2-2}$$

where: ε_{vol} = volumetric expansion

ε_{vol}^{max} = maximum volumetric expansion

Equations 2-1 and 2-2 are graphically depicted in Figure 2-8. The degradation of each property is represented as a line with a negative slope equal to $(1 - \beta)$. The material constant, β, is not necessarily the same for all material properties; unique values are possible for both strength and stiffness. As a reference, a smaller value of β was selected for the elastic modulus than for the compressive and tensile strengths in an example validation originally presented by the researchers. A smaller β would indicate that the elastic modulus decreases more than does the strength of concrete as was implied by the ISE Guidelines (1992). With regard to strength, the researchers indicated that β is the

same for both uniaxial compressive and tensile strengths. This is a departure from the ISE Guidelines (1992) which suggest that degradation of each type of strength is different. Further, values of β may be unique for different reactive concrete mixtures. No particular values for β were recommended, nor is there any analytical means provided to evaluate β. In practice, β could be algebraically computed from Equation 2-2 given knowledge of the amount of material property degradation at one level of volumetric expansion and a known maximum volumetric expansion. This is challenging, however, because the maximum volumetric expansion for a particular ASR-affected structure is difficult to anticipate given the sheer number of factors described in Section 2.3, such as concrete reactivity, restraint, and member size, which can influence expansion development. As a final note, this linear degradation model was adopted by Saouma and Perotti (2006) to use in combination with their ASR expansion model described in Chapter 4. Unlike Huang and Pietruszczak (1999) though, Saouma and Perotti (2006) suggested that only the tensile strength and elastic modulus degrade and that the compressive strength remains unaffected by ASR.

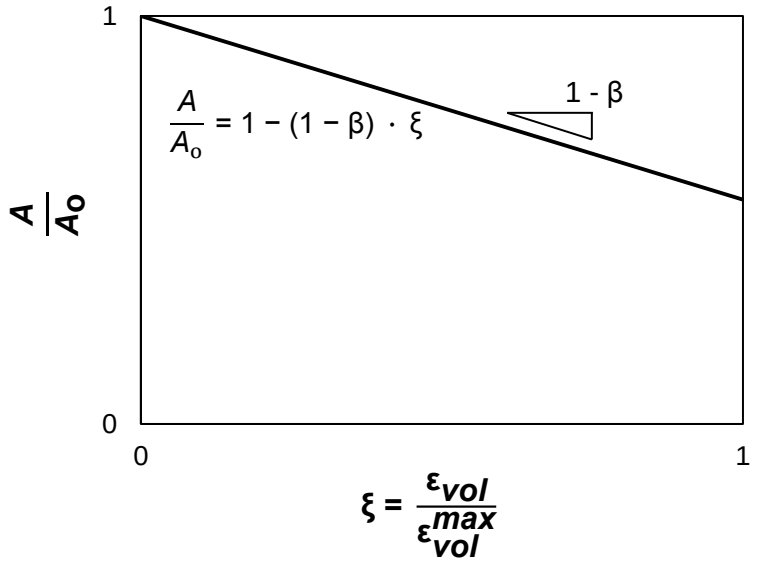

Figure 2-8: Huang and Pietruszczak (1999) material property degradation

2.6.7.2 Experimental Results

The results of materials testing of different ASR-affected concretes in five studies from the literature are collectively plotted in Figure 2-9. The data shown were collected by Swami and Al-Asali (1988), Ng and Clark (1992), Smaoui et al. (2006), Giannini and Folliard (2012), and Zetzman (2015). Note that this does not represent all data available in the literature. The retained percentages of each material property relative to 28-day values are shown for different levels of free unidirectional expansion. The lower-bound estimates of property degradation from the ISE guidelines (1992) are shown as well. The data clearly reveal that the splitting tensile strength and elastic modulus decrease with increasing expansion. Many of the data points for both cylinder and cube compressive strengths suggest that the compressive strength of concrete relative to 28-day values is marginally reduced, if at all, at least for expansions below 0.4-0.5 %. Beyond those levels of expansion, the compressive strength is shown to decline, but often to no less than about 85 % of 28-day values at the highest given levels of expansion. This is a noticeably lower amount of degradation compared to that for tensile strength which is shown to drop to 75 % or less of 28-day values at similar levels of expansion. Despite the widespread lack of significant degradation of compressive strength compared to 28-day values, the peak achievable strength appears to still be undermined by ASR. Within the range of 0-0.2 % expansion, the compressive strength reaches values greater than those at 28 days, likely due to continued hydration of cement leading to late-age strength gains. At expansions below 0.4-0.5 %, the compressive strength does trend downward with increasing expansions, although generally remaining in excess of 28-day values. Thus, the potential for typical strength gain in concrete after 28 days and degradation due to ASR appear to offset, negating some concern about severe loss of design strength due to ASR. At the same time, any possible late-age gains in tensile strength or elastic modulus appear to be overwhelmed by losses due to ASR. Comparatively, the loss of stiffness, albeit measured from fewer data points, appears to exceed the loss of both compressive

and tensile strength as suggested by both the ISE Guidelines (1992) and Huang and Pietruszczak (1999).

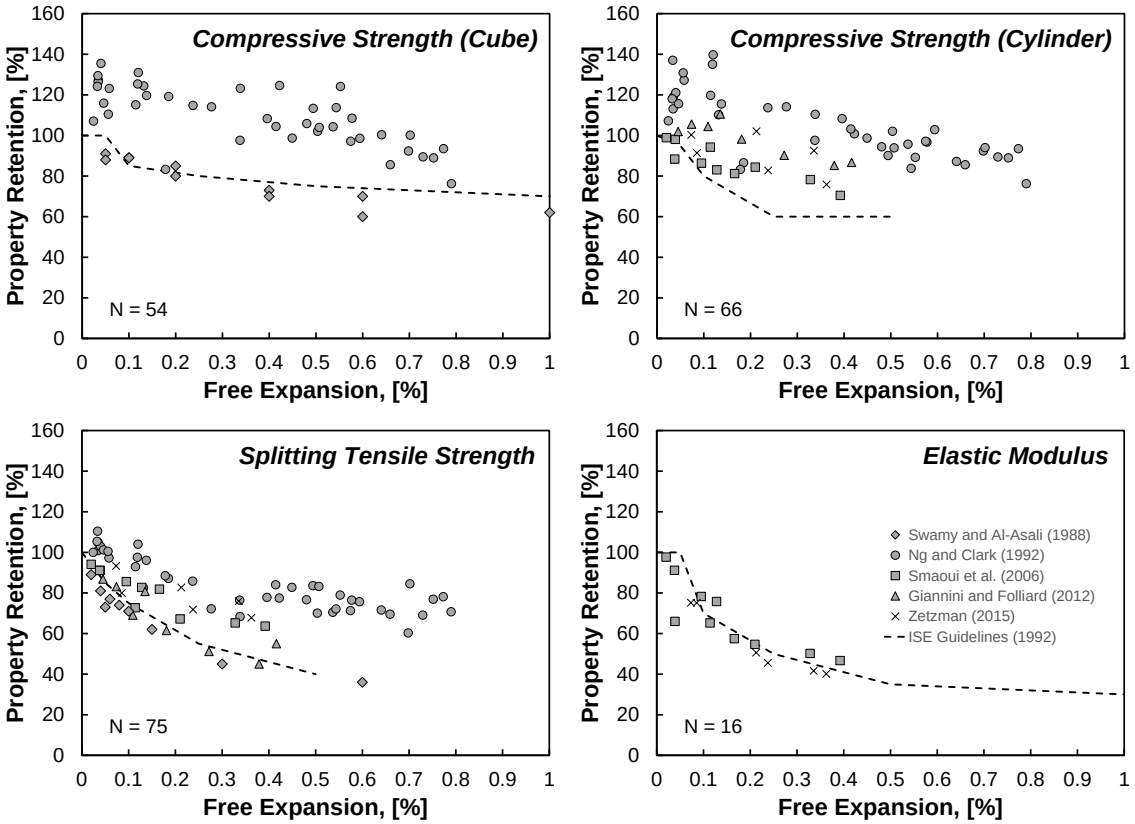

Figure 2-9: Measured material property degradation in literature

One outstanding issue with the data in Figure 2-9 is that material property values were linked to unidirectional expansions for test samples in the direction of loading. Obviously, a concrete element can expand in multiple directions, and it is not clear if or how the expansions in directions transverse to the loading direction may have influenced the results. If transverse expansions do affect property degradation in small-scale samples of unrestrained concrete, the aspect ratio of the samples may be a critical factor. Cylindrical specimens used for compressive strength, splitting tensile strength, and elastic modulus testing typically have an aspect ratio of about 2:1 and are hypothetically prone to increased expansions in the long direction due to that being the casting direction and/or

due to increased potential for alkalis leaching from radial surfaces. As a point of reference, the unrestrained prisms used to evaluate ASR expansion potential via ASTM C 1293 (2008) are solely measured in their long direction and purposely sized to 75 x 75 x 285 mm to minimize transverse expansions given increased surface area while still promoting significant longitudinal expansions. A lack of transverse expansion measurements in these prisms may be acceptable given the aspect of ratio 3.75:1, but not in cylinders with nearly half of that aspect ratio. Therefore, successfully linking property degradation to expansions may actually require a two-parameter input: loading direction expansions and transverse expansions. Alternatively, property degradation may be linked to volumetric expansion development, but as stated previously, this would suggest isotropy of the degradation. More testing and more complete monitoring of all expansions in materials samples would be necessary to improve knowledge.

With regard to the validity of the aforementioned property degradation estimation techniques, both appear to have some credence when assessing the data in Figure 2-9. The ISE Guidelines (1992) provide strong lower-bound estimates of all properties, as intended. They do not however, provide accurate estimates of property degradation given the data shown, except for the degradation of the modulus of elasticity. On that note, given the scatter of data at similar levels of expansion, it would appear difficult to accurately predict many of the individual data points by any means purely as a function of the level of expansion without consideration of other factors such as concrete composition, ASR reactivity, aggregate size, and cracking. Still, it may be possible to predict average degradation as a function of expansion. Meanwhile, many of the data points for all properties appear to align in a band with a decreasing linear trend, thus supporting the suggested formulations by Huang and Pietruszczak (1999). Of course, that is assuming that the unidirectional expansions correlate with volumetric expansions.

2.6.7.3 Application of ASR Material Behavior

In discussing material property degradation, it is valuable and often essential to raise questions about how the material properties of ASR-affected concrete should be

applied in the analysis and assessment of afflicted structures. In particular, engineers may find value in knowledge of any inter-relationships between different material properties, overall compressive stress-strain behavior, and the effects of multi-directional loading on properties as they pertain to ASR. The following are issues that may garner attention:

- The elastic modulus of unaffected concrete is often related to its compressive strength. For example, the ACI Building Code (2014) permits designers take the elastic modulus as $57000\sqrt{f_c'}$ (in psi). One might consider whether a similar relationship applies to ASR-affected concrete. This could be used in lieu of evaluating the modulus based on expansions or attempting to directly measure the modulus for an actual structure using cylinders or cores.
- Generally, the tensile strength of typical concrete is not measured or specified but is rather evaluated empirically for any design calculations or modeling as a function of the compressive strength of concrete. One might consider whether the tensile and compressive strengths of ASR-affected concrete can likewise be related through formulation to use in lieu of evaluating the tensile strength based on expansions or attempting to directly measure the strength for an actual structure using cylinders, cores, or dog-bones. It should also be noted that many modeling approaches for RC make use of tensile and compressive strength relationships even if a measured tensile strength is otherwise known for input.
- The direct, splitting, and bending tensile strengths, each commonly used in different aspects of concrete design, are different from one another. These tensile strengths are often approximated as $4\sqrt{f_c'}$, $6\sqrt{f_c'}$, and $7.5\sqrt{f_c'}$ (in psi), respectively. As previously indicated, material property degradation models and experimental results for ASR provide estimates of splitting tensile strength degradation. Splitting tensile tests, performed on cylinders or cores, are the most readily available way to obtain a tensile strength. However, the direct and bending tensile strengths are more useful for design and analysis; the direct tensile strength is

typically input in finite element models and important for the consideration of shear while the bending tensile strength is useful for evaluating flexural cracking loads. Limited evaluation of these strengths for ASR-affected concrete has been performed. Thus, it is vital to determine if the aforementioned relationships apply equally to unaffected and ASR-affected concrete or if alternative relationships can be established for the latter. If so, one might be able to convert the expansion-dependent values of degraded splitting tensile strength provided by the ISE Guidelines (1992) and Huang and Pietruszczak (1999) into expansion-dependent direct and flexural tensile strengths.

- Due to nonlinearity, the modulus of elasticity of concrete is not constant. In particular, the initial tangent modulus, as measured on a stress-strain curve, differs from a secant modulus taken between the zero point and a nonzero amount of stress. Generally, measured and reported moduli of elasticity are secant moduli determined at low levels of stress. For example, in the U.S., secant moduli are measured up to 40 % of the peak compressive strength in accordance with ASTM C 469 (2010). With regard to ASR, values of elastic modulus degradation from the ISE Guidelines (1992) were derived from materials samples in which secant moduli were likely measured. By comparison, an initial tangent stiffness is only measured through analysis of stress-strain data. Ultimately, the initial tangent stiffness and low-stress secant moduli do not often differ significantly, at least in unaffected concrete, such that the secant modulus may be used in lieu of an initial tangent stiffness for design. In fact, the ACI Building Code (2014), specifically states that a computed modulus value equal to $57000\sqrt{f_c'}$ (in psi) was derived from secant stiffness data. However, tangent stiffnesses are needed in the definition of compressive stress-strain curves, and it is not certain whether existing methods of determining material property degradation pertain to both secant and tangent stiffnesses.

- Full compressive stress-strain behavior of concrete is valuable in developing moment-curvature relationships for flexural members and imperative for finite element modeling. Unidirectional stress-strain curves for concrete are typically characterized by peak stresses, peak strains, and elastic moduli. While some researchers, including Cope et al. (1994) and Barbosa and Hanson (2014), have measured limited amounts of stress-strain behavior in ASR-affected elements, it does not appear as though stress-strain curves have been measured for particular levels of expansion. There are also no known analytical models for ASR-affected stress-strain behavior, and expansion-dependent values for peak strains are absent in the literature. Consequently, one is currently left to assume that: a) the general shapes of measured unaffected and ASR-affected stress-strain response match, or b) stress-strain models for unaffected concrete equally apply to ASR-affected concrete, simply with modified parameters. Simple stress-strain models, such as Hognestad's parabola, can be defined solely given a peak stress and a secant modulus from the zero point for any stress level. The initial tangent modulus and peak strain are not needed and can subsequently be derived. Since the degradation of compressive strength and the secant elastic modulus can be measured or computed, stress-strain behavior for ASR-affected concrete can be defined. Alternatively, more advanced models, like that of Popovics (1973), cannot be defined without both an initial tangent modulus and a peak strain. Even if the initial tangent modulus of unaffected concrete is known and the degradation of this parameter is the same as the degradation of the secant modulus, the lack of knowledge of how peak strains are affected by ASR renders it impossible to modify these models. Ultimately, a greater focus on measuring stress-strain behavior and peak strain response is needed to be able to modify existing models to begin with and validate a modification approach or otherwise develop new models.
- The uniaxial compressive strength, stiffness, and deformation capacity of unaffected concrete differ from that in concrete under multiaxial states of stress.

In the presence of transverse tension, the compressive strength and stiffness reduce due to compression softening. Under states of biaxial or triaxial compression, the compressive strength and deformation capacity increase due to confinement. It is unclear whether the compressive strength, stiffness, and deformation capacity of ASR-affected concrete vary in the same ways or to the same degrees as unaffected concrete under multiaxial states of stress. Further, the applicability of existing compression softening and confinement models to ASR-affected concrete is unknown.

2.6.7.4 Validity of Relating Property Degradation to Unrestrained Expansions

If there is indeed a correlation between material property degradation and expansions, the greatest remaining unknown is whether or not it is appropriate to correlate degradation to unrestrained expansions. This is specifically a question of applicability to restrained expansions. As mentioned in Section 2.4, restrained ASR-affected concrete physically differs from unrestrained ASR-affected concrete in the way the material cracks. Differences in the amount, size, and orientation of cracking in concrete may affect properties.

Of all cracking features, cracking orientation may play the most prominent role in evaluating material property degradation. As previously described, unrestrained concrete will exhibit randomly oriented cracks while restrained concrete will exhibit cracking in the direction of restraint. The compressive and tensile strength and stiffness of concrete may be negatively impacted more so when ASR-induced cracks are oriented perpendicular to the direction of loading/resistance as opposed to parallel to the direction of loading/resistance. Such response is illustrated in Figure 2-10 and has been confirmed through the testing of cores extracted from an ASR-affected structure by Barbosa and Hanson (2014). Additionally, these researchers showed that the overall compressive stress-strain response of concrete with perpendicularly oriented cracks is less brittle than that for concrete with cracks oriented parallel to the direction of compression.

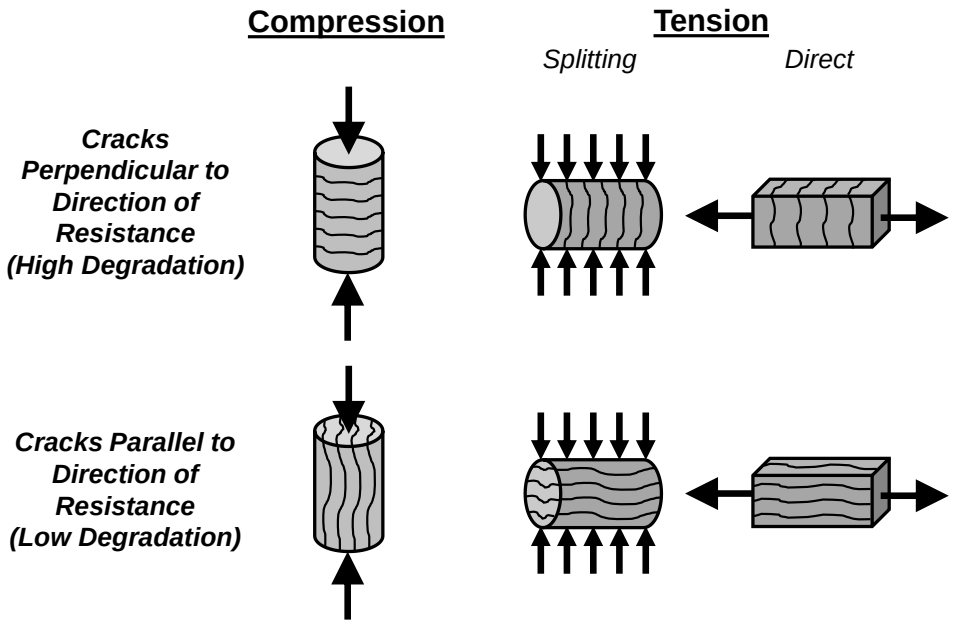

Figure 2-10: Influence of cracking orientation on strength degradation

These findings do cast some doubt as to the existence of a single set of values relating property degradation to expansions. Perhaps three new relationships can be formulated distinguishing property degradation for free expansions with randomly-oriented cracks, unrestrained expansions perpendicular to restraint-oriented cracking, and restrained expansions parallel to restraint. A final assessment of the effects of cracking orientation may not yet be complete without consideration of how multi-directional restraint influences crack patterns. More work is needed on these topics in the future.

2.6.7.5 Use of Materials Samples or Cores to Evaluate Property Degradation

In the discussion of material property degradation, it is important to briefly address the methods that might be used to evaluate degradation in RC structures in support of or in lieu of expansion-degradation relationships. Notably, tests on cylinders cast alongside, or cores extracted from, structural components may be tested to assess property degradation.

Cylinders are easy to fabricate and may be cast in large quantities with an ASR-affected laboratory specimen, but the mechanical properties of cylinders are likely not

representative of in-situ properties. For one, the amounts, sizes, and orientation of cracking will be different amongst structures and their companion cylinders. Specifically, properties for these elements are likely to differ due to cylinders experiencing randomly oriented cracking and a greater amount of macrocracking relative to their volume. Second, the development of expansion and cracking in cylinders will likely be slower than in real structures due to a lack of restraint, smaller size, and larger surface area. Cylinders will contain fewer alkalis to contribute to the chemical reaction, be more prone to alkalis leaching faster and in greater quantities, and be more sensitive to fluctuations in external environmental conditions, even when conditioned in the same space. Further, the peak expansions will be less in cylinders then in the full structures. Finally, the ASR-affected elements will be subject to the same differences between unaffected elements including varied curing, bleeding and segregation, and compaction. As an additional note, poor results from cylinder testing given a limited number of available specimens can present a problem.

Results from cores potentially provide a closer measure of in-situ properties in both laboratory and field structures since the cores can directly capture the influence of environmental conditions and cracking behavior; however, the results still may not be perfectly representative of in-situ properties. In extracting cores, there may be a removal of in-situ restraint with the potential for a "recovery" of expansion deformations (i.e., an opening of ASR-induced cracks). This may particularly yield lower values for the elastic modulus if the increased straining of the cracked concrete under compression is partly due to the rigid closing of cracks and not just gross deformation of the concrete material. Additionally, the properties obtained from cores in one location of a structure may not be indicative of properties at other locations and in other directions due to differences in local restraint and cracking behavior. Unfortunately, it is neither possible nor practical to extract cores in multiple directions of most RC structures, and only a limited number of cores would typically be taken to avoid removing an excessive amount of concrete or damaging the structure.

2.6.8 Other Potential Implications of ASR

In addition to the aforementioned implications of ASR, ASR may also result in the following:

- Imposed deformations which can lead to the buildup of unanticipated forces or deformations in joints and connections or other members of structural assemblies
- Fracture of reinforcement, which has been observed by Miyagawa et al. (2006)

2.7 SUMMARY

ASR expansion behavior in RC is a complex phenomenon requiring consideration of many different factors to effectively address concerns about the safety and operability of ASR-affected structures. Expansions are not only the direct product of ASR and the most readily measurable parameter of distress, but they serve as a direct link, both physically and computationally, to any changes in the load-carrying response of the concrete material or performance of structures that may be observed. It is important to have some basic understanding of the role ASR plays in the concrete material alone; however, it is more critical to shift the discussion of ASR toward behavior of the actual structures built from the deleterious material, identifying how structural details like loading and reinforcement influence expansion behavior and what the global implications of ASR are. ASR is not only a materials science problem; it is a structural engineering problem as well and should be emphasized as such much more.

The development of expansions and cracking in concrete, in terms of the rates, amounts, and patterns of distress, are influenced by numerous factors. Expansion behavior is related to the chemical and physical makeup of the concrete material and environmental conditions (i.e., temperature and humidity) which have been well-researched by materials scientists. In RC structures, design and construction details, which must be acknowledged by materials scientists but are under the purview of structural engineers, greatly increase the complexity of expansion behavior. Attributes like loading conditions, reinforcement amounts and layouts, component size and shape,

and casting direction result in different behavior in RC structures than would be evidenced in plain concrete. These are issues that have been explored to a degree, but still require more investigation through experimentation and analytical work.

It is vital to acquire information on expansion behavior through field studies or experimentation to advance our knowledge of ASR and pave the way for numerical modeling and future investigations. Expansions can be measured using internal devices like strain gages, external methods such as caliper-based surface measurements, and visual crack inspection. Each technique has its advantages and disadvantages related to factors such as cost, applicability to field or laboratory structures, subjectivity, and accuracy. Ultimately, the differences in these techniques and their common inability to measure widespread expansions complicates assessment and can make it more challenging to draw meaningful and reliable conclusions from collected data or use the data properly in validating analytical models.

Expansions are correlated to ASR-induced cracking in concrete and a myriad of possible unanticipated effects that may alter, potentially negatively, the way in which structures respond to load or serve their intended purposes. ASR can lead to the impairment of a structure's durability and functionality. Expansions and cracking may hinder effective load transfer, disrupt the bond between concrete and steel, lead to unexpected yielding of reinforcement, and/or cause a degradation of concrete material properties (i.e., strength and stiffness). Meanwhile, these behaviors may be counteracted by chemical prestressing and confinement that occurs in RC as a compatibility-related response to expansion in the concrete material. As a whole, structural performance may or may not be compromised by ASR, though such an assessment cannot be made without adequate experimental or analytical investigation.

CHAPTER 3: EXPERIMENTAL INVESTIGATIONS*

3.1 OVERVIEW

This chapter includes a detailed description of experimental work that has been conducted to identify ASR expansion behavior in concrete in the presence of structural restraint, i.e., reinforcement and/or sustained applied loading. First, a review of major expansion monitoring studies that have been conducted by previous researchers is presented. Then, two new experimental investigations conducted by the author of this dissertation are outlined.

3.2 EXISTING EXPANSION MONITORING STUDIES

Numerous researchers have conducted experimental investigations in which expansions have been monitored for ASR-affected concrete elements under a variety of different restraint conditions. Amongst these studies, ASR expansion development has been tracked with time for plain concrete specimens under sustained loads, unloaded RC specimens, and RC specimens under sustained loads in an effort to gauge the independent and combined influences of active and passive restraint conditions. Typically, researchers

* Portions of this chapter have been extracted directly from the following publications written by the author of this dissertation, with figures and tables reformatted for use in this dissertation:

Wald, D., Arrieta Martinez, G., and Bayrak, O. (2017). "Expansion Behavior of a Biaxially Reinforced Concrete Member Affected by Alkali-Silica Reaction." *Structural Concrete*, 11 pp. https://doi.org/10.1002/suco.201600143

- Dissertator contribution: Primary author and lead researcher; experiments conducted with Gloriana Arrieta Martinez, PhD

Wald, D. M., Allford, M. T., Bayrak, O., and Hrynyk, T. D. (2017). "Development and Multi-Axial Distribution of Expansions in Multi-Directionally Reinforced Concrete Elements Affected by Alkali-Silica Reaction." *Structural Concrete*, 15 pp. https://doi.org/10.1002/suco.201600220

- Dissertator contribution: Primary author and lead researcher; experiments conducted jointly with Morgan T. Allford, M.S.E. as part of combined masters/doctoral research

have explored how the amounts of applied loading or reinforcement may affect ASR expansion behavior. These studies have been carried out on concrete elements of varying sizes and shapes, with different reactive concrete mixtures, environmental exposure conditions, and restraint configurations (e.g., reinforcement layouts or number of reinforced/loaded directions). In addition to advancing the general knowledge of ASR expansion behavior for structural engineering applications, experimental findings from existing research have helped to guide the development of existing materials and structural engineering modeling procedures, discussed in Chapter 4, that are intended to capture the effects of ASR. Moreover, these findings have shaped the setup and practical focus of newer expansion monitoring studies, described later in this chapter, and the development and validation of a newly developed ASR expansion modeling approach, outlined in Chapters 5 and 6.

The following sections briefly detail the experimental programs and principal results or conclusions that may be drawn from prominent ASR expansion monitoring studies in the literature. Note that the list of studies described is not exhaustive. Further, most of these studies focused on specimens with only one type or configuration of restraint, such as:

- Plain concrete under load (uniaxial or biaxial loading)
- Unloaded RC (typically with uniaxial or triaxial reinforcement)
- RC under load

The studies covered are generally lumped together in the following sections with respect to the main form of restraint investigated. Afterward, a summary of major consistencies and inconsistencies of results seen amongst these studies is provided. Additionally, the review of prior research concludes with a brief critique of the experimental programs that have been employed in the past, highlighting prevalent issues that undermine the goal of addressing how ASR may influence structural performance.

3.2.1 Studies Focusing on Loaded, Plain Concrete

3.2.1.1 Le Roux et al. (1992)

The researchers monitored axial expansions in uniaxially loaded, 69 x 120 mm concrete cores that were extracted from an ASR-affected structure in an effort to identify an applicable method to mitigate continued expansion in the original structure. The cores were subjected to sustained compressive stresses of 1, 3, or 5 MPa and stored in tap water at 20ºC to mimic exposure conditions of the real structure.

Results showed that increasing the amount of applied compression resulted in reduced expansions compared to those in an unloaded specimen. The greatest percent reduction in expansions between load levels occurred for the lowest level of applied stress (1 MPa) in which expansions were reduced by more than one-half compared to those in an unloaded specimen. Additional reductions were achieved, although disproportionately, with further increases in applied load. Ultimately, under 5 MPa of compression, continued expansions of the concrete material were effectively stopped.

3.2.1.2 Larive (1997)

The researcher examined the influence of sustained, uniaxial compressive stresses on the expansion behavior of 130 x 240 mm concrete cylinders. The cylinders were subjected to 5, 10, or 20 MPa of compression. Longitudinal expansions in the direction of applied stress and expansions in transverse directions were monitored. Volumetric expansions were also examined.

Significant results from this study were identified as follows:

- Compared to free longitudinal expansions, restrained longitudinal expansions decreased with increasing applied stress. At 5 and 10 MPa, expansions were nonzero, but small. At 20 MPa, expansions were negligible.
- At 5 MPa and 10 MPa, the decrease in longitudinal expansions was coupled with an increase in transverse expansions. The transverse expansion was greater for the higher stress level.

- The terminal volumetric expansions of unrestrained cylinders and those under 5 and 10 MPa of compression were found to be 0.40 %, 0.33 %, and 0.43 %, respectively. Despite the somewhat out-of-place lower value for the cylinders under 5 MPa, these volumetric expansions were deemed to be of comparable magnitude. The volumetric expansions were similar as a result of decreasing longitudinal expansions being offset by increasing transverse expansions.
- The cylinders under 20 MPa of compression reached a terminal volumetric expansion of only 0.25 %. Transverse expansions did increase relative to free values as the longitudinal expansion dropped to negligible values; however, the transverse expansion was lower than that for cylinders under 5 and 10 MPa of compression. The drop in volumetric expansion was believed to be caused by the absorption of ASR gel in microcracks under high levels of compression, effectively limiting the amount of gel available to expand.

3.2.1.3 Dunant and Scrivener (2012)

The researchers monitored longitudinal and lateral expansions in 160 x 335 mm concrete cylinders subjected to various levels of uniaxial compression. The cylinders were loaded at 5, 10, or 15 MPa and instrumented with longitudinal and radial fiber optic gages. The cylinders were conditioned at 38ºC in a low-alkali solution to minimize alkali leaching while not influencing the overall reactivity of the concrete mixture. The ASR expansions of the concrete material were computed by eliminating creep and elastic strains from measurements.

The presence of restraint resulted in a significant reduction in both the longitudinal and lateral expansions of the cylinders compared to unloaded specimens undergoing free expansion. The longitudinal and lateral free expansions at the conclusion of the study were approximately 0.175 and 0.125 %, respectively. Under 5 MPa of compression, longitudinal expansions were almost entirely restricted, reaching terminal values of approximately 0.002 %. Cylinders under 10 and 15 MPa of compression did not expand in the longitudinal direction. Thus, the three load levels had essentially the same

influence on longitudinal expansion behavior. Conversely, lateral expansion behavior was significantly different amongst cylinders at the three load levels. While the lateral expansions of the loaded specimens were essentially lower than the free lateral expansion at all times, the more heavily loaded cylinders expanded greater amounts laterally than did cylinders subjected to smaller loads. In other words, the cylinder under 15 MPa expanded more than that under 10 MPa, which in turn expanded more than that under 5 MPa. Evidently, there was an interaction in load-expansion behavior beyond the one loaded direction. More interestingly, the net combinations of lateral and longitudinal expansions for the different load cases imply that volumetric expansions developed more quickly given increasing, not decreasing, levels of restraint.

3.2.1.4 Gautam et al. (2015)

The researchers monitored expansions along the three axes of 250 mm cubes subjected to uniaxial and biaxial states of applied compression. Specimens were post-tensioned in either one or two directions using unbonded, high-strength rods that were placed within each specimen and externally anchored with large end plates, ensuring uniform distributions of stress in each direction. Results were reported for one uniaxially loaded cube and one equal biaxially loaded cube, each subjected to 3.9 MPa of compression in the restrained directions. The cubes were conditioned at 50ºC and at a relative humidity of 100 %. Through-dimension expansions were measured between opposite faces of the specimen using a micrometer between sets of target points.

A few significant findings have been drawn from this study based on reported terminal expansion results. The volumetric expansions of the uniaxially loaded cube (0.38 %) and a plain concrete cube (0.37 %) were nearly identical. The volumetric expansion of the biaxially loaded cube (0.31 %) was less, though not necessarily outside the range of measurement variability. Expansions in the loaded directions of each restrained cube were less than those in the unloaded directions. The differences in such expansions were greater for the biaxially loaded cube than the uniaxially loaded cube. Meanwhile, the expansions in the three directions of the unreinforced cube were nearly

identical. These results imply that the applied loads served primarily to redirect expansions to the unloaded directions, with a greater redirection occurring given more loaded directions.

3.2.2 Studies Focusing on Unloaded RC

3.2.2.1 Inoue et al. (1989)

The researchers monitored expansions in a series of 1700 x 200 x 200 mm, singly reinforced beams with stirrups. The beams contained different amounts of longitudinal tension reinforcement with tension steel reinforcement ratios consisting of either 0.77 %, 1.20 %, or 1.74 %. The transverse reinforcement ratio for all beams was 0.30 %. No compression reinforcement was used. The beams were subject to a conditioning environment at 40ºC and 100 % relative humidity. Expansions were measured at the compression face of each beam and by way of reinforcement strain gages.

Based on terminal expansions measured at the end of the conditioning period, results indicated that increasing the tension reinforcement ratio resulted in a clear reduction of both the longitudinal and transverse steel strains. The expansion of the concrete at the compression face was also affected, with both the intermediately and highly reinforced beams expanding less than the lightly reinforced beam. While these trends were not perfectly consistent, or as severe in magnitude at other times during the conditioning period, they suggest that increasing reinforcement ratios may not solely influence expansions in the direction of that reinforcement.

3.2.2.2 Koyanagi et al. (1992)

The researchers monitored expansions in a series of 100 x 100 x 1000 mm prisms that were longitudinally reinforced with a single bar at the center of each specimen. The reinforcement percentages used were 0.07, 0.30, 0.70, 1.3, and 2 %. The prisms were stored at 100 % relative humidity and exposed to temperature cycles between 43ºC and 20ºC. Expansions were measured only in the longitudinal direction using an external concrete strain gage with a gauge length of 250 mm.

An increasing amount of reinforcement resulted in an increasing reduction in expansions in the reinforced direction of a prism. This was found to be true at all times during conditioning. The terminal expansions of the reinforced prisms ranged from 0.23 % to 0.08 % whereas the terminal expansion of a companion unreinforced prism was 0.27 %. As such, the presence of only a slight amount of reinforcement (0.07 %) was enough to restrain expansions. Only this most-lightly reinforced prism reached an expansion capable of causing yielding of the reinforcement. Meanwhile, 2 % reinforcement was not enough to entirely resist expansion. It is also noted that the relative reduction in expansions from one prism to the next was not proportional to the associated change in reinforcement ratio. The greatest reduction in expansions occurred in a prism containing 0.30 % reinforcement, for which the terminal expansion was nearly one-half of the free expansion value. Beyond 0.30 % reinforcement, terminal expansions steadily declined (in absolute units) by 0.02-0.03 % per increasing reinforcement level.

3.2.2.3 Jones and Clark (1996)

The researchers monitored expansions in the three orthogonal directions of a 450 x 300 x 600 mm block containing 0.36, 0.25, and 0.17 % reinforcement in the three directions. The block was conditioned in water at 38ºC and instrumented with Demec studs at a gauge length of 100 mm.

The expansions in the three directions of the block differed due to the differences in reinforcement ratios and the influence of casting direction. The direction containing 0.36 % reinforcement expanded the least. The direction constructed with 0.25 % reinforcement, which was also the casting direction, expanded more than the direction containing 0.17 % reinforcement.

3.2.2.4 Ballivy and Khayat (2000)

The researchers monitored expansions in 350 mm concrete cubes that were either unreinforced or triaxially reinforced with four 15M (nominal bar diameter = 16 mm) bars in each direction. The cubes were subject to a conditioning environment at 38ºC and

100 % relative humidity. Expansions for each cube were measured in two ways: 1) with pairs of vibrating wire gages (one in the vertical casting direction and another in a horizontal direction), and 2) via surface measurements between pairs of Demec studs.

At the conclusion of the study, the researchers identified the following:

- Expansions in the vertical and horizontal directions of reinforced cubes were highly comparable. This was confirmed using both measurement techniques.
- In unreinforced cubes, vertical expansions exceeded horizontal expansions. This was only confirmed with surface measurements. The cause for this behavior was deemed to likely be related to the vertical direction being the casting direction and/or a heightened variability of behavior in near-surface concrete.
- Restrained expansions in the triaxially reinforced cubes were approximately 30-35 % lower than the free expansions in the unreinforced cubes.
- Internal expansion values found with the vibrating wire gages closely matched surface expansion values in reinforced cubes, reflecting the "homogenization" of expansions given well-distributed restraint. Conversely, surface expansion values were greater than internal expansion values in unreinforced cubes.

3.2.2.5 Mohammed et al. (2003)

The researchers monitored the expansions of 250 x 250 x 600 mm prisms to identify interior and exterior expansion behavior in the presence of different forms of passive restraint. These included the use of deformed reinforcing bars, smooth bars, and smooth bars with welded end plates. The majority of specimens were uniaxially reinforced with a single reinforcing bar located in the center of the specimen cross section while a few prisms contained bars near each corner of the specimen. The prisms were conditioned in seawater at 40ºC. Each prism was instrumented with reinforcing bar strain gages and Demec studs to measure surface expansions. Surface expansions were measured on one long face and one short face of each specimen. Only the longitudinal expansions and lateral expansions in one direction were reported.

The relative amount of restraint against ASR provided by the different types of reinforcing schemes was assessed by comparing ratios of lateral to longitudinal surface expansions. Specimens with greater ratios of these expansions were identified to provide more effective restraint under the premise that, regardless of how lateral expansions were affected, increasing restraint would counter longitudinal expansions more and create a greater differential between the longitudinal and lateral expansions. The following significant findings were drawn from this study:

- The different reinforcement schemes, ordered from the least restraint provided to the greatest, were: using smooth bars, using deformed reinforcement, and using smooth bars with end plates. Comparisons of these reinforcement schemes were made from specimens containing a single 13-mm diameter longitudinal bar, giving a reinforcement ratio of 0.20 %. Despite the lack of deformations, smooth bars did provide some restraint against ASR compared to specimens without reinforcement. The use of end plates, covering 4 % of the concrete surface area, was determined to have helped better distribute longitudinal restraint, resulting in reduced longitudinal surface strains compared to using a deformed bar alone.
- The expansion behaviors for prisms with 13-mm and 25-mm diameter, smooth bars with end plates were found to be essentially identical despite the difference in bar size. The researchers stated that these similarities were due to having used the same size end plates. This raises more questions, however, when considering reinforcement percentages and observed steels strains. The prism with a larger bar contained a reinforcement percentage of approximately 0.80 % (i.e., about four times that in the prism with a smaller bar). Meanwhile, the larger bar was strained about half as much as the smaller bar at all times. In combination, these factors would suggest that the amount of prestress induced in the more heavily reinforced prism was twice that induced in the lightly reinforced prism, which seemingly conflicts with the observation of comparable expansion behaviors.
- Surface expansions were found to be much larger than measured strains in the reinforcement. No reinforcing bars in any case were found to have yielded, while

all prisms with a single bar exhibited longitudinal surface expansions well in excess of 0.20 % (an approximated yield strain). The longitudinal surface expansions in prisms containing multiple reinforcing bars, while still high compared to steel strains, plateaued prior to reaching "yield" levels of expansion. At the same time, concrete continued to expand in transverse directions.

3.2.2.6 Smaoui et al. (2007)

The researchers monitored expansions in sets of 230 x 230 x 810 mm prisms made from three different reactive concrete mixtures and reinforced in up to three directions. The prisms were longitudinally reinforced with four bars apiece to produce reinforcement ratios of 0.38, 0.77, or 1.53 %. Some prisms were also reinforced transversely using either smooth or deformed stirrups. The prisms were conditioned at 38ºC and a relative humidity targeting 95 % or greater. Expansions were measured in each prism direction using at least one of four different techniques: 1) surface measurements with target studs attached to concrete, 2) vibrating wire gages, 3) measurements with cover-isolated studs welded to reinforcement, and 4) fiber-optic gages welded to reinforcement. In most specimens, all four methods were used to measure expansions in the longitudinal direction. Only vibrating wire gages and surface measurements were used in the transverse direction parallel to the casting direction. Only surface measurements were used in the transverse direction perpendicular to the casting direction.

Significant findings from reported data on expansions at 228 days after casting included the following:

- In all cases, surface expansions measured in the casting direction of each prism exceeded the surface measurements in all other directions, reflecting the influence of casting direction on expansion behavior.
- No discernable trend could be found when comparing expansion values using different techniques. Measurements were occasionally similar and often dissimilar. This applied when comparing concrete measurements (surface and

vibrating wire gages) to each other, when comparing steel measurements (studs and fiber-optic gages) to each other, or when comparing concrete and steel measurements to each other. Further, surface measurements often did not represent the greatest expansion measurement.

Due to the variability of different measurement techniques and the uncertainties associated with proper selection of data for comparison, no efforts are made here to comprehensively assess the overall expansion behaviors of these specimens and the influences of different reinforcement layouts and concrete mixtures.

3.2.3 Studies Focusing on Loaded RC

3.2.3.1 Jones and Clark (1996)

The researchers monitored the axial expansions of 100 x 200 mm cylinders under various combinations of axial reinforcement and sustained axial compression or tension. Reinforcement ratios of 0.125, 0.25, 0.50, 1, and 2 % were achieved using single threaded rods cast in the centers of specimens. Compressive stresses of 1, 2, 4, or 7 MPa and tensile stresses of 2 or 4 MPa were applied. Specimens under tension were always reinforced to prevent failure under sustained loading. The cylinders were conditioned underwater at 38ºC. Expansions were monitored using Demec studs at a gauge length of 100 mm.

The expansion behavior of cylinders that were either only under compression or only reinforced matched that identified in other research studies. As had been observed by Le Roux et al. (1992), axial expansions reduced with increasing sustained compression, with the greatest reduction amongst any specimens occurring given the application of a low stress (1 MPa) and disproportionate additional reductions at subsequent stress levels. In this case, expansions were nearly, although not entirely, resisted under 7 MPa of compression, more than the limiting 5 MPa previously identified. As had been observed by Koyanagi et al. (1992), axial expansions reduced with an increasing axial reinforcement ratio, but with larger ratios having a lower relative influence on influencing values in comparison to free expansions.

Ultimately, the researchers identified terminal expansions for all restrained specimens, having eliminated any existing pre-expansion, non-ASR strains (namely creep and elastic strains) from overall measurements. In assessing the behavior of cylinders that were both reinforced and loaded, the following results were identified:

- The combination of reinforcement and applied compression provided some additional benefit to restraining expansion over the explicit use of either type of restraint. However, as the amount of sustained compression was increased, the reinforcement percentage influenced expansions less. This was especially noticeable for cylinders subjected to compressive stresses of 2 MPa or greater.
- Given low reinforcement percentages (i.e., 0.25 % or less), the presence of applied tension appeared to have either a neutral or partially negative effect, thus counteracting the restraint to expansion provided by the reinforcement.
- Given high reinforcement percentages (i.e., 1 % or more), the presence of applied tension appeared to have a beneficial effect, resulting in slightly lower expansions than in reinforced specimens alone. This effect was more noticeable at higher levels of tension and with the highest reinforcement percentages. Cylinders under tension with 1 % reinforcement expanded similarly to like-reinforced cylinders under 1 MPa of compression.

3.2.3.2 Multon and Toutlemonde (2006)

The researchers monitored expansions in 130 x 240 mm cylinders that were actively and/or passively restrained in up to three directions. Longitudinal restraint was provided via 10 or 20 MPa of sustained applied compression. Radial, passive restraint in two directions was provided using sets of isolated steel rings, 3 or 5 mm in thickness, enclosing the cylinders. Cylinders were either restrained in either one direction with applied loading only, in two directions with passive restraint only, or in all three directions with applied loading and passive restraint. Longitudinal and radial expansions were measured at various locations with an automated device with displacement transducers to measure changes in specimen dimensions.

For comparative analysis, the imposed expansions in the concrete material alone were determined by removing elastic, creep, and Poisson strains from total measured expansions. Based on the results of imposed expansions in the concrete alone, significant results from this study were identified as follows:

- For cylinders under axial compression only, the presence of load resulted in a reduction in longitudinal expansions compared to free expansions. These expansions were similar under both 10 and 20 MPa of compression, reaching near-zero terminal expansions of 0.02 %. Increasing the applied load from 10 to 20 MPa resulted in an increase in radial expansions; however, these expansions did not exceed free expansion measurements.
- For cylinders with radial passive restraint only, the presence of radial restraint resulted in slightly reduced radial expansions and slightly increased longitudinal expansions. Cylinders with larger steel rings expanded more in both directions than those with the smaller steel rings.
- For cylinders with a given amount of radial passive restraint and some amount of applied compression, increasing the load resulted in an increase in both longitudinal and radial expansions. These expansions, however, were all generally less than free expansions.
- For cylinders with both applied compression and radial passive restraint, expansion behavior was unaffected by the size of the steel rings.
- The imposed volumetric expansions for all cylinders were subjectively stated to be "quite close." At the conclusion of the study, these volumetric expansions ranged between 0.15-0.35 %. The terminal volumetric free expansion of these cylinders was approximately 0.30 %; the terminal volumetric expansions of some restrained cylinders were above this value while others were below. For any amount of radial passive restraint, volumetric expansions were higher given 20 MPa of axial compression compared to 10 MPa. For any amount of nonzero axial compression, volumetric expansions were similar given 3 mm or 5 mm steel rings used as passive restraint.

Ultimately, the results from this study represent much uncertainty, as directional and volumetric expansions did not display any consistent trends.

3.2.3.3 Deschenes et al. (2009)

The researchers monitored expansions in a series of 8435 x 1065 x 535 mm beams as part of an investigation on the shear behavior of ASR-affected members containing transverse reinforcement. Each beam was divided into two regions and detailed with different amounts of transverse reinforcement for the testing of both sectional shear (SS) and deep beam (DB) behavior. The transverse reinforcement ratios were 0.15 % and 0.30 % for the SS and DB regions, respectively. The beams were heavily reinforced in the longitudinal direction, with a tension steel reinforcement ratio of 3.1 % and a compression steel reinforcement ratio of 1.0 %. Expansive strains were measured for both concrete and steel in the longitudinal direction and the transverse direction. Strains were not measured in the out-of-plane (i.e., through-thickness) direction. Further, strains were only measured on the tension face and one side face of each beam. An extensometer was used to measure deformations between studs either embedded in the concrete or welded to reinforcement prior to casting. Blockouts were used to isolate the measurement points from the influence of expanding cover concrete.

The beams were cast at different times, but all were subjected to an external moisture conditioning and loading regime beginning at the same time. The beams were stored outdoors and exposed to seasonal ambient temperatures in Austin, Texas and cyclic wetting and drying. The beams were loaded in a manner to induce constant shear forces of approximately 220 kN and 358 kN in the SS and DB regions, respectively. These corresponded to shear stresses of 0.45 and 0.73 MPa over the effective depth of each beam. Note that, for a 28-day concrete strength of 34.5 MPa specified for these beams, these stresses were well below a value of 0.97 MPa [= $2\sqrt{f_c'}$ (in psi)] estimated to cause shear cracking per the ACI Building Code (2014).

Significant results identified from this study are summarized as follows:

- For all beams, the rate of expansion and amounts of expansion at all times were greater in the lightly reinforced transverse direction than in the heavily reinforced longitudinal direction.
- For most beams, the transverse reinforcement yielded (at a steel strain of approximately 0.20 %) while the longitudinal reinforcement did not yield. After yielding, there was a noticeable and abrupt increase in the rate of transverse expansion. A change in the rate of expansion in the longitudinal direction was not observed.
- In each beam after yielding of the transverse reinforcement, the rate of transverse expansion in the more lightly reinforced SS region was greater than that in the DB region. Prior to yielding, transverse expansion behavior was very similar between the two regions. Longitudinal expansion behavior appeared to be unaffected by differences in transverse expansion behavior.
- Prior to the apparent subsidence of continued overall expansions in many beams, the expansions in the longitudinal direction appeared to have somewhat plateaued while expansions continued to develop in the transverse direction. The longitudinal expansions generally peaked at approximately 0.05-0.10 %.
- Many of the beams began expanding prior to the initiation of the external moisture conditioning and loading regime. As a whole, the increased moisture and application of load did not cause any abrupt changes in expansion behavior.
- In most cases, the expansions of the reinforcement exceeded the expansions found using the studs directly embedded in concrete. The absolute differences between the two, however, were generally not greater than about 0.05 %. Isolation of the studs from cover concrete may have contributed to the agreement amongst the measured expansions.

3.2.3.4 Bracci et al. (2012)

The researchers monitored expansions in 7620 x 1220 x 610 mm longitudinally post-tensioned beams containing reinforcement in all directions as part of a study on the

lap-splice behavior of ASR-affected columns. Expansions were measured in the test region of each beam containing six pairs of spliced longitudinal bars and stirrups. The gross reinforcement ratios in the longitudinal and two transverse directions were 1.6 %, 0.22 %, and 0.11 %, respectively. An axial compressive stress of 3.45 MPa was introduced via post-tensioning of unbonded strands. The beams were stored outdoors, exposed to seasonal temperature variations in Bryan, Texas, and subjected to periodic wetting and drying cycles. Expansions were primarily measured at the surface of specimens in all three directions using embedded Demec studs.

The expansion behavior of each of these beams was consistent with the findings of others. Concrete expanded little in the heavily restrained longitudinal direction, never exceeding an approximated yield expansion of 0.20 %. Concrete expanded in excess of this yield expansion in the transverse directions. The expansions in the more lightly reinforced transverse direction were greater than those in the more heavily reinforced transverse direction. It is also noted that the beams were cast in the direction of the more lightly reinforced transverse direction.

3.2.4 Summary of Findings from Literature Review

Following a review of the different experimental investigations available in the literature and aimed at studying ASR expansion behavior, the following primary conclusions were drawn:

1. Restraint in one element direction appears to influence expansions in all element directions and not only the expansion in the restrained direction. There is likely an interaction between expanding directions which is related to the number of restrained directions, amounts of restraint in each direction, and the distribution of restraint, namely with regard to the type and layout of reinforcement/passive restraint. Consequently, broad conclusions should not be drawn about the relatability of an increasing restraint-decreasing expansion relationship to overall expansion behavior from studies measuring expansions solely in a restrained direction.

2. Volumetric expansion development may be related to the type of restraint provided, the number of restrained directions, and the amounts of restraint in each direction. However, there is conflicting evidence as to what such a volumetric expansion-restraint relationship may be. For example, some results would suggest that increasing restraint (at least as measured by applied compression) would result in a reduction in volumetric expansion development whereas other results would suggest that there would be an increase in volumetric expansion development.
3. In elements containing different amounts of reinforcement in different directions, expansions appear to generally be higher in those directions with less reinforcement.
4. Expansions in directions with applied loads may stop or approach near-zero values under some upper-bound load. While it appears that 10 MPa is a fairly consistent upper-bound stress from many studies, any value ranging from 5 to 20 MPa may be appropriate.
5. The casting direction may play a role in influencing expansion behavior, leading to expansions that may be higher than otherwise expected in that direction.
6. There is much uncertainty when comparing expansions measured using different techniques, specifically when comparing surface and internal expansions for both reinforced and unreinforced concrete elements. Differences, often large, can be observed in surface measurements and internal concrete or steel measurements, possibly as a function of element size, distribution of restraint, or exposure conditions.

3.2.5 Limitations and Difficulties of Existing Experimentation

Despite the significant amount of work that has been done on the topic of ASR expansion behavior, there are notable differences and inconsistencies in past expansion monitoring programs that have limited the practicality and generality of results and hampered progress toward a comprehensive understanding of expansion phenomena.

Differences in specimen size and aspect ratio, boundary conditions, restraint type, loading conditions, reinforcement conditions (e.g., bar size and layout), concrete mixture reactivity, and environmental conditioning can lead to unreliable comparisons amongst much of the currently available data. This is especially true when attempting to compare expansion behavior on the basis of time. The use of different expansion measurement techniques and the uncertain reliability of those techniques – especially surface measurement methods – raise many questions. Further, a frequent lack of expansion measurements reported in three orthogonal directions (typically comprising reinforcement or loading axes) prevents the ability to properly assess any multi-axial interaction amongst expanding directions or to evaluate volumetric expansion trends. Thus, the role of reinforcement and applied load in influencing expansion behavior beyond a single direction is yet to be well-defined.

These are all concerns that must be acknowledged and should be thoughtfully addressed as newer expansion monitoring studies are developed and conducted. The studies described subsequently in Sections 3.3 and 3.4 were carried out with many of these considerations in mind.

3.3 WALD ET AL. (2017A): EXPANSION BEHAVIOR OF A BIAXIALLY REINFORCED CONCRETE MEMBER AFFECTED BY ALKALI-SILICA REACTION

3.3.1 Study Overview

A biaxially reinforced concrete element represents one structural design that is particularly susceptible to ASR. Structural walls, retaining structures, shells, membranes, slabs, footings, beams lacking closed stirrups, and RC silos are all common examples of components that are reinforced in two of the three orthogonal directions. The interaction in expansion behavior between the restrained directions and orthogonal unrestrained direction is of special interest.

The development and multi-axial distribution of mechanical expansions caused by ASR were quantified for a large-scale RC beam containing top and bottom mats of bidirectional reinforcement with no reinforcement through its depth. The effects of

different conditioning environments and the influence of reinforcing bar size and layout on the expansion behavior of the beam were also considered.

3.3.2 Experimental Investigation

3.3.2.1 Specimen Design and Conditioning Regime

Expansions caused by ASR were monitored in a rectangular RC beam serving as a representative field-scale structural component containing reinforcing bars in only two of three orthogonal directions. The beam was 8435 mm long with a 910 x 610 mm cross-section. Reinforcement details are shown in Figure 3-1. All reinforcement was ASTM A615 (2016) Grade 60 with U.S. bar designations. The entire expansion monitoring region (middle 75 % of length) contained two mats of horizontal (x-direction) and vertical (y-direction) reinforcement with no through-thickness (z-direction) reinforcement. Each mat of reinforcement consisted of three No. 11 (36 mm diameter) horizontal bars spaced within 910 mm and No. 9 (29 mm diameter) vertical bars spaced at 305 mm, corresponding to gross reinforcement ratios in x and y of 1.1 % and 0.7 %, respectively. Torqued mechanical heads were secured at the ends of each No. 9 bar to ensure full bar anchorage. The clear cover to each mat of reinforcement was 50 mm on one surface and 75 mm on the opposite surface. No. 5 (16 mm diameter) closed stirrups were provided at both specimen ends for ease of construction.

A highly reactive concrete mixture was selected to rapidly generate ASR expansions. The concrete consisted of a high-alkali Type I/II cement (with alkali content of 1.1 %), a half-and-half blend of low- and highly-reactive, 19 mm crushed coarse aggregates, and highly reactive concrete sand. The highly-reactive coarse aggregate contained quartz and granite, and the fine aggregate contained quartz, chert, and feldspar. A 50 % NaOH reagent was added to the mixing water to boost the equivalent alkali content of the mixture to 1.25 %. A water-to-cement ratio of 0.50 was chosen to obtain a target 28-day cylinder compressive strength of 31.0 MPa. The concrete was used to cast the monitoring specimen along with companion 100 x 200 mm cylinders for strength testing and 75 x 75 x 285 mm prisms to gauge ASR expansion potential in accordance

with ASTM C 1293 (2008). The measured 28-day strength of the concrete was 33.0 MPa. Prism expansions reached 0.61 % after one year.

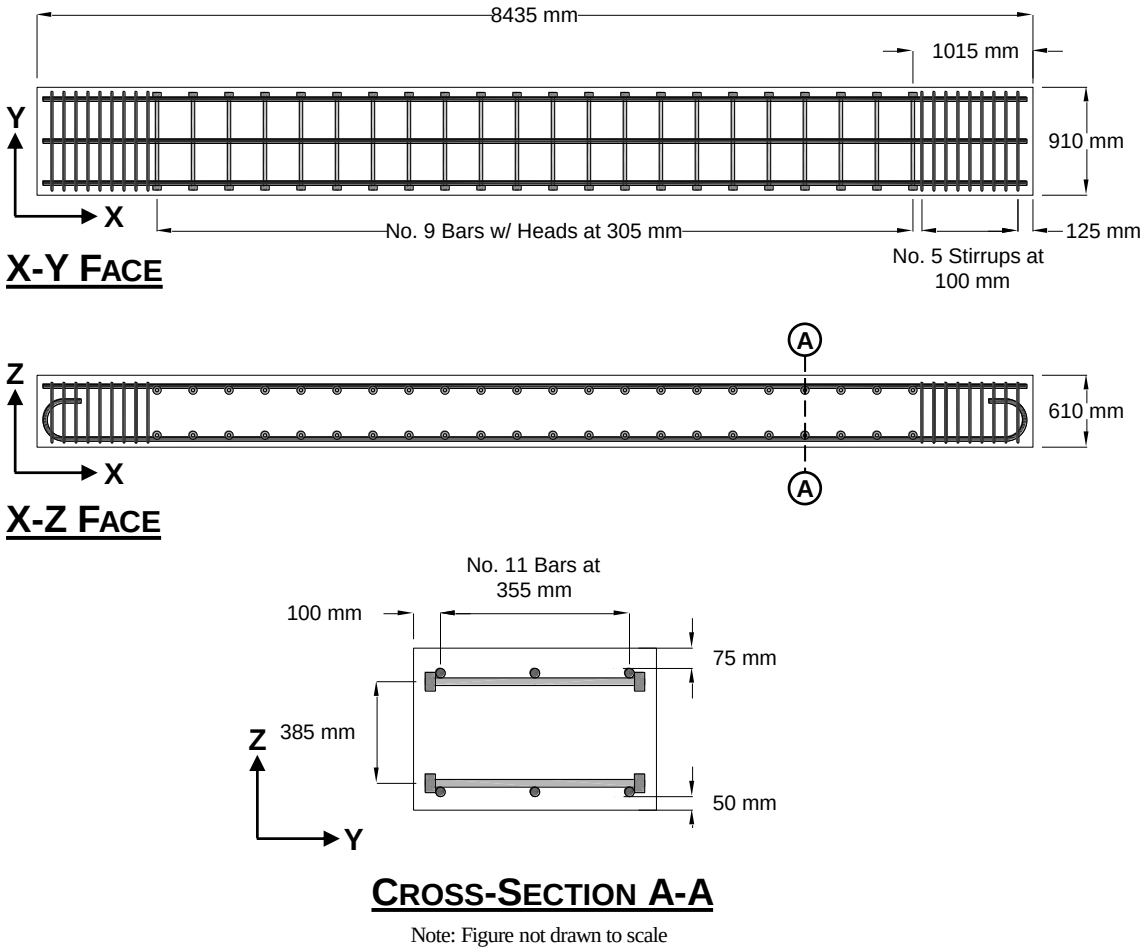

Figure 3-1: Beam specimen reinforcement

In order to expedite expansions, the specimen was subjected to a high temperature and humidity environment approximately two months after fabrication. The specimen was cast in an indoor laboratory space at an ambient temperature of 10.6°C and relative humidity below 80 %. The specimen was subsequently stored in an enclosed, outdoor environmental conditioning facility (Figure 3-2). Within the conditioning space, the specimen was exposed to temperatures on the order of 5-10°C greater than seasonal ambient outdoor temperatures. In central Texas, ambient temperatures typically ranged

between 5°C and 40°C from winter to summer. The entire specimen was subjected to alternating, week-long wet and dry conditioning cycles using mist foggers to produce a periodic state of 90-100 % relative humidity within the storage space.

Figure 3-2: Environmental conditioning facility

3.3.2.2 ASR Expansion Monitoring

Expansions were monitored within three regions (Zones A, B, and C) of the specimen to investigate whether the reinforcing details of one portion of a structure influence expansion behavior in an adjacent portion with different detailing (Figure 3-3). Additionally, the portion of the specimen encompassing Zone C was wrapped in a continuously wetted burlap sheeting (Figure 3-4) to investigate expansion behavior under differential conditioning environments.

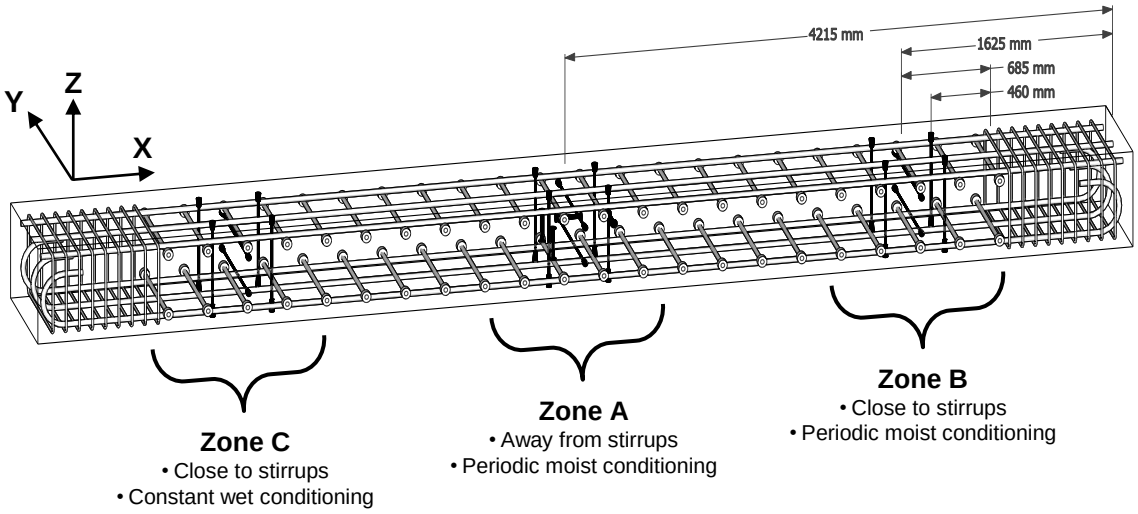

Figure 3-3: Instrumentation layout and monitoring zones

Figure 3-4: Wet conditioning of Zone C

The specimen was instrumented to accommodate two expansion measurement techniques: calipers and vibrating wire gages (VWGs). Expansions were primarily determined using a pair of centerline calipers to measure axial deformations between pairs of cast-in-place targets. These targets consisted of machined thumb screws attached to the drilled and tapped ends of six solid, stainless steel rods arranged and cast within each monitoring zone (Figure 3-5). The rods were undeformed and rust-resistant to minimize the possibility that they would provide additional passive restraint to expansion. Removable nylon blockouts with depths equal to the cover concrete were provided at rod

ends during concrete placement to isolate cover concrete so that recorded expansions would be reflective of behavior at the boundary of the reinforced core (i.e., at a depth equal to the cover). Placement of the rods facilitated ten measurements in each monitoring zone: two x-direction and two y-direction measurements on both 910 mm wide faces of the specimen and one z-direction measurement on each 610 mm wide face. The deformations of the specimen between targets included crack opening displacements. Expansions reported were taken as the measured deformations averaged over the gauge lengths between corresponding measurement points. The nominal initial gauge lengths for measurements were 450 mm in the x- and y-directions and 230 mm in the z-direction. Additional expansion data were collected using a set of four vibrating wire gages embedded within the specimen core near midspan (Figure 3-6). Gages measuring x- and y-direction expansions were placed in the center of the core. Two gages were used to measure z-direction expansions: one at the core center and another near the core boundary approximately 100 mm from the specimen surface.

Both caliper and vibrating wire gage measurements were taken at midspan (Zone A). Caliper measurements were also taken closer to each specimen end (Zones B and C) at locations centered 685 mm away from the nearest No. 5 stirrup (refer to Figure 3-3). Caliper measurements were taken every two weeks over 18 months. Although no additional data were collected, there was no evidence that the concrete had finished expanding at that time. VWG measurements were taken every two weeks during the first three months of expansion and one additional time after six months before the working range of the instruments was exceeded. Measured expansions included strains due to ASR, shrinkage, thermal effects, Poisson effects, and mechanical stresses developed in the specimen following initial measurements. Initial (zero) measurements were taken using calipers and VWGs at fourteen and three days after casting, respectively. Preceding each set of caliper measurements, the device was tared relative to a calibrated invar reference. The precision of the calipers and VWGs were 0.013 mm and 0.1 microstrain, respectively.

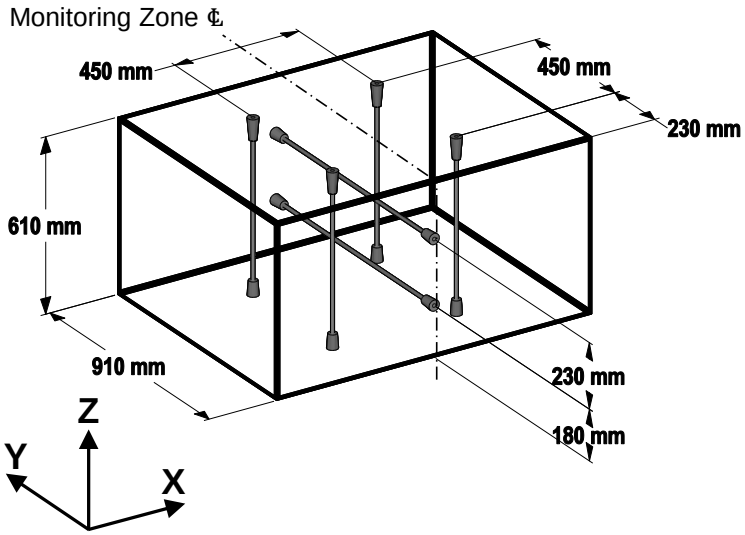

(a) Expansion Rod Layout

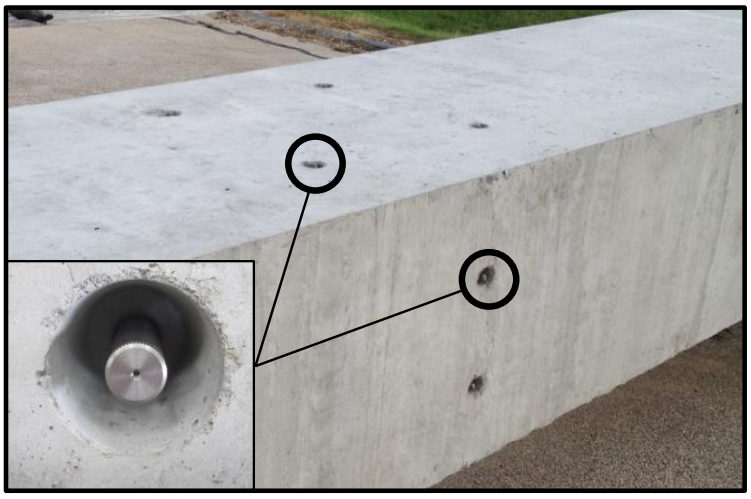

(b) Measurement Targets After Casting

Figure 3-5: Instrumentation for caliper measurements

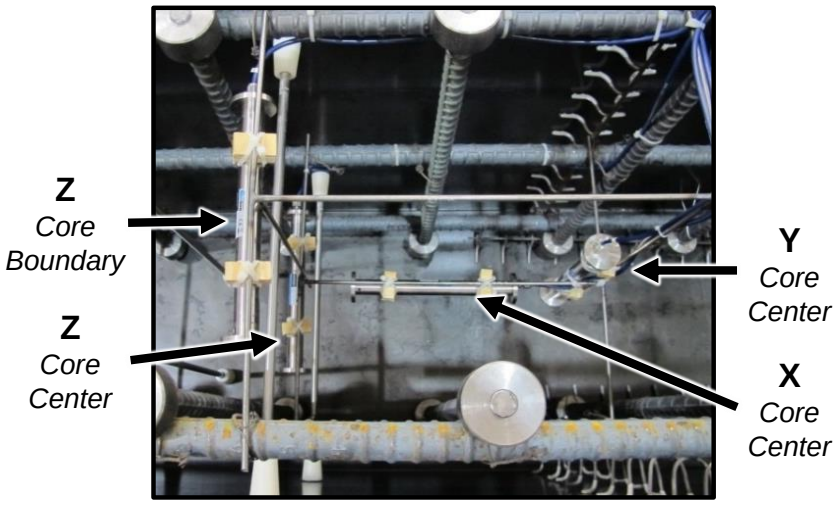

Figure 3-6: Vibrating wire gages

3.3.3 Results and Discussion

The development over time and the geometric distribution of expansions in the biaxially reinforced, ASR-affected beam were carefully tracked. Caliper measurements served as the main source of data collected and analyzed in this study. The expansions in each orthogonal direction were taken as the average of the strains computed for that direction from appropriate caliper readings. VWG measurements served as a secondary source of data for comparison and validation.

It is important to acknowledge that the measured expansions represent strains for the entire RC element and not only those strains chemically imposed in the ASR-affected concrete material. For the purposes of this discussion, ASR expansions in the concrete itself are imposed concrete material strains and may be termed as concrete "prestrains." They are conceptually equivalent to shrinkage strains, only in reverse and with direction dependency. Overall element strains are influenced by the mechanical interaction of expanding concrete with embedded reinforcing bars. Under the assumption of perfect material bond, reinforcement will be tensioned by the expanding concrete which will in turn be compressed to maintain force equilibrium. As with shrinkage, the compatible strain local to and in the direction of the reinforcement will be less than the ASR-induced strain in concrete. The passively induced compression in concrete will generate

transverse strains via the Poisson effect. Further, three-dimensional continuum effects in RC elements may result in significant nonuniform strain distributions. Measured results may be influenced by where and how measurements are taken or averaged in such cases. Thus, users or analysts of the presented or any other ASR data should carefully consider structural mechanics and not automatically assume that measurements satisfactorily reflect concrete material behavior without fail.

3.3.3.1 Expansion Behavior over Time

The directional expansions measured using calipers in each of the three monitoring zones are shown over time in Figure 3-7 along with the average surface temperature of the specimen obtained with an infrared thermometer. Each biaxially restrained portion of the beam exhibited a similar expansion response. At all times, expansions in the unreinforced direction (z) were greater than those in the reinforced directions (x and y). Despite differences in gross reinforcing ratios for the x- and y-directions, the beam expanded nearly identically in the two directions. At approximately 90-100 days after casting, there was a relatively abrupt shift in expansion behavior. The data indicate that the expansions in the reinforced directions effectively stopped while the beam continued to expand in the unreinforced direction. The expansions in x and y reached maxima of approximately 0.1-0.15 %. These expansions were less than an approximate yielding strain of 0.2 % for the reinforcement. Continued expansion of the beam in z was sensitive to thermal fluctuations with less additional expansion occurring during colder months. The rate of this expansion in z was increased in Zone C, which was under constant wet conditioning.

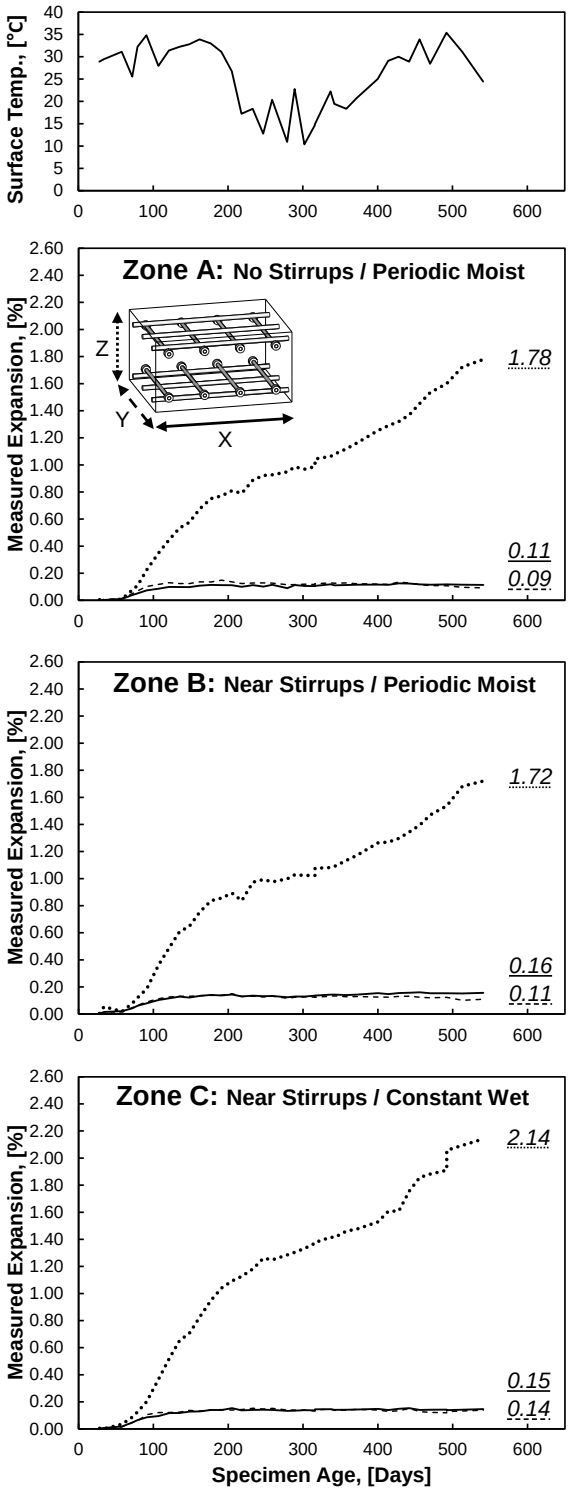

Figure 3-7: Measured directional expansions (calipers) vs. specimen age

The aforementioned expansion behavior transition period was also marked by the formation and subsequent growth of large cracks on the side (x-z) surfaces of the specimen perpendicular to the mats of reinforcement (Figure 3-8). The cracks were located midway between the mats of reinforcement and oriented parallel to the x-direction reinforcement. The cracks were only located in the biaxially reinforced part of the beam; they did not extend into the beam ends where stirrups were present.

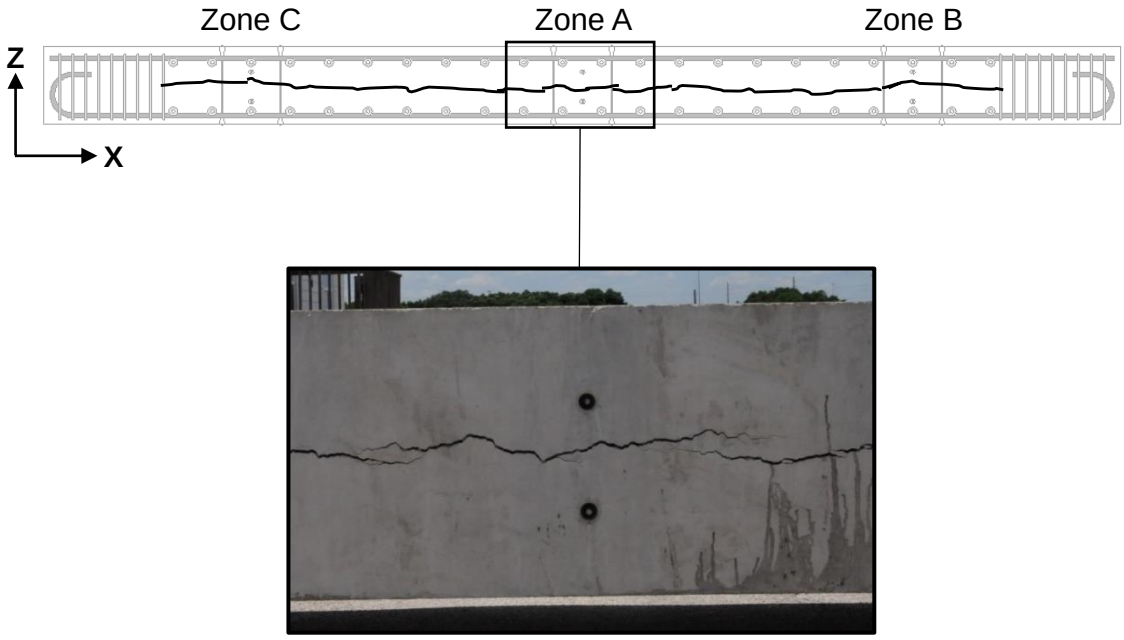

Figure 3-8: Mid-depth surface crack on X-Z specimen face

The cracks on the x-z faces of the specimen were identified to be caused largely by a mechanical boundary effect rather than purely due to ASR expansion perpendicular to the cracks (i.e., in the z-direction). It is suggested that the cracks formed due to tension induced in the outer fibers of the specimen from non-uniform restraint to expansion provided locally by the two discretely placed mats of reinforcement. The concrete between these reinforcing layers, separated by more than 350 mm, was freer to expand. The net effect was a concentrated deformation of concrete near the reinforced surfaces

with the interior concrete outwardly “bending” between reinforcement locations which acted as supports.

This behavior was verified using a finite element analysis in VecTor2, a program capable of analyzing RC structures in two dimensions with applied direction-dependent concrete prestrains (Wong et al. 2013) (Figure 3-9). A transverse cross-section of the beam (in the y-z plane) was modeled using a mesh of quadrilateral elements for concrete and discrete truss bar elements for reinforcement. Only the in-plane (y-direction) reinforcement was necessary for this model. The measured concrete compressive strength (33.0 MPa), nominal steel yield strength (414 MPa), and assumed modulus of elasticity for steel (200,000 MPa) were input. The initial tangent modulus of elasticity and tensile strength for concrete were evaluated as 25,970 MPa and 1.9 MPa, respectively, using default VecTor2 material models. To show that ASR did not solely contribute to mid-depth crack formation, a uniform expansive concrete prestrain was incrementally applied only in the y-direction. At a prestrain of 0.14 %, representative of experimental observations, elements located at the edge and near mid-depth of the cross-section cracked, with the cross-section slightly bulging outward between the layers of reinforcement.

The analysis shows that applying a uniform concrete material prestrain in the y-direction results in an element-level strain differential and the generation of a non-uniform compressive stress field in concrete through the cross-section in y. Strains in elements at the edge and mid-depth of the cross section were equal to the prestrain and thus unaffected by restraint provided by the reinforcement. Strains in elements local to reinforcement were less than the prestrain. The maximum strain differential between elements was approximately 0.1-0.2 millistrain (0.01-0.02 %). Although this differential was relatively small in the context of ASR expansions, it was significant enough to prompt the generation of tensile strains and stresses in edge elements in the z-direction and thus promote mechanical cracking.

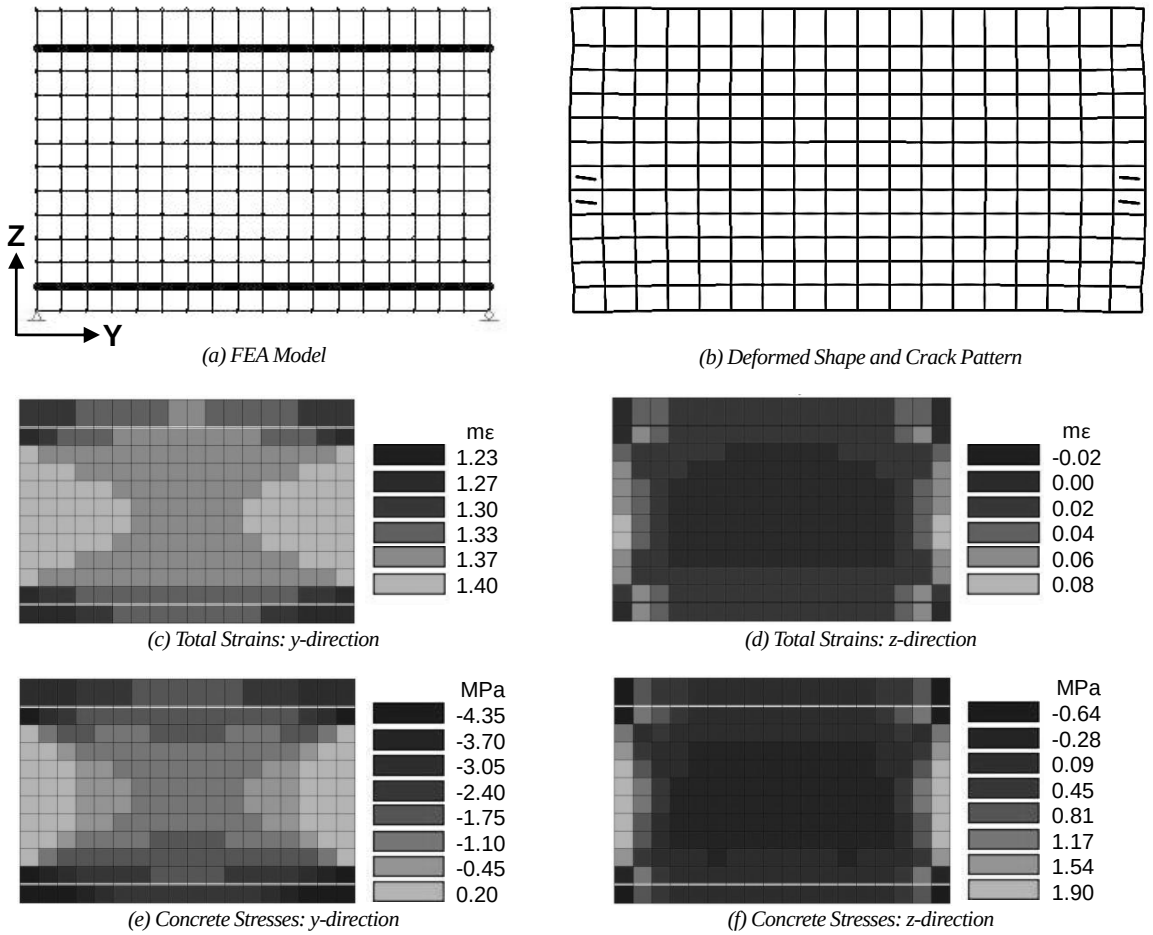

(a) FEA Model

(b) Deformed Shape and Crack Pattern

(c) Total Strains: y-direction

(d) Total Strains: z-direction

(e) Concrete Stresses: y-direction

(f) Concrete Stresses: z-direction

Figure 3-9: VecTor2 finite element analysis of mid-depth surface crack (0.14 % concrete prestrain applied in y)

Expansions in the unreinforced direction of the specimen nearer the surface were concentrated at mid-depth close to the macrocracks that developed at that location on the x-z faces of the specimen. This was evidenced by the continual widening of these cracks without significant formation or growth of other macrocracks on the x-z surfaces. It is believed that the mid-depth cracks served as weak points in the concrete with substantially reduced resistance to expansion compared to other locations. In particular, these cracks likely permitted increased local moisture ingress and accelerated swelling of ASR reaction product. It is highly likely that z-direction expansions were more uniformly distributed through the depth within the core of the specimen. Although the distribution of z-direction expansions was not uniform through the depth near the surface, it is also

believed that the full-depth average expansion at the surface was similar to the average expansion within the core. While this may be true, the measured z-direction expansions were only averaged over a 230 mm gauge length which crossed the mid-depth cracks. Consequently, the reported z-direction expansions from after the formation of the mid-depth cracks are undoubtedly greater than would have been measured over a full-depth gauge length of 610 mm. On a similar note, expansions would have been severely underestimated if the discrete cracks had formed just outside the original gauge length. This highlights the precautions that must be taken when interpreting data from ASR-affected elements. In particular, an average expansion should never be automatically assumed to be a uniform expansion.

The cessation of expansions in the reinforced directions was not caused by the exhaustion of all ASR reactants in the specimen. Neither the number of reinforced directions, in this case two, nor the development of the mid-depth cracks are believed to be causation for this behavior. Existing expansion data collected on beams with triaxial restraint (longitudinal bars and closed stirrups) and no significant isolated cracks have evidenced that expansions can stop in one direction and continue in others (Deschenes et al. 2009, Bracci et al. 2012). In those cases, the heavily reinforced longitudinal direction stopped expanding.

Reinforcement layout, bar size, and reinforcing percentage may have all contributed to the observed expansion behavior. These factors will influence the magnitude and distribution of induced compressive stresses in concrete when passively restrained against ASR. According to many experimental and analytical sources, there exists a maximum compressive stress in concrete at which expansions in a direction will stop (Le Roux et al. 1992, Larive 1997, Saouma and Perotti 2006, Charlwood et al. 1992, Cope et al. 1994). Although there is much discrepancy concerning what this value may be and whether it applies equally to applied and passively induced stresses, such a limit may have been at work in this study.

Despite different specimen sizes, materials, and loading conditions during ASR generation, the biaxially restrained specimen discussed here and the aforementioned

triaxially restrained beams (Deschenes et al. 2009, Bracci et al. 2012) were similarly reinforced in one direction with No. 11 bars lumped in top and bottom layers. With larger diameter bars placed at discrete locations, compared to smaller diameter bars spaced uniformly, induced compressive stresses in concrete local to the reinforcement are likely to be greater. With greater stresses, it becomes more likely that a limit would be reached and expansions would stop prior to the reinforcement yielding and concrete stresses stabilizing. On the other hand, stresses between bars would be lower, thus implying that concrete should continue to expand at these locations. As discussed later, the data in this study more strongly support the likelihood of a uniform ASR expansion in concrete for the specimen monitored. As such, it may be more suitable to compare an average compressive stress in concrete to a limit than to perform such a comparison using local concrete stresses.

Assuming perfect bond between concrete and steel, the average steel stress in an element with smeared reinforcement (with a modulus of elasticity of 200,000 MPa) at a representative total strain of 0.14 % would be 280.0 MPa. With reinforcement ratios of 1.1 % and 0.7% respectively, the passively induced compressive stress in concrete determined by axial equilibrium in the x- and y-directions would be 3.1 MPa and 2.0 MPa, respectively. These values fall below an upper-bound limiting concrete stress suggested by some researchers (Le Roux et al. 1992, Larive 1997, Saouma and Perotti 2006, Charlwood et al. 1992) above which ASR expansion does not occur: between 5.0 MPa and 10.0 MPa. It should be noted that suggested compressive stress limits were typically derived from experiments on unreinforced concrete under sustained loads. These lower values suggest that applied and passively induced compressive stresses in concrete may not be one and the same in the context of restraint against ASR.

3.3.3.2 Volumetric Expansions

Figure 3-10 shows the development of volumetric expansions in the beam with time for each monitoring zone. The volumetric expansion is the summation of the three caliper-based expansions in the x-, y-, and z-directions at each point in time. The

development of volumetric expansion in Zones A and B was nearly identical. Zone C expanded more volumetrically than the other zones; however, trends in behavior were similar amongst each zone. Zone C began to expand more than the other zones after the formation of the mid-depth cracks on the x-z faces of the specimen.

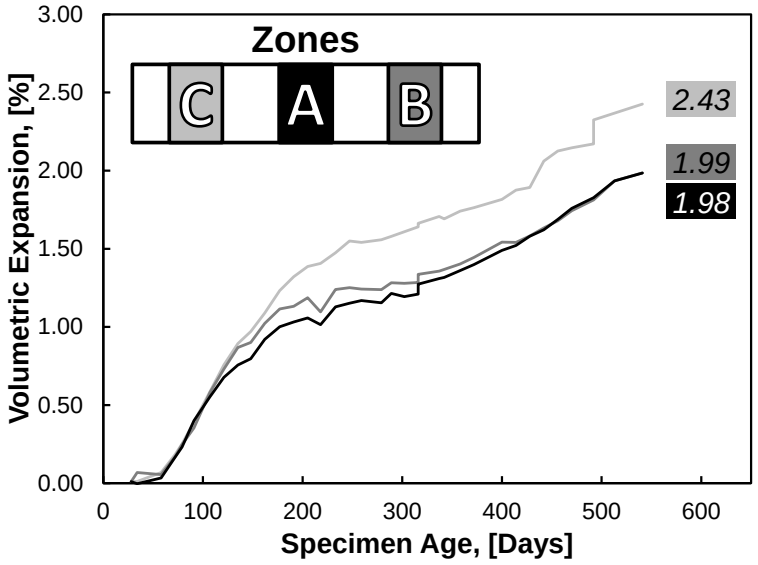

Figure 3-10: Volumetric expansion (calipers) vs. specimen age

3.3.3.3 Distribution of Volumetric Expansions

At each point in time, measured directional expansions algebraically contribute to computed volumetric expansions. Figure 3-11 presents the measured caliper expansions in the x-, y-, and z-directions that simultaneously comprised the developing volumetric expansion in each monitoring zone. The presentation of the data in this form is extremely valuable for analysis and assessment of ASR expansion behavior in multiple or interacting directions. The plots essentially filter out temporal variations in expansion behavior, such as those caused by changes or differences in environmental exposure conditions. The underlying assumption in doing so is that the distribution of volumetric expansions amongst different directions is independent of factors such as temperature, humidity, and chemical reactivity. Consequently, ASR-affected elements that are geometrically identical but that are constructed with different concretes, cast at separate

times, and/or conditioned differently can be compared more appropriately. The plots of data from this study suggest an additional advantage for interpretation and ASR model development: nonlinear trends for directional expansions with time can potentially be re-evaluated as a series of linear trends with changing volumetric expansion.

The volumetric expansion distribution behavior was essentially identical in all zones. Up until approximately 0.50 % volumetric expansion, each direction contributed to changes in volumetric expansion. Each zone reached 0.50 % volumetric expansion at approximately 100 days. The plots clearly show that, beyond 0.50 % volumetric expansion, not only did expansions in the x- and y-directions stop, but the change in volumetric expansion was solely attributed to additional expansion in the z-direction. It should be highlighted that these trends in distribution behavior continued to apply in Zone C where the volumetric expansion exceeded the maxima in Zones A and B.

The approximate linearity of each plotline in Figure 3-11 prior to the cessation of expansions in x and y implies that the directional expansions were in constant proportion to one another during this time. As such, each direction contributed some more-or-less fixed fraction of volumetric expansion. The unreinforced direction is of particular interest. Table 3-1 gives the contribution of the z-direction expansions, ε_z, to volumetric expansions, ε_{vol}, in each zone prior to expansions stopping in other directions. The data suggest that, on average, the unreinforced direction accounted for approximately half of the total volumetric expansion at any point in time prior to expansions stopping in the other directions. Afterward, the contribution of the z-direction expansions increased with increasing volumetric expansion. On a related note, the incremental contribution of z-direction expansions to incremental additions in volumetric expansion was essentially 100 % after the x- and y-directions stopped expanding.

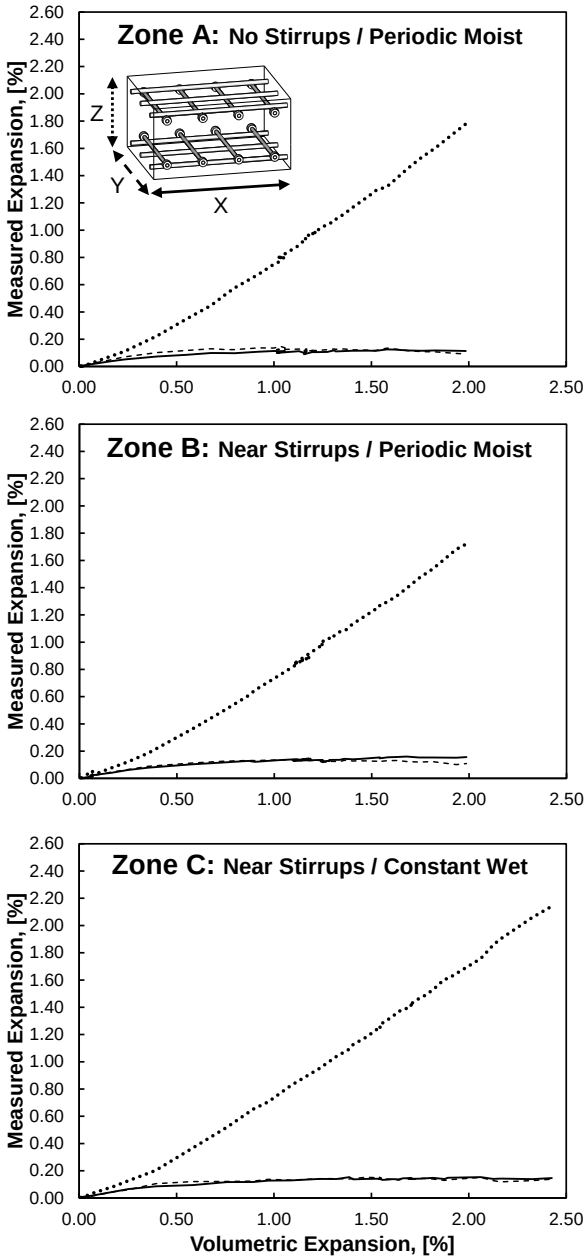

Note: Volumetric Expansion = X + Y + Z

Figure 3-11: Measured directional expansions (calipers) vs. volumetric expansions

Table 3-1: Contribution of z-direction (caliper) expansions to volumetric expansions

	Zone A			Zone B			Zone C		
Age (Days)	ε_{vol} (%)	ε_z (%)	$\varepsilon_z/\varepsilon_{vol}$	ε_{vol} (%)	ε_z (%)	$\varepsilon_z/\varepsilon_{vol}$	ε_{vol} (%)	ε_z (%)	$\varepsilon_z/\varepsilon_{vol}$
28	0.0102	0.0045	0.44	0.0102	0.0045	0.44	0.0102	0.0045	0.44
34	-0.0030	-0.0123	---*	0.0687	0.0546	0.79	0.0109	0.0017	0.16
58	0.0339	0.0100	0.29	0.0554	0.0183	0.33	0.0687	0.0351	0.51
72	0.1660	0.0769	0.46	0.1695	0.0796	0.47	0.1833	0.0879	0.48
79	0.2320	0.1103	0.48	0.2482	0.1214	0.49	0.2520	0.1267	0.50
91	0.4000	0.2247	0.56	0.3532	0.1854	0.52	0.3922	0.2016	0.51
107	0.5530	0.3500	0.63	0.5801	0.3636	0.63	0.5850	0.3687	0.63
		AVG:	0.48		AVG:	0.52		AVG:	0.46
		STD:	0.116		STD:	0.148		STD:	0.145
		COV:	0.243		COV:	0.282		COV:	0.314

*Ratio of z-direction expansion to volumetric expansion not evaluated for negative expansions

3.3.3.4 Zone of Influence of Reinforcement Details on Expansion Behavior

Zone B was monitored to assess whether the expansion behavior of a biaxially reinforced portion of a structure is influenced by an adjacent triaxially reinforced region. As previously indicated, the expansion behavior of Zone B, located near a specimen end with stirrups, very closely matched behavior in Zone A, located at midspan far from the specimen ends. Behavior was comparable when analyzing data in the context of either time or volumetric expansions.

The results suggest that differently reinforced regions of a structure may respond to the effects of ASR independently. Consequently, an ASR-affected structure could be subdivided into discrete portions which could then be individually analyzed or computationally modeled without having to consider interaction effects. Being able to reliably model a structural component without having to model the entire structure would offer significant computational savings.

It is plausible that, much like with tension stiffening or crack spacing effects in RC, there is a distance-related zone of influence of a reinforcing bar on ASR expansion behavior. The distance between the closest measurement point in Zone B to a stirrup was 460 mm. This equates to 29 stirrup bar diameters. The similarity of results for Zones A

and B suggest that this distance was great enough to preclude any interaction between the triaxially and biaxially reinforced portions of the beam.

3.3.3.5 Role of Conditioning on Expansion Behavior

As illustrated by the results for Zone C, constant wet conditioning increased the speed of expansion development but not the directional distribution of volumetric expansions. The increase in expansion rate was only evidenced in the unreinforced direction after the formation of the mid-depth cracks. The heightened moisture seemingly promoted increased expansion at the surface which, as described earlier, was concentrated at the crack locations and captured by the measurements taken across the cracks. Because expansions had stopped in the reinforced directions during this time, additional volumetric expansion was attributed to additional expansion in the z-direction. The net result was that the rate of volumetric expansion with time was greater in Zone C, under constant wet conditioning, than in Zone B, under periodic moist conditioning, but trends in the distribution of volumetric expansion were identical.

3.3.3.6 Comparison of Caliper and Vibrating Wire Gage Measurements

Figure 3-12 compares caliper and VWG measurements taken for each direction in Zone A. Prior to the formation of the mid-depth cracks at approximately 100 days, the data from the two monitoring techniques were in excellent agreement. The final VWG measurements differed from caliper measurements more substantially, notably in the y- and z-directions. Despite the single variable result in y (a difference in caliper and VWG values of 0.06 %), the data as a whole for the x- and y-directions indicate that the concrete expanded relatively uniformly across the entire core in each reinforced direction. With the exception of final z-direction VWG measurements, the overall VWG data suggest that expansions in the unreinforced direction were also relatively uniform through the core. The last VWG measurement at the core boundary was 0.11 % greater than that at the core center. However, the final caliper measurement was much greater (0.39 %) than the VWG measurement at the core boundary. This again highlights how

measurement averaging (as was done with calipers in a short gauge length across cracks) can influence data interpretation. Regardless of which set of z-direction measurements better reflects late-age expansion behavior, it is important to note that substitution of one value for another would not alter trends in the directional distribution of volumetric expansions. Such a change would be no different numerically than considering different z-direction values due to the type of conditioning employed.

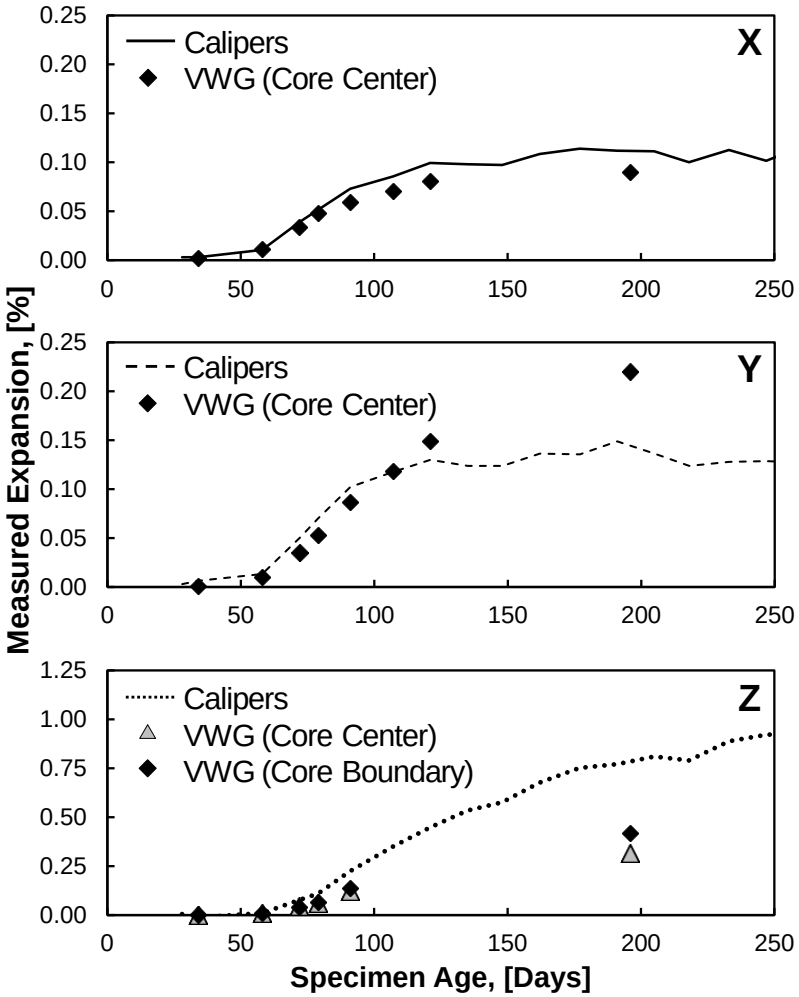

Figure 3-12: Comparison of VWG and caliper measurements in Zone A

The uniformity of expansions in reinforced directions through the cross-section again raises consideration of a zone of influence for a reinforcing bar in influencing

expansion behavior. The layers of No. 11 bars in the x-direction were spaced 450 mm apart. The layers of No. 9 bars in the y-direction were spaced 385 mm apart. These values equate to spacings of 12.6 and 13.4 bar diameters, respectively. The corresponding distances between each bar and the center of the core were one-half of these values: 6.3 and 6.7 bar diameters, respectively. At these distances, the interior of the core was effectively reinforced and thus restrained against ASR expansion.

3.3.4 Conclusions

The expansion behavior of a biaxially reinforced, ASR-affected concrete beam was investigated. The time development of expansions, interaction of simultaneously expanding directions, and the distribution of volumetric expansions were explored. The effects of different conditioning environments and the likely influences of reinforcing bar size and layout on behavior were also considered. The principal findings from this study were as follows:

1. The expansions in the reinforced directions were less than those in the unreinforced direction at all times. The directional distribution of volumetric expansions showed that expansion in the unreinforced direction accounted for more than one-third of any given volumetric expansion. While all three primary orthogonal directions continued to expand, the unreinforced direction contributed an average of approximately 50 % of the volumetric expansion.
2. Different types of environmental exposure conditions promoting ASR expansion affected only the rates of expansion but not the distribution of volumetric expansions amongst primary orthogonal directions.
3. According to caliper measurements, the reinforced directions stopped expanding between 0.1 % and 0.15 %, prior to steel yielding and before the unreinforced direction stopped expanding. At an expansion of 0.14 %, the induced compressive stresses in concrete in these directions were computed to be 2.0 MPa and 3.1 MPa. These values are lower than a limit between 5.0 MPa and 10.0 MPa above which ASR expansion does not occur. These limits are commonly identified from

studies of applied compression but accepted for use with any stress, regardless of its source.

4. Expansion behavior within the biaxially reinforced portion of the specimen was not influenced by triaxial restraint conditions at nearby specimen ends. The closest expansion measurement zone to the end region of the specimen was sufficiently separated (by nearly 30 bar diameters) from the nearest stirrup.
5. Expansion behavior in reinforced directions was relatively uniform through the specimen depth. The top and bottom layers of reinforcement were spaced close enough (less than 15 bar diameters) such that the effective restraint against expansion was uniform in each direction.
6. Large, mid-depth cracks formed on specimen side surfaces due to strains in the unreinforced direction. Nonuniform restraint against expanding concrete in the transverse direction generated by lumped reinforcement layers resulted in tensile stresses developing in the unreinforced direction at the edges of the cross-section. ASR expansions near the surface were concentrated at these crack locations rather than well-distributed across the depth.

3.4 WALD ET AL. (2017B): DEVELOPMENT AND MULTI-AXIAL DISTRIBUTION OF EXPANSIONS IN REINFORCED CONCRETE ELEMENTS AFFECTED BY ALKALI-SILICA REACTION

3.4.1 Study Overview

Understanding the development and multi-axial distribution of expansions is of critical importance in the appraisal of structures affected by alkali-silica reaction. Such expansions were monitored for thirty-three 480 mm reinforced concrete cubes in an effort to develop an improved understanding of the expansion mechanisms in reinforced concrete and broaden the database of experimental results available from which to build tools to aid in the performance assessment of affected structures. The cubes were fabricated using three different concrete mixtures of varying reactivity and contained

uniaxial, biaxial, and triaxial reinforcement layouts with different reinforcement ratio combinations.

3.4.2 Experimental Investigation

3.4.2.1 Specimen Design and Conditioning Regime

A total of 33 ASR-affected, 480 mm RC cubes were fabricated for this study. Four specimens were unreinforced to examine free expansion behavior. The remaining specimens were reinforced in either one, two, or three orthogonal directions (x, y, and z) to examine expansion behavior under uniaxial, biaxial, and triaxial restraint conditions. Different combinations of gross reinforcing ratios (ρ_x, ρ_y, and ρ_z) were incorporated using ASTM A615 (2016) Grade 60 deformed steel reinforcing bars with U.S. designations. Reinforcement ratios of 0.5, 1.1, and 1.5 % were achieved using varying amounts of No. 4, 5, 6, and 7 reinforcing bars with nominal diameters of 13, 16, 19, and 22 mm, respectively. The reinforcing bars were placed in either three distributed layers spaced at 150-200 mm, or in two layers at the top and bottom spaced at 360-410 mm. The different reinforcing schemes employed are depicted in Figure 3-13. The majority of specimens were reinforced in one, two, or three directions with three layers of reinforcing bars in each of those directions. However, a few of the cube specimens were biaxially reinforced using either a two-layer (L1, L2) or two- and three-layer combination (L3) reinforcing bar layout (refer to Figure 3-13d, e, and f). All reinforcing bars were end-threaded, and small washer plates and nuts were used to ensure that each bar would provide effective restraint against expansion along its full length.

a) 3-Layer Uniaxial Reinforcement

b) 3-Layer Biaxial Reinforcement

c) 3-Layer Triaxial Reinforcement

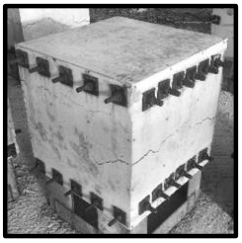

d) 2-Layer Biaxial Reinforcement (L1)

e) 2-Layer Biaxial Reinforcement (L2)

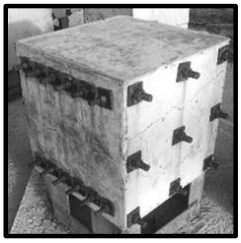

f) Combined 2-Layer / 3-Layer Biaxial Reinforcement (L3)

Figure 3-13: Cube specimen reinforcement layouts

Each cube specimen was fabricated from one of three concrete mixtures which were selected to examine the influence of using reactive fine aggregates with low-reactivity coarse aggregates (Mixture C), nonreactive fines with highly reactive coarse aggregates (Mixture B), or both reactive fines and reactive coarse aggregates (Mixture A). The fine aggregate used for Mixtures A and C was a highly reactive concrete sand containing quartz, chert, and feldspar. An even blend of low- and high-reactivity, 19 mm crushed stone was used as the coarse aggregate for Mixtures A and B. The highly reactive coarse aggregate contained quartz and granite and was approximately 2.5 times as reactive as the low-reactive coarse aggregate which contained granite. The reactive fine aggregate used was at least 3-3.5 times as reactive as the highly reactive coarse aggregate. A high-alkali Type I/II cement, with an alkali content of 1.1 %, was used for all three mixtures. Each mix nominally consisted of 220, 820, and 860 kg/m^3 of cement, fine aggregate, and coarse aggregate, respectively. A 50 % NaOH reagent was added with the water to increase the equivalent alkali content of each mixture to 1.25 %. A water-to-

cement ratio of 0.50 was selected to achieve a target 28-day cylindrical compressive strength of 31 MPa.

A total of 25 cube specimens were cast using Mixture A, while four specimens were cast from both Mixtures B and C. Specimens from each mixture were cast at different times. Further, the Mixture A cubes were cast in three separate sets (Set 1, 2, and 3), also at different times. The Set 3 specimens were used to investigate the influence of reinforcing layout on expansion behavior. All but the Set 3 specimens were cast in the y-direction. Companion 100 x 200 mm cylinders were cast with each mixture for material property testing, the results of which are provided in Allford (2016). Additionally, 75 x 75 x 285 mm prisms were cast with each mixture to monitor ASR expansion potential in accordance with ASTM C 1293 (2008). At the conclusion of this study (approximately 15 months), the Mixture A, B, and C prisms expanded 0.65 %, 0.10 %, and 0.68 %, respectively.

Each specimen is designated using either a two- or three-part identifier such as B-101 or A3-102-L1. The first part of the identifier gives the mixture designation and the set number for the case of Mixture A specimens. The second part is a three-digit code indicating the reinforcing percentages used in the x-, y-, and z-directions, respectively. The digits 0, 1, 2, and 3 represent reinforcement ratios of 0, 0.5, 1.1, and 1.5 %, respectively. As an example, the code "102" indicates that a specimen was unreinforced in the y-direction and contained 0.5 % and 1.1 % reinforcement in the x- and z-directions, respectively. Multiple cube specimens with common details are denoted with "a", "b", etc. The third part of the identifier is reserved for the Mixture A specimens from Set 3 which used one of the two-layer reinforcing layouts (i.e., L1, L2, or L3). Specimens with a two-part identification contained bars in three layers in each reinforced direction. Additional details of the RC cube specimens comprising the monitoring program are available in Allford (2016).

To promote expedited ASR-induced cracking and expansion under elevated temperature and humidity conditions, the cube specimens were moved into the aforementioned enclosed, outdoor environmental conditioning facility (ECF)

approximately two weeks after casting. As previously described, the temperature within the ECF was typically 5-10°C higher than the ambient outdoor temperature in Austin, Texas which ranged between 5°C and 40°C over the course of the year. Specimens were subjected to alternating, week-long wet and dry cycles, with wet cycles consisting of periods of 80-100 % external relative humidity that was maintained using mist foggers within the ECF. The relative humidity within the ECF during dry cycles was 20-60 %.

3.4.2.2 ASR Expansion Monitoring

The axial expansions of the cubes were monitored by taking measurements of the deformations between opposite specimen faces. Sets of 6.4 mm-diameter stainless steel target points were adhered to each specimen face to establish the measurement locations. Modified long-jaw calipers with a precision of 0.0127 mm were used to periodically measure the distance between pairs of opposite target points, as shown in Figure 3-14a. Prior to taking measurements, the device was tared using a steel reference bar. During data collection, two or three measurements were taken at each measurement location to ensure repeatability of results. The average change in specimen dimension at each measurement location was documented every two weeks over a period of 15 months. All specimens, with the exception of the five A3 specimens, were outfitted with six target points on each face (Figure 3-14b). The A3 specimens were outfitted with sixteen target points on the side faces (x- and z-directions) and eight points on the top and bottom faces (y-direction), six of which were placed at the same locations as those placed on all other specimens (Figures 3-14c and 3-14d). More target points were used for the A3 specimens to better examine differences in expansion behavior given different specimen reinforcing bar layouts.

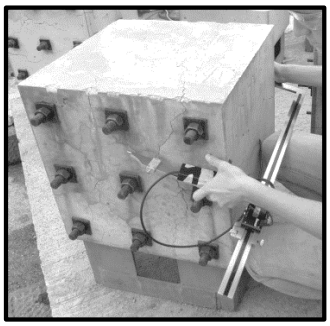

a) Caliper Measurements

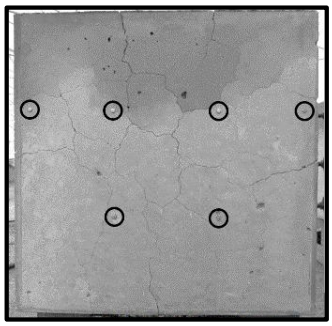

b) Six Target Points in x, y, and z (Mixture A1, A2, B, and C)

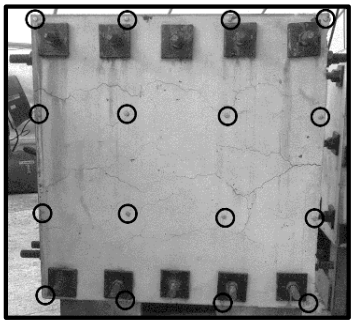

c) Sixteen Target Points in x and z (Mixture A3)

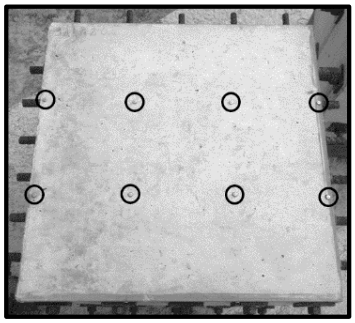

d) Eight Target Points in y (Mixture A3)

Figure 3-14: Expansion measurement device and measurement locations

Note that the reported axial expansions of the cubes were computed by averaging several expansion measurements taken for a given direction (i.e., in the x-, y-, or z-directions). Except where explicitly noted, the reported axial expansions are the average of expansions at all six, eight, or sixteen locations described above.

3.4.3 Results and Discussion

The following sections outline the development and multi-axial distribution of the average expansions of the cube specimens monitored in this study. Note that in the case of the RC cube specimens, the reported expansions are measured element expansions and, as such, do not represent ASR-induced concrete material expansions. The reported element expansions may actually be comprised of ASR-induced expansions in the concrete, shrinkage and thermal strains, Poisson effects, creep, and mechanical strains developed due to the compatibility between concrete and steel.

3.4.3.1 Expansion Behavior with Time

The development of axial (i.e., x-, y-, and z-direction) expansions of the cubes over time is described in this section. Although the discussions provided largely reference Mixture A specimens, many trends in expansion behavior described also apply to Mixture B and C specimens. Data for all specimens from this study may be found in Allford (2016).

3.4.3.1.1 Influence of Reinforcement Direction and Ratio

Figure 3-15 shows the measured expansion behavior for two unreinforced, plain concrete Mixture A specimens (A1-000a and A1-000b). These specimens served as element free expansion specimens. The two plain concrete cubes did not exhibit identical behavior; the three axial expansions for A1-000b matched very closely at all times while the y-direction expansions for A1-000a were greater than the x- and z-direction expansions. It is believed that the unequal axial expansions for A1-000a were a consequence of the typical high variability of expansions of plain concrete specimens that has been identified by others in the past (Larive 1997). Although the y-direction was the casting direction of the cubes, it is not believed that casting direction played any major role in the measured differences. There was generally no tendency for other specimens to expand more in the casting direction than in any other direction containing the same reinforcement ratio. Despite any individual differences amongst the three directions, the average axial expansions for A1-000a and A1-000b at an age of 450 days were found to be 0.61 % and 0.64 %, respectively. These values correlate closely with the terminal ASTM C 1293 (2008) prism expansion of 0.65 %.

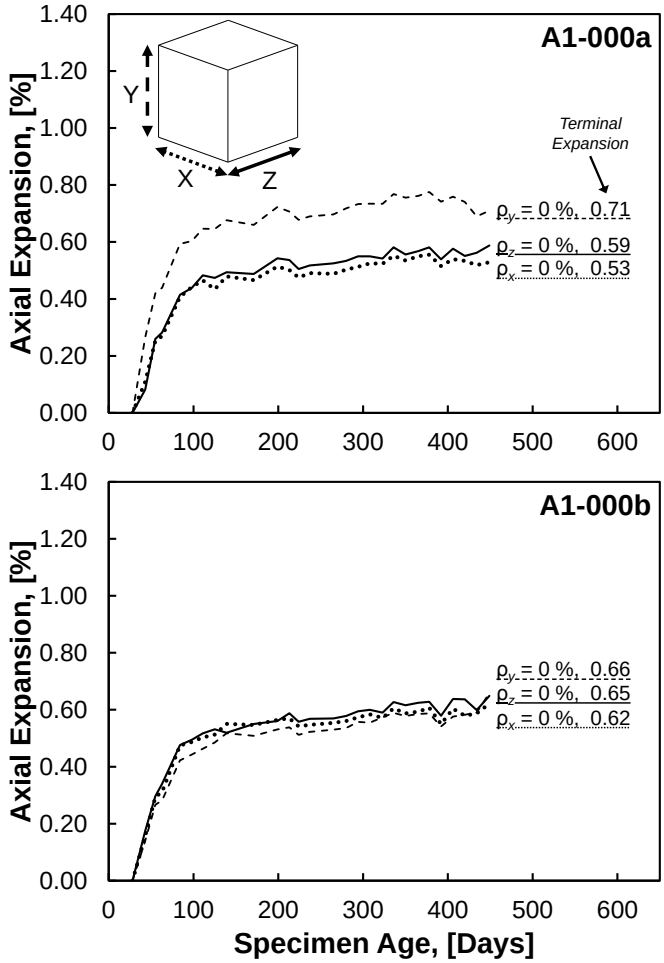

Figure 3-15: Axial expansions vs. specimen age – unreinforced A1 specimens

Figures 3-16, 3-17, and 3-18 show the expansion behavior for the A1 specimens that contained reinforcement in one, two, or three orthogonal directions. Expansions in the unreinforced directions of all uniaxially or biaxially reinforced specimens were greater than those in the directions containing reinforcement. At approximately 100 days after casting, there was a relatively abrupt shift in expansion behavior of all specimens including those that were unreinforced. All expansion rates were reduced; however, the expansion rates for the unreinforced directions were slightly less affected than those for reinforced directions within the same specimens. Similar transitions in expansion rates have been evidenced in other studies, including that by Larive (1997), and may be the result of a transition from internal to external moisture contribution to the reaction.

Expansions in unreinforced specimen directions may have been more sensitive to variations in temperature and external relative humidity within the ECF.

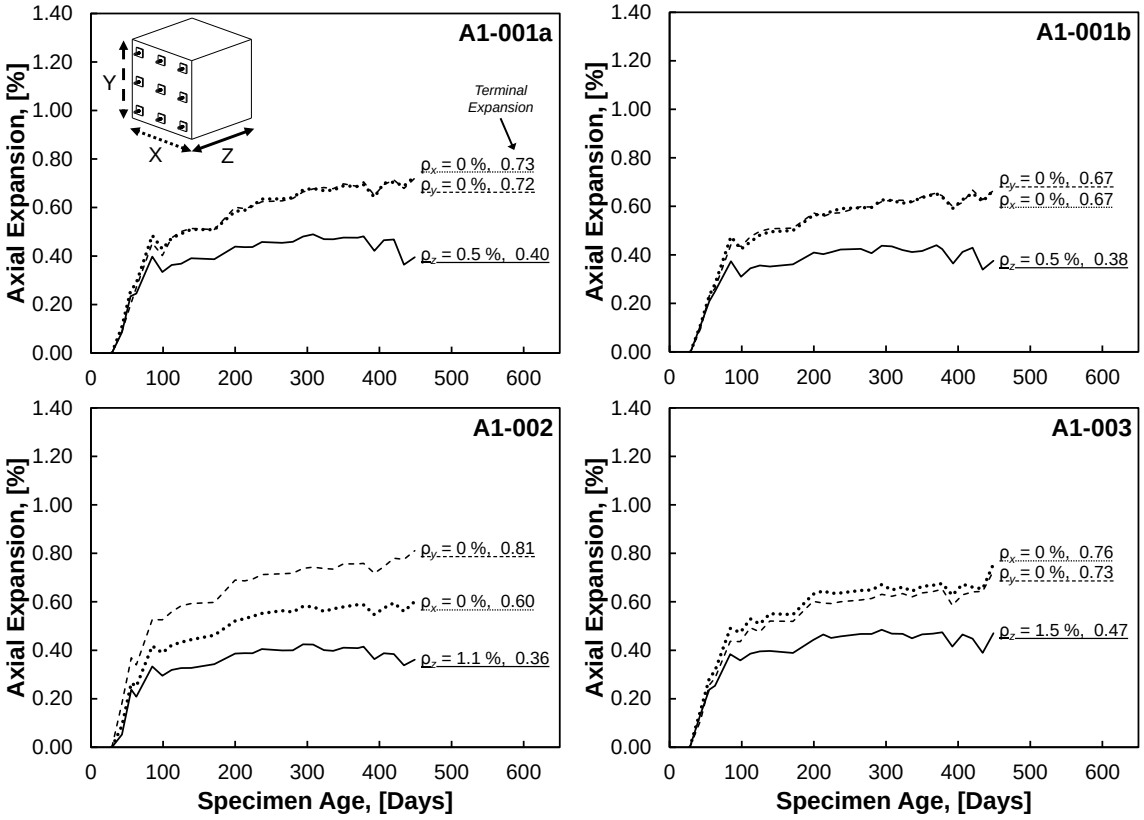

Figure 3-16: Axial expansions vs. specimen age – uniaxially reinforced A1 specimens

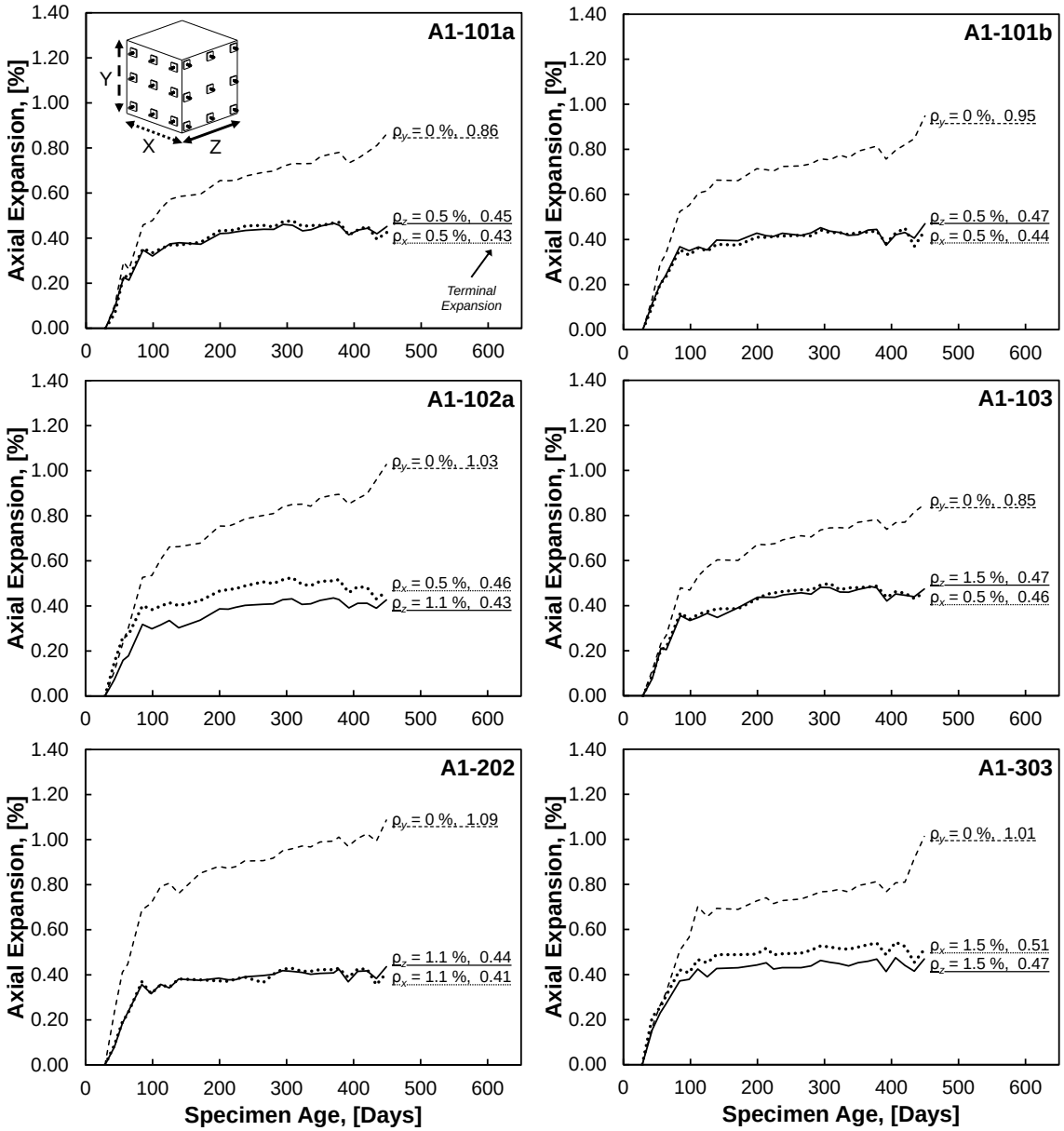

Figure 3-17: Axial expansions vs. specimen age – biaxially reinforced A1 specimens

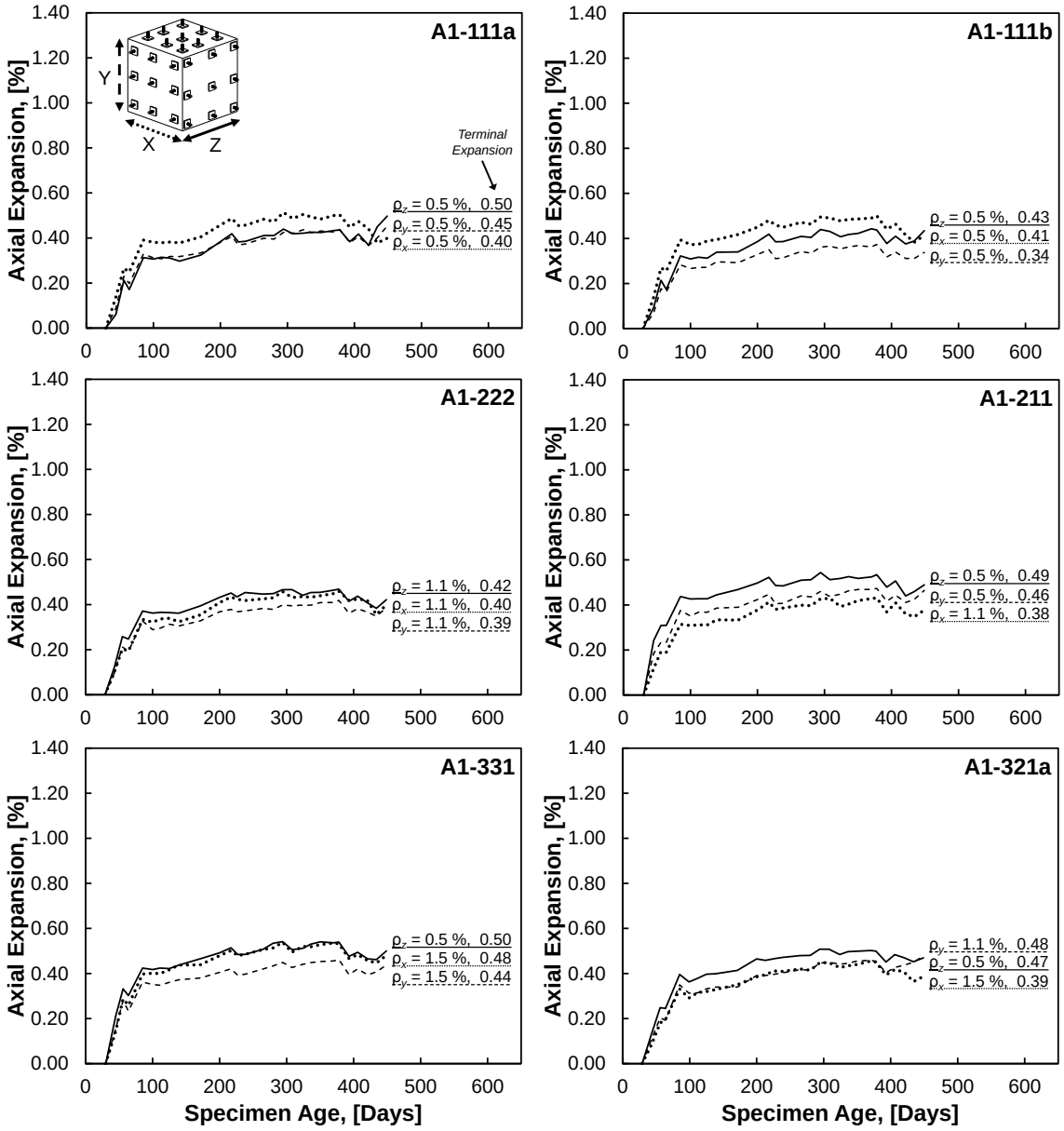

Figure 3-18: Axial expansions vs. specimen age – triaxially reinforced A1 specimens

The expansions in the reinforced directions of all A1 specimens exceeded the approximate yield strain of 0.20 % for the reinforcement. Given the magnitude of expansions well in excess of 0.20 %, it is likely that reinforcement yielded; however, it is unclear whether yielding commenced exactly at this expansion level. In this study, the strains in reinforcing bars were not measured directly; however, it is believed that the

measured expansions provide a reasonable estimate of average bar strains due to a better distribution of restraint achieved through the end-anchoring of the bars. This would suggest that the reinforcement did yield when expansions reached approximately 0.20 %. At the same time, it is recognized that local expansion measurements may have been influenced by the location of the measurement points. If there existed higher localized expansions of the concrete with increasing distance away from reinforcing bars then measured expansions would likely have been greater than the actual strains in those bars, thus suggesting that the reinforcement yielded only at higher levels of expansion. As discussed previously, this uncertainty represents a prominent issue with ASR expansion-related research that is yet to be resolved. Again, other researchers, including Smaoui et al. (2007) and Deschenes et al. (2009), have used various techniques for simultaneously measuring concrete expansions and steel strains during ASR evolution only to show that the two are at times similar and at other times may differ significantly. Such discrepancy may be related to differences in the zones of influence of restraint, locations of measurement points, and potential for bar-slip for specimens monitored in these studies.

The number of reinforced directions was also shown to have influenced the magnitude of expansions in unrestrained directions over time and the relative magnitudes of those expansions. With an increase in the number of reinforced directions, specimens expanded greater amounts over time in the unreinforced directions. For A1 specimens, the average expansions in unreinforced directions were found to be 0.60-0.65 %, 0.65-0.75 %, and 0.80-1.1 % for unreinforced, uniaxially reinforced, and biaxially reinforced specimens, respectively. Similarly, the difference between the average expansions in unreinforced and reinforced directions in these specimens was greater with an increase in the number of reinforced directions. This behavior is very clear for the uniaxially and biaxially reinforced specimens in Figures 3-16 and 3-17 where the gaps between plotlines for unreinforced and reinforced directions were larger for the biaxially reinforced specimens.

The data show that the presence of 0.5 % reinforcement in at least one direction influenced the magnitude and development of ASR-induced expansions in all three

orthogonal directions. However, the actual percentages of reinforcement at or above 0.5 %, and the reinforcing bar sizes, may not have played a significant role in influencing expansion behavior observed over time. As identified from Figures 3-16, 3-17, and 3-18, specimens detailed with the same amount of reinforcement in each reinforced direction (i.e., detailed with only one unique reinforcement ratio) expanded over time independently of the selected amount of reinforcement. In other words, all uniaxially reinforced specimens expanded similarly to one another, as did specimens that were equally biaxially or equally triaxially reinforced. In the case of some biaxially and triaxially reinforced specimens that contained different reinforcement ratios in the orthogonal directions, there was a tendency for specimens to expand more in the lightly reinforced direction(s) than in the more heavily reinforced direction(s). One unequal biaxially reinforced specimen (A1-102a) and all unequal triaxially reinforced specimens exhibited approximately a 0.1 % variation in expansions between the reinforced axes. Note that, unless explicitly indicated, any variations in expansion data reported refer to absolute differences in expansion values with units of "%" and not relative percent differences between values. A few specimens expanded the same or slightly more in more highly reinforced directions. These observations, to some degree, conflict with previously reported experimental data which suggest that increased reinforcement levels result in lower expansion rates and reduced maximum element expansions (Jones and Clark 1996, Koyanagi et al. 1992). However, previous experimentation has often been conducted on uniaxially reinforced cylinders or prisms in which expansions were only monitored in the reinforced direction. An assessment of the influence of reinforcement level is arguably incomplete without examining the role that the reinforcement ratio has on influencing element expansion behavior in transverse directions as well. The data from this study suggest that the proportionality of expansions amongst the reinforced and unreinforced element directions may be independent of the amount of reinforcement present, at least in cases where all reinforced directions contain equal reinforcement ratios.

3.4.3.1.2 Influence of Reinforcement Layout

Biaxially-reinforced A3 specimens were fabricated to investigate the influence of reinforcing bar layout on element expansion behavior. The reinforcing bars comprising each specimen were placed along designated axes in either three uniformly distributed layers or in two layers located near the edges of the specimen. Figure 3-19 shows the axial expansions for these specimens over time. Unlike the A1 specimens, these specimens did not reach their peak expansions at the end of this study.

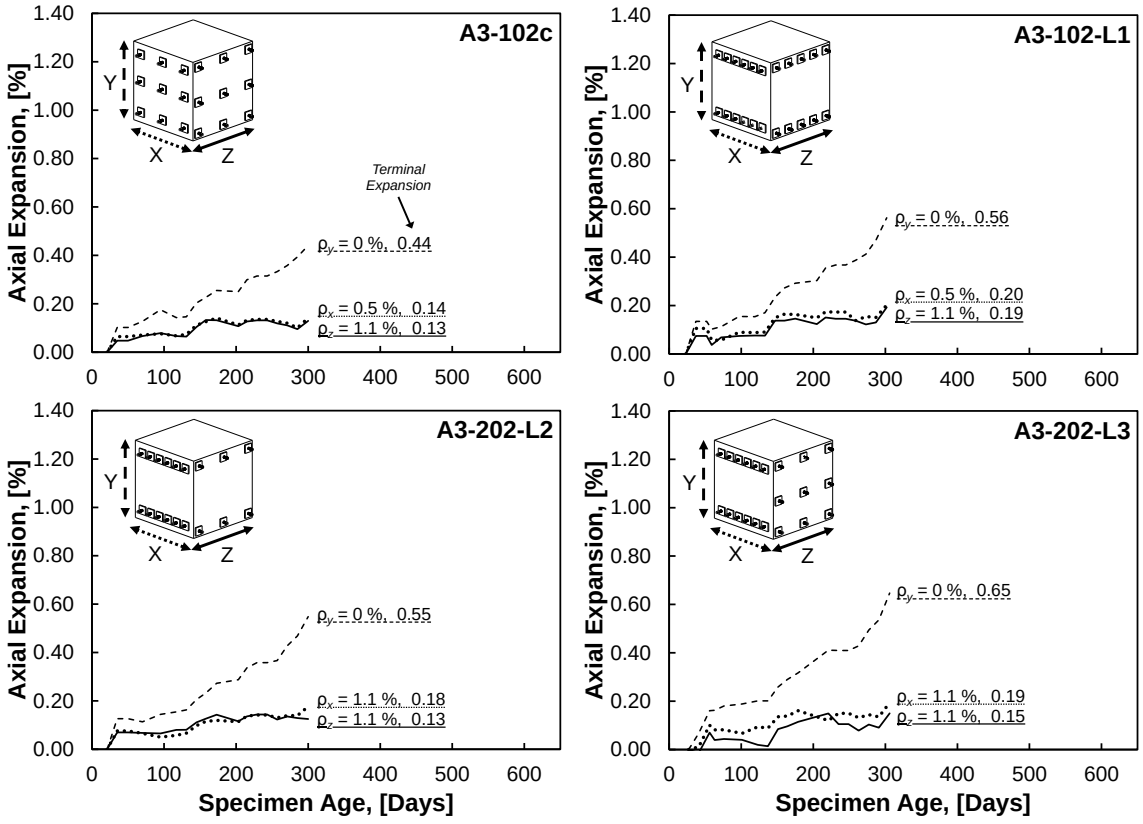

Figure 3-19: Axial expansions vs. specimen age – A3 specimens with variable biaxial reinforcement layouts

Expansions in the reinforced directions of the two specimens constructed with unequal biaxial reinforcement ratios (A3-102c, A3-102-L1) differed over time. As was the case for A1-102a, these specimens expanded less over time in the direction with

1.1 % reinforcement than in the direction with 0.5 % reinforcement. The difference in reinforcing bar layout for these specimens was found to primarily influence the rates of expansion. The specimen with reinforcement lumped in two layers (A3-102-L1) expanded more quickly than that with reinforcement distributed in three layers (A3-102c). This resulted in average axial expansions of 0.32 % and 0.24 % at 300 days for A3-102-L1 and A3-102c, respectively. The increased expansions for A3-102-L1 are believed to be a consequence of having a larger zone of effectively unreinforced concrete between two layers of reinforcement than between three layers of reinforcement. Figure 3-20 shows the development of average interior, exterior, and overall combined expansions in the reinforced directions of A3-102-L1. These expansions were derived from measurements taken from the middle eight, outer eight, and all sixteen measurement points, respectively, in the reinforced directions of this specimen. From the data presented, it is clearly seen that the specimen expanded more near its interior than it did at the target points located closer to the reinforcing bars. Given the bar sizes (13 and 16 mm diameter) and spacing of the reinforcement layers (360-410 mm) in A3-102-L1, the concrete comprising the mid-height location of the specimen was less effectively restrained and thus was more free to expand.

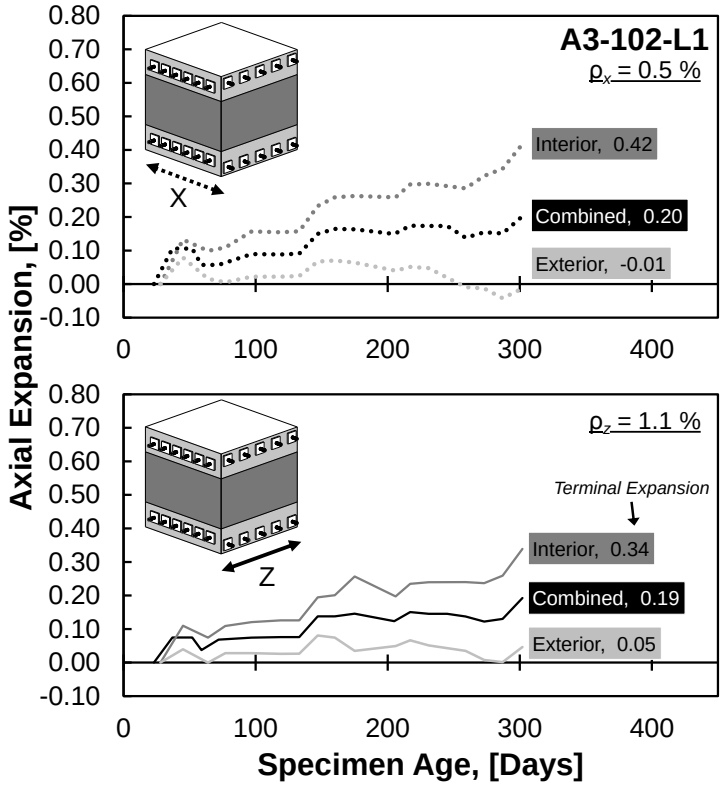

Figure 3-20: Development of expansions in reinforced directions amongst interior and exterior zones for A3-102-L1 with reinforcement in two layers

The two different reinforcing bar layouts provided in A3-202-L3 appear to have affected expansion behavior. Unlike the trends developed for specimen A1-202, in which two directions containing equal reinforcement placed in three layers expanded nearly identically with time, there was a clear difference in expansion behavior resulting from the different reinforcing bar layouts in A3-202-L3. The expansions for the x-direction, reinforced in three layers, were greater than those for the z-direction, reinforced in two layers, at nearly all times. In other words, the expansion rate-bar layout relationship previously identified from a cube containing a two-layer reinforcement layout for each reinforced direction was not seen in this case.

3.4.3.1.3 Influence of Mixture Reactivity

Mixture reactivity influenced expansion rates but did not appear to affect trends in the distribution of axial expansions over time. These findings are illustrated in Figure 3-21 which shows expansion behavior for uniaxially reinforced specimens from all three mixtures with 0.5 % reinforcement. The Mixture A and C specimens expanded much faster than the Mixture B specimen; the last measured average axial expansion for Mixture A, B, and C specimens was 0.57 %, 0.08 %, and 0.57 %, respectively. The ratio of these expansions from either of the highly reactive specimens to the low-reactive specimen – approximately 7.0 – closely matched that for the companion prisms constructed with these mixtures. Despite containing different amounts of high- and low-reactivity coarse aggregates, the expansion development for Mixture A and C specimens was similar. In this case, expansion development was primarily controlled by the much higher reactivity of the fine aggregate used for the two mixtures. Expansions for the Mixture B specimen were small, as the presence of some reactive coarse aggregate could not compensate for a lack of reactive fines. Additionally, each specimen was found to expand more in the unreinforced directions than in the reinforced direction. As expansions approached peak values under the conditioning regime employed, each specimen had expanded approximately 1.5-2 times more in the unreinforced directions as in the reinforced direction, regardless of the concrete mixture used.

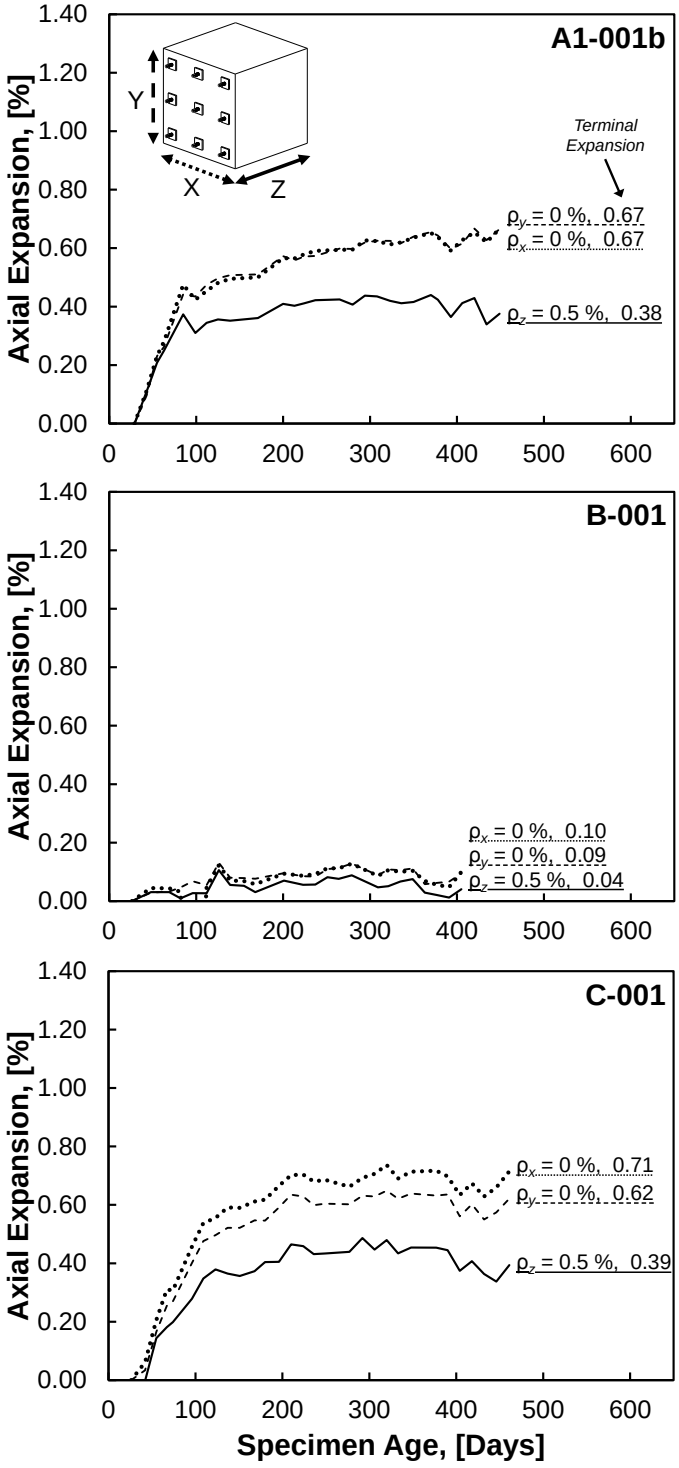

Figure 3-21: Comparison of axial expansions vs. specimen age for similar uniaxially reinforced specimens with different concrete mixtures

3.4.3.1.4 Influence of Environmental Conditioning

At the conclusion of this study, many specimens appeared to stop expanding under the conditioning regime employed. It is possible that specimens could have expanded further given additional time and increased or less variable temperatures and moisture. Upon final measurements, the uniaxially and biaxially reinforced A1 specimens appeared to still be expanding slightly while the unreinforced and triaxially reinforced specimens from the same set appeared to achieve peak expansions.

The role that element conditioning played on expansion behavior in this study may be identified from Figure 3-22 which shows the development of average axial expansions in representative Mixture A specimens cast at different times. The specimens (A1-102a, A2-333, and A3-102c) from each Mixture A casting set exhibited different expansion behavior despite using the same reactive concrete mixture. The oldest specimen (A1-102a), from Set 1, quickly expanded to an average of approximately 0.40 % within the first 100 days when the temperature and humidity (RH) within the ECF were relatively high before slowing at the onset of colder winter weather and a three-month period of low humidity. The low humidity was a consequence of the foggers within the ECF being turned off to accommodate simultaneous experimental programs. Despite an eventual rise in temperatures and shift back to high humidity within the ECF, the expansion rate for this specimen did not increase. The youngest specimen (A3-102c), from Set 3, experienced a near constant average axial expansion rate with no expansion limit reached at the conclusion of the study. Conditioning for this specimen began at colder temperatures and high humidity. With time, the temperature within the ECF increased and the high humidity was maintained. Thus, there were no changes in environmental conditions that would cause any form of expansion rate reduction. Similar to A1-102a, the specimen from Set 2 (A2-333) experienced a quick initial rise in expansions followed by a reduced expansion rate. However, this specimen only expanded approximately 0.20 % on average before the expansion rate changed, and shortly after this transition, the specimen essentially stopped expanding despite increasing temperatures and high humidity within the ECF. The lower initial expansion was the

result of the specimen being subjected to a high temperature and humidity environment for a shorter amount of time than A1-102a before the drop in temperature and humidity.

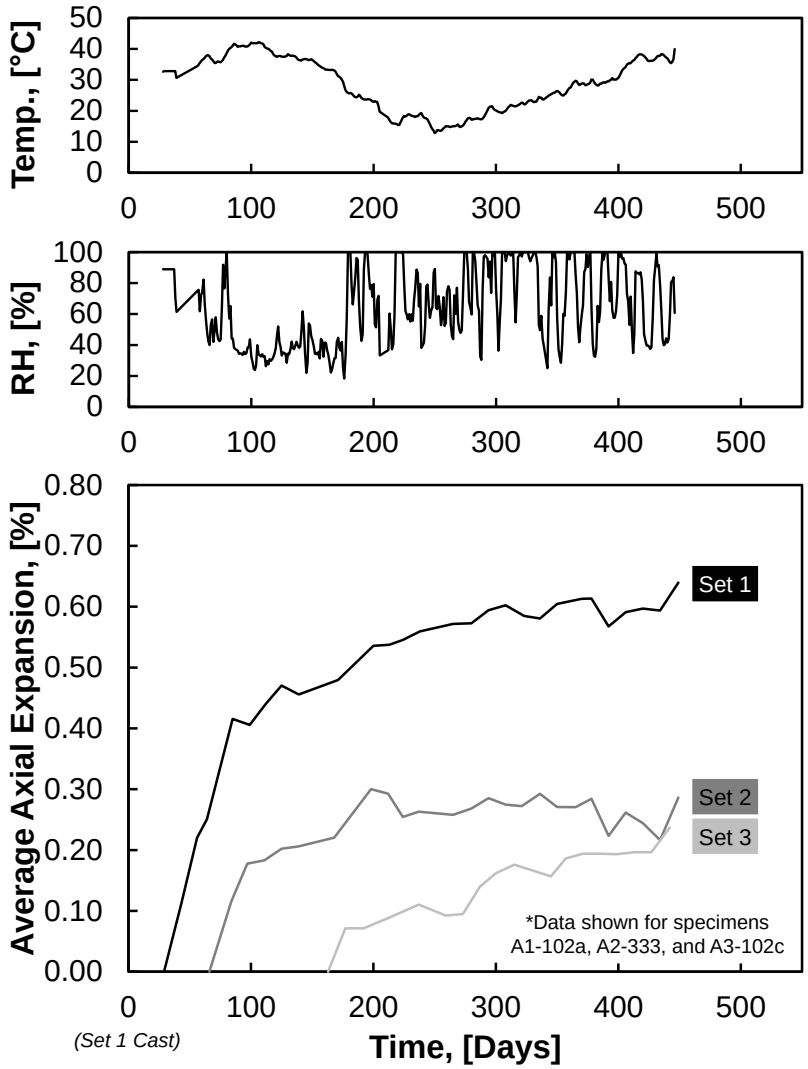

Figure 3-22: Development of average axial expansions in Mixture A specimens from different casting sets

It is believed that the inability of A2-333 to continue expanding was due to the specimen being subjected to a low humidity environment for an extended amount of time before considerable expansions could occur. The internal relative humidity of the specimen during this time likely prematurely declined below 80 % (i.e., the approximate

threshold below which swelling of ASR gel is restricted), and the external moisture provided within the ECF was inadequate to restore the high internal humidity for further expansion. This hypothesis was validated by subjecting eight companion Mixture A prisms cast with Set 1 specimens to various external moisture conditions. Given the small volume but large surface area-to-volume ratio, prisms are unable to sustain a high internal relative humidity on their own and require external moisture to promote ASR expansions. Four prisms were placed in partially water-filled, polyethylene buckets heated to 38°C, following the procedures of ASTM C 1293 (2008), to achieve a 100 % relative humidity environment. Two prisms were stored at all times with the specimens within the ECF. The final two prisms were stored in the ECF until approximately one month prior to the conclusion of this study, and thereafter were relocated to partially water-filled buckets at 38°C for subsequent conditioning. Figure 3-23 shows the evolution of average expansions over time for the three groups of prisms. All prisms initially stored in the ECF exhibited shrinkage while the humidity within the ECF was low. When the humidity was increased, the prisms quickly expanded to approximately 0.30-0.40 % before plateauing. The prisms left in the ECF did not continue to increase toward the level of expansion (0.60-0.65 %) exhibited by the prisms initially stored in buckets. However, the prisms that were moved from the ECF to buckets quickly began expanding again, reaching the 0.60-0.65 % threshold. This indicates that the moisture content within the ECF was not great enough to promote continued expansions for prisms nor cube specimens. However, this lack of moisture did not compromise the maximum expansion potential of the prisms. Thus, it is believed that that the peak expansions reached by the A2 specimens under the conditioning regime employed were not maximum possible expansions that might be obtained were the specimens conditioned longer while exposed to additional moisture in the ECF.

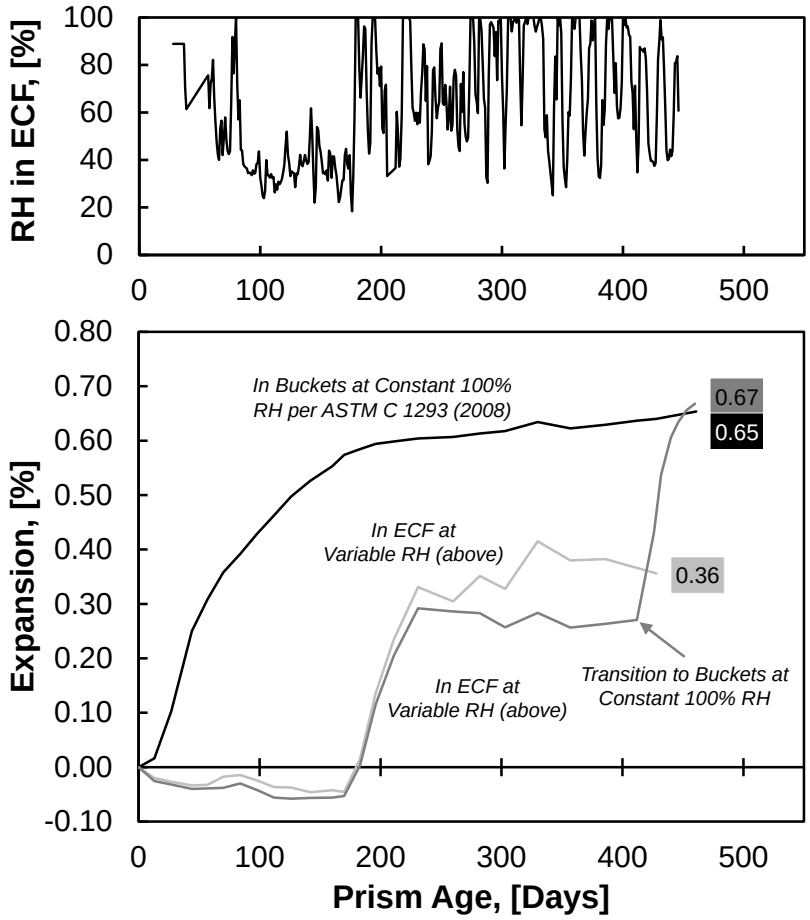

Figure 3-23: Development of expansions in 75 x 75 x 285 mm prisms with variable moisture conditioning

3.4.3.2 Volumetric Expansion with Time

The volumetric expansion of a specimen is taken as the summation of the x-, y-, and z-direction expansions of that specimen at any given time. Figure 3-24 shows the development of volumetric expansions over time for representative A1 specimens that were unreinforced or reinforced in one, two, or three directions. Volumetric expansion vs. time plots for all specimens may be found in Allford (2016) or extracted from axial expansion vs. time plots. The greatest variations in volumetric expansions between individual specimens with the same number of reinforced directions occurred after the aforementioned 100-day transition in expansion behavior; however, such variations were relatively small. The range between maximum and minimum volumetric expansions

within groups of similarly reinforced specimens did not exceed 0.20-0.25 %. In other words, the standard deviation of expansion values was on the order of 0.10 %. It should also be emphasized that there was no apparent correlation between the reinforcement amounts or layouts used and the slight variations of volumetric expansion development seen amongst specimens reinforced in the same number of directions.

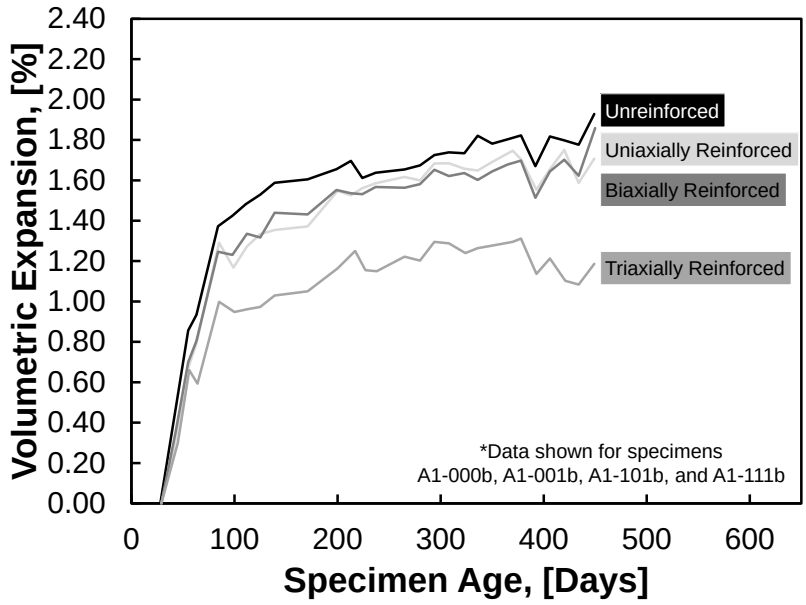

Figure 3-24: Volumetric expansion vs. specimen age for representative specimens with a varied number of reinforced directions

The data in Figure 3-24 suggest that: i) the presence of reinforcement in at least one direction of an element will reduce the amount of ASR-induced volumetric expansion that develops over time, ii) reinforcement provided in three orthogonal directions will result in the greatest reduction of ASR-induced expansion, and iii) there is not a significant difference in the development of volumetric expansion in uniaxially and biaxially reinforced elements. Relatively, the volumetric expansions for triaxially and biaxially/uniaxially reinforced specimens were approximately 60-70 % and 80-90 %, respectively, of the free volumetric expansions at each point in time. Data from Mixture B and Mixture C specimens and Mixture A specimens from Sets 2 and 3 support these observations, although the actual amounts of volumetric expansion varied for each

mixture and set due to the aforementioned differences in mixture reactivity and element conditioning.

3.4.3.3 Axial Distribution of Volumetric Expansions

Figure 3-25 presents expansion data for comparable Mixture A, B, and C equal biaxially reinforced specimens in two forms. Figure 3-25a shows the time development of axial and volumetric expansions while Figure 3-25b presents the distribution of the axial expansions which sum to the developing volumetric expansions for each specimen. The presentation of data in this second form combines the information plotted in axial expansion vs. time and volumetric expansion vs. time plots while effectively filtering out the influence of time on expansion distribution. Although specimens from the three mixtures expanded differently with time due to variations in mixture reactivity or environmental conditioning, the plots illustrate that the specimens expanded similarly in element directions when compared on the basis of volumetric expansion development.

Axial expansion vs. volumetric expansion plots of this form permit a unique interpretation of data in which the interaction between simultaneously expanding directions can be identified while assuming that factors influencing expansion rates do not affect this interaction. Specimens from a single study or from multiple studies cast at different times, with different mixtures, and/or under different environmental conditioning regimes can be very easily compared in this manner. Further, trends in axial expansion with volumetric expansion appear to be more distinct and linear than those obtained when plotting against time.

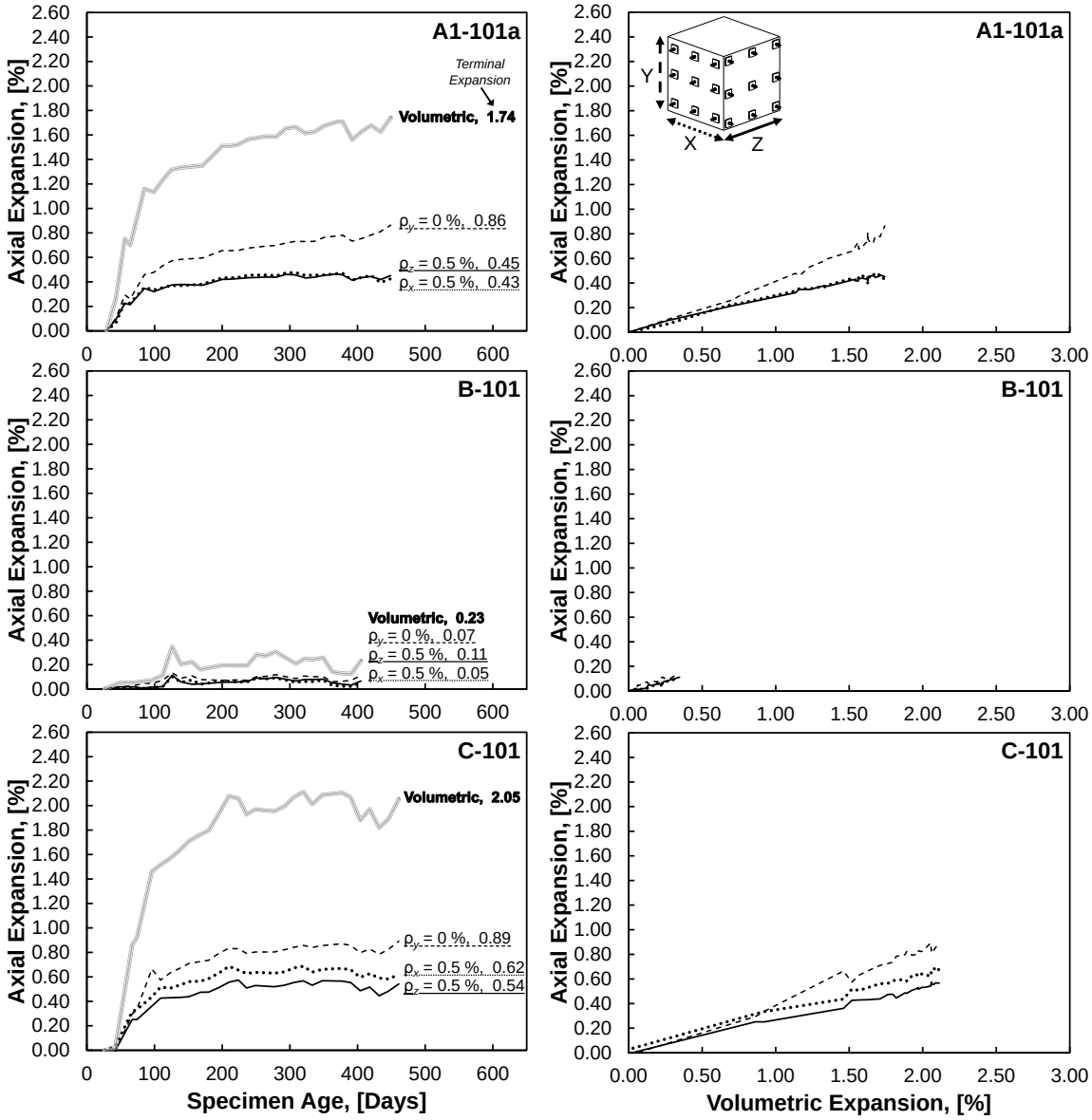

a) Axial Expansion vs. Time Plots *b) Axial Expansion vs. Volumetric Expansion Plots*

Figure 3-25: Comparison of axial expansion development with specimen age and with volumetric expansion for similar biaxially reinforced specimens with different concrete mixtures

Figure 3-26 provides a comparison of the axial distribution of volumetric expansions for pairs of A1 specimens with different amounts of uniaxial, equal biaxial, or equal triaxial reinforcement. The plots confirm the aforementioned finding that expansion behavior was similar for like specimens with only one reinforcement ratio used in the

reinforced directions. Figure 3-27 compares the axial distribution of volumetric expansions for pairs of A1 specimens with different amounts of unequal biaxial or triaxial reinforcement. These plots show that when multiple reinforcement ratios are used in a single specimen, there is a greater likelihood that the amounts of reinforcement may influence the distribution of ASR-induced expansions.

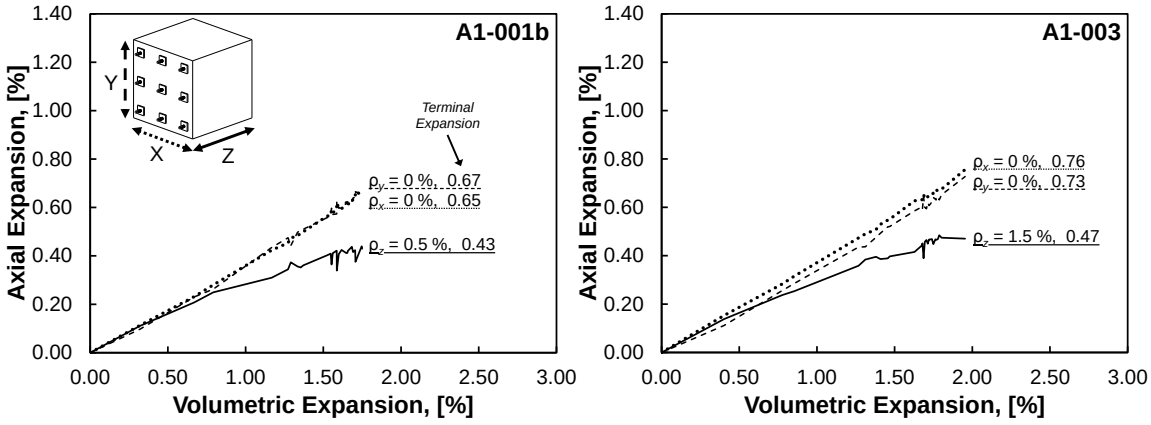

a) Uniaxially Reinforced Specimens

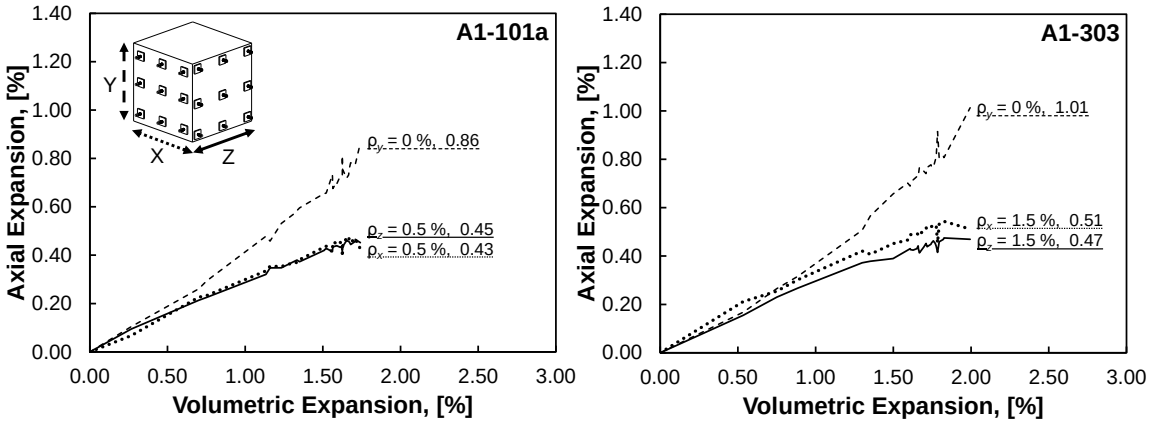

b) Equal Biaxially Reinforced Specimens

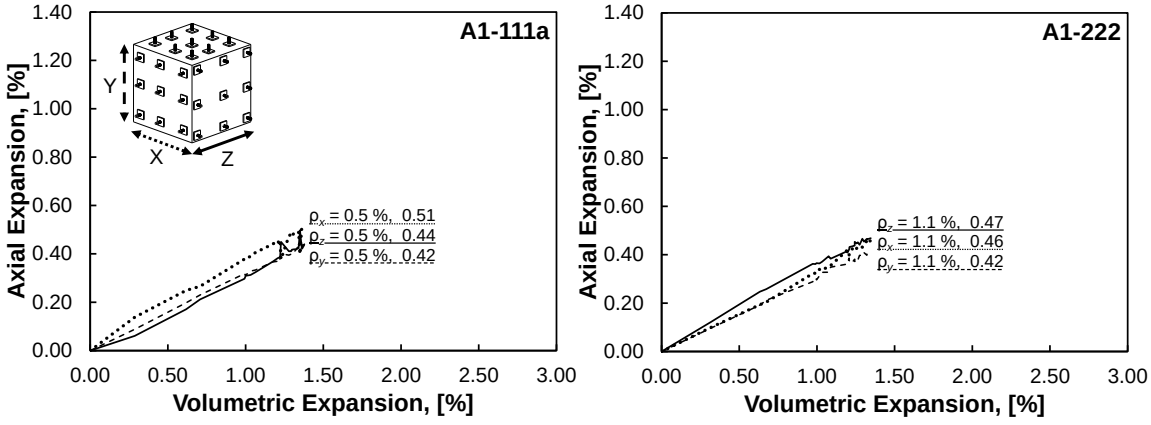

c) Equal Triaxially Reinforced Specimens

Figure 3-26: Axial expansions vs. volumetric expansion – uniaxially, equal biaxially, and equal triaxially reinforced A1 specimens

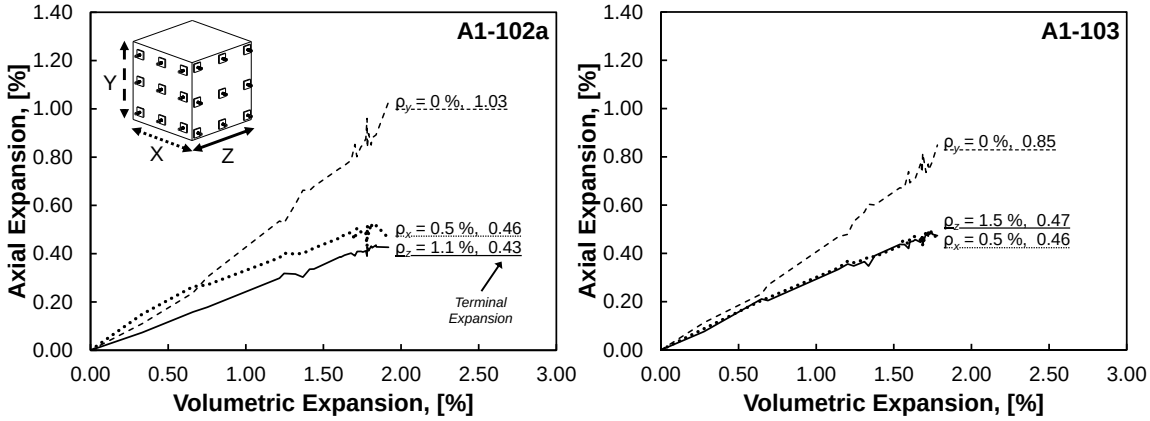

a) Unequal Biaxially Reinforced Specimens

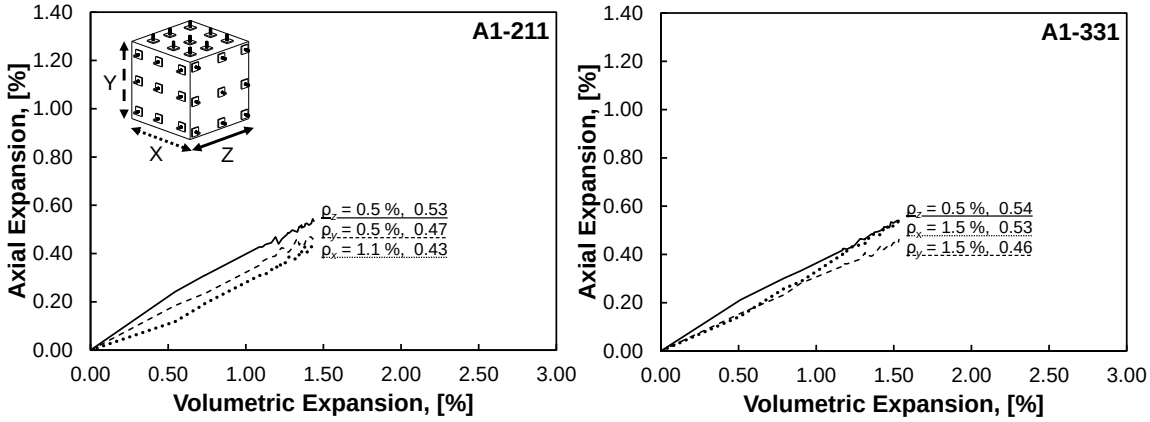

b) Unequal Triaxially Reinforced Specimens

Figure 3-27: Axial expansions vs. volumetric expansion – unequal biaxially and unequal triaxially reinforced A1 specimens

3.4.4 Conclusions

The time development and triaxial distribution of expansions for 33 large-scale RC cubes affected by ASR were monitored over a 15-month period. The influence of the number of reinforced directions comprising the elements, reinforcement ratios and bar layouts, concrete mixture reactivity, and environmental conditioning were considered. Principal findings from this study were as follows:

1. The number of reinforced directions comprising the RC cube elements influenced the development of volumetric expansions and the interaction of expansions between unreinforced and reinforced directions. Increasing the number of

reinforced directions resulted in a reduction in volumetric expansion and a relative increase in expansions in the unreinforced directions.

2. Expansions were reduced due to the presence of reinforcement; however, the actual reinforcing ratios used (0.5, 1.1, 1.5 %) did not appear to significantly influence the overall development or distribution of expansions. No correlation between reinforcing percentages and volumetric expansion development was discernable amongst specimens reinforced in the same number of directions. The multi-axial distribution of expansions for uniaxially, equal biaxially, and equal triaxially reinforced specimens were independent of the reinforcement ratios employed. The multi-axial distribution of expansions for unequal biaxially or triaxially reinforced specimens was only slightly dependent on the two or three reinforcement ratios used.
3. Mixture reactivity and environmental conditioning influenced axial and volumetric expansion rates but not the overall axial distribution of volumetric expansions. This was identified using plots of axial expansion vs. volumetric expansion which can be used to filter out the effects of time and effectively compare specimens with different casting and conditioning profiles.
4. The layout of reinforcing bars can influence expansion behavior, as was seen for specimens with reinforcement in either two or three layers. Concrete at some critical distance from reinforcement may expand as if unreinforced. Thus, averaging expansions across an entire cross-section with reinforcement not well distributed throughout may not be appropriate for analysis in some cases.

3.5 SUMMARY

Much experimental work on ASR expansion behavior has been conducted. Past studies have endeavored to identify the roles that various forms of applied loading (e.g., compression or tension) and passive restraint (e.g., reinforcement) have in restraining expansions. Principal findings have included that the amounts of applied load or reinforcement, types of loading or reinforcement bond characteristics, distribution of

restraint, and casting direction can influence expansion behavior. Depending on the method of instrumentation used to measure expansions, differences in induced concrete and steel strains may be discovered, as can variations in material expansions throughout the individual directions of an element. This can notably include differences in near-surface and core expansions of concrete elements, which may be a function of restraint distribution or exposure conditions, amongst other factors. At the same time, differences in the types, amounts, and locations of instrumentation used amongst various studies can complicate interpretation and comparison of experimental results. Dissimilar concrete reactivities, specimen sizes and shapes, conditioning, and restraint conditions can worsen this situation, especially when attempting to draw broad conclusions from results on the basis of the time-development of expansions.

Many existing studies are particularly lacking in their focus of how restraint influences expansion behavior beyond a given direction of restraint. In other words, there is little attention paid to any multi-directional interaction of expanding directions or the influence of restraint on volumetric expansion development. Amongst studies that do investigate volumetric expansions and/or expansions in multiple directions, there is much uncertainty as to what direction-to-direction expansion and restraint-volumetric expansion relationships exist. This is especially true given more than one direction of restraint. With regard to such relationships, some of the most readily apparent insufficiencies in the literature were identified to be related to the expansion behavior of RC structures. It had been less clear how the amounts and layouts of reinforcement, in both single or multiple directions, influenced overall expansions behavior, especially in larger specimens. It has also been uncertain if passive and active restraint influence expansion behavior in the same way, specifically as a function of applied or induced stress states.

In order to expand the base of knowledge on ASR expansion behavior in RC while overcoming some of the problems identified in past research, two new experimental studies were conducted. These studies focused on the development of expansions in all directions of large-scale specimens with respect to both time and

volumetric expansions. Amongst the variables considered were reinforcement amounts, number of reinforced directions, reinforcement layouts, and response given different concrete mixture reactivities or types of conditioning. Unique behaviors like mid-reaction plateauing of expansions in individual directions and significant mechanical cracking due to nonuniform restraint were evidenced. Also, a new means of presenting expansion data – plotting individual expansions against volumetric expansions as opposed to time – was introduced. This makes it possible to identify time- or conditioning-independent behavioral trends and more suitably compare elements from the same or different studies whose experimental programs do not match. Through such data analysis, it was found that the multi-directional distribution of volumetric expansions may be independent of environmental conditioning and less affected by reinforcement percentages in certain situations than might otherwise be anticipated, largely implying that active and passive restraint conditions do not influence behavior identically.

CHAPTER 4: INTRODUCTION TO NUMERICAL MODELING OF ASR EXPANSION BEHAVIOR*

4.1 OVERVIEW

This chapter provides relevant background material pertaining to the numerical modeling of ASR expansion behavior. First, information is provided to contextualize how element expansion modeling fits in the overall hierarchy of ASR modeling. The advantages of expansion modeling, particularly as they pertain to supplementing or being used in lieu of experimentation and field monitoring, are outlined. Then, several different ways in which expansion modeling results can be utilized are detailed. These include evaluating ASR-affected structure performance by way of additional structural analyses and finite element modeling or assessing structure durability and performance using more conventional engineering mechanics and reinforced/prestressed concrete design and analysis approaches.

The remainder of this chapter covers the characteristics and details of different ASR expansion models. The focus of the discussion is primarily placed on single-phase, macroscopic expansion distribution models which are arguably the most suitable for structural engineering applications. An overview of the common attributes of these types of models is presented along with an in-depth summary of three principal modeling approaches that exist in the literature.

* Portions of this chapter have been extracted directly from the following prospective publication (unpublished at time of dissertation submission) written by the author of this dissertation:

Wald, D. M., Hrynyk, T. D., and Bayrak, O. (2017). "The Distributed Volumetric Expansion Pressure Model for ASR Expansion Behavior in Reinforced Concrete Elements – Part 1: Background and Development." (submitted to *ASCE Journal of Structural Engineering*)

- Dissertator contribution: Primary author and lead researcher

4.2 BACKGROUND

Numerically estimating the effects of ASR is of interest in assessing the ramifications of expansion behavior on the performance of afflicted structures. Numerical modeling can be used to develop mathematical and theoretical explanations of behavior, confirm the results of experimental studies and in-situ investigations, evaluate the current-state durability and integrity of structures, and ideally forecast future structure performance.

ASR-related numerical modeling generally begins with the modeling of the ASR-induced expansions in the concrete. By first modeling these expansions, cracking and material property degradation can be estimated with consideration of chemical, physical, environmental, and structural parameters that influence expansion behavior. Estimated expansions can then be validated against measured expansions and subsequently applied to computer models or appropriate engineering formulations to evaluate structural performance.

It is important to bear in mind that the development of a successful ASR modeling strategy requires validation of the expansion estimation method coupled with validation of modeled structure response (e.g., load carrying capacity or ductility). Matching of experimental and analytical results for structural performance does not prove that the individual materials models, in this case an expansion model, are correct. Further, engineers may not yet be in a position to confidently assess structural performance with analytical models due to a continued lack of information or uncertainty pertaining to material property degradation and concrete-steel bond behavior. Given these difficulties, focus should be placed on completing one task at a time. The work presented in this dissertation is focused on developing and validating ASR expansion models.

4.2.1 Practical Benefits of Expansion Modeling

Numerical modeling of ASR expansion behavior offers numerous benefits to materials scientists or structural engineers as they attempt to better understand ASR phenomena, characterize distress, and identify if, how, and when the durability and

integrity of structures may be compromised. Not only can modeling supplement experimentation or field studies, but it can also serve as a reliable and efficient alternative to physical data gathering. Some of the practical benefits of expansion modeling include the following:

- Modeling can be used to provide confirmation of behavior identified through experimental and field expansion monitoring studies. Further, successful matching of computational results and experimental or in-situ results can validate the underlying mathematical or theoretical formulations embedded in the modeling approach.
- Modeling can assist in the evaluation of expansion behavior in portions of structures that cannot be easily or readily monitored. Attempting to correlate overall structural performance in the presence of ASR to expansions measured at a limited number of locations may be unwise and lead to poor assessments. This can especially be true if only relying upon measurements of near-surface expansions or expansions from regions where design detailing or boundary conditions differ significantly from those in other structure components. Modeling can thus help preclude unwarranted assumptions about widespread expansion behavior given limited physical monitoring.
- Modeling can be used to estimate expansion behavior for structures or components that cannot be physically monitored in the field or replicated in the laboratory.
- Field structures are not known to be affected by ASR until after some level of damage or deterioration (e.g., cracking) is discovered. As such, any attempts to monitor deleterious behavior following discovery of ASR cannot account for the expansions, induced stresses, material property degradation, and other consequences that occurred beforehand. Therefore, numerical modeling can provide a means of characterizing a structure's entire ASR-response history, enabling engineers to assess structural performance without inadvertently neglecting pre-existing conditions.

- Modeling can be used to reduce assessment costs and time requirements relative to conducting experimental or field studies to monitor expansions. Expansion monitoring programs require significant contributions of money and time to generate meaningful data. Experimentation necessitates the time-intensive and laborious fabrication of specimens whose cost of construction and subsequent conditioning can become prohibitive as the number and sizes of specimens grow, more unique concrete materials must be acquired, and special facilities and equipment are needed. All expansion monitoring programs can require large amounts of instrumentation devices which can often be very expensive. Further, the process of physical data collection is exceptionally time-consuming. In field structures, ASR expansions develop over decades. While expansions in laboratory specimens are expedited through the use of more reactive concrete mixtures and high temperature and humidity conditioning environments, it still generally takes a few years for the entire ASR process to work its course. Further, expansion monitoring generally requires frequent participation of individuals to mechanically measure expansions or visually inspect cracks.
- Perhaps most importantly, the contributions of expansion monitoring to the overall assessment of the performance of ASR-affected structures can provide an immediate indication as to whether ASR-induced response mechanisms are likely to pose any immediate or long-term threat to the safety and functionality of those structures.

4.2.2 Types of Expansion Modeling

ASR expansion models may be divided into many categories based on the physical scale at which ASR behavior is being captured, the mechanisms of distress as pertaining to the kinetics and chemo-mechanics of ASR, and how the expanding concrete is represented (i.e., as a homogeneous, single-phase material or as a heterogeneous, multi-phase material comprised of solids and expansive ASR gel). These models, notably those working with ASR at larger scales, are most often either semi-empirical or

mathematical. The different types of models are well-explained by Pan et al. (2012) and Jurcut (2015) and are primarily summarized as follows:

- Micro-models – These are models aimed at capturing behavior at a microscopic scale (below 1 cm) in which the genesis of expansion is explored via modeling of ASR gel behavior, including its development and swelling through chemical transport phenomena. In this case, concrete is treated as a heterogeneous material in which ASR gel can form within a matrix of aggregates and cement paste. Examples of micro-models include those proposed by Bažant and Steffens (2000), Puatatsananon and Saouma (2013), Schlangen and Garboczi (1997).
- Meso-models – These are models which explore the local interaction of expanding ASR gel and surrounding concrete solids at a scale of 1-10 cm, identifying resulting deformations and cracking of the concrete microstructure. An example of a meso-model includes that proposed by Dunant and Scrivener (2010).
- Macro-models – These are models useful for evaluating expansions and the consequences of expansions at a global, structural scale, taking into account stresses and strains, the influence of loads and reinforcement, and visible deformations, deflections, and cracking. Concrete is treated as either a single-phase or multi-phase material, although models that do not break concrete down into separate solid and gel fractions are arguably more suitable for structural engineering applications. These models generally aim to capture the influence of restraint on expansion behavior primarily through mathematical formulation guided by empirical observation. Examples of macro-models include those proposed by Charlwood et al. (1992), Cope et al. (1994), and Saouma and Perotti (2006).

4.2.3 Use of Expansion Information Obtained Through Modeling

As stated previously, expansion distribution models provide valuable contributions toward assessing the overall performance of an ASR-affected structure. It is

important to recognize that these models are aimed at providing one primary piece of information –estimates of ASR expansion behavior. Just as would be the case for expansions found through experimentation or in-situ monitoring, numerically estimated expansions are of limited use on their own. However, when ASR-induced element expansions are combined with, or used as input for, engineering calculations or numerical modeling (e.g., structural analysis and finite element modeling), an engineer may be able to gauge the impact of ASR on structure performance. The following summarizes some of the various ways in which expansions identified via numerical models can be subsequently utilized:

- Expansions can be applied directly to a finite element model to assess the behavior of a structure under a pre-existing set of load conditions, overall load-deflection or load-deformation behavior, and ultimate capacity or ductility. Response can be identified at one particular level of expansion, whether that be a current or anticipated future level of expansion. Response can also be tracked at successive levels of expansion during ASR generation to quantify if and how structural performance changes over time. Through finite element modeling, a structural engineer may be able to identify global ASR-induced macrocracking of a structure due to nonuniform restraint conditions and differential expansions, the level and distribution of prestressing throughout a structure, the extent of any yielding of reinforcement, and the interaction between expanding and/or nonexpanding components within a structural assembly. Subsequent changes to load transfer, load resistance, and deformations or deflections of the loaded structure can be quantified. The amounts and distributions of expansions used as input to a finite element model may be obtained via expansion models programmed into a finite element analysis program, hand calculations, or other computational methods. The expansions should be introduced as direction-dependent, imposed strains (i.e., prestrains) in the concrete material. This procedure is identical to the way in which shrinkage or thermal expansion/contraction are introduced in the concrete material in finite element

models, although the imposed ASR strains will not be uniform like other imposed strains.

- Expansions in given directions of a structural component can easily be converted into gross deformations as a function of the component's dimensions. A measure of these deformations can directly alert individuals as to whether an expanding component will interfere with any machinery or equipment in proximity. These deformations can also be input directly into structural analysis programs as imposed deformations to evaluate any unexpected forces or deformations that may be introduced in joints, connections, and other members within structural assemblies.
- Using simple engineering mechanics calculations that take into consideration equilibrium and compatibility, gross levels of induced prestress in reinforced directions of a structure can be approximated from expansions without the need for finite element modeling. RC elements can then be analyzed as prestressed concrete elements as a first approximation. Codified prestressed concrete shear equations, equations for concrete under combined axial applied compression and shear, prestressed concrete axial load-bending interaction diagrams, and prestressed concrete moment-curvature plots can all be subsequently used in an effort to evaluate changes in anticipated structural cracking behavior, stiffness response, and serviceability.
- Expansions can be correlated to material property degradation using the methods described in Section 2.6.7. Degraded properties can then be used in tandem with traditional sectional analyses and codified equations to evaluate any changes in structural performance and stability.
- Confinement due to multi-axial levels of prestressing can be estimated. Confined concrete properties (e.g., enhanced peak compressive stress and strain) can be used in code equations or with sectional and moment-curvature analyses.
- Although a precise method for doing so is not currently available, expansions may eventually be correlated to levels of cracking or damage to help define the level of

concern for structures with regard to durability issues and structural repair/rehabilitation assessment. In effect, ASR-affected structures may be assigned performance classifications or criteria to meet based upon the amount/distribution of expansions evidenced, similar to how seismically affected structures are evaluated with performance-based guidelines.

- In the future, new code equations or assessment formulations, perhaps as an extension of current reinforced and prestressed concrete design equations, may be developed to relate expansions directly to ASR-affected structural capacities.

4.3 SINGLE-PHASE, MACROSCOPIC EXPANSION DISTRIBUTION MODELS

The primary focus of numerical modeling of ASR expansion behavior presented in this dissertation is on single-phase, macroscopic expansion distribution models. Expansion distribution models can be used to identify the amount and directionality of ASR-induced expansions that simultaneously occur within concrete elements under various restraint conditions. Expansion "distribution," as referred to in this dissertation, implies that an appropriate assessment of ASR expansion behavior necessitates the characterization of expansion in more than one direction at a time. The models in question often focus more on how restraint alters the development and directionality of otherwise free expansions within an element as opposed to the chemo-mechanics behind the development of free expansions of plain, unrestrained concrete to begin with.

4.3.1 Typical Features and Characteristics of Existing Models

4.3.1.1 Incremental Analysis

Existing techniques used to estimate the development of restrained ASR expansions commonly utilize an incremental analysis approach (Charlwood et al. 1992; Cope et al. 1994; Saouma and Perotti 2006). Increments or rates of concrete expansion are considered to be influenced by the mechanical stresses that already exist, or predevelop, in concrete during ASR generation. These stresses arise from the application of external loading or via passive restraint. The progressive nature of ASR results in a

gradual buildup of strain and stress, crack widening and propagation, and possible changes in concrete stiffness leading to stress or force redistribution. Thus, the stress-strain history of the concrete is of critical importance; one cannot simply identify the level of ASR expansion given the current state of concrete stresses without knowing when and how those stresses developed. Expansions must be correlated to each unique stress state that pre-exists during ASR generation. Consequently, unless the stress state in concrete remains constant, an incremental approach is thus necessitated.

The greatest challenge associated with the use of an incremental analysis approach lies in the selection of the increment size. Use of a small increment is computationally expensive, while use of a large increment may lead to error accumulation.

4.3.1.2 Analysis as a Function of Time

Time is often used as the primary input parameter for estimating expansion behavior. Selecting time as an independent variable for analysis is desirable for many reasons: laboratory and field studies universally monitor ASR expansion behavior in concrete structures over time, the durability and functionality of affected structures are time-sensitive, and time-stepping is a commonly-employed incremental structural analysis approach. When analyzing a structure as a finite element assembly, time can be used to help distinguish differential expansion development between elements due to local variations in reactivity, environmental exposure, and restraint conditions throughout the structure.

4.3.1.3 Use of Principal Stress System

Generally, existing expansion distribution models identify ASR-induced expansions in principal stress directions. Evaluating expansions in these directions is appropriate for multiple reasons. Analysis of RC is traditionally conducted in the principal system with compressive and tensile stress-strain relationships defined in principal directions. Strains due to Poisson's effect are often computed in these

directions. Perhaps most importantly, the principal stress system consists of only normal stresses, including the largest compressive stress. Expansions are only affected by normal stresses in existing restrained expansion formulas; any applied shear stresses on an element are taken into account by working in the principal stress system. Meanwhile, a stress state comprising the largest compressive stress may present the "most extreme" restraint scenario.

The major difficulty with evaluating expansions in a principal stress system is that the principal directions of an element are generally not constant during ASR generation. The principal directions will change as expansions increase if an element contains any nonorthogonal reinforcement or there are any applied shear stresses acting on the element oriented in alignment with an orthogonal array of reinforcement. External applied loading and load transfer between elements commonly result in the presence of these shear stresses. As a result, the principal directions, principal stresses, and expansions must be iteratively solved for at every step of the analysis. This is a process not easily or quickly done by hand.

4.3.1.4 Interaction of Expanding Directions

In general, a concrete element will expand due to ASR in more than one direction. Many stress-based expansion modeling algorithms, such as those developed by Charlwood et al. (1992) and Cope et al. (1994), are formulated such that directional expansions can be computed independently of one another. The approach developed by Saouma and Perotti (2006) stands in stark contrast to its predecessors as it accounts for an interdependency of expansion behavior amongst simultaneously expanding directions within an element.

The debate between independence or the interaction of expanding directions is in essence a debate over whether ASR expansion behavior should be viewed as a set of unidirectional expansions in orthotropic directions or as the distribution of a volumetric expansion amongst those directions. The volumetric expansion is comprised of the directional expansions within an element, and its distribution reflects the presence and

effects of stresses and reinforcement. Thus, a volumetric expansion distribution approach represents efforts to treat ASR-affected RC as a continuum material.

4.3.1.5 Restraint to ASR

Existing modeling approaches largely operate under the premise that ASR expansions are reduced with increasing compressive stress. This stress may be comprised of applied compression from external loading or passively induced compression due to the presence of reinforcement or external restraint. These two forms of compression are mathematically indistinct. The expansions in a given direction are reduced linearly or logarithmically with increasing stress according to the models proposed by Cope et al. (1994) and Charlwood et al. (1992), respectively. The model by Saouma and Perotti (2006) uses an alternative formulation to consider expansion development in simultaneously interacting directions that is rooted in a linear relationship between stress and expansion. Again, each of these models evaluates expansions in principal stress directions.

According to these models, concrete will stop expanding in a given direction if the compressive stress in that direction exceeds some upper-bound limit, except in the case of a triaxially restrained element per Saouma and Perotti (2006). This limit is recommended to be taken as 5-10 MPa per Charlwood et al. (1992) and 10 MPa per Saouma and Perotti (2006). Numerous experimental studies (Le Roux et al. 1992; Jones and Clark 1996; Larive 1997; Multon and Toutlemonde 2006; Dunant and Scrivener 2012) on small-scale cylinders have supported a limit, ranging anywhere between 5-20 MPa, for plain concrete elements under applied compression. Whether such limits are suitable for passively restrained elements, however, remain in question.

The presence of reinforcement in an element influences expansion behavior; however, there is no consensus regarding the influence of reinforcement ratio on RC element expansion. Existing modeling approaches would suggest that expansion rates and the distribution of expansions in multiple directions depend on the specific reinforcement conditions of an ASR-affected element. Experimental work on small-scale specimens

monitored by Koyanagi et al. (1992) and Jones and Clark (1996) support such procedures, having shown that expansion rates and ultimate expansions in the reinforced direction of small-scale, uniaxially reinforced specimens reduce with increased reinforcement levels. Accurately interpreting these and other results, however, is challenging given that expansions are often not measured or reported for three orthogonal directions of a specimen. This makes it difficult to gauge the relative, rather than absolute, influence of reinforcement on expansions. The absolute influence of reinforcement is not highly valuable if the overall volumetric expansions of specimens being compared are not similar. Results from the recent study performed on large-scale RC cubes (Wald et al. 2017b) indicate that reinforcing ratios may have little influence on the multi-axial distribution of volumetric expansions for unloaded elements that are reinforced equally (i.e., have the same amount and same reinforcement layout) in any reinforced directions. Meanwhile, this and other studies (Deschenes et al. 2009; Bracci et al. 2012) indicate that elements with different combinations of two or more reinforcing ratios may expand differently, with greater concrete expansions developing in more lightly reinforced directions.

4.3.1.6 Expansion Transfer

ASR "expansion transfer," a term introduced by Multon and Toutlemonde (2006), has commonly been used to describe the interaction between simultaneously expanding directions of an element and the multi-directional influence of restraint. Under idealized conditions, plain concrete will expand equally in orthogonal element directions. Expansion transfer refers to the redistribution of these otherwise "free" expansions in response to restraint conditions, while still preserving the volumetric expansion of the element. For example, in a uniaxially restrained element, a reduction in expansion in the restrained direction will be matched with increased expansions in unrestrained orthogonal directions. Thus, expansion potential in the restrained direction is not lost; rather, it is "transferred" to the other directions to maintain the element's volumetric expansion. Expansion transfer may be thought of as concrete expanding along paths of least

resistance: if concrete cannot or does not expand in one direction due to a certain level of restraint then it will attempt to expand in other, less restrained directions. This phenomenon is supported by the results of multiple studies in which different amounts of restraint have resulted in different multi-axial expansion distribution patterns for specimens exhibiting similar volumetric expansions (Multon and Toutlemonde 2006; Wald et al. 2017b). Expansion transfer has been incorporated in the approach developed by Saouma and Perotti (2006). In this approach, increments of volumetric expansion are distributed in principal stress directions using weighting factors computed as functions of multi-directional restraint in the form of concrete principal stresses.

4.3.2 Details of Existing Models

4.3.2.1 Cope et al. (1994) – Generalized and Linear Expansion-Stress Relationships

Cope et al. proposed a general methodology to estimate restrained ASR expansions in concrete in individual directions of an element. Increments of restrained expansion, $d\varepsilon_{ex}$ in a given direction are related to increments of unidirectional free expansion, $d\varepsilon_{ex}^{f}$ as a function of the normal compressive stress in concrete, σ_c, acting in that direction, according to Equation 4-1a. Note that, in general, the compressive stress will not be constant.

$$d\varepsilon_{ex} = f(\sigma_c) \cdot d\varepsilon_{ex}^{f} \qquad \textit{Equation 4-1a}$$

This relationship may also be expressed in terms of expansion rates per unit time, d*t*:

$$\dot{\varepsilon}_{ex} = f(\sigma_c) \cdot \dot{\varepsilon}_{ex}^{f} \qquad \textit{Equation 4-1b}$$

where: $\dot{\varepsilon}_{ex}$ = rate of restrained ASR expansion (= $d\varepsilon_{ex}/dt$)

$\dot{\varepsilon}_{ex}^{f}$ = rate of free ASR expansion (= $d\varepsilon_{ex}^{f}/dt$)

Any mathematical relationship with functional dependency upon compressive stress may be valid for use in Equations 4-1a and 4-1b. These can include linear, higher-order polynomial, and exponential relationships, all of which were considered by the researchers. In particular, the researchers largely discussed usage of a linear relationship,

illustrated in Figure 4-1, in which expansion rates (or increments of expansion) reduce linearly with an increasing compressive stress. Tensile stresses do not influence the expansion rate. Concrete continues to expand as long as the compressive stress does not exceed an upper-bound limit, σ_c^o. This relationship is described by Equations 4-2a (in terms of incremental expansions) and 4-2b (in terms of expansion rates):

$$d\varepsilon_{ex} = \left(1 - \frac{\sigma_c}{\sigma_c^o}\right) \cdot d\varepsilon_{ex}^f \qquad \textit{Equation 4-2a}$$

$$\dot{\varepsilon}_{ex} = \left(1 - \frac{\sigma_c}{\sigma_c^o}\right) \cdot \dot{\varepsilon}_{ex}^f \qquad \textit{Equation 4-2b}$$

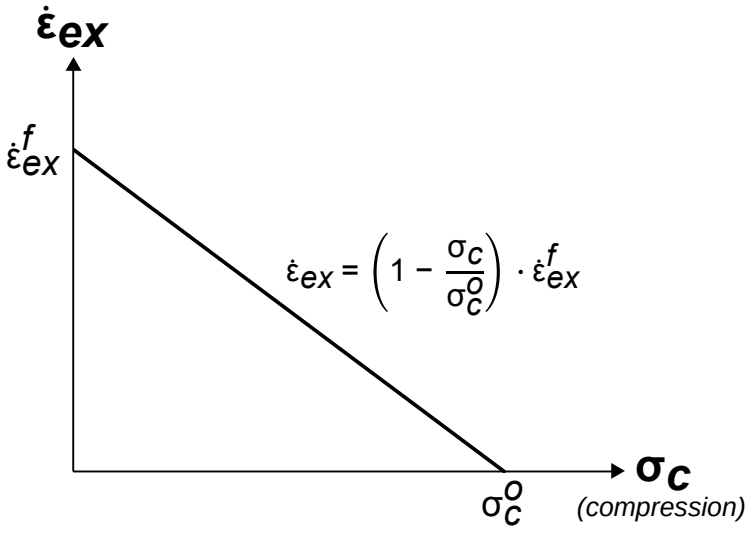

Figure 4-1: Cope et al. (1994) Linear Expansion Rate-Stress Relationship

The expansion-stress relationships are applicable to concrete restrained in any form, that is concrete under both actively applied and passively induced compressive stresses. As such, σ_c^o is intended to be used the same way for ASR-affected concrete that is either loaded and/or reinforced. The authors did not recommend a particular value for σ_c^o; however, they found that 100 x 200 mm cylinders experienced very small to negligible expansions under sustained axial compression between 4 and 6 MPa. Use of a limiting stress value in this range may be appropriate, but it must be cautioned that, by the researchers' own experimental results, use of a single value of σ_c^o may actually be

incorrect. The researchers estimated that RC cylinders, not under sustained applied loading, continued to expand given passively induced compressive stresses in excess of 4-6 MPa. This lends credence to the possibility that active and passive restraint may influence expansion behavior differently.

Although not explicitly noted, the expansion-stress relationship is expected to be applied in each of the element's principal stress directions and under the assumption that each direction, if unrestrained, would experience the same unidirectional free expansion with time. One commonly obtained principal stress, the maximum normal compressive stress acting on an element, will represent the most extreme case of restraint to expansion. Identifying expansions in principal directions will also take into consideration the combined effects of applied shear and normal stresses. However, it should be recognized that shear-induced normal compressive stresses (i.e., those geometrically transformed from shear stresses) are assumed to influence expansion behavior in the same way as directly applied normal stresses. Various expansion-stress relationships have been conceived in large part from experimentation on concrete elements only under directly applied normal stresses. Thus, the role of shear stresses on expansion behavior is not well defined. As such, given the approximate nature of expansion-stress relationships, one cannot dismiss the possibility that relationships may be just as applicable in non-principal stress directions.

The total restrained expansion at any point in time, ε_{ex}, is the integration of incremental expansions up until that point in time:

$$\varepsilon_{ex} = \int d\varepsilon_{ex} \qquad \textit{Equation 4-3}$$

If the compressive stress in a direction under consideration is constant, as may be the case for plain concrete under a sustained axial load, the total restrained expansion at any point, ε_{ex}, is simply taken as a linear reduction of the total free expansion, ε_{ex}^{f}:

$$\varepsilon_{ex} = \left(1 - \frac{\sigma_c}{\sigma_c^o}\right) \cdot \varepsilon_{ex}^{f} \qquad \textit{Equation 4-4}$$

As stated before, σ_c, will generally not be constant. Passively induced compressive stresses gradually build in RC with increasing expansion. Long-term loading conditions on structures can change. Stresses can also redistribute within a structure due to changes in material stiffness (e.g., ASR-induced stiffness degradation). In such cases, expansions must be estimated incrementally and Equation 4-3 must be used. At every step of the analysis, concrete stresses will need to be evaluated and updated. While not explicitly notated, σ_c is implied as being a function of expansions of the form $\sigma_c(\varepsilon_{ex})$.

The researchers presented closed form solutions for evaluating the total expansion, ε, in unloaded RC with a linear expansion-stress relationship. Recall that the total expansion in unloaded RC consists of the ASR-induced expansion, ε_{ex}, in the concrete material and the net strain due to stress in the concrete from the mechanical interaction of concrete and steel. The expansions that develop prior to yielding of reinforcement and after yielding of reinforcement are given by Equations 4-5 and 4-6, respectively:

$$\varepsilon = \frac{\sigma_c^o}{\rho E_s}\left(e^{\frac{\rho E_s}{\sigma_c^o(1+m\rho)}\varepsilon_{ex}^f} - 1\right) \qquad \textit{Equation 4-5}$$

$$\varepsilon = \left(1 + \frac{\rho E_s \varepsilon_y}{\sigma_c^o}\right)\left[\varepsilon_{ex}^f - \frac{\sigma_c^o(1+m\rho)}{\rho E_s}\ln\left(1 + \frac{\rho E_s \varepsilon_y}{\sigma_c^o}\right)\right] + \varepsilon_y \qquad \textit{Equation 4-6}$$

where: $m =$ modular ratio (E_s/E_c)

$\varepsilon_y =$ yield strain of reinforcement

These closed-form solutions were derived from first principles using the aforementioned continuous incremental expansion-stress relationship given by Equation 4-2. Note that concrete was treated as a linear-elastic material with a constant modulus of elasticity, E_c. The solutions account for the gradual increase in passively induced compressive stress in concrete due to the presence of reinforcement. According to Jones (1994), these closed-form solutions give mathematical upper-bounds on expansions. Alternate closed-form solutions developed by the model researchers are reported by Jones (1994) which are used to generate lower-bound expansions in unloaded RC based on the assumption that RC expands as though it were plain concrete under a sustained,

constant stress equal to the maximum passively induced stress expected. In such a case, expansions are estimated to be lower due to the presence of a large, initial stress rather than an initial stress of zero that gradually increases. These solutions were derived using the total expansion-stress relationship given by Equation 4-4. Lower-bound total expansions prior to yielding of reinforcement and after yielding of reinforcement are given by Equations 4-7 and 4-8, respectively:

$$\varepsilon = \left(\frac{1}{\frac{E_c \varepsilon_{ex}^f}{\sigma_c^o} - \frac{1 + m\rho}{m\rho}} + \frac{1}{1 - \frac{m\rho}{1 + m\rho} \cdot \frac{E_c \varepsilon_{ex}^f}{\sigma_c^o}} \right) \varepsilon_{ex}^f \qquad \textit{Equation 4-7}$$

$$\varepsilon = \left(1 + \frac{\rho E_s \varepsilon_y}{\sigma_c^o} \right) \varepsilon_{ex}^f - m\rho\varepsilon_y \qquad \textit{Equation 4-8}$$

Jones and Clark (1996) also used the modeling approach to develop closed-form solutions to identify the total expansion, ε, for RC under a sustained compressive stress acting in the direction of reinforcement. Note that total expansions given by these formulas include strains due to elastic shortening under a compressive stress. Upper-bound total expansions for loaded RC prior to yielding of reinforcement and after yielding of reinforcement are given by Equations 4-9 and 4-10, respectively:

$$\varepsilon = \frac{\sigma_c^o - \sigma_c(1 + \rho)}{\rho E_s} \left(e^{\left[\frac{\rho E_s}{\sigma_c^o (1 + m\rho)}\right] \varepsilon_{ex}^f} - 1 \right) + \frac{\sigma_c (1 + \rho) e^{\left[\frac{\rho E_s}{\sigma_c^o (1 + m\rho)}\right] \varepsilon_{ex}^f}}{(1 + m\rho) E_c} \qquad \textit{Equation 4-9}$$

$$\varepsilon = \left(1 + \frac{\rho E_s \varepsilon_y}{\sigma_c^o} - \frac{\sigma_c (1 + \rho)}{\sigma_c^o} \right) \left\{ \frac{\sigma_c^o (1 + m\rho)}{\rho E_s} \left[\varepsilon_{ex}^f - \ln\left(1 + \frac{\rho E_s \varepsilon_y}{\sigma_c^o - \sigma_c (1 + \rho)} \right) - \ln\left(1 + \frac{\sigma_c (1 + \rho) m\rho}{(1 + m\rho)\left[\sigma_c^o - \sigma_c (1 + \rho)\right]} \right) \right] \right\} + \varepsilon_y \qquad \textit{Equation 4-10}$$

Lower-bound total expansions for loaded RC prior to yielding of reinforcement and after yielding of reinforcement are given by Equations 4-11 and 4-12, respectively:

$$\varepsilon = \left[\frac{1}{\frac{E_c \varepsilon_{ex}^f}{\sigma_c^o} - \frac{1 + m\rho}{m\rho}} + \frac{1}{1 - \frac{m\rho}{1 + m\rho} \cdot \frac{E_c \varepsilon_{ex}^f}{\sigma_c^o}} \right] \left(\varepsilon_{ex}^f - \frac{\sigma_c (1 + \rho)}{m\rho E_c} \right) + \frac{\sigma_c (1 + \rho)}{m\rho E_c} \qquad \textit{Equation 4-11}$$

$$\varepsilon = \left(1 + \frac{\rho E_s \varepsilon_y}{\sigma_c^o} - \frac{\sigma_c (1 + \rho)}{\sigma_c^o} \right) \varepsilon_{ex}^f - m\rho\varepsilon_y + \frac{\sigma_c (1 + \rho)}{E_c} \qquad \textit{Equation 4-12}$$

Closed-form solutions cannot be readily obtained for loaded RC in which loading and reinforcement directions do not coincide, where nonlinear expansion-stress relationships are used, or where concrete is not treated as a linear-elastic material with a constant modulus of elasticity. Thus, in applying such an approach with any of the conditions noted above, the restrained expansions will likely need to be estimated as a summation of discrete incremental expansions, $\Delta\varepsilon_{ex}$, instead of using the previously defined continuous formulations. The formulas for using discrete increments are given by Equations 4-13a and 4-13b:

$$\varepsilon_{ex} = \sum \Delta\varepsilon_{ex} \qquad \textit{Equation 4-13a}$$

$$\Delta\varepsilon_{ex} = \left(1 - \frac{\sigma_c}{\sigma_c^o} \right) \cdot \Delta\varepsilon_{ex}^f \qquad \textit{Equation 4-13b}$$

The size of the free expansion increment, $\Delta\varepsilon_{ex}^f$, selected can greatly influence the accuracy of the results and the required computation time.

Free expansion increments should also be chosen such that any considered changes in restraint conditions or stresses that are explicitly time-dependent are appropriately accounted for. Such changes may be caused by creep of concrete, relaxation of steel, or abrupt changes in loading conditions. The problem which arises in this situation is that free expansion development is not a linear function of time. Consequently, a constant increment of free expansion does not correspond to a constant increment of time, and most time-dependent effects may be ill-predicted with variable time increments. If time-dependent changes in restraint are considered, it may be better to

estimate restrained expansion increments using constant increments of time, Δt, with variable free expansion increments defined as a function of time, t, per Equation 4-14:

$$\Delta\varepsilon_{ex}(\Delta t) = \left(1 - \frac{\sigma_c(t)}{\sigma_c^0}\right) \cdot \Delta\varepsilon_{ex}^{f}(\Delta t) \qquad \textit{Equation 4-14}$$

Performing an analysis on the basis of time also permits identification of differential free expansion development between different portions of a structure due to varying chemical reactivity or environmental conditions. The researchers, however, did not address these considerations.

4.3.2.2 Charlwood et al. (1992) – Logarithmic Expansion-Stress Relationship

Within the same general framework established by Cope et al. (1994), Charlwood et al. (1992) proposed a logarithmic expansion-stress law to estimate restrained expansion rates in independent principal stress directions. According to the described modeling approach, the rate of restrained expansion, $\dot{\varepsilon}^r$, reduces from the free expansion rate, $\dot{\varepsilon}^u$, logarithmically with increasing compressive stress in the concrete, σ_c. This rate reduction does not occur for either tensile stresses or for compressive stresses below a lower-bound stress, σ_{cL}, set at 0.3 MPa. Concrete will stop expanding at compressive stresses above an upper-bound stress, σ_{cMAX}, between 5-10 MPa. The full stress-expansion law is diagrammed in Figure 4-2 and given by Equation 4-15:

$$\dot{\varepsilon}^r = \begin{cases} \dot{\varepsilon}^u, & 0 \le \sigma_c < \sigma_{cL} \\ \dot{\varepsilon}^u - K \cdot \log\dfrac{\sigma_c}{\sigma_{cL}}, & \sigma_{cL} \le \sigma_c < \sigma_{cMAX} \\ 0, & \sigma_c \ge \sigma_{cMAX} \end{cases} \qquad \textit{Equation 4-15}$$

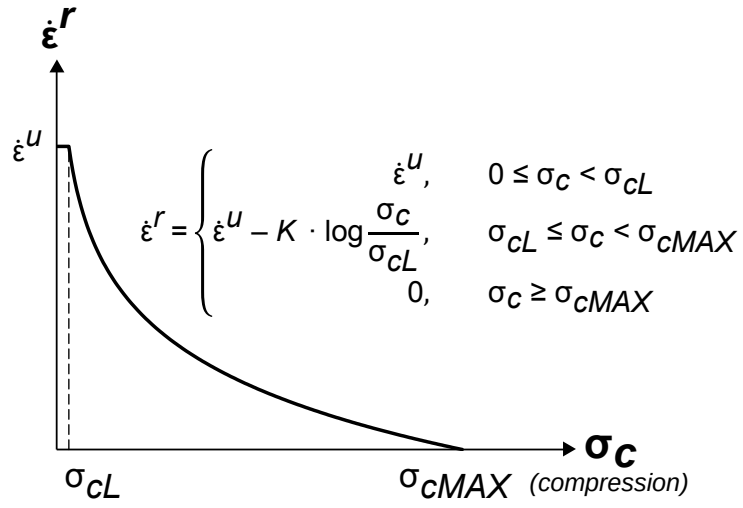

Figure 4-2: Charlwood et al. (1992) Logarithmic Expansion Rate-Stress Relationship

The parameter, *K*, is an expansion rate constant (units of expansion/time) which can be derived from Equation 4-16 by setting $\dot{\varepsilon}^r$ equal to zero when σ_c equals σ_{cMAX}:

$$K = \frac{\dot{\varepsilon}^u}{\log\frac{\sigma_{cMAX}}{\sigma_{cL}}} \qquad \textit{Equation 4-16}$$

The stress-expansion law can be rewritten in terms of discrete incremental expansions as:

$$\Delta\varepsilon^r = \begin{cases} \Delta\varepsilon^u, & 0 \le \sigma_c < \sigma_{cL} \\ \Delta\varepsilon^u - k \cdot \log\frac{\sigma_c}{\sigma_{cL}}, & \sigma_{cL} \le \sigma_c < \sigma_{cMAX} \\ 0, & \sigma_c \ge \sigma_{cMAX} \end{cases} \qquad \textit{Equation 4-17}$$

In this case, the parameter, *k*, is an incremental expansion constant evaluated as:

$$k = \frac{\Delta\varepsilon^u}{\log\frac{\sigma_{cMAX}}{\sigma_{cL}}} \qquad \textit{Equation 4-18}$$

The total restrained expansion, ε^r, at a given point can be estimated as a summation of the discrete incremental expansions:

$$\varepsilon^r = \sum \Delta\varepsilon^r \qquad \textit{Equation 4-19}$$

As was discussed for the model proposed by Cope et al. (1994), the expansion increment size will dictate updated stress states in passively restrained concrete as well as influence model accuracy and computational time. If the concrete stresses do change during ASR generation then the choice of expansion increment will complicate things further by influencing the value of *k*.

If σ_c is a constant between σ_{cL} and σ_{cMAX}, the total restrained expansion, ε^r, will be related to the total free expansion, ε^u, given by Equation 4-20:

$$\varepsilon^r = \varepsilon^u \cdot \left(1 - \frac{1}{\log \frac{\sigma_{cMAX}}{\sigma_{cL}}} \right) \qquad \textit{Equation 4-20}$$

Similarly to Cope et al. (1994), Charlwood et al. (1992) did not address how to estimate free expansion with time as a function of chemical reactivity and environmental conditions, limiting successful application of the modeling approach where multiple elements might exhibit differential expansion development. Léger et al. (1996) proposed a parametric modeling approach capable of capturing differential elemental expansions in which the restrained ASR expansions found using the current expansion model are directly adjusted by multipliers to account for the effects of chemical reactivity, temperature, and humidity. These multipliers are illustrated in Figure 4-3.

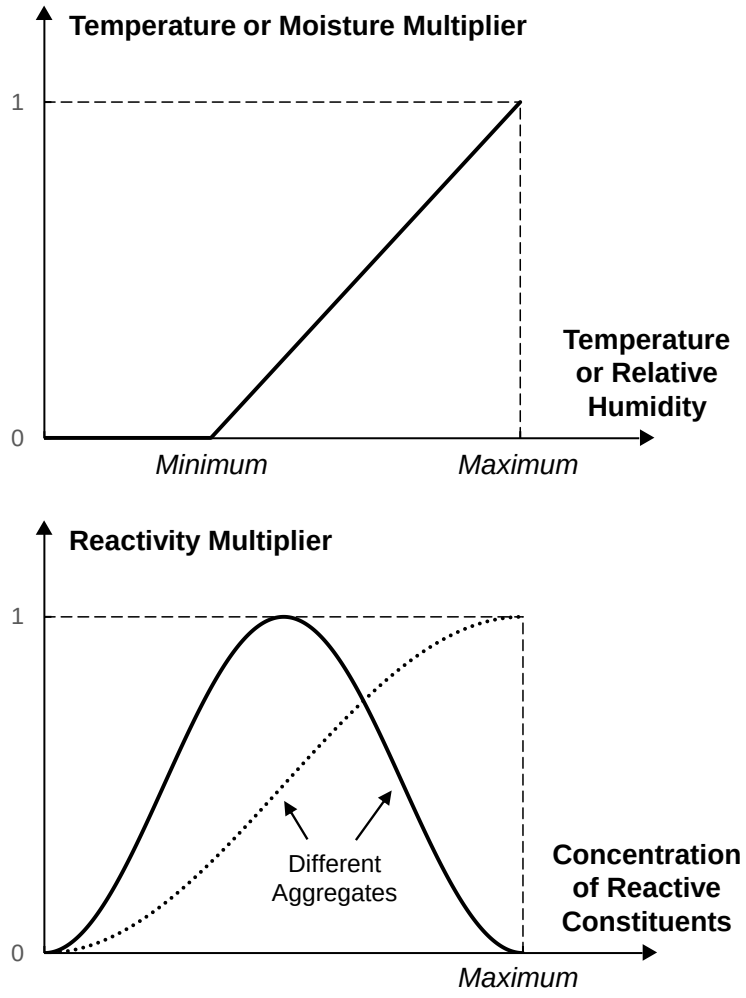

Figure 4-3: Léger et al. (1994) Expansion Development Modifiers

4.3.2.3 Saouma and Perotti (2006) – Interacting, Multi-Axial Expansion-Stress Relationship

The modeling approaches proposed by Cope et al. (1994) and Charlwood et al. (1992) are used to directly evaluate restrained expansions in each principal stress direction of an element, independent of concurrent behavior in other principal directions. In effect, expansions are computed for and entirely distributed to only the direction under consideration. These models mainly convey "what" expansions to distribute; "how" to distribute those expansions is self-explanatory. The modeling approach proposed by Saouma and Perotti (2006) differs significantly in that expansions are evaluated in each

principal stress direction as a three-way distribution of an overall volumetric expansion, with each direction influencing the others. As with the other models, expansions are determined on an incremental basis. The modeling approach is carried out in two repeated steps. First, increments of restrained volumetric expansion are evaluated. Second, the increments of restrained volumetric expansion are distributed amongst the three current principal stress directions in concrete as a mathematical function the pre-existing overall state of principal concrete stresses. It is this second part of the procedure that dictates "how" to distribute expansions within an element.

According to the researchers' model, the time-dependent development of volumetric expansion is a function of temperature, humidity, principal stresses, and the ability of tensile macrocracks and compressive microcracks to absorb ASR gel and restrict expansion. Volumetric ASR expansion develops with time, *t*, according to a thermo-chemo-mechanical formulation that accounts for the kinetics of the chemical reaction and the influence of mechanical stresses:

$$\dot{\varepsilon}_{vol}^{ASR}(t) = \Gamma_t\left(f_t^{'},\sigma_1|COD\right) \cdot \Gamma_c\left(\bar{\sigma},f_c^{'}\right) \cdot \mathrm{f}(h) \cdot \dot{\xi}(t,\theta) \cdot \varepsilon^{\infty}|_{\theta=\theta_o} \qquad \textit{Equation 4-21}$$

where: $\dot{\varepsilon}_{vol}^{ASR}$ = rate of restrained volumetric ASR expansion in concrete

$\dot{\xi}$ = rate of reaction progress

ε^{∞} = maximum free volumetric ASR expansion

Γ_t = reduction factor accounting for absorption of ASR gel by tensile macrocracks

Γ_c = reduction factor accounting for absorption of ASR gel by compressive microcracks

σ_1 = maximum principal tensile stress [MPa]

$\bar{\sigma}$ = average principal stress [MPa]

COD = crack opening displacement

h = relative humidity (0 to 1)

θ = temperature [K]

θ_o = reference temperature [K]

Equation 4-21 may be rewritten in terms of increments of volumetric expansion, $\Delta\varepsilon_{vol}^{ASR}$, and increments of ASR reaction progress, $\Delta\xi$, as:

$$\Delta\varepsilon_{vol}^{ASR}(t) = \Gamma_t\left(f_t',\sigma_1|COD\right)\cdot\Gamma_c\left(\bar{\sigma},f_c'\right)\cdot f(h)\cdot\Delta\xi(t,\theta)\cdot\varepsilon^{\infty}|_{\theta=\theta_o} \qquad \textit{Equation 4-22}$$

ASR reaction progress, ξ, is given in Equation 4-23 as a function of the sum of the three principal stresses (i.e., the first invariant of the stress state), I_σ, and the characteristic and latency times, τ_C and τ_L , of the chemical reaction. The characteristic and latency times are given by Equations 4-24 and 4-25. The latency time is independently a function of I_σ, given by Equation 4-26. Note that the formulation given by Equation 4-23 was developed by Larive (1997) without consideration of the influence of principal stresses on reaction progress. The formulations for characteristic and latency times were developed by Ulm et al. (2000), also without consideration of the influence of principal stresses. Saouma and Perotti introduced the dependency on principal stresses to these formulations; however, it is unclear what data were used in the validation of the modified formulations.

$$\xi(t,\theta) = \frac{1 - e^{-\frac{t}{\tau_C(\theta)}}}{1 + e^{-\frac{t - \tau_L\left(\theta,I_\sigma,f_c'\right)}{\tau_C(\theta)}}} \qquad \textit{Equation 4-23}$$

$$\tau_C(\theta) = \tau_C(\theta_o)\cdot e^{U_C\left(\frac{1}{\theta}-\frac{1}{\theta_o}\right)} \qquad \textit{Equation 4-24}$$

$$\tau_L(\theta) = f\left(I_\sigma,f_c'\right)\cdot\tau_L(\theta_o)\cdot e^{U_L\left(\frac{1}{\theta}-\frac{1}{\theta_o}\right)} \qquad \textit{Equation 4-25}$$

$$f\left(I_\sigma,f_c'\right) = \begin{cases} 1, & I_\sigma > 0 \text{ (tension)} \\ 1 + \alpha\dfrac{I_\sigma}{3f_c'}, & I_\sigma \le 0 \text{ (compression)} \end{cases} \qquad \textit{Equation 4-26}$$

where: U_C = activation energy required for reaction at characteristic time
(= 9400 ± 500 K)

U_L = activation energy required for reaction at latency time
(= 5400 ± 500 K)

α = calibration factor (= 4/3)

Formulations for the influence of humidity and absorption of ASR gel in Equations 4-21 and 4-22 are provided in the researchers' technical paper (Saouma and Perotti 2006).

Equations 4-21 or 4-22 are necessary for finite element modeling where structures are modeled as a collection of individual elements that may be subject to different thermal, moisture, and restraint conditions. In other words, this modeling approach can formulaically estimate differential volumetric expansion throughout a structure. This differs significantly from the approaches proposed by Cope et al. (1994) and Charlwood et al. (1992) and is more comparable to the approach proposed by Léger et al. (1996).

In light of recent experimental findings, there are some questions regarding the suitability of some aspects of the formulation comprising Equations 4-21 and 4-22. First, it is unknown whether the correlation between restraint, as taken into consideration through principal stresses, and volumetric expansion development is appropriate. As indicated in Chapter 3, experimentation has not shown a consistent relationship between the two. Second, the presence of the humidity factor as a multiplier on top of the reaction progress factor suggests that volumetric expansion development will not only be slowed, but will be altogether prevented if adequate moisture is not supplied over the course of ASR gel formation. According to this, when gel formation finishes as the reaction is completed, at $\xi = 1$, no further expansion can occur, regardless of how much moisture is present. In other words, if the internal relative humidity of an element drops below 100 % at any point, the maximum amount of volumetric expansion will be reduced and no future exposure to moisture will 'make-up' for the previously limited expansion development. Recently gathered experimental data from the cube study presented in Section 3.4 suggests that delayed exposure to moisture may not necessarily hinder ultimate expansion development. Finally, the formulation is also based on the assumption that increments of volumetric expansion develop as some fraction of the maximum free volumetric expansion, thus requiring an accurate measure of that free expansion. It is extremely difficult to predict the final free expansion that would be achieved by the unrestrained version of a given structure. The researchers indicated that the free expansion could be

derived from laboratory specimens or estimated in some other way. Unfortunately, laboratory-determined free expansions do not correlate to those in real structures due to differences in size and alkali leaching. Unreinforced versions of actual structures cannot be readily produced at proper scale. Even if that were possible, doing so would be a costly and time-consuming effort, and having to wait multiple years, at a minimum, to assess ultimate expansions defeats the purpose of using expansion models to estimate current and near-future behavior. Also, there does not appear to be any existing computational formulation to estimate ultimate expansions.

Once an increment of volumetric expansion for an element has been identified, it is distributed amongst the three principal directions of an element using a weighting distribution system. Fractions of volumetric expansion – weight factors – are evaluated for each principal concrete direction as a function of the three principal concrete stresses that exist during generation of a volumetric expansion increment. These weight factors, *w*, may vary during the course of ASR generation as stress states in concrete change due to changes in applied loading, a build-up of passively induced stresses, or a redistribution of stresses related to changes in material stiffness and/or time-dependent effects. Each weight factor ranges in value from 0 to 1.0, with the factors for the three considered directions summing to 1.0 at all times. For accounting purposes, the three principal directions are denoted as k, l, and m, where k is the direction currently under consideration and l and m are the directions perpendicular to k. Note that directions l and m are denoted arbitrarily.

The researchers provided weight factors, listed in Table 4-1, for 48 combinations of stress in k, l, and m. Specified weight factors apply to what the researchers referred to as "known" or "common sense" stress states. These weight factors are given for stresses equal to 0, $f_t^{'}$, $f_c^{'}$, or a limiting compressive stress, σ_u. Note that tensile stresses are positive and compressive stresses are negative. Tensile stresses are not considered to influence expansion distribution behavior; thus, weight factors are identical for stress states with a positive principal stress, regardless of its value. As a result of this and the interchangeability of k, l, and m depending on which of the three weight factors is being

evaluated, there are actually only 20 unique triaxial stress states for which weight factors are given. The limiting compressive stress serves a similar function as the upper-bound compressive stress limit in the modeling approaches from previous researchers. For some stress states in which a principal compressive stress in a given direction equals or exceeds σ_u, expansions will stop in that direction. The model accounts for this behavior by assigning a weight factor of 0 to that direction during distribution of the current increment of volumetric expansion. A limiting value of -10 MPa is recommended. According to the factors provided, expansions will only stop in uniaxially or biaxially restrained elements (i.e., where at least one principal stress equals zero or is tensile). In triaxially compressed elements, the stress limit does not apply. In this case, concrete will continue to expand in all directions up until at least one principal direction reaches a stress level equal to the uniaxial compressive strength of concrete. Although concrete can be stressed to higher values of compression due to confinement, weight factors are not provided given principal stresses beyond f_c'. It should be noted, however, that it is neither likely nor practical for most concrete structures to achieve such high compressive stresses in service. Sustained, applied compression is limited by designers to mitigate creep effects, and any reinforcement will yield well before such large compressive stresses can be passively induced.

Table 4-1: Saouma and Perotti (2006) weight distribution factors

Perpendicular stress combinations		Weight factors for given stress in Direction k		
Direction l	*Direction m*	≥ 0	σ_u	f_c'
0	0	1/3	0	0
σ_u	0	1/2	0	0
σ_u	σ_u	1	1/3	0
0	σ_u	1/2	0	0
f_c'	0	1/2	0	0
f_c'	σ_u	1	1/2	0
f_c'	f_c'	1	1	1/3
σ_u	f_c'	1	1/2	0
0	f_c'	1/2	0	0
f_t'	f_c'	1/2	0	0
f_t'	σ_u	1/2	0	0
f_t'	0	1/3	0	0
f_t'	f_t'	1/3	0	0
0	f_t'	1/3	0	0
σ_u	f_t'	1/2	0	0
f_c'	f_t'	1/2	0	0

Table 4-1 is used to determine weight factors in two steps:

1. For a given principal stress in k, linear interpolation is used between the three tabulated columns to identify weight factors for each listed combination of stresses in l and m.
2. For a given combination of stresses in l and m, bilinear interpolation is used between four appropriate sets of the 16 listed stress combinations, with their associated weight factors found in Step 1, to compute the weight factor of interest.

The researchers also provided a graphical interpretation of this process, illustrating how the bilinear interpolation from Step 2 matches that used in finite element analyses with bilinear shape functions. This may be found in the researchers' technical paper (Saouma and Perotti 2006).

Once the three weight factors have been evaluated, the portion of the incremental volumetric expansion assigned to each principal direction, *i*, is computed as:

$$\Delta\varepsilon_i^{ASR} = w_i \cdot \Delta\varepsilon_{vol}^{ASR} \qquad \textit{Equation 4-27}$$

Subsequently, the increments of directional expansions are added to previous directional expansions totals, stress states in the concrete material are updated in response to those expansions, and the weight distribution process is repeated for the next increment of volumetric expansion.

As a final note, if the stress state in an element does not change with time, increments of volumetric expansion will always be distributed the same way amongst the principal concrete directions. This will be true regardless of the sizes of the volumetric expansion increments. In other words, the directional expansions will always remain in constant proportion to one another. Consequently, the total expansion in a direction at any time, ε_i^{ASR}, will be directly related to the total volumetric expansion, ε_{vol}^{ASR}, according to Equation 4-28. In general, however, the stress state will not be constant due to shear transfer and a redistribution of load amongst multiple, connected elements or the presence of reinforcement which leads to the passive induction of stresses.

$$\varepsilon_i^{ASR} = w_i \cdot \varepsilon_{vol}^{ASR} \qquad \textit{Equation 4-28}$$

4.4 SUMMARY

Numerical modeling of ASR expansion behavior is the first step toward numerically estimating a structure's overall response to ASR-induced expansions. Analytical tools can be used to provide estimates of expansion as cost-effective alternatives to experimental or field monitoring results. While computational identification of these expansions can serve as a starting point for continuing computational analysis of structural behavior, the expansions could also potentially be

used in the context of codified and concept-based engineering design and analysis formulas or tools to evaluate a structure's response to ASR.

For practical structural engineering applications, single-phase, macroscopic expansion distribution modeling approaches are arguably of the greatest value amongst those available in the literature. These techniques permit the estimation of multi-directional expansion patterns in concrete elements at a global scale, with consideration of the restraint to ASR provided by loading and reinforcement conditions. Existing modeling approaches generally use time-dependent, incremental methodologies to estimate restrained expansions or expansion rates in principal stress directions of concrete elements as a function of existing stress states. These restrained expansions or rates are determined relative to free values. Depending on the specific modeling approach being used, this process is done either directly in individual directions of an element without consideration of any multi-axial interaction between expanding directions or on a volumetric basis, after which expansions are divided up amongst different directions based on the directional distribution of restraint.

The information summarized in this chapter supplies context for the development of an alternative single-phase, macroscopic expansion distribution modeling approach that is presented in Chapters 5 and 6.

CHAPTER 5: DISTRIBUTED VOLUMETRIC EXPANSION PRESSURE MODEL – BACKGROUND AND DEVELOPMENT*

5.1 OVERVIEW

The formulation of the Distributed Volumetric Expansion Pressure (DVEP) model, a mechanics-based approach for estimating the multi-directional distribution of volumetric expansions in RC elements occurring as a result of ASR, is presented in this chapter. Successful identification of the amounts and patterns of expansion in RC is important for the evaluation of ASR-induced material stresses and concrete property degradation, parameters which should be considered in assessing the life-cycle performance of structures affected by ASR. Key differences and features of the proposed modeling procedure (as compared to existing procedures described in Chapter 4), model details, and model limitations are discussed. A non-incremental, time-independent procedure is used to determine simultaneous ASR-induced concrete expansions in orthogonal reinforcement directions of RC elements. In calculating element expansions, the modeling procedure considers independent influences associated with applied loading and passive restraint effects stemming from steel reinforcement, the influence of orthogonal steel reinforcement ratios and reinforcing bar configurations, and expansion behavior prior to and following yielding of reinforcement.

* Portions of this chapter have been extracted directly from the following prospective publication (unpublished at time of dissertation submission) written by the author of this dissertation, with figures and tables reformatted for use in this dissertation:

Wald, D. M., Hrynyk, T. D., and Bayrak, O. (2017). "The Distributed Volumetric Expansion Pressure Model for ASR Expansion Behavior in Reinforced Concrete Elements – Part 1: Background and Development." (submitted to *ASCE Journal of Structural Engineering*)

- Dissertator contribution: Primary author and lead researcher

5.2 DISTRIBUTED VOLUMETRIC EXPANSION PRESSURE MODEL – AN OVERVIEW

Ongoing research efforts at the University of Texas at Austin have resulted in the development of the Distributed Volumetric Expansion Pressure (DVEP) model, a simple procedure aimed at estimating the multi-axial distribution of ASR-induced volumetric expansions within RC elements. The DVEP model is distinguished from existing modeling approaches by the following: 1) a non-incremental analysis approach is used, 2) expansions are not identified as a function of time, 3) expansions are evaluated in a fixed, rather than principal, coordinate system, 4) the influences of applied stresses and passive restraint are treated independently, and 5) expansion behavior is assumed to occur in stages delineated by points where reinforcement yields or expansions plateau prior to the yielding of reinforcement.

5.2.1 Non-incremental Analysis Approach

The DVEP model employs an approach in which ASR expansions develop according to constitutive laws related to internal expansion pressures that build over time. Expansions in orthotropic directions, summing to a volumetric expansion, are assumed to be interrelated and are developed in response to distributed, direction-dependent expansion pressures comprising a volumetric expansion pressure (VEP). The VEP is divided into orthogonal components with due consideration of the influences of applied stresses, reinforcing bar layouts, and yielding of reinforcement.

A non-incremental analysis approach is utilized in which prior stress-strain history need not be considered. That is, the directional distribution of a total volumetric expansion can be evaluated without having to progressively build up to the target expansion using increments or steps. Such a technique is computationally expedient, it eliminates inaccuracies associated with increment size selection, and it is particularly beneficial for potential performance assessment applications in which behavior at some threshold expansion level is of interest.

5.2.2 Time-Independent Approach

The manner in which concrete expands in adjacent orthogonal directions of an element is isolated from temporal factors such as temperature, humidity, and creep. The model is based on the assumption that time only influences when expansions and cracking occur but not how and why concrete expands in certain patterns with specific interactions in behavior amongst different directions. Regardless of how quickly or slowly an element expands volumetrically, any amount of volumetric expansion that is expected to develop can be distributed amongst orthogonal reinforcement directions. This process is performed in response to reinforcement layouts and percentages in those directions, nondegraded concrete and steel material properties, and any initial applied loading conditions sustained during ASR generation. Although estimating expansion behavior with time would be useful for addressing durability-related concerns, the proposed model is largely intended for use in assessing current and future structural behavior and performance.

The requirement to estimate ASR expansions over time is eliminated because: a) structures are subdivided into lumped zones of like volumetric expansion development, and b) expansions are identified with constitutive formulations rather than as a function of pre-existing stress states. Portions of a structure with the same approximate reactivity, temperature and moisture profiles, and number of reinforced orthogonal directions (up to three) are assumed to develop common volumetric expansions. The volumetric expansion within individual elements in a zone is distributed to orthogonal axes in accordance with element applied stresses and reinforcement conditions. Redistribution of stresses between elements due to changes in concrete stiffness or phenomena like creep are assumed to have a negligible influence on overall expansion behavior. Further, only the initially applied stresses on an element are considered in analysis, barring any abrupt changes in sustained external loading on the structure.

One possible method of relating differential volumetric expansion development between zones with varying environmental or restraint conditions is to use constant scaling factors, much in the same way as multipliers were introduced by Leger et al.

(1996). Scaling factors related to the number of effective reinforcement directions of an element are suggested based on experimental results from Wald et al. (2017b). No scaling factors are currently proposed to account for the role of applied loading on volumetric expansion development due to a lack of consensus among the findings of research studies performed to date and as a result of a limited set of relevant data.

5.2.3 Reinforcement Coordinate System

Expansions are evaluated in orthogonal directions aligned with the reinforcement; however, these expansions can be related to any desired coordinate system (e.g., the principle stress directions) using simple transformation methods. Expansions are determined in this "reinforcement coordinate system" (RCS) to accommodate constitutive formulations that are defined relative to reinforcement directions. The effects of applied restraint are also considered in the RCS.

5.2.4 Distinction between Effects of Applied and Passive Restraint

The DVEP model distinguishes between how active restraint (i.e., sustained applied loading) and passive restraint (e.g., that associated with embedded reinforcement) influence expansion development and distribution. This approach was developed in response to experimental results demonstrating continued ASR expansion development in RC specimens given passively induced stresses exceeding the applied stresses found to mitigate expansions in plain concrete specimens (Cope et al. 1994).

Rather than adopting mathematical relationships between expansions and passively induced stresses, the DVEP model evaluates expansions as the net result of the kinematic compatibility between expanding concrete and any internally embedded or externally anchored reinforcement. Other forms of passive restraint within a structure, such as adjacent nonexpanding structural components, resist expansions and instigate localized compressive stresses but are not considered by the model to change the way expansions are distributed within the structure.

Applied stresses influence the distribution of expansions in accordance with the expansion transfer concept. The model accounts for expansion transfer indirectly by allowing the applied stress state to influence the multi-directional distribution, or the "transfer," of the expansion pressures which ultimately lead to element expansions.

5.2.5 Staged Behavior

Experimental evidence has suggested that ASR expansion distribution behavior in RC elements can change abruptly over time. In one case (Bracci et al. 2012), the rate of expansion (and thus contribution to volumetric expansion) for a reinforced direction was shown to be influenced after the measured expansions exceeded the yield strain of the steel. In another case (Wald et al. 2017a), the expansions in the reinforced directions of a test specimen plateaued before yielding of the steel while a third orthogonal direction continued to expand. These phenomena are depicted in Figure 5-1, which shows the breakdown of volumetric expansions into orthogonal components for two representative ASR-affected specimens. During early development of volumetric expansions for both specimens, the directional expansions were approximately proportional, as illustrated by the initial linearity of plotlines. However, after reaching some level of volumetric expansion, the slopes of these plotlines either became zero at pre-yield levels of expansion (indicating expansion plateauing) or significantly changed at approximately 0.2 % expansion (i.e., the approximate yield strain of steel reinforcing bars used in these cases). The DVEP model accounts for these abrupt changes in expansion behavior by treating ASR expansion behavior as a multi-stage phenomenon in which behavior is described using different formulae, corresponding to pre- and post-yield reinforcement response and the plateauing of expansions.

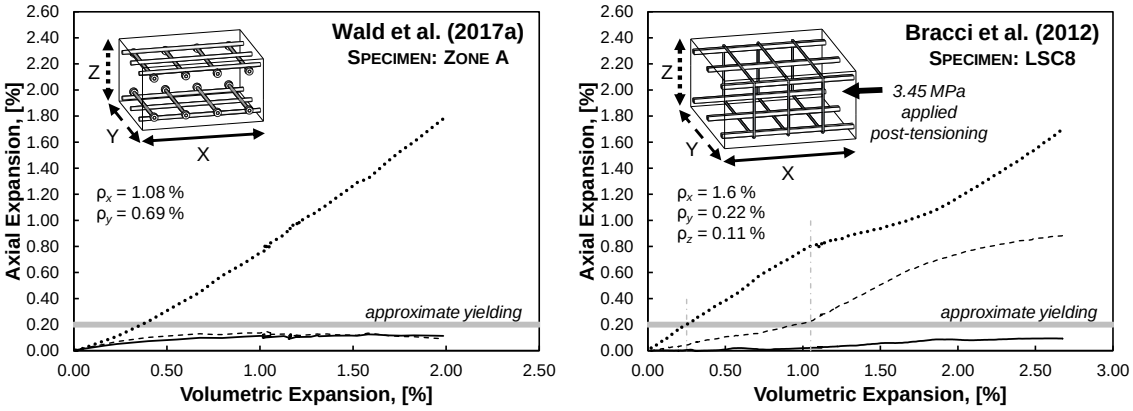

(a) Pre-yield Plateauing (b) Reinforcement Yielding

Figure 5-1: Experimental evidence of transitions in expansion behavior

5.3 DETAILS OF DVEP MODEL

A two-phase process is used to identify the distribution of ASR-induced expansions of RC elements. In Phase I, definition of the constitutive relationships and their input parameters is done to describe how concrete will expand in interacting directions of the RCS in response to some overall VEP. Required user input parameters include concrete and steel reinforcement material strengths and stiffnesses, reinforcement ratios and reinforcing bar spacings, and initially applied, sustained loads. In Phase II, the constitutive formulations defined in Phase I can be used to evaluate the associated expansion distribution pattern for any level of volumetric ASR expansion.

5.3.1 Phase I

Preceding any calculations of ASR expansion distribution, a RC structure being analyzed should first be divided into separate zones with similar properties for analysis. Namely, a structure will be separated into regions of unreinforced, uniaxially reinforced, biaxially reinforced, and/or triaxially reinforced concrete, each with a given set of concrete and steel material properties (e.g., moduli of elasticity). Individual structural members (e.g., beams) or laboratory specimens (e.g., cylinders or prisms) are generally recommended to be represented by single lumped zones to assess global, average expansion behavior. In such cases, these structures are considered to be entirely

"effectively" reinforced in all RCS directions containing at least one reinforcing bar. If desired, these components may be broken down into multiple zones to investigate any potential, differential local expansion behavior, particularly if there are prominent regions of plain concrete located between widely-spaced layers of reinforcing bars. In larger, continuous structures (e.g., walls or dams) detailed with multiple reinforcement configurations or regions of differential volumetric expansion development, the structure should be subdivided into multiple zones. Where multiple analysis zones are used, concrete may be considered "effectively" reinforced in an RCS direction when within 7.5 bar diameters (d_b) from at least one reinforcing bar. This value stems from that employed in crack spacing calculations (CEB-FIP Model Code 1990), and it was selected in accordance with experimental findings from Wald et al. (2017a) in which ASR expansions were identified to be fairly uniform for concrete within $7d_b$ of a bar.

Regardless of the number of analysis zones considered, each zone may be further divided, as needed, into any number of individual elements for analysis. Within a given region of a structure, an element which is effectively reinforced in a particular direction is assigned the gross reinforcement ratio (area of steel divided by area of concrete) of the structural region in that direction. It is important to note that element reinforcement ratios are not computed according to zonal areas.

The following sections detail the three primary computational features of Phase I that are used to describe ASR expansion behavior of an RC element: 1) constitutive formulations relating element expansions to expansion pressures in the three RCS directions, 2) division of VEPs into directional components, and 3) identification of stage-specific behavior such as reinforcement yielding or expansion plateauing in a given direction. The three items are presented in the above order for clarity; however, note that these items are not mutually exclusive. The constitutive relationships and VEP distribution needed to estimate expansions during a particular stage depend on specific behavior that is in turn a function of the expansions generated during earlier stages. The Phase I response calculations are performed using a subsequently outlined step-by-step procedure.

5.3.1.1 Constitutive Relationships for Expansion Pressures and Expansions

ASR expansions in concrete are designated as concrete material prestrains with the notation, ε^{ASR}. These prestrains are treated as stress-independent "free" strains for analysis much like the prestrains in concrete due to shrinkage or thermal expansion. The total strain in the concrete element, ε, consists of all prestrains plus the net strain due to stress, ε_c, in the concrete. Compressive or tensile stress-strain relationships pertain to the net strain which develops in response to applied loads and via passive restraint to the prestrains.

ASR expansions in concrete are related to developing expansion pressures in the three RCS directions using multi-part formulations. The first part is used to identify expansions in a given direction prior to the yielding of any reinforcement in that direction. The second is used to identify expansions in either an unreinforced direction or in a direction with reinforcement that has yielded. These constitutive relationships are described below and depicted in Figures 5-2 to 5-5.

5.3.1.1.1 Reinforced Directions before Yielding

Expansions in pre-yielded, reinforced directions of an element are computed in response to an increasing internal expansion pressure using conventional RC equilibrium and compatibility relations. Derivation of the relationship between expansions and expansion pressures begins with Equation 5-1, which is used to describe the uniaxial response of an unloaded RC element subject to concrete ASR prestrains and assuming perfect bond between concrete and embedded reinforcement:

$$\overline{E}_c\left(\varepsilon - \varepsilon^{ASR}\right) + \rho E_s \varepsilon = 0 \qquad \textit{Equation 5-1}$$

where ρ is the axial reinforcement ratio, E_s is the elastic modulus of steel, and $\overline{E}_c$ is the secant modulus of elasticity of compressed concrete.

The model postulates that the reinforcement is tensioned with a force equal to an internal expansion pressure due to ASR, σ^{exp}, acting uniformly over the cross-sectional area of concrete. This ASR-induced prestressing effect results in the following expression in terms of the smeared steel stress ($\rho\sigma_s$):

$$\rho\sigma_s = \rho E_s \varepsilon = \sigma^{exp} \qquad \textit{Equation 5-2}$$

Equations 5-1 and 5-2 are combined to give Equation 5-3 identifying the ASR expansion in concrete in the pre-yielded, reinforced direction, *i*, corresponding to the direction-dependent expansion pressure, σ_i^{exp}:

$$\varepsilon_i^{ASR} = \sigma_i^{exp} \cdot \left(\frac{1}{\overline{E}_c} + \frac{1}{\rho E_s}\right)_i \qquad \textit{Equation 5-3}$$

RC is treated as a smeared material where stresses and strains in an element reflect average material behavior. The reinforcement ratio and modulus of elasticity of steel in Equation 5-3 are constants that can be easily defined. For practicality, the secant modulus for concrete in compression, $\overline{E}_c$, may be replaced with a constant, nondegraded initial tangent modulus of concrete, E_c, due to the fact that the comparatively low stiffness of the smeared reinforcement (ρE_s) will typically have a much greater influence on the expansion response of the RC element than will the stiffness of the concrete.

Equation 5-3 directly captures the influence of reinforcement, through the use of ρ, acting as restraint to expansion in a single direction. Increased reinforcement ratios will result in reductions in expansions stemming from a given expansion pressure. If an element is unreinforced in a considered direction, Equation 5-3 becomes unsolvable, thus necessitating a different formulation to estimate expansions. As discussed later, the influence of applied loads and the mechanism by which reinforcement influences expansions in other expanding directions are indirectly captured through the value of expansion pressure, σ_i^{exp}, that is input into Equation 5-3. This expansion pressure is not a wholly independent variable that can be arbitrarily selected; expansion pressures in all three RCS directions are interrelated and sum to a VEP, σ_{vol}^{exp}. In other words, the VEP must be selected with a corresponding set of appropriately proportioned expansion pressures for use in the constitutive formulations for each independent direction. For clarity, Equation 5-3 is rewritten in functional form in Equation 5-4. The functional dependency of directional expansions and pressures on volumetric pressures is implied henceforth where not explicitly noted.

$$\varepsilon_i^{ASR}\left(\sigma_{vol}^{exp}\right) = \sigma_i^{exp}\left(\sigma_{vol}^{exp}\right) \cdot \left[\frac{1}{\bar{E}_c} + \frac{1}{\rho E_s}\right]_i \qquad \textit{Equation 5-4}$$

It is important to clarify that any simplifications made in deriving or using Equations 5-3 and 5-4 pertain only to the process of estimating ASR expansions. These simplifications include treating concrete as a linear-elastic material, using a nondegraded concrete stiffness, ignoring other concrete prestrains, and not considering applied stresses as part of the original equilibrium expression. Once expansions have been identified, the response of a structure to those expansions and/or applied loads may be identified with traditional methods while treating concrete as a nonlinear material, using any appropriate degraded concrete properties, and considering other concrete prestrains.

5.3.1.1.2 Unreinforced Directions or Reinforced Directions after Yielding

It is proposed that yielding of reinforcement in a given direction represents a loss of effective passive restraint (EPR) to subsequent element expansions that occur in that direction after yielding. An element is treated approximately, though not precisely, as if reinforced in one fewer direction following every instance of yielding in one of the three RCS directions. This results in up to four stages of ASR expansion behavior (one pre-yield and three post-yield) to consider during analyses. In the most extreme case, an element reinforced in three orthogonal directions may experience stages of effective triaxially restrained, biaxially restrained, uniaxially restrained, and unrestrained expansion. Note that yielded reinforcement is not physically removed from an element nor do the yield-level stresses passively developed in the element dissipate; the amount, but not the presence and layout, of such reinforcement is conceptually neglected for post-yield expansion evaluation. Meanwhile, an element that is unreinforced in a direction lacks effective passive restraint in that direction from the outset. Biaxially reinforced, uniaxially reinforced, and unreinforced elements are thus analyzed as being equivalent to triaxially reinforced elements that have “pre-yielded” in one, two, or three directions, respectively.

Equation 5-5 is used to compute the total expansion in any unreinforced direction or in a reinforced direction after yielding at a given point of interest (POI) during ASR stage *n*:

$$\varepsilon_i^{ASR} = \varepsilon_{i,py}^{ASR} + \sum_{\substack{\text{1st post-}\\ \text{yield stage}}}^{n\ (\text{POI})} \Delta\varepsilon_{i,n}^{ASR} \qquad \textit{Equation 5-5}$$

where $\varepsilon_{i,py}^{ASR}$ is the expansion in *i* developed prior to a loss of effective passive restraint and $\Delta\varepsilon_{i,n}^{ASR}$ is the expansion in *i* developed during stage *n*.

The total expansion is comprised of any expansion in *i* prior to and after a loss of effective passive restraint (first and second terms of Equation 5-5, respectively). The term $\varepsilon_{i,py}^{ASR}$ equals zero in an unreinforced direction which lacks effective passive restraint from the start. In a reinforced direction, $\varepsilon_{i,py}^{ASR}$ is evaluated from Equation 5-3 using the expansion pressure identified to cause yielding.

Without effective passive restraint, continued expansions develop on a stage-by-stage basis. At a particular point of interest during stage *n*, the additional expansion developed in a direction lacking effective passive restraint will be the summation of all stage-specific expansions which develop after the loss of effective passive restraint up until the point of interest. A transition between stages occurs any time reinforcement in one of the three RCS directions yields (i.e., a loss of effective passive restraint) or if expansions plateau prior to yielding in one of the three directions. Each of these transitions is referred to as a "critical event" (CEV).

The stage-specific expansions which develop following a loss of effective passive restraint are computed as:

$$\Delta\varepsilon_{i,n}^{ASR} = \begin{cases} \dfrac{\Delta\sigma_{i,n}^{exp}}{\Sigma\Delta\sigma_{eprd,n}^{exp}} \cdot \Sigma\Delta\varepsilon_{eprd,n}^{ASR} & \text{for } n = 2, 3 \\ \dfrac{\Delta\sigma_{i,n}^{exp}}{\Delta\sigma_{vol,n}^{exp}} \cdot \Delta\varepsilon_{vol,n}^{ASR} & \text{for } n = 4 \end{cases} \qquad \textit{Equation 5-6}$$

While at least one RCS direction maintains effective passive restraint during Stages 2 or 3, the stage-specific expansion developing in a considered direction without effective passive restraint, $\Delta\varepsilon_{i,n}^{ASR}$, is evaluated as being proportional to the sum of same-

stage expansions in the direction(s) with maintained effective passive restraint, $\Sigma\Delta\varepsilon^{ASR}_{eprd,n}$. The constant of proportionality will be the ratio of stage-specific expansion pressure in the direction considered, $\Delta\sigma^{exp}_{i,n}$, to the sum of stage-specific pressures in the direction(s) with maintained effective passive restraint, $\Sigma\Delta\sigma^{exp}_{eprd,n}$.

During Stage 4, all RCS directions will have either yielded or stopped expanding. At this point, the partial volumetric expansion, $\Delta\varepsilon^{ASR}_{vol,n}$, developed during Stage 4 is simply distributed in some fixed proportion amongst the three orthogonal directions. The fraction of volumetric expansion distributed to a given direction is equal to the ratio of the partial directional expansion pressure to the partial VEP, $\Delta\sigma^{exp}_{vol,n}$, developed during Stage 4.

As an example, consider a triaxially reinforced element with directions D1, D2, and D3 for which the expansion in D1 at a point during Stage 3 is to be determined. If the reinforcement in D1 yields at the end of Stage 1 (i.e., yielding in D1 before D2 and D3), the expansion developed after a loss of effective passive restraint will consist of that from Stage 2 and from Stage 3 up until the point of interest (Figure 5-2).

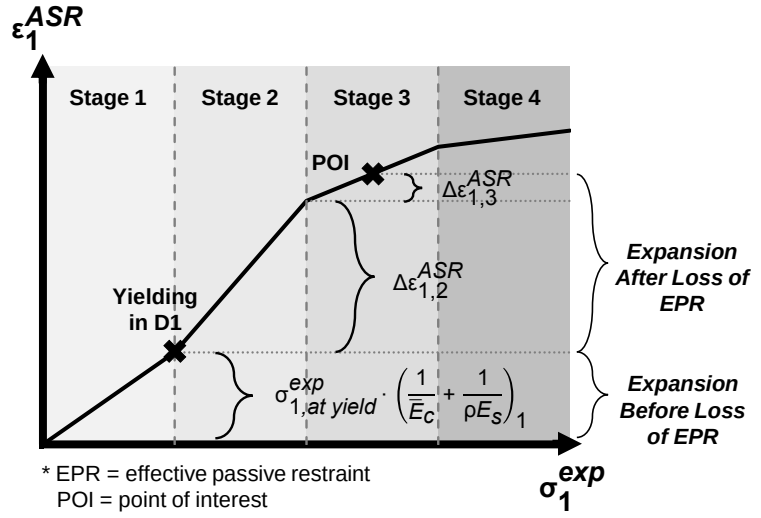

Figure 5-2: Graphical interpretation of computing expansion in a direction following yielding of reinforcement in that direction

5.3.1.1.3 Expansions Plateauing Prior to Yielding

As previously indicated, it is possible for concrete to completely stop expanding in a reinforced direction prior to yielding of the reinforcement (i.e., before a loss of effective passive restraint) or before a depletion of all ASR reactants while continuing to expand in other directions. Such a phenomenon is considered a type of critical event upon which ASR behavior transitions between stages. A limiting total expansion pressure, discussed later, is imposed for Equation 5-3 to cap expansions in that direction. Meanwhile, Equations 5-5 and 5-6 remain valid for directions that have lost effective passive restraint. Although a direction with a plateaued expansion still maintains effective passive restraint, that direction is "critically restrained" such that no additional expansion or pressure can develop. Consequently, this direction contributes zero-values to the summation terms of Equation 5-6.

5.3.1.1.4 Summary of Constitutive Response

Ultimately, each of the three RCS directional expansion versus expansion pressure relationships defined across all stages of expansion behavior will take on one of six generic forms depicted in Figure 5-3. Type A curves reflect behavior when reinforcement in a given direction yields while Type B curves reflect behavior when expansions plateau prior to yielding of reinforcement. Type 1, 2, and 3 curves illustrate whether critical events associated with a given direction occur first, second, or third, respectively, amongst the three orthogonal directions. For the three RCS directions, there will be only one of each of the numbered curves represented.

The curves highlight the simplicity of the DVEP model: ASR constitutive relationships are defined as piecewise continuous functions of linear segments. For clarity, as behavior transitions between stages where different formulae are used, the slopes of the line segments are depicted to change. The actual slopes will be determined once the expansions and expansion pressures are identified for critical events. Note that these slopes will not necessarily decrease in steepness from one stage to the next as is shown in Figure 5-3; however, the slopes will always be non-negative. For an element

with one or more unreinforced directions, the curves will simplify to consisting of fewer segments. As an example, in a biaxially reinforced element, each curve will only consist of three line segments. The first critical event – a "loss" of effective passive restraint in the unreinforced direction – occurs immediately before any expansion pressure builds, such that nothing actually happens during Stage 1 and the associated line segment resolves to a point at the origin of the plot. It should also be noted that, generally, the three curves for an element will be uniquely different except where two or three directions of the RCS are both unreinforced or contain identical reinforcement conditions (e.g., same amount, properties, and basic layout of reinforcement).

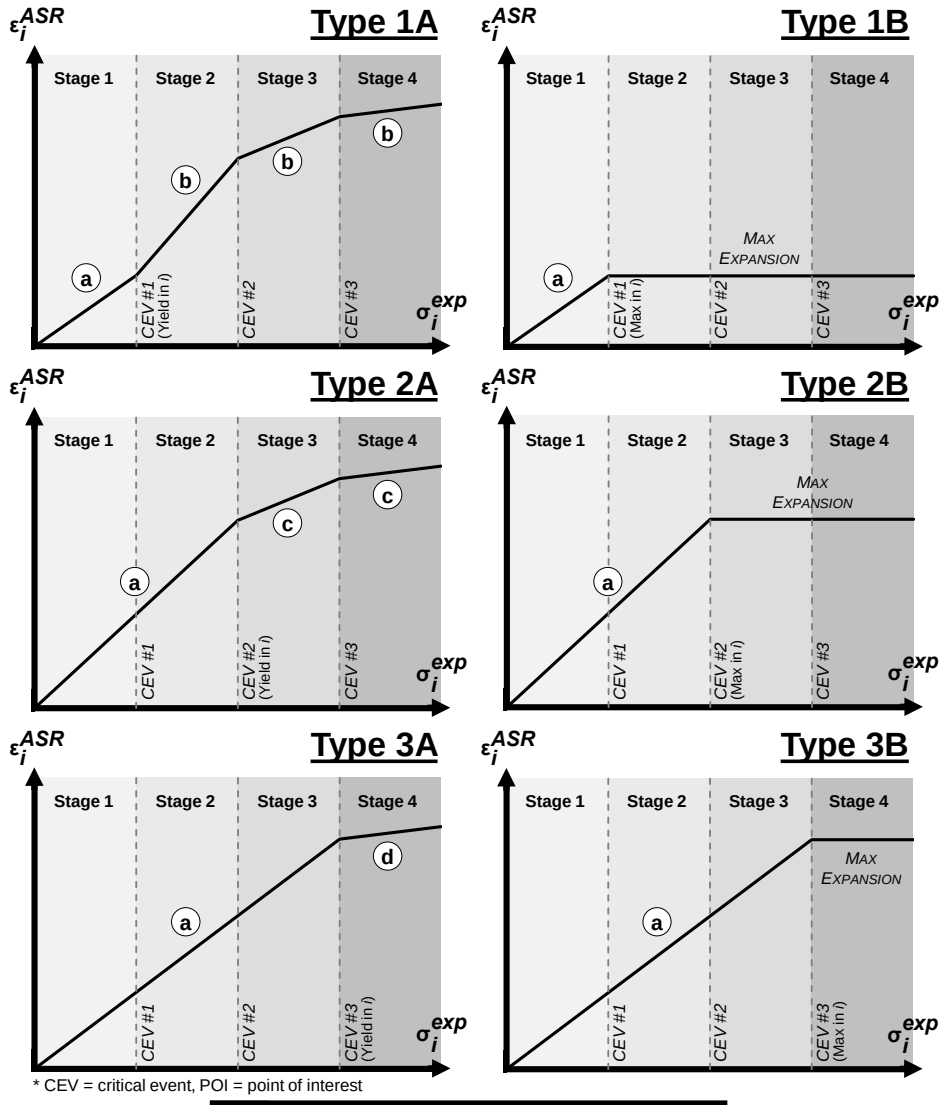

* CEV = critical event, POI = point of interest

Formulas

(a) $\varepsilon_i^{ASR} = \sigma_i^{exp} \cdot \left(\frac{1}{\bar{E}_c} + \frac{1}{\rho E_s}\right)_i$

(b) $\varepsilon_i^{ASR} = \varepsilon_{i,py}^{ASR} + \sum_{n=2}^{2,3, \text{ or } 4 \text{ (POI)}} \Delta\varepsilon_{i,n}^{ASR}$

(c) $\varepsilon_i^{ASR} = \varepsilon_{i,py}^{ASR} + \sum_{n=3}^{3 \text{ or } 4 \text{ (POI)}} \Delta\varepsilon_{i,n}^{ASR}$

(d) $\varepsilon_i^{ASR} = \varepsilon_{i,py}^{ASR} + \sum_{n=4}^{4 \text{ (POI)}} \Delta\varepsilon_{i,n}^{ASR}$

where: $\Delta\varepsilon_{i,n}^{ASR} = \begin{cases} \frac{\Delta\sigma_{i,n}^{exp}}{\Sigma\Delta\sigma_{eprd,n}^{exp}} \cdot \Sigma\Delta\varepsilon_{eprd,n}^{ASR} & \text{for } n = 2, 3 \\ \frac{\Delta\sigma_{i,n}^{exp}}{\Delta\sigma_{vol,n}^{exp}} \cdot \Delta\varepsilon_{vol,n}^{ASR} & \text{for } n = 4 \end{cases}$

Figure 5-3: Directional expansion vs. direction expansion pressure curves

5.3.1.2 Directional Distribution of Volumetric Expansion Pressures

Analogous to the weighting factors used to distribute incremental volumetric expansions in the model proposed by Saouma and Perotti (2006), the DVEP model incorporates pressure distribution factors, κ_{ni}, to distribute VEP amongst the three RCS directions. Up to four sets of three pressure distribution factors must be identified to describe behavior during the four potential stages of ASR behavior. The use of these factors implies that the stage-specific partial VEP that builds is distributed amongst the three directions in constant proportion during that stage. The partial expansion pressure in *i* that develops during stage *n* is given as:

$$\Delta\sigma_{i,n}^{exp} = \kappa_{ni} \cdot \Delta\sigma_{vol,n}^{exp} \qquad \textit{Equation 5-7a}$$

The stage-specific partial VEP is the sum of all same-stage directional expansion pressures:

$$\Delta\sigma_{vol,n}^{exp} = \sum_{i=1}^{3} \Delta\sigma_{i,n}^{exp} \qquad \textit{Equation 5-7b}$$

Figure 5-4 illustrates the relationship between directional and volumetric expansion pressures. At a given point of interest, the total pressure in *i* is simply taken as the sum of stage-specific pressures in that direction up until the point of interest:

$$\sigma_{i}^{exp} = \sum_{1}^{n\,(\mathrm{POI})} \Delta\sigma_{i,n}^{exp} \qquad \textit{Equation 5-8a}$$

The total VEP is the sum of all directional expansion pressures:

$$\sigma_{vol}^{exp} = \sum_{i=1}^{3} \sigma_{i}^{exp} \qquad \textit{Equation 5-8b}$$

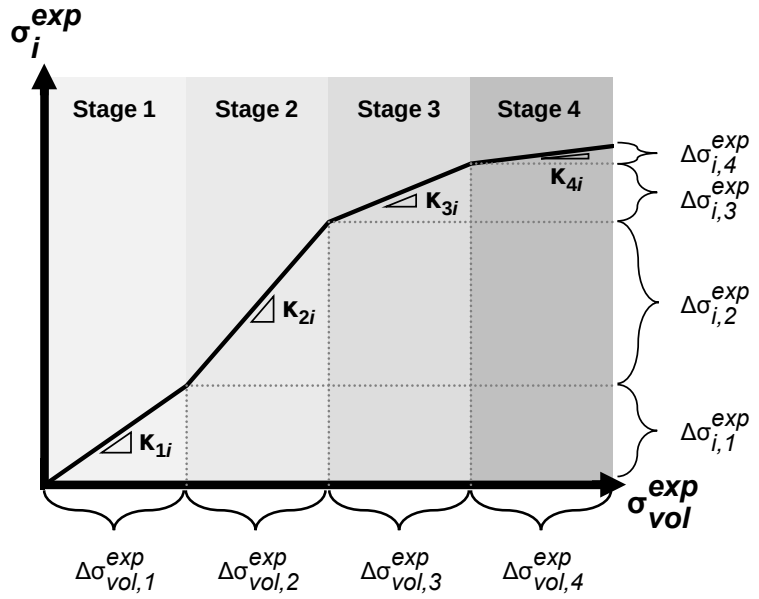

Figure 5-4: Directional expansion pressure vs. volumetric expansion pressure relationship

Combining Equations 5-7a and 5-8a with 5-3 and 5-6 results in expanded expressions for pre-yield directional expansions and stage-specific expansions developed after a loss of effective passive restraint which now reflect dependence on a VEP:

Pre-yield: $$\varepsilon_i^{ASR} = \left(\sum_1^{n\,(\mathrm{POI})} \kappa_{ni} \cdot \Delta\sigma_{vol,n}^{exp}\right) \cdot \left(\frac{1}{\bar{E}_c} + \frac{1}{\rho E_s}\right)_i$$ *Equation 5-9*

Post-EPR-loss: $$\Delta\varepsilon_{i,n}^{ASR} = \begin{cases} \frac{\kappa_{ni}}{\Sigma\kappa_{n,eprd}} \cdot \Sigma\Delta\varepsilon_{eprd,n}^{ASR} & \text{for } n = 2, 3 \\ \kappa_{ni} \cdot \Delta\varepsilon_{vol,n}^{ASR} & \text{for } n = 4 \end{cases}$$ *Equation 5-10*

where $\Sigma\kappa_{n,eprd}$ is the sum of pressure distribution factors for directions with maintained effective passive restraint during stage *n*.

Figure 5-5 depicts updates to Figure 5-3 with relationships between directional expansions and pressures transformed into relationships between directional expansions and VEPs. Note that these relationships are still linear during each stage. Further, due to this linearity, the overarching relationship between volumetric expansions (i.e., the sum of directional expansions) and VEPs will also be linear during each stage of expansion.

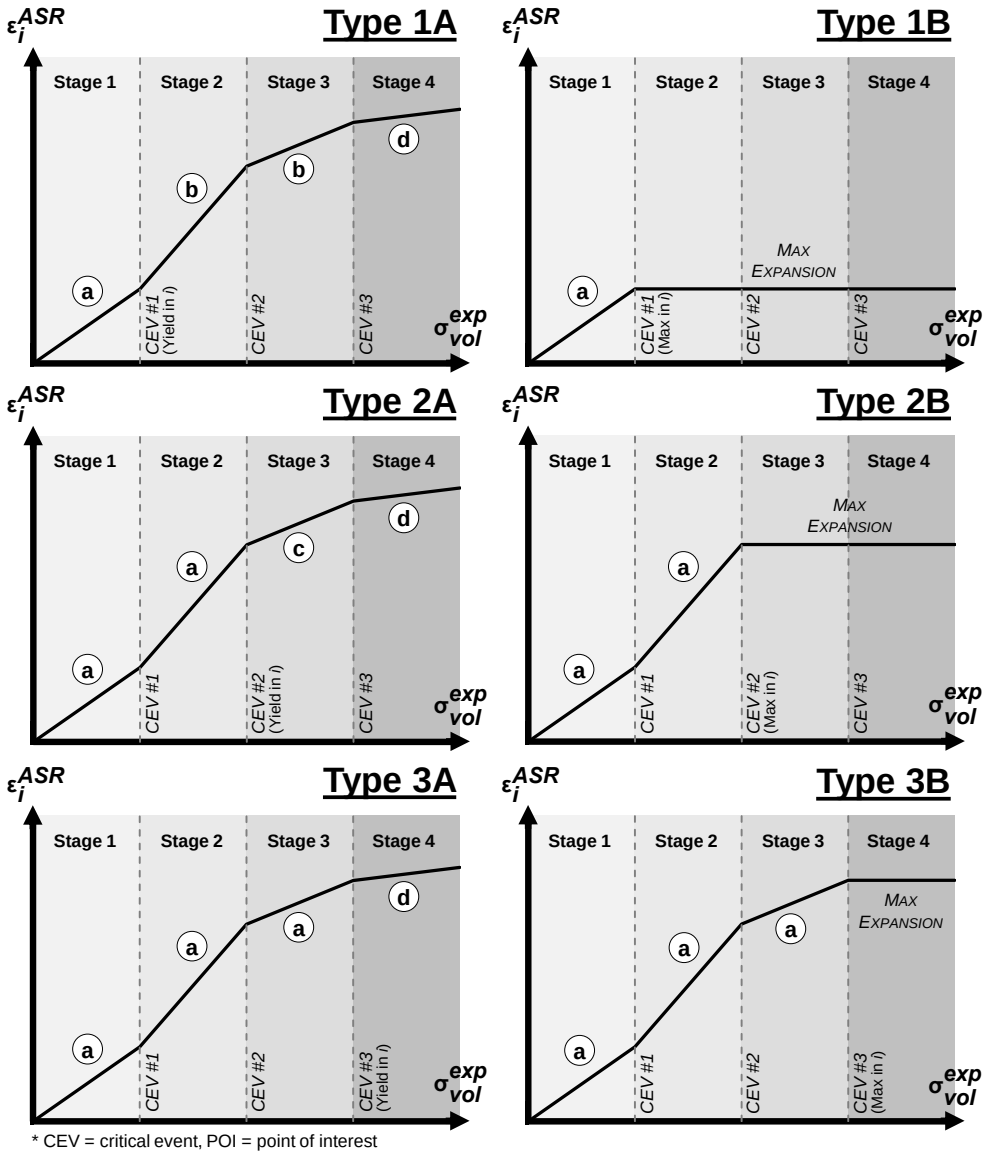

Figure 5-5: Directional expansion vs. volumetric expansion pressure curves

5.3.1.2.1 Background on Pressure Distribution Factors

A VEP is distributed uniquely during each stage of behavior in response to the initial applied stress state for an element, reinforcing bar layouts, and critical event behavior. Through this pressure distribution, the influence of applied restraint and the multi-axial influence of reinforcement, both previously unaccounted for during constitutive relationship development, are addressed. The fraction of VEP that develops in a direction is given by κ_{ni}. Each individual factor ranges from 0 to 1.0, while the three factors for any individual stage of behavior must sum to 1.0 (i.e., the direction-dependent pressures must sum to the VEP).

The DVEP model originated under a mechanics-based assumption of uniform internal expansion pressure distribution for an element given uniform restraint conditions (i.e., same amount and layout of reinforcement and/or applied loading in all directions). Any deviation from uniformity of restraint will result in a nonuniform distribution of expansion pressures. Assessment of the nonuniformity of expansion pressures is driven by two experimental observations: 1) the expansion transfer concept, and 2) differential expansion distribution behavior given different reinforcement layouts.

Recall that it has been suggested that an element under an increasing applied compressive stress will expand less in the stressed direction and more in other directions to preserve a constant volumetric expansion. The DVEP model accounts for expansion transfer indirectly by adopting a similar, expansion pressure transfer concept. Conceptually, an applied stress in one direction counteracts expansion pressure development in that direction but promotes increased pressure development in other directions to preserve a VEP.

Reinforcement layouts, namely bar spacing, appear to influence expansion behavior as well. Figure 5-6 compares the axial distribution of low-level volumetric expansions for two biaxially-reinforced specimens monitored at the University of Texas at Austin: a 610 mm deep beam with reinforcement provided in two layers spaced 380 to 450 mm apart and a 480 mm cube element with reinforcement spaced in three layers at approximately 200 mm (Wald et al. 2017a, b). These specimens were fabricated using the

same concrete mixture designs and contained similar gross reinforcing ratios (1.1 % and 0.7 % for the beam; 1.1 % and 0.5 % for the cube). Thus, the primary difference in specimen design was the bar spacing. While each specimen generally expanded more in the unreinforced direction than in reinforced directions on average, the difference in expansions between the reinforced and unreinforced directions was greater for the beam. A larger bar spacing resulted in a greater transfer of expansions to the unreinforced direction at each given volumetric expansion. It is thought that this behavior may relate to the fact that, given some internal expansion pressure, the compressive stresses developing in concrete local to reinforcement should be greater when using fewer bars spaced farther apart. The DVEP model accounts for this behavior by instituting increased expansion pressure transfer from a reinforced direction as the maximum bar spacing in that direction increases.

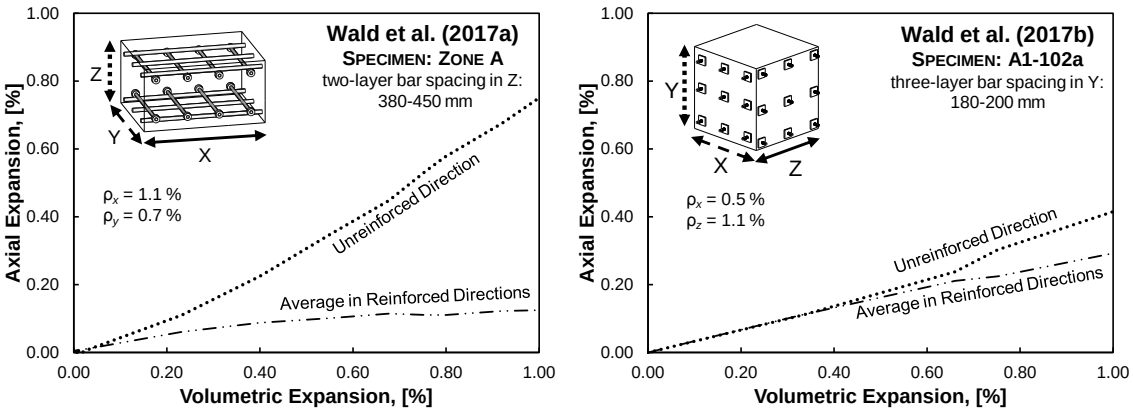

Figure 5-6: Experimental evidence of differential expansion behavior for variable reinforcing bar spacings

5.3.1.2.2 Evaluating Pressure Distribution Factors

Pressure distribution factors are computed in each RCS direction during each stage of behavior in two steps. First, a minimum fraction of VEP, λ_{ni}, is assigned to each direction as a function of applied stresses and reinforcing bar layouts. A minimum is necessitated because the expansion pressures cause expansions, and, in most instances, concrete will always expand to some degree in each direction. Second, the remaining

fraction of pressure not yet assigned is distributed amongst any direction(s) of "least resistance" in a manner that accommodates expansion pressure transfer and accounts for critical event behavior.

The λ_{ni} factors range in value from 0 to 1/3 and are computed as a function of influence factors accounting for sustained levels of applied stress, $\lambda_{\sigma i}$, and reinforcement layout, $\lambda_{\rho i}$:

$$\lambda_{ni} = 1/3 \cdot \lambda_{\sigma i} \cdot \lambda_{\rho i} \qquad \textit{Equation 5-11}$$

During any stages where expansions have plateaued in a given direction, λ_{ni} is taken as 0. Otherwise, λ_{ni} factors are computed with Equation 5-11 and will be constant during all stages with ongoing expansions. The $\lambda_{\sigma i}$ and $\lambda_{\rho i}$ factors range in value from 0 to 1.0. Applied stress factors are computed based on the initial, sustained normal compressive stress in the concrete material in each direction, σ_{ci}, and an upper-bound applied stress limit, σ_{max}, as:

$$\lambda_{\sigma i} = 1 - \frac{\sigma_{ci}}{\sigma_{max}} \qquad \textit{Equation 5-12}$$

The $\lambda_{\sigma i}$ factor linearly decreases with increasing applied compressive stress, thus reducing λ_{ni} and permitting a greater percentage of VEP to be transferred to other directions. This function is consistent with formulae incorporated in other models suggesting a linear reduction in expansions with increasing applied compression (Cope et al. 1994; Saouma and Perotti 2006). Only initial values of sustained compression are used; recall, the model considers any redistribution of applied stresses in an element due to factors such as creep or stiffness degradation to be negligible. Sustained tension is not considered to influence expansion pressure distribution. The DVEP model supports the use of a maximum applied stress limit beyond which expansions will stop in a direction. In the absence of an alternatively supported limit, a value of 10 MPa is recommended for consistency with other ASR expansion models.

The $\lambda_{\rho i}$ factor is computed from Table 5-1 based upon the maximum perpendicular spacing of reinforcing bars oriented in *i* within the vicinity of the element being analyzed. If a structural component is reinforced with only a single reinforcing bar,

as is often the case for laboratory-tested cylinders or prisms, the largest perpendicular dimension of the component should be used in conjunction with Table 5-1. If a structural component is unreinforced in *i*, a $\lambda_{\rho i}$ value of 1 will be assigned for all associated elements. When conducting a multi-zone analysis, if an element is not effectively reinforced in *i* but the entire structural component is still reinforced in that direction then the element will be assigned a $\lambda_{\rho i}$ value other than 1. The factor of 3/4 in Table 5-1 was calibrated to generate results consistent with experimental findings for the biaxially reinforced beam from Wald et al. (2017a). In that study, it was found that, on average, approximately one-half of developing volumetric expansions was attributed to expansion in the unreinforced specimen direction. Factors of 3/8 and 7/8 were chosen for bar spacings twice as large and one-half as large as those associated with a factor of 3/4.

Table 5-1: Proposed $\lambda_{\rho i}$ factors

Maximum Bar Spacing for Element, $d_{sp,i}$, in i (mm)	$\lambda_{\rho i}$
No reinforcement for structure	1
$0 \leq d_{sp,i} < 300$	7/8
$300 \leq d_{sp,i} < 600$	3/4
$600 \leq d_{sp,i}$	3/8

Note: See discussion of bar spacings for use with Table 5-1

Once the λ_{ni} factors have been computed, the remaining fraction of expansion pressure not yet assigned to any direction, γ_n, is evaluated as:

$$\gamma_n = 1 - \sum \lambda_{ni} \qquad \textit{Equation 5-13}$$

The remainder of the expansion pressure is distributed to the single RCS direction or equally amongst the two or three RCS directions of an element qualified as those of "least resistance." The resistance for each direction is categorized in one of nine groups during each stage according to Table 5-2 based on uniformity of restraint. In general: a) a direction under load offers more resistance than an unloaded direction, b) a direction containing yielded reinforcement offers less resistance than a direction containing unyielded reinforcement but the same resistance as a direction for which the entire

structure is unreinforced, c) if conducting a multi-zone analysis, a direction for which the element is effectively unreinforced but the entire structure still contains reinforcement offers more resistance than a direction for which the entire structure is unreinforced, and d) a direction with small reinforcing bar spacings (higher $\lambda_{\rho i}$) offers more resistance than a direction with large reinforcing bar spacings.

Table 5-2: Resistance categories for expansion pressure transfer

Resistance Category	Description of Restraint for Element in *i* (increasing order of resistance)
1	Unloaded with yielded reinforcement Unloaded with no structural reinforcement ($\lambda_{\rho i} = 1$)
2	Unloaded with lowest $\lambda_{\rho i}$
3	Unloaded with intermediate $\lambda_{\rho i}$
4	Unloaded with highest $\lambda_{\rho i}$
5	Loaded with yielded reinforcement Loaded with no structural reinforcement ($\lambda_{\rho i} = 1$)
6	Loaded with lowest $\lambda_{\rho i}$
7	Loaded with intermediate $\lambda_{\rho i}$
8	Loaded with highest $\lambda_{\rho i}$
9	Maximum expansion reached Maximum load applied ($\lambda_{\sigma i} = 0$)

Note: Categories 2-4 and 6-8 apply where the element contains unyielded reinforcement in *i* or where the entire structure is reinforced in *i* but the element contains no reinforcement in *i*

The γ_n factor is equally divided amongst the direction(s) in the lowest resistance category (RSTC) to give $\gamma_{ni,dist}$ factors which are added to the λ_{ni} factors to give κ_{ni} factors for the given stage:

$$\kappa_{ni} = \lambda_{ni} + \gamma_{ni,dist} \qquad \textit{Equation 5-14}$$

5.3.1.3 Identifying ASR Stages

To evaluate required pressure distribution factors and employ appropriate constitutive formulations during each ASR stage, one must identify critical event behavior. That is, the VEP, directional pressures, and directional expansions must be determined at every instance when reinforcement in an RCS direction yields or where

concrete stops expanding in a direction. Assessing which of the two types of critical events occurs and the order in which the three RCS directions experience critical events are essential.

A critical event occurs at the end of a stage given the minimum VEP that will cause any still-expanding directions with effective passive restraint to either yield or stop expanding. The ASR expansion causing yielding of reinforcement is approximated from the axial equilibrium expression for RC (treated as linear-elastic) with perfect material bond under an applied normal stress, σ_i:

$$E_c\left(\varepsilon_{yi} - \varepsilon_{yi}^{ASR}\right) + \rho_i E_s \varepsilon_{yi} = \sigma_i \qquad \textit{Equation 5-15}$$

where ε_{yi} and ε_{yi}^{ASR} are the yield strain of reinforcement and expansion causing yielding in direction *i*. The VEP associated with ε_{yi}^{ASR} can then be found using Equation 5-9. Note that if the element is not under an applied normal stress, Equation 5-15 is the same as Equation 5-1 at yielding, and the directional expansion pressure causing yielding, per Equation 5-2, is equal to the smeared yield strength (ρf_y) of the reinforcement.

Meanwhile, the VEP causing expansions to plateau in a direction is that for which the associated directional expansion pressure reaches the tensile strength of concrete, f_t', but is only applicable if the critical bar spacing density, *bsd*, in that direction is greater than 0.5. This VEP may be found using Equations 5-7a and 5-8a. Note that a bar spacing density is defined as the spacing of bars oriented in a given direction divided by the associated parallel specimen dimension. Generally, a direction may have two associated densities – one each for bars spaced in two transverse directions. It is recommended that the critical bar spacing density be taken as the largest of the two computed values. A critical bar spacing density of 0.5 was chosen based on results from Wald et al. (2017a, b) for which the large-scale beam specimen, with bar spacing densities ranging from 0.63 to 0.73, stopped expanding in the reinforced directions prior to yield while cube specimens, with densities ranging from 0.32 to 0.42, continued expanding after the onset of steel yielding. The tensile strength of concrete was selected as the limiting pressure based on estimates of upper-bound equilibrating concrete stresses from Wald et al. (2017a).

5.3.1.4 Phase I Solution Approach

Expansion behavior during each stage as described by the previously formulated constitutive relationships and pressure distribution factors requires knowledge of critical event behavior that occurred beforehand. However, determination of critical event behavior via assessment of critical VEPs requires knowledge of the pressure distribution factors from the previous stage. This challenge is overcome because all analyses may begin with the same starting point – Stage 1 behavior in which no reinforcement has yielded and expansions have not had the opportunity to plateau. Expansion behavior can be defined using the step-by-step procedure outlined in Figure 5-7 in which stage and critical event behavior are evaluated in a repeated loop. In the process, the applicable range of volumetric expansions and volumetric pressures are determined for each stage.

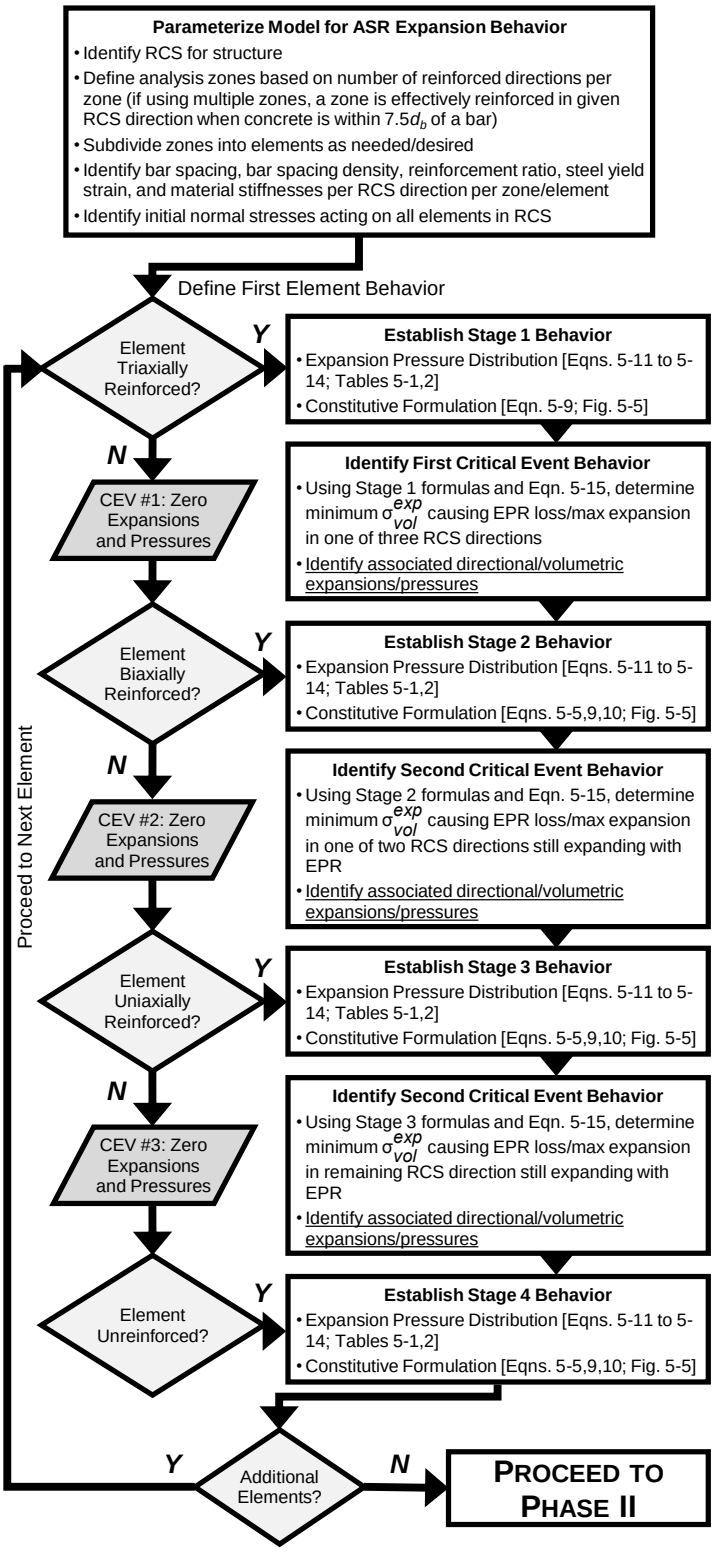

Figure 5-7: Phase I procedure

5.3.2 Phase II

After fully defining all formulae and parameters in Phase I, it is then possible to employ a VEP or volumetric expansion and related constitutive formulations to identify the distribution of expansions in an element under consideration. Knowing the applicable range of volumetric expansions and pressures for each stage, one can immediately identify the associated stage of behavior and the formulations to use for any particular value of volumetric expansion or pressure. Given a VEP, one can directly use the formulations to evaluate the volumetric and directional expansions. Given a volumetric expansion, one must first identify the matching VEP before directional expansions can be evaluated with the formulations. This may be done using an iterative trial-and-error approach or by solving a system of equations. In lieu of such a procedure, all calculations may be simplified by taking advantage of critical event behavior determined during Phase I and the fact that all pressure and expansion relationships are linear during each stage. Linear interpolation between known directional and volumetric pressures or expansions at stage bounds (i.e., critical events) can be used. For a single element, any process used can easily be done by hand or using a spreadsheet.

When conducting a multi-zone analysis, the zone-specific volumetric expansion for contained elements will depend on the number of reinforced directions considered for each zone. Assuming that all zones are equally reactive and conditioned the same way, volumetric expansion development is proposed to be taken as a scaled percentage of that in an unreinforced element exhibiting free expansion. Suggested scaling factors, based on the experimental findings outlined in Section 3.4.3.2, are as follows: 1.0 if unreinforced, 0.85 if uniaxially/biaxially reinforced, and 0.65 if triaxially reinforced. Note that these suggestions are simply initial estimates that may warrant revision based on further study.

5.4 MODEL LIMITATIONS

It is important to conclude the discussion of the proposed modeling approach by noting its primary limitations.

One limitation of the DVEP model is that it relies upon on an orthogonal arrangement of reinforcement in a structure in order to estimate expansions. Although it is less common, RC elements/structures may be detailed with reinforcing bars that are not orthogonal to each other. The model may still be used; however, the nonorthogonal arrangement of reinforcement would need to be considered as an equivalent orthogonal arrangement of reinforcement.

A second limitation is that the DVEP model may not estimate there to be as much macroscopic cracking in a structure as other expansion modeling approaches would predict using finite element-based analyses. This is simply a consequence of modeling structures using a single analysis zone or multiple large zones exhibiting uniform expansion behavior. However, it should be noted that, in the application of the proposed procedure to finite element continuum modeling, cracking can be identified for: 1) structures with multiple analysis zones (i.e., with a varied number of reinforced directions) containing differential volumetric expansions and directional expansion patterns, 2) structures with a single analysis zone where multiple elements comprising the zone are differentially loaded and exhibit different directional expansion patterns, and 3) unloaded structures with a single analysis zone assigned uniform concrete expansions but containing discretely-modeled, nonuniform reinforcement layouts that promote cracking. For instance, mid-depth cracks forming on the side surfaces of the biaxially reinforced beam monitored by Wald et al. (2017a) were effectively captured by modeling the beam's cross-section with a uniform concrete prestrain and discretely placed top and bottom mats of reinforcement.

5.5 SUMMARY

The Distributed Volumetric Expansion Pressure (DVEP) model was developed as a tool to simply estimate the multi-axial distribution of volumetric expansions in ASR-affected reinforced concrete elements given multi-axial states of active and passive restraint. Constitutive relationships were formulated to identify directional expansions as caused by a set of internal expansion pressures comprising a volumetric expansion

pressure. The effects of active and passive restraint on expansion behavior were distinguished, mid-behavior plateauing of expansions were acknowledged, and the influence of yielding and reinforcement layouts were incorporated. With this information in hand, an analyst may be able to rapidly identify expansions and subsequent mechanical stresses in structures at any given level of volumetric expansion with a non-incremental, time-independent approach. Such a technique is suitable for both hand calculations and implementation within the framework of nonlinear finite element analysis procedures. Successful usage of the DVEP model also requires awareness of its limitations and challenges that may have to be overcome, including working with non-orthogonal arrangements of reinforcement and capturing cracking behavior introduced by differential expansions throughout a structure.

CHAPTER 6: DISTRIBUTED VOLUMETRIC EXPANSION PRESSURE MODEL – IMPLEMENTATION AND VALIDATION*

6.1 OVERVIEW

The methodology of implementation and validation for the DVEP model is presented in this chapter. The DVEP model is used to estimate the multi-directional distributions of volumetric expansions due to ASR for RC elements. The adequacy of the proposed modeling procedure is validated against data from six independent experimental studies. Nine application examples are provided to illustrate the model's usage and robustness in capturing pre- and post-yield expansion behavior, mid-behavior plateauing of expansions, and RC element expansion response stemming from different combinations of reinforcement layouts, reinforcement percentages, and applied loads.

6.2 MODEL IMPLEMENTATION AND INTERPRETATION OF RESULTS

The DVEP model is used to determine ASR expansions in the concrete material. In practice, measured and reported expansions are for a composite RC system rather than concrete alone. Due to steel-concrete compatibility, restraint provided by bonded steel reinforcement results in a reduced element total strain as compared to concrete free expansion. It is important to distinguish this mechanical response from the constitutive response captured by the DVEP model in which ASR behavior of the concrete material is physically altered by the presence of reinforcement. The difference between ASR expansion in concrete and total expansion of an RC element is generally much smaller

* Portions of this chapter have been extracted directly from the following prospective publication (unpublished at time of dissertation submission) written by the author of this dissertation, with figures and tables reformatted for use in this dissertation:

Wald, D. M., Hrynyk, T. D., and Bayrak, O. (2017). "The Distributed Volumetric Expansion Pressure Model for ASR Expansion Behavior in Reinforced Concrete Elements – Part 2: Implementation and Validation." (submitted to *ASCE Journal of Structural Engineering*)

- Dissertator contribution: Primary author and lead researcher

than the difference between ASR expansion in the concrete material itself with and without embedded reinforcement. This is qualitatively illustrated in Figure 6-1. For the purposes of relating expansions to cracking or evaluating changes in element dimensions, it may be suitable to approximate the overall RC element expansions from ASR-induced concrete expansions estimated using the DVEP model, without consideration of the compatibility-related mechanical restraint provided by reinforcement.

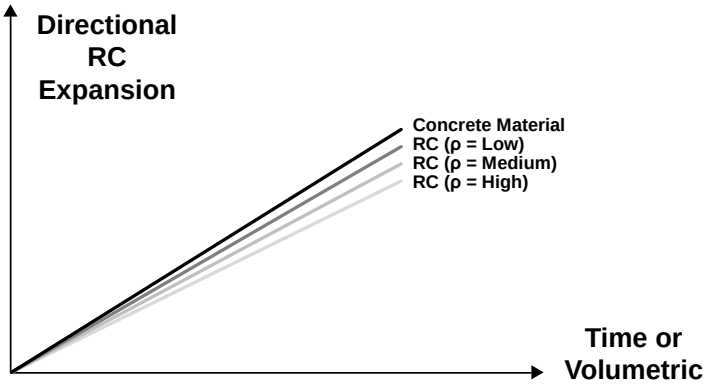

a) Compatibility Response

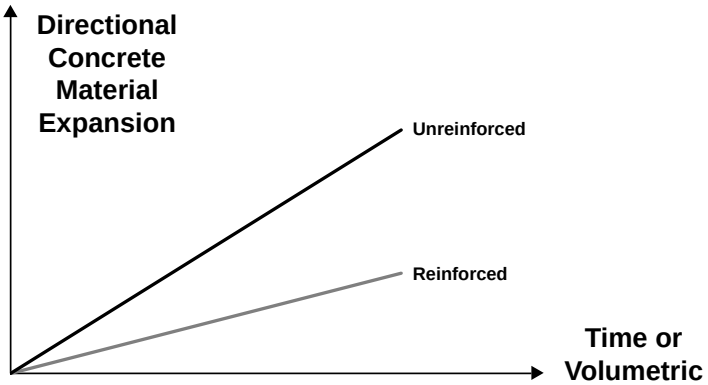

b) Constitutive Response

Figure 6-1: Compatibility and constitutive restraint to expansions

Where the integrity or load-carrying capacity of an ASR-affected structure is in question, expansions may be required to estimate induced stresses in a structure. In this case, concrete expansions estimated with the DVEP model should be applied as material-specific strains to account for the mechanical interaction between expanding concrete and

bonded steel, to generate induced stress states, and, if desired, to assign concrete material property degradation.

The DVEP model is intended to serve as a tool to identify expansion behavior and subsequently assess structural response at threshold or critical levels of volumetric expansion. Such levels might be established in the future by the engineering community as realistic, upper-bound expansions expected to be reached during a structure's service life or as expansions that may be tolerated by a structure while maintaining necessary serviceability and functionality.

6.3 MODEL VALIDATION

The DVEP model is validated via comparisons of computed and experimental results for ASR-affected specimens from six research studies. Element expansions were monitored in three orthogonal directions for all specimens described. A total of nine multi-part examples illustrate the suitability of the modeling approach in estimating ASR expansion behavior under different restraint scenarios. These include cases of concrete reinforced in a single or multiple directions, concrete with reinforcement conditions that promote yielding, concrete with reinforcement conditions that promote pre-yield plateauing of expansions, concrete under uniaxially or biaxially applied normal stresses, and concrete that is both reinforced and subjected to sustained loading conditions.

The validation cases discussed in the following sections are summarized in Figure 6-2. The figure presents three-dimensional illustrations and cross-section details for the portions of the RC structures under consideration. Critical parameters related to material properties, loads, and reinforcement conditions used as model input are also provided. Table 6-1 and Tables A-1 to A-14 in Appendix A provide more comprehensive output of the relevant parameters related to stage and critical event behavior that are developed in the Phase I analyses of these examples. Phase II results (i.e., computed distributions of volumetric expansions) are subsequently shown and compared with experimental results. Note that for all specimens with reinforcement, the plotted results represent average RC expansions which were obtained by applying expansions estimated with the DVEP model

as concrete prestrains to idealized, single-element RC models with smeared properties. For examples with applied loads, the plotted data reflect element deformations due to ASR which occur after, and do not include, deformations due to initial load application. Also, it is important to note that percentage comparisons between results refer to absolute differences in expansion values with units of "%" and do not represent relative percent differences between values.

In particular, the RC expansions were evaluated using a single-element, three-dimensional, smeared RC behavior and analysis program which was developed to capture stress-strain behavior of elements reinforced in multiple directions and under multi-directional states of applied stress and imposed deformations. The program incorporated the analysis methodology and numerous materials models employed by the VecTor Suite of RC finite element modeling tools, information about which may be found in Wong et al. (2013). Particularly, the RC expansions were taken as total element strains from analysis incorporating the Modified Compression Field Theory (Vecchio and Collins 1986) and models to account for Poisson effects (Variable Poisson's Ratio – Kupfer), compression softening (Vecchio 1992-A), tension stiffening (Modified Bentz 2003), and confinement (Kupfer/Richart). Perfect bond between the concrete and reinforcement was assumed, and no ASR material property degradation models were used.

Example	3D View of Expansion Zone	Scaled 2D Cross-Section of Expansion Zone	DVEP Model Parameters* (material properties / loads / reinforcement)
1 Wald et al. (2017a)	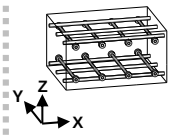	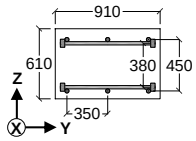	f_c' = 33.0 MPa; E_c = 33.0 GPa; f_t' = 1.9 MPa ρ_x = 1.1 % (6 No. 11) bsd_x = 450/610 = 0.74 ρ_y = 0.7 % (2 No. 9 at 305) bsd_y = 380/610 = 0.62
2 Wald et al. (2017b); Allford (2016)	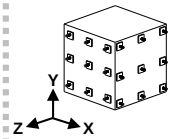	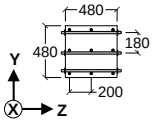	f_c' = 35.6 MPa; E_c = 35.6 GPa; f_t' = 2.0 MPa ρ_x = 0.5 % (9 No. 4) bsd_x = 200/480 = 0.42 ρ_z = 1.1 % (9 No. 6) bsd_z = 180/480 = 0.38
3 Wald et al. (2017b); Allford (2016)	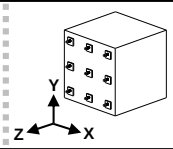	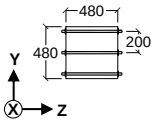	f_c' = 35.6 MPa; E_c = 35.6 GPa; f_t' = 2.0 MPa ρ_z = (a) 0.5 % (9 No. 4) bsd_z = 200/480 = 0.42 (b) 1.5 % (9 No. 7)
4 Smaoui et al. (2007)	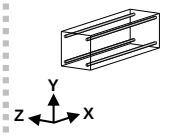	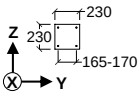	f_c' = 40.0 MPa†; E_c = 40.0 GPa; f_t' = 2.1 MPa ρ_x = (a) 0.38 % (4Ø8) bsd_x = 165/230 = 0.72 (b) 0.77 % (4Ø10) (c) 1.53 % (4Ø15)
5 Wald et al. (2017b); Allford (2016)	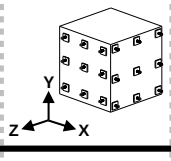	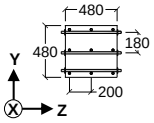	f_c' = 35.6 MPa; E_c = 35.6 GPa; f_t' = 2.0 MPa ρ_x = (a) 0.5 % (9 No. 4) bsd_x = 200/480 = 0.42 (b) 1.5 % (9 No. 7) bsd_z = 180/480 = 0.38 ρ_z = (a) 0.5 % (9 No. 4) (b) 1.5 % (9 No. 7)
6 Dunant and Scrivener (2012)	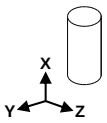	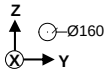	f_c' = 40.0 MPa†; E_c = 40.0 GPa; f_t' = 2.1 MPa σ_{cx} = (a) -5 MPa; (b) -10 MPa
7 Gautam et al. (2015, 2017)	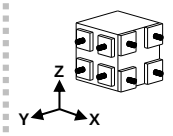	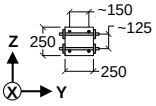	f_c' = 45.1 MPa; E_c = 45.1 GPa; f_t' = 2.2 MPa σ_{cx} = -3.9 MPa; σ_{cy} = -3.9 MPa Unbonded high-yield bolts in X/Y used to post-tension specimen and anchored after load applied to concrete bsd_x = 150/250 = 0.60 bsd_y = 125/250 = 0.50
8 Wald et al. (2017b); Allford (2016)	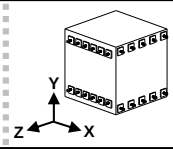	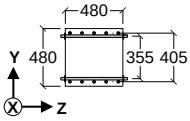	f_c' = 32.0 MPa; E_c = 32.0 GPa; f_t' = 1.9 MPa ρ_x = 0.5 % (10 No. 4) bsd_x = 405/480 = 0.84 ρ_z = 1.1 % (12 No. 5) bsd_z = 355/480 = 0.74
9 Bracci et al. (2012)	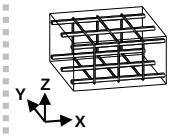	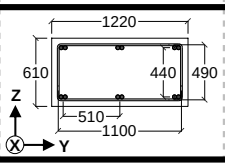	f_c' = 32.0 MPa†; E_c = 32.0 GPa; f_t' = 1.9 MPa σ_x = -3.45 MPa ρ_x = 1.6 % (12 No. 11) bsd_x = 440/610 = 0.72 ρ_y = 0.22 % (2 No. 5 @ 305) bsd_y = 490/610 = 0.80 ρ_z = 0.11 % (2 No. 5 @ 305) bsd_z = 1100/1220 = 0.90

*Notes: (All dimensions in mm) † Assumed Value

1) Computed modulus of elasticity and tensile strength of concrete used in lieu of measured values
   - Modulus taken as initial tangent stiffness for parabolic stress-stress strain curve with peak strain of 0.002: $E_c = 2f_c'/0.002 = 1000f_c'$
   - Direct tensile strength computed as: $f_t' = 0.33\sqrt{f_c'}$

2) ASTM 615 Grade 60 (f_y = 414 MPa) or CAN/CSA-G30.18 Grade 400 (f_y = 400 MPa) bars used in all cases except Example 7; yield strength of steel approximated with ~10% overstrength as 450 MPa and elastic modulus of steel estimated as 200 GPa in all cases

Figure 6-2: DVEP model validation examples

An in-depth, step-by-step discussion of the DVEP model usage with reference to the values presented in Table 6-1 and Appendix A is provided for Example 1. Note that Example 1 pertains to the biaxially reinforced concrete beam (Wald et al. 2017a) described in Section 3.3, which was used in the calibration of the bar spacing influence factors ($\lambda_{\rho i}$) and the incorporation of plateaued expansion response. Brief discussions are presented for Examples 2-9 with primary emphasis on the presentation of final results. A single-zone analysis was used to model global, average expansion behavior for all specimens. Example 8 illustrates the use of a multi-zone analysis for a specimen which was experimentally shown to exhibit significant differential local expansion behavior throughout its volume.

6.3.1 Example 1 – Step-by-Step Calibration Example: Unequal Biaxially Reinforced Element with Large Bar Spacing and Plateaued Expansions

Example 1 presents the case of the 8435 x 910 x 610 mm, biaxially reinforced concrete beam monitored by Wald et al. (2017a). The RC beam was constructed with 1.1 % reinforcement in the longitudinal (i.e., x-) direction and 0.7 % reinforcement in transverse (i.e., y-) direction. The following step-by-step discussion outlines the procedure for estimating the concrete expansion behavior using the DVEP model. Steps 1-8 describe Phase I procedures, and Step 9 describes Phase II procedures.

Table 6-1: Example 1 Calculations

		X	Y	Z			X	Y	Z
	$\lambda_{\sigma i}$	1.0	1.0	1.0		$\lambda_{\rho i}$	0.75	0.75	1.0
Stage 1	Eqn. 5-	---	---	---	**CEV#1**	CEV	---	---	NEPR
	λ_{1i}	0.25	0.25	0.333		σ_{vol}^{exp} (MPa)		--- 0 ---	
	γ_1		--- 0.167 ---			$\Delta\sigma_{vol,1}^{exp}$ (MPa)		--- 0 ---	
	RSTC	2	2	1		$\Delta\sigma_{i,1}^{exp}$ (MPa)	0	0	0
	$\gamma_{1,dist,\,i}$	0	0	0.167		σ_i^{exp} (MPa)	0	0	0
	κ_{1i}	0.25	0.25	0.5		$\Delta\varepsilon_{i,1}^{ASR}$ (%)	0	0	0
						ε_i^{ASR} (%)	0	0	0
						ε_{vol}^{ASR} (%)		--- 0 ---	
Stage 2	Eqn. 5-	9	9	5,10	**CEV#2**	CEV	MAX	---	---
	λ_{2i}	0.25	0.25	0.333		σ_{vol}^{exp} (MPa)		--- 7.58 ---	
	γ_2		--- 0.167 ---			$\Delta\sigma_{vol,2}^{exp}$ (MPa)		--- 7.58 ---	
	RSTC	2	2	1		$\Delta\sigma_{i,2}^{exp}$ (MPa)	1.90	1.90	3.79
	$\gamma_{2,dist,\,i}$	0	0	0		σ_i^{exp} (MPa)	1.90	1.90	3.79
	κ_{2i}	0.25	0.25	0.5		$\Delta\varepsilon_{i,2}^{ASR}$ (%)	0.092	0.141	0.233
						ε_i^{ASR} (%)	0.092	0.141	0.233
						ε_{vol}^{ASR} (%)		--- 0.467 ---	
Stage 3	Eqn. 5-	9	9	5,10	**CEV#3**	CEV	---	MAX	---
	λ_{3i}	0	0.25	0.333		σ_{vol}^{exp} (MPa)		--- 7.583 ---	
	γ_3		--- 0.417 ---			$\Delta\sigma_{vol,3}^{exp}$ (MPa)		--- 0 ---	
	RSTC	9	2	1		$\Delta\sigma_{i,3}^{exp}$ (MPa)	0	0	0
	$\gamma_{3,dist,\,i}$	0	0	0.417		σ_i^{exp} (MPa)	1.90	1.90	3.79
	κ_{3i}	0	0.25	0.75		$\Delta\varepsilon_{i,3}^{ASR}$ (%)	0	0	0
						ε_i^{ASR} (%)	0.092	0.141	0.233
						ε_{vol}^{ASR} (%)		--- 0.467 ---	
Stage 4	Eqn. 5-	9	9	5,10					
	λ_{4i}	0	0	0.333					
	γ_4		--- 0.667 ---						
	RSTC	9	9	1					
	$\gamma_{4,dist,\,i}$	0	0	0.667					
	κ_{4i}	0	0	1.0					

Note: CEV Types - NEPR = no EPR; Y = yielding of reinforcement; MAX = max expansion reached

6.3.1.1 Step 1

With a goal of identifying average, global expansion behavior, this beam is idealized as a single biaxially reinforced element comprised of one analysis zone. The zone is reinforced in the x- and y-directions using the gross reinforcement ratios for the structure (1.1 % and 0.7 %). Note that if an analyst alternatively elected to explore the possible use of a multi-zone analysis in this case, concrete would only be deemed effectively reinforced if located within a distance of $7.5d_b$ from at least one reinforcing bar. For reinforcing bars spaced less than $15d_b$ apart, the concrete between those bars is effectively reinforced in the bar orientation direction. In this example, the x-direction reinforcement (U.S. No. 11 bars with d_b = 36 mm) is spaced at a maximum of 450 mm ($12.5d_b$) and the y-direction reinforcement (US No. 9 bars with d_b = 29 mm) is spaced at a maximum of 380 mm ($13.1d_b$). Thus, all concrete, including the cover concrete, would be considered effectively biaxially reinforced, and this structural region would still be analyzed using a single lumped zone.

6.3.1.2 Step 2

Stage 1 behavior is defined by pressure distribution factors and constitutive relationships that reflect expansions developed on the basis that no RCS directions have yet experienced critical events. In this specific example, defining expansion behavior during Stage 1 is irrelevant because the beam is unreinforced in one direction. Consequently, non-zero expansion behavior begins with Stage 2. However, for completeness, Stage 1 relationships are also defined here.

To evaluate pressure distribution factors, applied load and reinforcement layout influence factors ($\lambda_{\sigma i}$ and $\lambda_{\rho i}$) must first be evaluated for each RCS direction. The $\lambda_{\sigma i}$ factors are given by Equation 5-12. Since the beam is not loaded, $\lambda_{\sigma i}$ is taken as 1.0 for each RCS direction. The $\lambda_{\rho i}$ factors are determined using Table 5-1, based on maximum bar spacings. Since the structure is unreinforced in the z-direction, $\lambda_{\rho z}$ is taken as 1.0. Given maximum bar spacings of 450 mm and 380 mm in x and y, respectively, $\lambda_{\rho x}$ and

$\lambda_{\rho y}$ are both taken as 0.75.

Minimum pressure distribution factors, λ_{mi} are subsequently evaluated per Equation 5-11. Values of 0.25, 0.25, and 0.333 are obtained for λ_{1x}, λ_{1y}, and λ_{1z}, respectively. The remaining fraction of pressure not yet assigned (γ_1) is 0.167. This fraction of pressure is distributed to the direction(s) of least resistance with the lowest-ranked resistance category, described in Table 5-2, during Stage 1. The z-direction is assigned a resistance category of 1 since the beam is unloaded and unreinforced in z, and the other two directions are assigned a resistance category of 2 since the beam is unloaded and each direction contains unyielded reinforcement during Stage 1 with equal $\lambda_{\rho i}$ factors. Consequently, γ_1 is distributed entirely to the z-direction ($\gamma_{1z,dist}$ = 0.25). When adding the λ_{1i} and $\gamma_{1i,dist}$ factors together in Equation 5-14, κ_{1i} factors of 0.25, 0.25, and 0.5 are obtained.

6.3.1.3 Step 3

The first critical event occurs when the first of the three RCS directions experiences a loss of effective passive restraint or stops expanding. In this case, the unreinforced z-direction has no effective passive restraint under all stages of the analysis. Thus, the first critical event occurs in the z-direction prior to any development of expansion pressures or expansions. In other words, all Stage 1 expansion pressures and material expansions are zero.

6.3.1.4 Step 4

Stage 2 behavior is defined by pressure distribution factors and constitutive relationships that reflect that one RCS direction has experienced a critical event (in this case a loss of effective passive restraint in the z-direction). Overall expansions in x and y during Stage 2 are given by Equation 5-9 since these directions have yet to experience a loss of effective passive restraint. Overall expansions in the z-direction during Stage 2 are given by Equations 5-5 and 5-10. The pre-yield expansion in z ($\varepsilon_{z,py}^{ASR}$) is zero, and the

expansion developed during Stage 2 after a loss of effective passive restraint, $\Delta\varepsilon_{z,2}^{ASR}$ will be proportional to the sum of same-stage partial expansions in x and y, $\Delta\varepsilon_{x,2}^{ASR}$ and $\Delta\varepsilon_{y,2}^{ASR}$, which expand with maintained effective passive restraint. Pressure distribution factors for Stage 2 are identical to those for Stage 1. In conjunction with Equation 5-10, the factor of 0.5 for z compared to the sum of factors in x and y (also equal to 0.5) indicates that the z-direction expansion is equal to the combined expansion in the x- and y-directions during Stage 2. This is consistent with the experimental findings for this beam (Wald et al. 2017a).

6.3.1.5 Step 5

The second critical event occurs when a second RCS direction experiences a loss of effective passive restraint or stops expanding. To identify this critical event, the minimum VEP causing a loss of effective passive restraint or plateauing of expansions in directions not yet experiencing a critical event (i.e., x and y) must be calculated.

Because the critical bar spacing densities in x and y (0.74 and 0.62) are greater than 0.5, expansions will plateau if a directional expansion pressure reaches $f_t^{'}$ (1.90 MPa in this case) before yielding of the reinforcement. Given no applied stresses on the beam, reinforcement will yield if the directional pressures in x or y reach $\rho_t f_{yi}$ (4.95 MPa or 3.15 MPa). Based on these computed values, it is estimated that the expansions will plateau prior to the onset of yielding.

The total pressures computed for Stage 2 are equal to the partial pressures developed from Stage 2 since, in this case, it was determined that no pressures would be developed during Stage 1. Based on Equations 5-7 and 5-8, the directional pressures in x and y during Stage 2 are equal to $0.25\sigma_{vol}^{exp}$. This means that expansions will plateau when the VEP reaches $4f_t^{'}$ (7.60 MPa). At this VEP, the directional expansion pressures in x, y, and z are $f_t^{'}$ (1.90 MPa), $f_t^{'}$ (1.90 MPa), and $2f_t^{'}$ (3.80 MPa), respectively. Expansions in the three directions are 0.092, 0.141, and 0.233 %, respectively, summing to a volumetric expansion of 0.467 %.

Because the x- and y-directions simultaneously experience critical events, expansion behavior during Stages 2 and 3 will be identical; however, for completeness and generalization, Stage 3 behavior will be assessed and the x-direction will be denoted as the second critical direction.

6.3.1.6 Step 6

Stage 3 behavior is determined and defined by pressure distribution factors and constitutive relationships that reflect that two RCS directions have already experienced critical events (in this case, an initial loss of effective passive restraint in the z-direction and secondary plateauing of expansions in the x-direction). Overall expansions in y and z during Stage 3 are given by the same equations used in Stage 2. Overall expansions in x during Stage 3 are given by Equation 5-9 since reinforcement is yet to yield, but values of the computed expansion will always resolve to the maximum of 0.092 %. Because expansions plateaued in x, the previous value for λ_x of 0.25 is changed to zero, resulting in a new γ of 0.417 for Stage 3. The resistance categories for x, y, and z are now 9, 2, and 1. Thus, γ is still distributed entirely to the z-direction, but the pressure distribution factors now become 0, 0.25, and 0.75, respectively.

6.3.1.7 Step 7

The third critical event is determined where the final RCS direction experiences a loss of effective passive restraint or stops expanding. To identify this critical event, the minimum VEP causing a loss of effective passive restraint or plateauing of expansions in the direction not yet experiencing a critical event (i.e., y) must be calculated. As computed in Step 5, the directional pressures causing plateauing and yielding in the y-direction are $f_t^{'}$ (1.90 MPa) and $\rho_y f_{yy}$ (3.15 MPa), respectively. Thus, it is estimated that the expansions will plateau. In accordance with Equations 5-7 and 5-8, the total directional pressure in y during Stage 3 will be the sum of the total directional pressure developed in earlier stages (1.90 MPa) and the partial pressure developed during Stage 3 ($0.25\Delta\sigma_{vol,3}^{exp}$). Since the directional pressure developed between Stages 1 and 2 is equal to

the limit of $f_t^{'}$, no additional VEP is required to cause expansion plateauing in the y-direction. Thus, the total VEP required for expansions to plateau in the y-direction remains 7.60 MPa, as determined previously in Step 5. Further, because the expansion pressures for the third critical event are the same as for the second critical event, all associated expansions will be the same as for the second critical event.

6.3.1.8 Step 8

Stage 4 behavior is defined by pressure distribution factors and associated constitutive relationships that reflect that all three RCS directions have experienced a critical event (in this case, an initial loss of effective passive restraint in the z-direction and secondary/tertiary plateauing of expansions in the x- and y-directions). Overall expansions in the three directions during Stage 4 are given by Equation 5-5, which indicates that these expansions are the sums of expansions from Stages 1-3 and partial expansions during Stage 4. The Stage 4 partial expansions are proportioned based on the Stage 4 pressure distribution factors. Because expansions are estimated to plateau in the x- and y-directions, the λ_{ni} factors for each direction are equal to zero, resulting in a new γ factor of 0.666 for Stage 4. The resistance categories for x, y, and z are updated as 9, 9, and 1, respectively. Thus, γ is still distributed entirely to the z-direction, but now the overall pressure distribution factors are taken as 0, 0, and 1.0, respectively. Ultimately, concrete will continue to expand, and 100 % of that expansion will be allotted to the z-direction during Stage 4, after plateauing of expansions.

6.3.1.9 Step 9

Following the procedures of Phase I outlined in the solution of Steps 1-8, the developed constitutive relationships are used in Phase II to distribute volumetric expansions amongst RCS directions. In general, an analyzed structure or element will expand volumetrically during one of the four stages of behavior that are mathematically bounded by the values of volumetric expansion and directional expansion distributions for critical events. As stated previously, linear interpolation may be used to establish the

distribution of directional expansions. For example, at a volumetric expansion of 0.3 %, the RC beam analyzed here will be experiencing Stage 2 behavior (i.e., between the first and second critical events corresponding to expansion levels of 0 % and 0.467 %, respectively). Using linear interpolation, the distribution of this volumetric expansion is estimated to be 0.059, 0.091, and 0.150 % in the x-, y-, and z-directions, respectively.

Step 9 can be repeated for any number of levels of volumetric expansion to generate a plot of directional expansions versus volumetric expansions. These concrete expansions can be further used as material prestrains, as described earlier, to generate RC element expansions which account for compatibility between concrete and steel reinforcement. Figure 6-3 compares the computed and measured RC expansions for the beam under consideration. It can be seen that the computed and reported results match very closely in this case; however, it should again be noted that this beam was considered in the original calibration of the DVEP model.

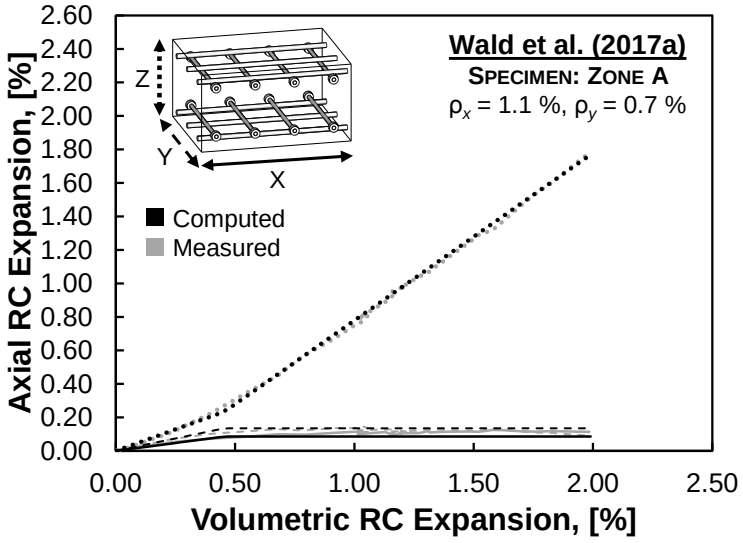

Figure 6-3: Example 1 computed and measured results

6.3.2 Example 2 – Unequal Biaxially Reinforced Element with Small Bar Spacing and Unlimited Expansions

Example 2 presents the case of a 480 mm, biaxially reinforced concrete cube (A1-102a) constructed with 0.5 % reinforcement in the x-direction and 1.1 % reinforcement in the z-direction. Additional details corresponding to the RC cube are presented in Wald et al. (2017b).

The reinforcement ratios provided in the RC cube were comparable to those used for the beam in Example 1. The cube largely differed from the beam in that reinforcement was distributed amongst three layers, with smaller bar spacings of 180 and 200 mm. For the given bar spacing, $\lambda_{\rho i}$ factors of 0.875 are assigned for each reinforced direction as opposed to the value of 0.75 that was used in Example 1. This implies that differential expansions between reinforced and unreinforced directions should be smaller for the cube than for the beam. Further, given that the bar spacing densities (0.42 for the x-direction and 0.38 for the z-direction) fall below 0.5, expansions in the reinforced directions are not estimated to plateau prior to yielding of reinforcement in either direction. The z-direction, which contains less reinforcement, will reach yielding first.

Figure 6-4 compares the computed and measured RC expansions for the cube. The measured expansions for the cube exceeded 0.20 % in the reinforced directions, which corresponds to approximate steel reinforcement yielding. The DVEP model correctly captures comparative experimental trends: the unreinforced direction generally expanded more than the lightly reinforced x-direction which, in turn, expanded more than the more heavily reinforced z-direction. For volumetric expansions up to 1.25 %, the model estimates the magnitude of all directional expansions within 0.05 %. There is greater discrepancy in x and y at larger volumetric expansions: while the model estimates that, after all reinforcement has yielded at a volumetric concrete expansion of 1.03 %, additional concrete expansions in x, y, and z develop during Stage 4 in a near-equivalent proportion of 0.319:0.361:0.319, the actual post-yield expansions were not similarly proportioned. However, the inability of the model to more closely estimate behavior at larger volumetric expansions may be attributed to high variability in expansion

distribution patterns seen when concrete elements are comprised of multiple directions lacking effective passive restraint against additional expansion. This is believed to be closely related to trends observed in fully unrestrained (i.e., plain concrete) elements, in which concrete has been shown to often expand much more in one direction than in others, possibly due to a weakened plane introduced perpendicular to the casting direction or due to inherent heterogeneity and variability of the concrete (Larive 1997).

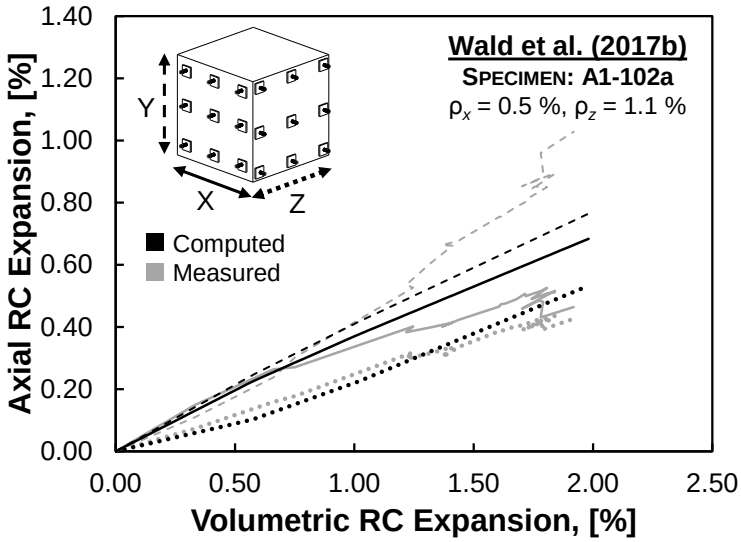

Figure 6-4: Example 2 computed and measured results

6.3.3 Example 3 – Uniaxially Reinforced Elements: Influence of Reinforcement Percentage

Example 3 presents the case of two 480 mm, uniaxially reinforced cubes monitored by Wald et al. (2017b). One of the cubes was constructed with 0.5 % reinforcement (A1-001b), and the other cube contained 1.5 % reinforcement (A1-003). The reinforcement for each cube was spaced in the z-direction in three layers at 200 mm, resulting in a bar spacing density of 0.42. Nonzero behavior for uniaxially reinforced specimens begins with Stage 3 given two directions lacking effective passive restraint from the outset of the analysis.

The DVEP model estimates that both specimens will exhibit virtually the exact

same concrete expansion behavior despite containing different reinforcement ratios. Recall that stage-specific expansions in directions without maintained effective passive restraint are proportional to the total of same-stage expansions in any direction(s) with maintained effective passive restraint. Further, it should also be reiterated that the constant of proportionality is a function of the stage-specific pressure distribution factors. During Stage 3, only one direction still maintains effective passive restraint; thus, the expansion in each unreinforced direction is simply proportional to the expansion in the sole reinforced direction. Further, the proportionality is the same for both cubes given identical Stage 3 pressure distribution factors. As long as the cubes can expand the same amount in the reinforced direction, they should experience similar and simultaneous expansions in the unreinforced directions. On the basis of Equation 5-9, the amount of reinforcement simply influences the amount of expansion pressure that must develop to attain a certain level of expansion; a greater pressure is needed in a more heavily reinforced element to reach the same level of expansion as in a more lightly reinforced element. Because expansion pressures are not limited for bar spacing densities below 0.5, the cubes in this example are able to reach similar levels of expansion.

Behavior of the two cubes primarily differs during, and after, the final critical event corresponding to reinforcement yielding. As presented in Tables A-2 and A-3 of Appendix A, the reinforcement in each cube yields given nearly the same concrete expansion, but with greater overall expansion pressure for the more heavily reinforced cube. The stage-specific directional expansions computed for the two cubes during Stage 4 behavior have the same directional proportions due to having the same pressure distribution factors. The distribution of total volumetric expansions during Stage 4 will be marginally different due to slight numerical differences in expansions during the final critical event.

Figure 6-5 compares the computed and measured RC expansions for the two cubes. The computed results for both cubes are similar, differing slightly as they reflect the stronger compatibility-related mechanical restraint against concrete expansion resulting from the greater amount of reinforcement. The DVEP model accurately

estimates behavior within 0.05 % for volumetric expansions up to values of 1.25 % for A1-001b and 1.75 % for A1-003. Discrepancies between computed and measured results are a consequence of differential expansions in the two unreinforced directions of each cube, which are idealized to be nominally identical. Inaccuracies at higher volumetric expansions are attributed to the Stage 4, post-yield variability, described previously for Example 2.

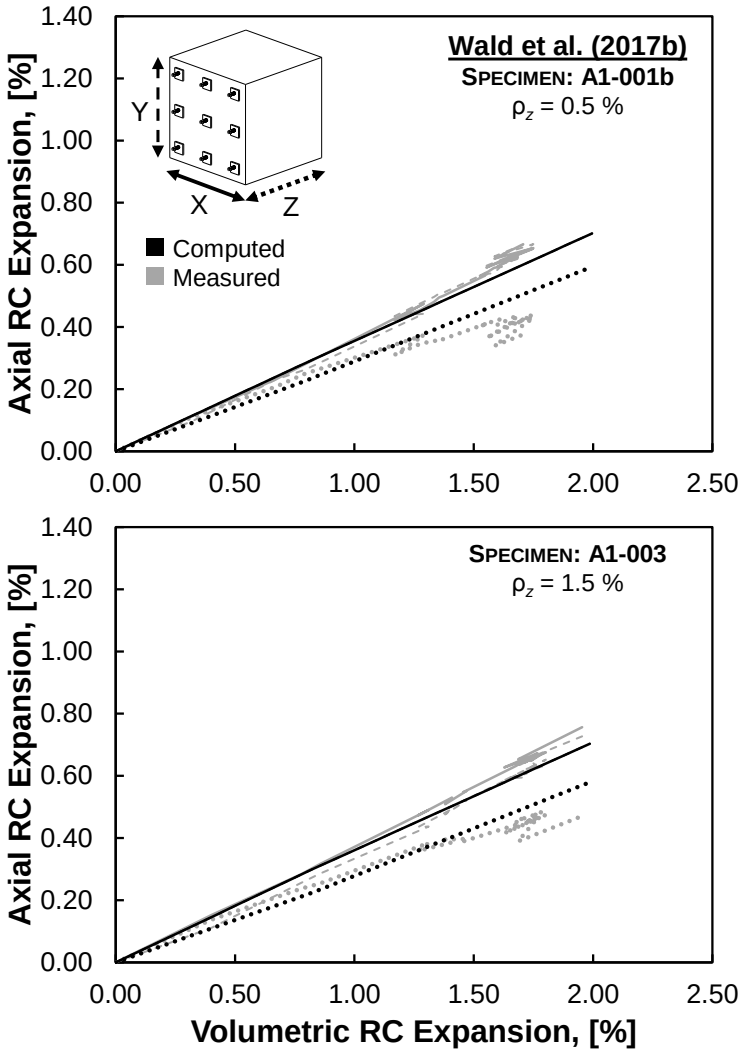

Figure 6-5: Example 3 computed and measured results

6.3.4 Example 4 – Uniaxially Reinforced Elements: Influence of Bar Spacing Density

Example 4 presents the case of six uniaxially reinforced, 230 x 230 x 810 mm concrete blocks monitored by Smaoui et al. (2007). Two of the blocks were constructed with 0.38 % reinforcement (Blocks 2 and 8), two blocks contained 0.77 % reinforcement (Blocks 3 and 9), and two blocks contained 1.53 % reinforcement (Blocks 4 and 11). Each block was longitudinally reinforced in the x-direction using four reinforcing bars provided in the specimen corner regions with a bar spacing of approximately 170 mm. Blocks 2, 3 and 4 were fabricated with a low-reactive concrete mixture and Blocks 8, 9, and 11 were fabricated with a moderately-reactive concrete mixture. The reinforced direction for each block is assigned a $\lambda_{\rho i}$ factor of 0.875 with a bar spacing density (0.72) above 0.5.

Figure 6-6 compares computed and measured RC expansions for the six blocks. Measured expansions were reported at 228 days after casting and were taken using four different monitoring techniques. The average data obtained from the measurements are plotted in Figure 6-6 against the volumetric expansion computed from those data. Mixture reactivity is not considered in the expansion distribution estimates developed from the model. Thus, measured results for each pair of similarly reinforced blocks are plotted together. Further, the modeling approach does not account for differences in measured expansions observed between the two unreinforced directions of each block; however, it is interesting to note that the presented model results in the y- and z-directions closely match the average values of expansions measured in the unreinforced directions. In this case, the model is also shown to estimate the expansions in the reinforced directions with high degrees of accuracy, especially for Blocks 2, 3, 4 and 11, in which computed and measured results differ by less than 0.03 %.

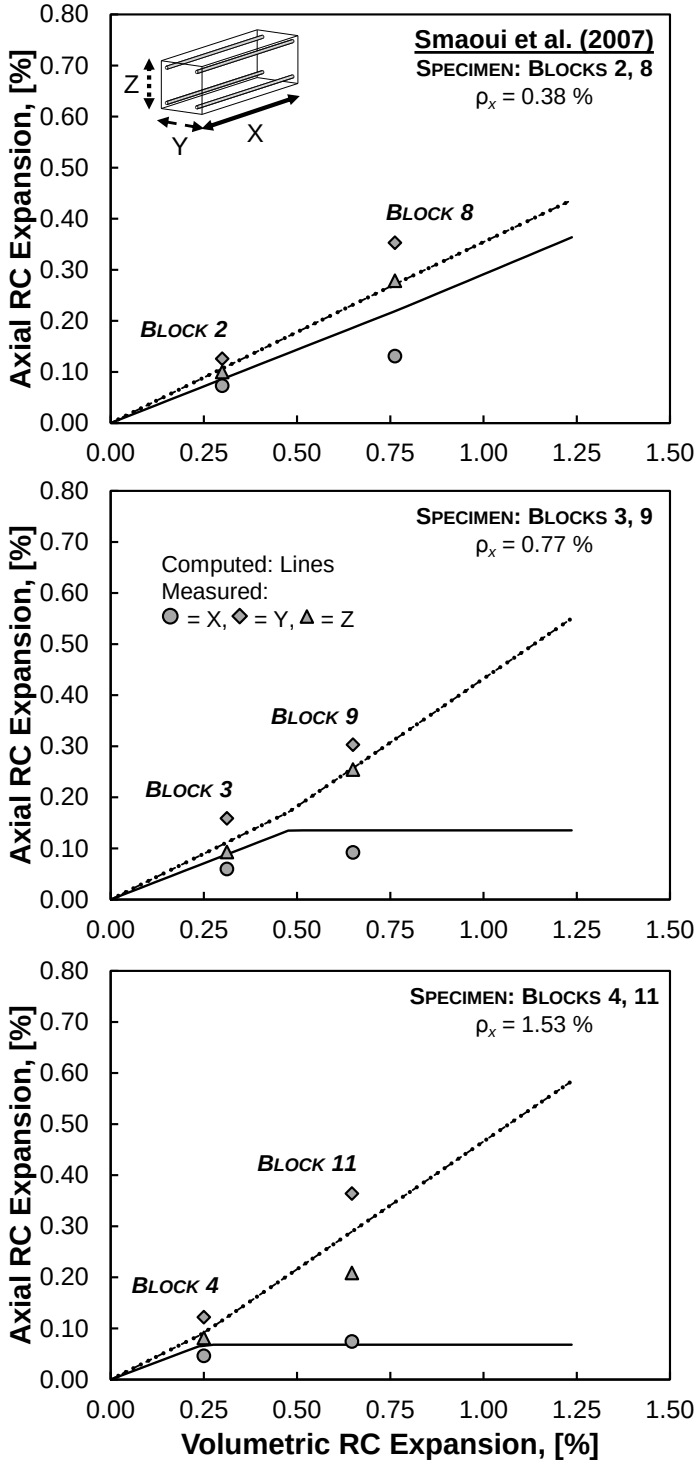

Figure 6-6: Example 4 computed and measured results

The model suggests that the blocks with 0.77 % or 1.53 % reinforcement were subject to plateauing expansion behavior prior to yielding of reinforcement. Recall that expansions plateau because the expansion pressure in the reinforced direction reaches a limit – the tensile strength of concrete – prior to reinforcement yielding. The tensile strength of concrete was estimated as 2.10 MPa on the basis of an assumed concrete strength of 40 MPa. Note that the actual concrete strength for these specimens was unreported. Blocks 3, 4, 9, and 11 reach this limit well before yielding. The reinforcement in Blocks 2 and 8 yield at an expansion pressure of approximately 1.70 MPa, or just before the occurrence of expansion plateauing. If a lower concrete tensile strength was assumed, or if increased reinforcing bar yield strength were considered, the DVEP model could indicate that expansions would plateau for these blocks. Due to a lack of additional experimental data, it is uncertain if any blocks truly exhibited plateaued expansions. However, it is noted that full expansion-time plots on similar specimens (Blocks 5 and 16) from the same study were shown to exhibit pre-yield plateauing behavior in the longitudinally reinforced directions while the concrete continued to expand in other directions.

The variations of the experimental results reported for these blocks are captured reasonably well with the proposed model because expansion plateauing is incorporated in the procedure. If plateauing is neglected, the model would predict near-identical concrete expansion distribution for all volumetric expansion levels, as was the case for Example 3 (refer to Figure 6-5). As illustrated from Figure 6-6, the distribution of expansions for each case is shown to be similar, prior to the occurrence of plateauing, but changes dramatically thereafter. Expansions are proportioned amongst RCS directions identically during Stage 3, but Stage 4 behavior, in which expansions are at a maximum in the reinforced direction, begins at a different volumetric expansion level for each specimen. Because greater expansion pressures are needed to generate similar levels of expansions in more highly reinforced specimens, Blocks 4 and 11 reach the limiting pressure at a smaller total expansion as compared to other blocks. In contrast, Blocks 2 and 8 experience greater expansion levels under a given pressure.

Collectively, Examples 3 and 4 highlight how the DVEP model addresses the dilemma of how reinforcement percentages actually influence ASR expansion behavior. One of the primary conclusions of the study by Wald et al. (2017b) was that reinforcement ratios did not influence expansion behavior if elements were detailed with only one ratio in any reinforced directions (i.e., if specimens contained uniaxial, equal biaxial, or equal triaxial reinforcement). Numerous studies, including those by Jones and Clark (1996), Koyanagi et al. (1992), and Smaoui et al. (2007), contradict this idea and suggest that uniaxial reinforcement ratios do influence expansion behavior. The DVEP model suggests that both scenarios are valid; reinforcement ratios may not strongly influence expansion behavior if expansions do not plateau prior to yielding, but reinforcement ratios will influence plateauing behavior and post-plateau expansion distribution patterns.

6.3.5 Example 5 – Equal Biaxially Reinforced Elements

Example 5 presents the case of two 480 mm, biaxially reinforced cubes monitored by Wald et al. (2017b). The RC cubes were constructed with equal reinforcement ratios in the x- and z-directions: one cube was constructed with 0.5 % reinforcement (A1-101b), and one cube was constructed with 1.5 % reinforcement (A1-303).

Figure 6-7 compares the computed and measured RC expansions for the two cubes. On the basis of the explanation provided in Example 3, the computed results for the two equal biaxially reinforced cubes are very similar despite the cubes containing different reinforcement ratios. Again, the results differ only slightly as they reflect the stronger mechanical restraint against concrete expansion provided with a greater amount of reinforcement. The computed results reflect that the difference in expansions between reinforced and unreinforced directions is greater with two directions of restraint as opposed to one. Given pre-yield pressure distribution factors of 0.292, 0.417, and 0.292 in x, y, and z, respectively, concrete expansions for these cubes are computed to be approximately 1.4 times (0.417/0.292) greater in the unreinforced direction than in each reinforced direction. With pre-yield pressure distribution factors of 0.292, 0.354, and

0.354 for the uniaxially reinforced cubes from Example 3, the concrete expansions were computed to be only 1.2 times (0.354/0.292) greater in the unreinforced directions.

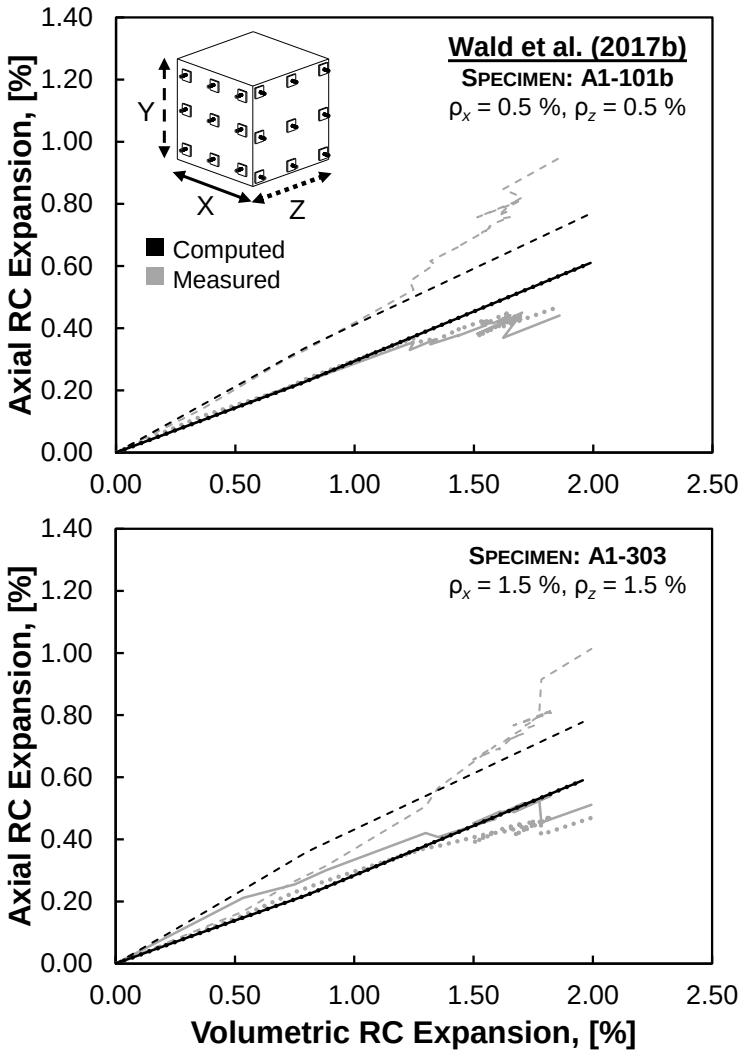

Figure 6-7: Example 5 computed and measured results

6.3.6 Example 6 – Unreinforced Elements under Uniaxial Load

Example 6 presents the case of 160 x 335 mm, plain concrete cylinders that were monitored by Dunant and Scrivener (2012) under different levels of sustained axial compression. The cylinders were subjected to compressive stresses of either 5 MPa or 10 MPa. In the modeling of these elements, nonzero expansion behavior occurs entirely

during Stage 4, given that the plain concrete cylinders begin expanding with all RCS directions containing no effective passive restraint. Consequently, the cylinders are assumed to expand at all times and in all directions in a constant proportion given by the Stage 4 pressure distribution factors. Using the DVEP model's upper-bound compressive stress limit of 10 MPa beyond which expansions are assumed to stop, the loaded element direction is assigned a $\lambda_{\sigma i}$ value of 0.5 for the 5 MPa sustained load and 0 for the 10 MPa sustained load. The other $\lambda_{\sigma i}$ and all $\lambda_{\rho i}$ factors are assigned values of 1.0. As a result, λ factors of 0.167, 0.333, and 0.333 are obtained for a cylinder subjected to the sustained load of 5 MPa for the loaded and two unloaded directions, respectively. Similarly, λ factors of 0, 0.333, and 0.333 are obtained for a cylinder subjected to 10 MPa. The remaining fraction of pressure not yet assigned, γ, is equally distributed to all directions with a resistance category of 1. For a cylinder subjected to 5 MPa of sustained compressive stress, all directions are assigned a resistance category of 1 since they contain no effective passive restraint and are not loaded to a maximum. For a cylinder subjected to 10 MPa of sustained compressive stress, the unloaded directions are assigned a resistance category of 1 since the third direction is loaded to a maximum (and thus assigned a resistance category of 9). This results in pressure distribution factors of 0.222, 0.389, and 0.389 for a cylinder under a 5 MPa sustained load and 0, 0.5, and 0.5 for a cylinder under a 10 MPa sustained load. In other words, the DVEP model indicates that a 5 MPa loaded cylinder will expand 1.75 times more in the unloaded directions than in the loaded direction, and that a cylinder subjected to a sustained load of 10 MPa will only expand in the unloaded directions.

Figure 6-8 compares the computed and measured concrete expansions for the cylinders. Note that expansions shown are ASR-induced strains and exclude elastic shortening and creep of the specimen under load. The DVEP model captures the response of a cylinder with a 10 MPa sustained load very well, which is to be expected given that the experimental study verified the limiting compressive stress of 10 MPa. The computed results provide less agreement with the results obtained for cylinders under a 5 MPa sustained load; however, the cause for this discrepancy is simply the unanticipated

experimental behavior at initial volumetric expansions (< 0.01 %) in which initial ASR expansion in the unloaded directions was slightly delayed. The plots of computed results are simply offset from the point where the unloaded directions began expanding. The slopes of the computed plotlines, representing the rates of directional-volumetric expansion development, closely match those of the measured data plotlines beyond 0.01 % volumetric expansion.

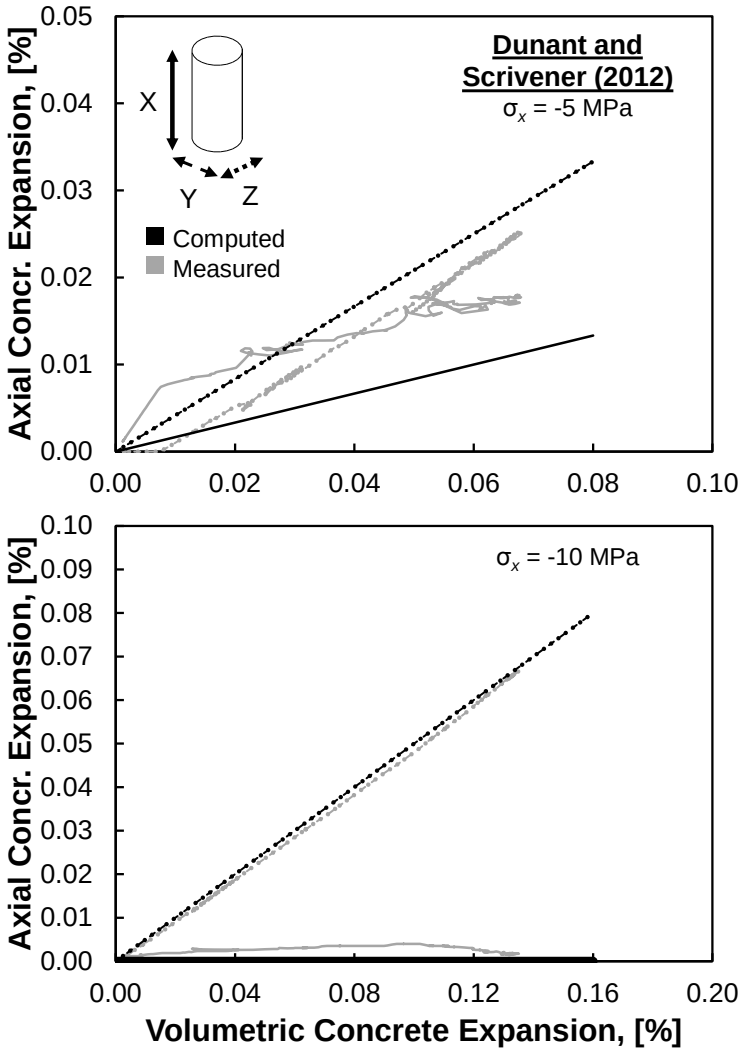

Figure 6-8: Example 6 computed and measured results

6.3.7 Example 7 – Elements under Biaxial Load

Example 7 corresponds to the work done by Gautam et al. (2015, 2017) involving a 250 mm cube subjected to 3.9 MPa of sustained biaxial compression. Loads were applied to the concrete via post-tensioning of unbonded rods (12.7 mm in diameter) that were anchored to the surfaces of the specimen. Given a lack of bonded reinforcement, the concrete stress in each loaded direction (x and y) was equal to the full 3.9 MPa of applied compression. This results in a $\lambda_{\sigma i}$ factor of 0.61 for both of the loaded directions. The externally anchored rods can be considered to provide 0.8 % effective passive restraint to the specimen in both the x- and y-directions. The rods, which were reported to be high-strength, were spaced far enough apart to give bar spacing densities at or above 0.5. Thus, the expansions are allowed and assumed to plateau well before the rods can yield.

Figure 6-9 compares the computed and measured expansions for the RC cube elements, illustrating that the experimental results are well-estimated with the DVEP model.

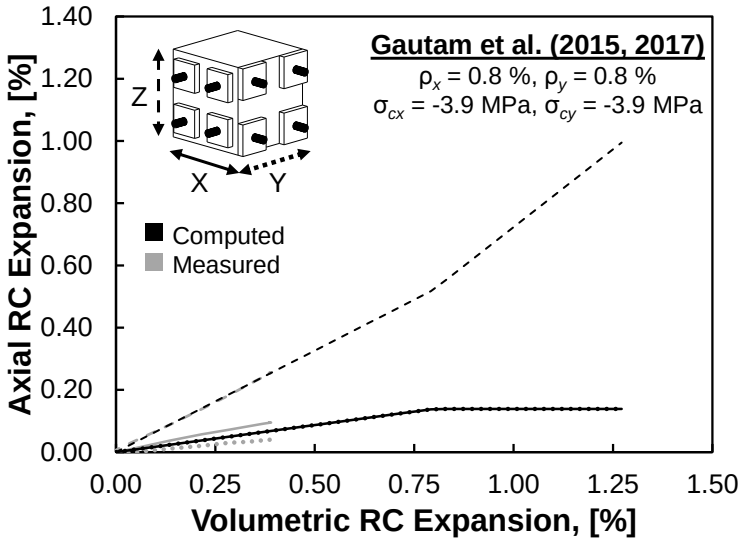

Figure 6-9: Example 7 computed and measured results

6.3.8 Example 8 – Structural Component with Multiple Analysis Zones

Example 8 presents the case of another 480 mm, biaxially reinforced cube (A3-102-L1) monitored by Wald et al. (2017b) with 0.5 % reinforcement in the x-direction and 1.1 % reinforcement in the z-direction (refer to Figure 6-10). Unlike the RC cube examined in Example 2, this cube was reinforced in two discrete layers as opposed to in three more-evenly distributed layers. Reinforcing bars were spaced in the x-direction at 405 mm and in the z-direction at 355 mm. The original monitoring study showed that expansions were not uniform throughout this specimen, with differential expansions developed between exterior reinforced regions and an effectively unreinforced interior. Consequently, it was concluded that it may be inappropriate to model such a specimen as a single element. Also note that differential expansion behavior was only confirmed because expansions were measured between opposite specimen faces rather than across individual specimen surfaces.

For the modeling of this specimen, the cube was separated into multiple analysis zones where concrete is only effectively reinforced in a direction if within $7.5d_b$ of a reinforcing bar. The x-direction was reinforced with US No. 4 bars (d_b = 13 mm) while the z-direction was reinforced with US No. 5 bars (d_b = 16 mm). For simplicity, an average bar diameter of 14.5 mm was considered for both directions and, as such, concrete within approximately 110 mm was deemed effectively reinforced. Given that the reinforcing bars were centered at approximately 45 mm, on average, from the nearest specimen edge, the cube was modeled as shown in Figure 6-10a, with a 170 mm-wide strip of unreinforced concrete between two 155 mm-wide strips of biaxially reinforced concrete at the top and bottom regions of the cube. Despite not encompassing the entire volume of the cube, the biaxially reinforced zones are assigned the gross reinforcement ratios of 0.5 % and 1.1 % in x and y, with the potential for expansions to plateau given bar spacing densities above 0.5. All zones are assigned $\lambda_{\rho i}$ factors of 0.75, 1, and 0.75 in x, y, and z, respectively, given maximum bar spacings for the entire cube. In both zones, γ is distributed only in the y-direction. The unreinforced zone exhibits only Stage 4 behavior, with expansions proportioned according to the computed pressure distribution

factors for the three directions in a 0.25:0.5:0.25 ratio.

Expansion behavior for the entire cube was estimated by averaging the axial expansions across all zones. Behavior in different zones was correlated by scaling zonal volumetric expansions relative to a free volumetric expansion (i.e., the expansion that would be expected everywhere if concrete were unrestrained). Expansions in the unreinforced zone were scaled by a factor of 1.0 because they already represent free expansions. Expansions in the biaxially reinforced zone were scaled by a factor of 0.85 based on conclusions drawn in the original experimental study. Figure 6-10b presents the axial expansion behavior for each biaxially reinforced zone against zonal and free volumetric expansions. Figure 6-10c plots axial expansion behavior for the unreinforced zone against zonal and free volumetric expansions.

Axial expansions in each zone were weight-averaged by zone volume at common free volumetric expansions. The zonal-averaged expansions were then replotted against a zonal-averaged volumetric expansion for comparison to average measured expansions for the entire specimen in Figure 6-10d.

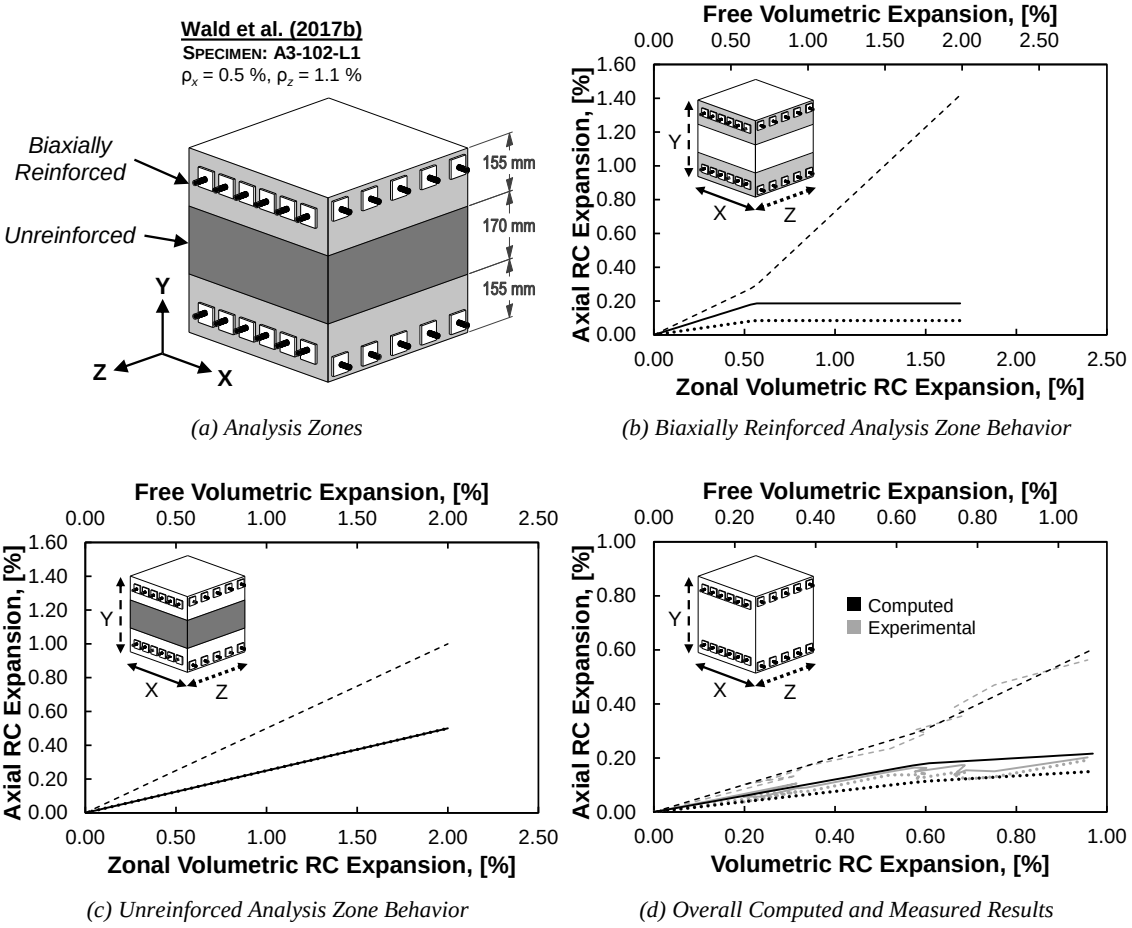

(a) Analysis Zones

(b) Biaxially Reinforced Analysis Zone Behavior

(c) Unreinforced Analysis Zone Behavior

(d) Overall Computed and Measured Results

Figure 6-10: Example 8 analysis and results using multi-zone analysis

For comparative purposes, Figure 6-11 compares the computed and measured RC expansion results for the cube when analyzing the specimen with a single, biaxially reinforced analysis zone. The computed results are identical to those shown in Figure 6-10b, with the expansions instead corresponding to the entire specimen volume rather than strips local to the reinforcement. The model results are deemed acceptable but are less accurate than those obtained using a multi-zone analysis. Notably, overall expansions in the two reinforced directions are estimated to be more distinct without the weighted influence of expansion behavior within an unreinforced core (refer to Figure 6-10c).

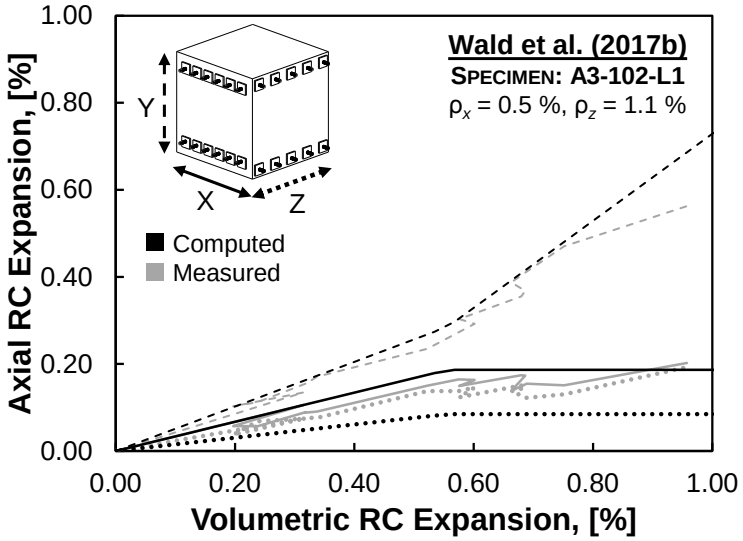

Figure 6-11: Example 8 computed and measured results using single-zone analysis

6.3.9 Example 9 – Triaxially Reinforced Structure under Load: Combining Restraint Types and Simplifying Analyses

Example 9 presents the case of two identical, triaxially reinforced, longitudinally post-tensioned RC beams (LSC1 and LSC4) reported by Bracci et al. (2012) with overall dimensions of 7620 x 1220 x 610 mm. Expansions were monitored at midspan locations where each beam contained six pairs of spliced US No. 11 bars in the longitudinal direction (i.e., the x-direction), and US No. 5 stirrups spaced regularly at 305 mm. The corresponding reinforcement ratios were 1.60 %, 0.22 %, and 0.11 %, in the x-, y-, and z-directions, respectively. This example represents a case in which the critical bar spacing density in a direction is not computed from the maximum bar spacing. The pairs of spliced longitudinal bars were spaced at 510 mm along the 1220 mm member dimension, giving a bar spacing density of 0.42. The same bars were spaced in two layers at 440 mm along the 610 mm dimension, giving a bar spacing density of 0.72. Thus, the maximum bar spacing and critical bar spacing density for this example are 510 mm and 0.72, respectively. The bar spacing densities in the y- and z-directions were above 0.5. At maximum bar spacings of 510, 490, and 100 mm in the x-, y-, and z-directions, respectively, the corresponding $\lambda_{\rho i}$ factors are 0.75, 0.75, and 0.375. A set of unbonded

post-tensioning strands were used to apply 3.45 MPa of axial compression to the specimen in the x-direction which was estimated to result in a sustained compressive stress in the concrete (σ_c) of approximately 3.13 MPa, with consideration the bonded mild reinforcement carrying a small portion of the applied load. This corresponds to a $\lambda_{\sigma i}$ factor of 0.687 in the x-direction. Also note that these strands have not been considered to contribute any added passive restraint to expansion in x, given that they were anchored near the ends of the beam, at distance of 3.8 m from midspan.

To estimate global, average expansion behavior, each beam was analyzed using a single analysis zone that is triaxially reinforced and loaded in the x-direction. It is noted that, given the small diameter of the No. 5 stirrups relative to the overall dimensions of the beam, a multi-zone analysis might provide additional information on possible variations in local expansion behavior. Such an analysis would result in a uniaxially reinforced interior zone, triaxially reinforced corner zones, and biaxially reinforced edge zones, each of which would also be loaded in the x-direction. The results from this process, however, are not presented herein. For model validation, a simpler approach is more appropriate here due to a lack of experimental data that could be used to evaluate differential volumetric expansion development and distribution throughout the beams.

In contrast to other examples presented, each element direction in this example falls in a different resistance category during the first nonzero stage of behavior (in this case, Stage 1). The x-direction is assigned a resistance category of 6 due to the combined presence of load and reinforcement. The y- and z-directions are assigned resistance categories of 3 and 2, respectively, with the z-direction falling in the lower category given a lower $\lambda_{\rho i}$ of 0.375. Thus, during Stage 1, γ is entirely distributed to the z-direction, which when combined with the lowest reinforcement ratio of 0.11 % results in yielding of the z-direction reinforcement as the first critical event. During Stage 2, the resistance category for the z-direction changes to 1 with γ still entirely being distributed to z. The second critical event occurs when the y-direction reinforcement yields, after which the resistance category for the y-direction also changes to 1 and γ is evenly distributed between the y- and z-directions during Stage 3. The final critical event occurs

when expansions in the x-direction reach a maximum without yielding of the reinforcement due to the combination of applied load and the large reinforcement ratio provided in the longitudinal direction of the beam.

Figure 6-12 compares computed and measured RC expansion results for the two beams. The DVEP model estimates the measured expansions with high accuracy and notably captures the abrupt shifts in behavior in the y- and z-directions when expansions in each of these directions reach the approximate yield strain of steel (0.20 %).

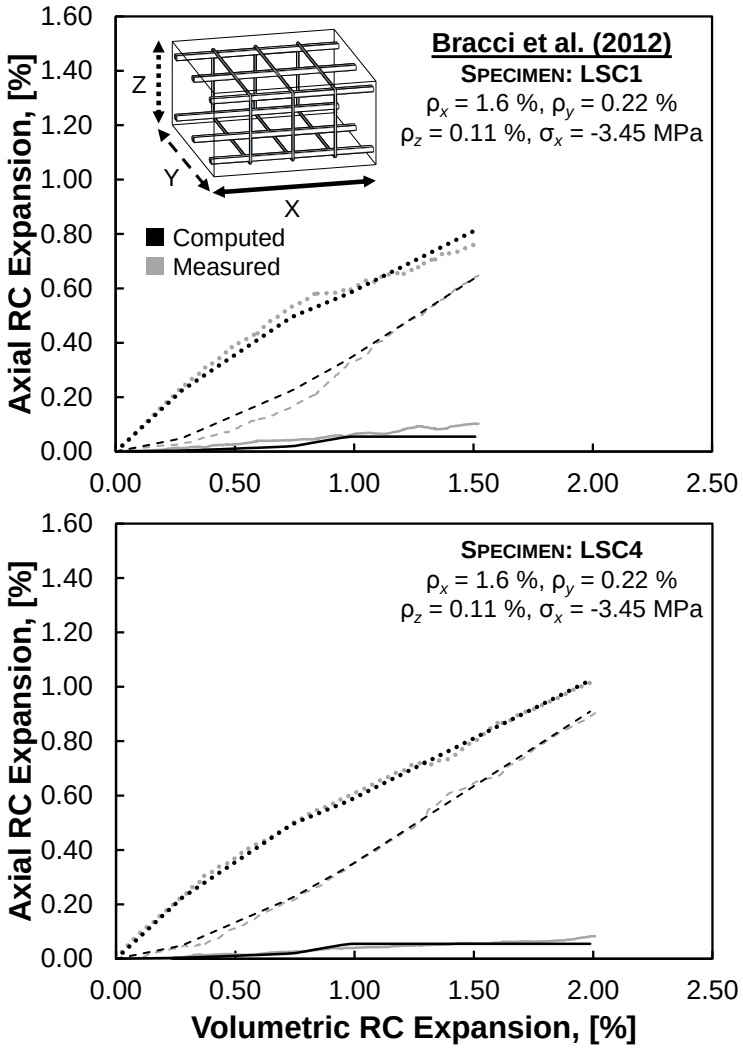

Figure 6-12: Example 9 computed and measured results

6.4 SUMMARY

The DVEP model was shown to be capable of reliably estimating the multi-directional distribution of ASR-induced expansions in concrete elements that are reinforced and/or subjected to sustained loads. The application of the modeling approach was illustrated through the step-by-step performance of nine examples pertaining to ASR-affected concrete specimens, from six independent experimental studies reported in the literature. Despite differences in concrete mixtures, environmental conditioning, and ASR reactivity amongst the different studies, it was shown that the DVEP model was able to capture the triaxial distribution of volumetric expansions in RC elements using a time-independent, non-incremental, mechanics-based approach. The model was able to estimate expansions adequately as a function of reinforcement percentages, reinforcement layouts, concrete and steel material properties, and sustained loads.

CHAPTER 7: EXPANSION DISTRIBUTION MODEL APPLICATION AND RESULTS

7.1 OVERVIEW

In this chapter, different ASR expansion distribution models are compared in terms of the process by which each may be implemented and the computational results obtained. The discussions offer additional perspective on the robustness of the DVEP model and the potential advantages the model offers relative to other computational approaches in the literature. First, major similarities and differences between the models are briefly reiterated. Then, the application of the different modeling approaches within the framework of a finite element program, notably employing a total load, secant stiffness solution methodology, is covered. Finally, computational results obtained using each model are compared to experimental results to illustrate how successful the models are relative to one another given the most basic analyses conducted.

7.2 REVIEW OF MODEL CHARACTERISTICS

Table 7-1 provides a comparison summary of key features of various expansion distribution models which includes information pertaining to how each model is applied, what aspects of structural design and ASR each model can account for, and the means by which those aspects are considered. Much of the information listed in Table 7-1 is covered in Chapters 4 and 5, while more in-depth discussion of model application is covered in later sections within this chapter. Details are given for the DVEP model and the expansion distribution models from Cope et al. (1994), Charlwood et al. (1992), and Saouma and Perotti (2006).

Table 7-1: Comparison summary of expansion distribution models

	Cope et al. (1994)	***Charlwood et al. (1992)***	***Saouma and Perotti (2006)***	***DVEP Model***
Analysis Type	Incremental	Incremental	Incremental	Non-incremental
Basis	Empirical	Empirical	Empirical	Mechanics/Semi-empirical
Coordinate System for Evaluation	Principal	Principal	Principal	Reinforcement-oriented
Input	Free unidirectional expansion	Free unidirectional expansion	Free/restrained volumetric expansion	Restrained volumetric expansion
Method used to Develop Input Parameter Considering Reactivity, Restraint and Environmental Conditions	None specified	None specified, but modification factors can be used according to Léger et al. (1996)	Kinetics law	Modification factors suggested for number of reinforced directions; none specified for reactivity, applied stresses, temperature, or humidity
Distinction Between Active and Passive Restraint?	No	No	No	Yes
Method used to Account for Restraint	Pre-existing concrete stresses	Pre-existing concrete stresses	Pre-existing concrete stresses	Initial applied loading and reinforcement percentages in mechanics formulation
Multiaxial Restraint Interaction? (i.e., Expansion Transfer)	No	No	Yes	Yes
Method used to Account for Reinforcement Distribution	Continuum modeling	Continuum modeling	Continuum modeling	Explicit formulation
Method used to Account for Reinforcement Yielding	Continuum modeling	Continuum modeling	Continuum modeling	Explicit formulation

7.3 MODEL APPLICATION

The four ASR expansion distribution models discussed in this document were introduced within the framework of nonlinear finite element analysis programs employing a total load, secant stiffness solution algorithm. In a total load, secant stiffness approach, the response of an RC element to a given set of loads and/or imposed deformations is computed directly without the need for increment-based load/displacement stepping procedures. Material stress and strain states are determined on the basis of constitutive formulations and are used to evaluate secant moduli that relate element total loads to element total deformations.

For reference, an alternative to a secant stiffness approach is one that utilizes updating tangent moduli developed from material stress-strain relations. With a tangent stiffness approach, loads and/or imposed deformations are applied and computed as increments that accumulate over the course of the analysis. Unfortunately, incremental analysis procedures can introduce numerical errors in results or be computationally expensive, all as a consequence of the specific increment size selected for analysis. With a secant stiffness approach, the application of secant moduli permits evaluation of material stress-strain behavior without necessarily requiring knowledge of prior material stress and strain conditions. Consequently, a secant stiffness approach may be more suitable for analyses utilizing the DVEP model. Note, however, that load-stepping analyses can still be conducted using a secant stiffness solution methodology, as will be discussed shortly.

When using a secant stiffness approach, loads and/or imposed deformations acting on an element are introduced into the solution algorithm as normal and shear stresses or strains acting in the element's local or principal coordinate system. For any particular input set of applied strains, the algorithm will generate one unique solution for RC response. Regardless of how the input was selected, the same solution will always be obtained for those input parameters. In other words, an analysis would give the same results if a set of applied strains were arbitrarily selected or if the same exact set of input parameters were evaluated with some material model. For example, if the DVEP model

were used to show that the orthogonal, axial concrete expansions in an ASR-affected element at some point were 0.1, 0.2, and 0.3 %, the overall RC response to those expansions found with a secant stiffness approach would be exactly the same as that given expansions of 0.1, 0.2, and 0.3 % input arbitrarily without utilizing the expansion model. Note that this would be true for all expansion distribution models.

The differentiating factor between the various expansion distribution models in a secant stiffness-based analysis program lies not in the solution approach itself but in each model's implementation within the framework of that approach. In a finite element analysis, the response of a structure to loads and/or imposed deformations can be analyzed in multiple load stages, as desired, to capture ranged behavior. This is often done to examine full load-deformation response of a structure until failure under monotonically varying or cyclic inputs. At other times, behavior for only one load stage (i.e., one set of inputs) may be desired. In any event, a secant stiffness solution algorithm can be executed regardless of the number of load stages employed. In fact, the number of load stages, load/deformation increment sizes per load stage, and behavior during each load stage will not in any way alter how the secant stiffness algorithm works. The behavior identified for one load stage may, however, influence the input parameters for the next load stage. For example, when assessing cyclic or loading-unloading behavior of an element, it is important to track the development of permanent deformations (i.e., plastic strains) and include them as inputs for subsequent load stages. In such a situation, load history is a vital consideration, and more than one load stage must be used to identify the buildup of plastic strains in the materials prior to and behavior after a load reversal. Meanwhile, for monotonically increasing loads, loading history is arguably less critical, as behavior at any load level can typically be estimated independent of response at lower load levels. Ultimately, in the case of modeling ASR-induced expansions, the model that is employed dictates whether a "load history considered" or "load history not considered" type of approach must be used.

Incremental ASR expansion distribution models (Cope et al. (1994), Charlwood (1992), Saouma and Perotti (2006)) are implemented with a "load history considered"

approach in which expansions are incremented through successive load stages. Each load stage begins with the input of an increment of time, free unidirectional expansion, free volumetric expansion, or restrained volumetric expansion. Next, the amount and distribution of restrained directional expansion increments are estimated as a function of the pre-existing concrete stresses from the prior load stage. Then, these expansion increments are added to the total expansions accrued from previous load stages to give new total directional expansions. Finally, the RC response to the set of total direction expansions is determined for the current load stage and concrete stress state information can be extracted for the next load stage.

Conversely, as a non-incremental expansion distribution tool, the DVEP model is implemented with a "load history not considered" approach in which expansions can be identified for any given input of volumetric expansion in a single load stage without any dependency on the buildup of concrete stresses. An analyst may still run multiple successive load stages, incrementing the applied volumetric expansion to track the progress of expansion distribution behavior during volumetric expansion development; however, doing so is optional and will generally not influence the results.

7.3.1 Comparison of Model Implementation Subjectivity and Computational Expense

Expansion behavior estimated using each expansion distribution model may not only be a function of the model's numerical formulation but also the method by which the model is implemented. In general, modeling a structure one way may lead to different results than doing so another way, with no assurance as to which is "correct." Sometimes, a simpler approach will yield more accurate results than using a complex approach, while other times the exact opposite is true. Ultimately, more subjectivity can raise questions about the validity of a model and delegitimize its intended purpose of generating a reliable estimate of current or future behavior.

Incremental expansion distribution models suffer from the issue of subjectivity. User-selected time or expansion increments (or the number of load stages to perform)

dictate the magnitude of end-stage, total accumulated expansions. Meanwhile, the state of stress in concrete will be updated uniquely per load stage based on those previously accumulated expansions, which will differ from one analysis to the next given alternate increment sizes. The use of a smaller increment size (i.e., more load stages to identify behavior at a given point) will permit more frequent updating of stress states and more closely satisfy the original intent of the models – to capture behavior given expansion rate-stress or continuous, rather than discrete, expansion-stress relationships. Meanwhile, the use of a larger increment size (i.e., fewer load stages to identify behavior at a given point) may fail to provide adequate updating of stress states and notably mistime when and if any yielding of reinforcement occurs. Often, an increment size will be selected to achieve a satisfactory balance between "accuracy" or satisfying "model intent" and computational expense. Smaller increments equate to increased computation time given more load stages, which is expounded as a finite element mesh size becomes finer.

Figure 7-1 illustrates how ASR expansion results can change given different increment sizes and numbers of load stages. The relationship between restrained RC expansions (in the direction of restraint) and free expansions is plotted for a uniaxially reinforced element with 1 % smeared reinforcement behaving in accordance with the linear expansion reduction model proposed by Cope et al. (1994). The concrete compressive strength and steel yield strength were specified at 40 and 450 MPa, respectively. The limiting compressive stress was set at 10 MPa. Unidirectional free expansions were incremented in 1, 2, 5, or 10 load stages until reaching a value of 0.5 %. The restrained RC expansions were found by analyzing the element with the same computer program and materials models used when validating the DVEP model in Chapter 6.

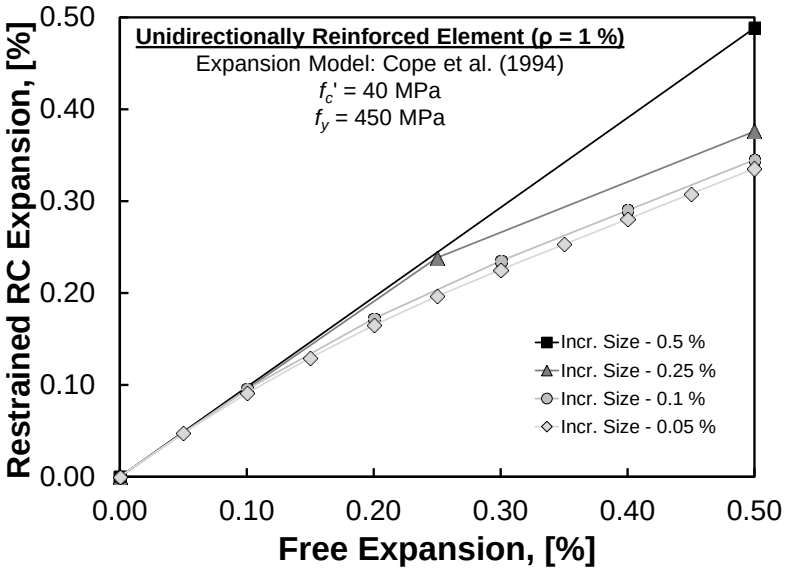

Figure 7-1: Influence of expansion increment selection

As can be seen, the sensitivity to restraining stresses increases with a greater number of load stages. Expansions are estimated to be higher given fewer load stages as increments are less frequently adjusted by the developing concrete stress states. Given only a single load stage, the concrete stresses are never updated from their zeroed states to capture any influence of restraint on expansion behavior. Most of the discrepancy between the different analyses occurs beyond approximately 0.2 % restrained expansion (i.e., where the reinforcement yields), especially when using only one or two load stages. When the reinforcement yields, concrete stresses become constant due to equilibrium. As such, the restrained-free expansion relationship becomes perfectly linear after yielding is detected. If too few load stages are used, the analysis can overshoot the yield-level expansion and delay when constant stresses are actually accounted for. Clearly, there will be some increment size beyond which further refinement will not result in a significant difference in estimated expansion response. In this case, the response for increment sizes of 0.1 % (given 5 load stages) and 0.05 % (given 10 load stages) were nearly identical, with estimated expansions from each analysis differing by only 0.01-0.02 % at the end of each load stage. It should be noted, however, that a practical limit on increment size may not be the same for all expansion models or analyses. This may be complicated further

when incrementing volumetric expansions (as in the model by Saouma and Perotti (2006)) in which expansions in different directions are inter-related. Also, a limit placed on increment size does not negate the fact that more load stages will still be needed if response estimates are required for higher levels of expansion.

The DVEP model has the advantage of eliminating much of the implementation subjectivity, or application burden, as the user is not required to select, or parametrically evaluate, appropriate increment sizing. RC expansion behavior for any given volumetric concrete expansion can be found immediately using a single load stage. If a structural component is modeled as a single element, the multi-axial distribution of concrete material expansions can be computed without using a finite element program.

It should also be noted that, within the framework of finite element procedures, all expansion distribution models are subject to mesh sensitivity. Analysis results may vary depending on the number of finite elements used to analyze a structure (i.e., mesh size), and computational expense is directly correlated to this mesh size. As more finite elements are used, any nonuniform distributions of concrete stress throughout a structure can be better captured, especially where reinforcement is not well distributed. How well these stress distributions are modeled can influence results when using any of the incremental expansion distribution models. Consideration of moisture and temperature variations throughout a structure can also necessitate the use of many finite elements when using these models. Unfortunately, there is no guidance on how many finite elements is appropriate for use with these models. With the DVEP model, a structure may be analyzed with multiple zones as a function of the number of effectively reinforced directions present in different structural regions. These zones can be further subdivided into a collection of finite elements, although doing so is only necessary if there are sustained nonuniform applied stresses acting throughout the structure during ASR generation. At the very least, defined procedures for splitting a structure into analysis zones offers a starting point for subsequently dividing the structure into finite elements. Of course, structural components (especially smaller laboratory specimens) can often be

modeled as individual elements with the DVEP model, completely eliminating subjectivity associated with mesh size selection.

7.4 COMPARISON OF MODEL RESULTS

To compare the accuracy of the four primary expansion models considered, each model was used to estimate expansions for select RC specimens monitored in the studies described in Chapter 3. Specifically, the three incremental models were applied for specimens from six of the nine DVEP model validation examples in Chapter 6. All specimens described were modeled with single elements rather than an assembly of multiple finite elements. The plots presented in the following sections show measured and computed axial expansions versus volumetric expansions for entire RC elements. The expansions are given in an element's RCS (i.e., in the x-, y-, and z-directions). As was noted in Chapter 6, the expansions plotted are not only those for the concrete material alone. The computed RC expansions were evaluated using the same single-element behavior and analysis program and general materials models used previously when validating the DVEP model.

For additional reference, RC expansion behavior for one of these specimens was estimated using an assumption of uniform concrete expansion in which equal amounts of expansion in the concrete material were applied in all element directions. Such an approach is identical in concept to uniformly applying shrinkage or thermal expansion/contraction strains in an element. As will be seen, the RC expansions in different element directions will reflect the influence of compatibility restraint provided by reinforcement. This will result in slightly different RC expansions being obtained for directions that contain different amounts of reinforcement. However, the influence of applied loading and reinforcement in altering the development of expansions in the concrete material will obviously not be considered.

The different modeling approaches were utilized as follows:

- Uniform expansion assumption – Total directional concrete expansions were uniformly applied in single load stages in all element directions, including in RCS directions. RC expansions were then evaluated in the RCS.
- Cope et al. (1994) and Charlwood et al. (1992) – For a given increment of free, unidirectional concrete expansion during a load stage, increments of restrained concrete expansion were evaluated in the principal directions and as a function of associated principal stresses from the previous load stage. These expansion increments were transformed into expansion increments in RCS directions and combined with previously applied concrete expansions in those directions. These new total concrete expansions in RCS directions were then applied to the element to obtain current-stage RC expansions and updated principal stresses and directions to use for the next load stage. All directions were assumed to experience the same development of free expansion. Free expansion was incremented at 0.05 % per load stage, and a maximum limiting compressive stress of 10 MPa was used.
- Saouma and Perotti (2006) – During individual load stages, given increments of restrained volumetric expansion were distributed to the principal directions as a function of associated principal stresses from the previous load stage. These expansion increments were transformed into expansion increments in RCS directions and combined with previously applied concrete expansions in those directions. The new total concrete expansions in RCS directions were then applied to the element to obtain current-stage RC expansions and updated principal stresses and directions to use for the next load stage. Increments of restrained volumetric expansion were applied directly without the use of Equation 4-22 since the specimens were idealized as single elements. Restrained volumetric expansion was incremented at 0.1 % per load stage, and a maximum limiting compressive stress of 10 MPa was used.
- DVEP model – Total volumetric concrete expansions were applied in single load stages to obtain concrete expansions in RCS directions and subsequent RC

expansions in those directions. An applied compressive stress limit of 10 MPa was used.

Note that the results presented herein are primarily meant to offer perspective on the suitability of the DVEP model to estimate expansion behavior relative to the performance of other modeling approaches when applied with common features (e.g., singular elements with smeared reinforcement and a limiting compressive stress of 10 MPa). The DVEP model results shown were already presented and discussed in Chapter 6. The accuracy of results, or lack thereof, given as-used incremental models are commented upon; however, it is important to recognize that analyses conducted are not meant as a validation or invalidation of the models themselves. It should be kept in mind that computed results with these models may improve or worsen when employing alternate modeling parameters (e.g., use of multiple finite elements with discretely modeled reinforcement, variation in number of increments, or use of an alternate limiting compressive stress).

Figure 7-2 illustrates the results obtained using a uniform expansion assumption. In this case, results are shown for the unequal biaxially reinforced cube A1-102a from Example 2 in Chapter 6 with 0.5 % and 1.1 % reinforcement in two directions. Note that the application of the main expansion distribution models for this particular specimen is discussed later. It can be seen that the computed RC expansions in the reinforced directions are only slightly less than those in the unrestrained direction. These marginal reductions are the result of the compatibility-related restraint to expansion provided by bonded reinforcement. The constitutive-related role of reinforcement in altering the development of expansions in the concrete material itself is not accounted for in this modeling approach. Consequently, the computed and measured results match poorly. An application of uniform expansions to subsequent example specimens is not provided, but similar and often worse discrepancy between computed and measured results would be obtained. The remainder of this section covers the results obtained when using the four primary expansion distribution models.

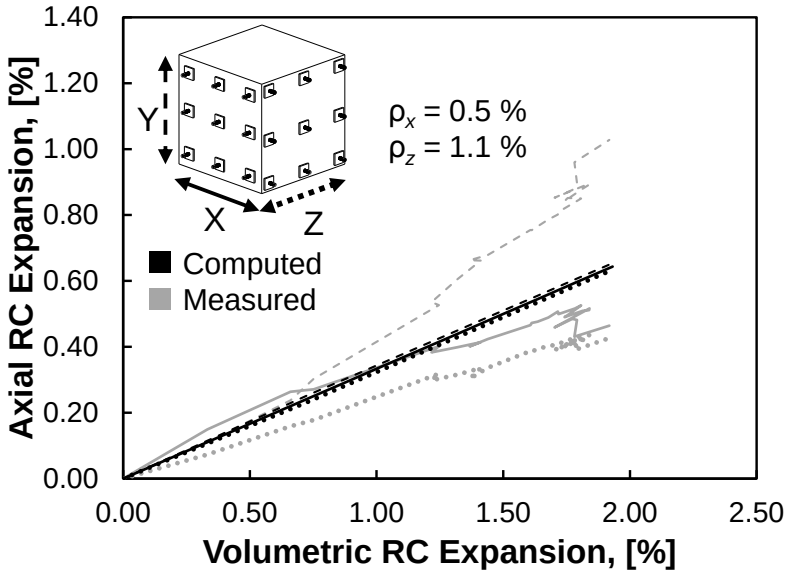

Figure 7-2: Use of uniform expansion assumption with biaxially reinforced cube A1-102a

Results shown in Figure 7-3 are for the uniaxially reinforced cube A1-001b from Example 3 in Chapter 6, with 0.5 % reinforcement. Each model performs well, with the model by Charlwood et al. (1992) generating estimates of expansions in the reinforced direction that are less accurate than those obtained using other models. It is noted here that while the models by Cope et al. (1994) and Charlwood et al. (1992) provide accurate results, as shown in plots of directional expansion versus volumetric expansion, the input used for these models was not a volumetric expansion as was the case for the DVEP model or the model by Saouma and Perotti (2006). Results were obtained through the input of numerically arbitrary free expansions which may or may not be consistent with actual material behavior.

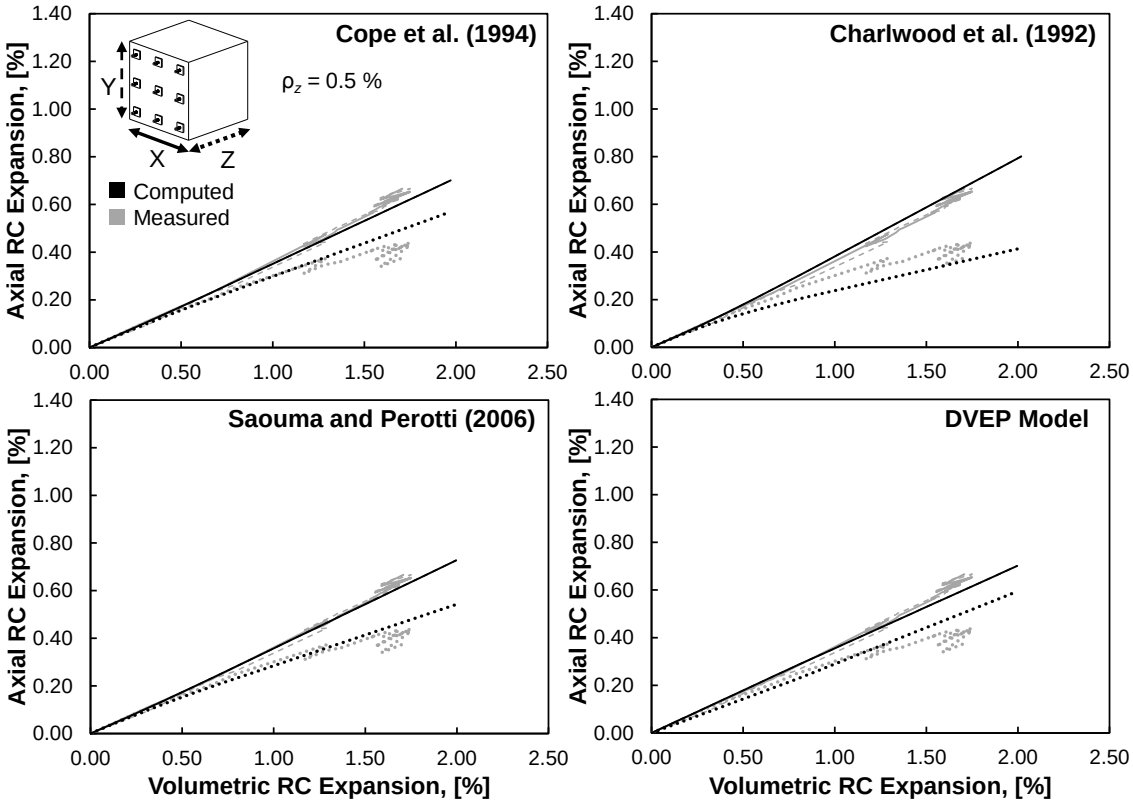

Figure 7-3: Comparison of modeling results for uniaxially reinforced cube A1-001b

Results shown in Figure 7-4 are for the uniaxially reinforced cube A1-003 from Example 3 in Chapter 6 with 1.5 % reinforcement. Recall that the DVEP model estimates RC expansions very well in this case, with the concrete material expansions being identical to those for the uniaxially reinforced cube with 0.5 % reinforcement. The model's mechanics-based formulation suggests that, where reinforcement is allowed to yield, the concrete in elements containing only one common reinforcement ratio in any reinforced directions will expand the same regardless of the particular reinforcement ratio present. The incremental models, which rely upon concrete stress states, provide less accurate expansion estimates, especially in the reinforced direction. Given a higher reinforcement ratio, passively induced stresses develop more quickly, thus resulting in an earlier reduction in expansions in the restrained direction and increased expansion transfer to unreinforced directions according to Saouma and Perotti (2006). Consequently, the results for the cube with 1.5 % reinforcement differs significantly from

that with 0.5 % reinforcement, with expansions in the reinforced and unreinforced directions deviating at lower levels of volumetric expansion and more severely.

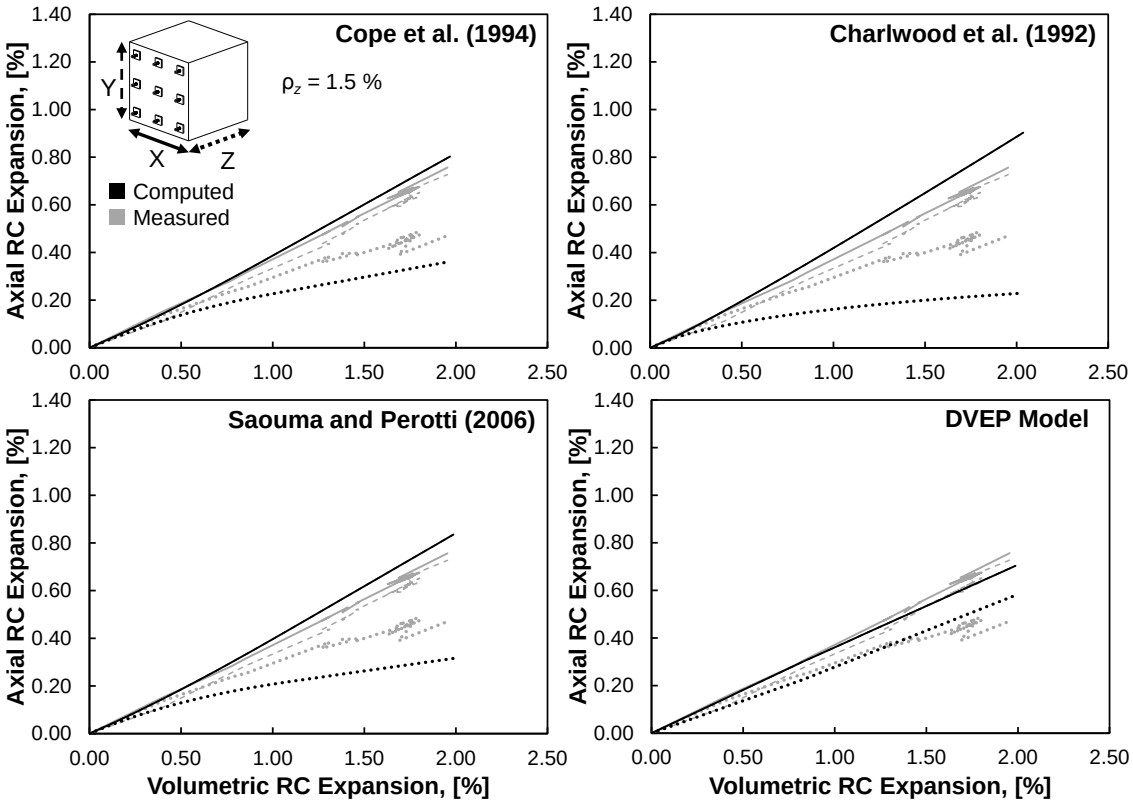

Figure 7-4: Comparison of modeling results for uniaxially reinforced cube A1-003

Results shown in Figure 7-5 are for the equal biaxially reinforced cube A1-101b from Example 5 in Chapter 6 with 0.5 % reinforcement in two directions. In this case, the model by Charlwood et al. (1992) produces the most accurate results overall; however, the other models arguably still provide meaningful expansion response estimates. Up to approximately 1.25 % volumetric expansion, measured and computed results match closely for all models. At higher levels of volumetric expansions, the response estimates obtained using the Cope et al. (1994) model, the Saouma and Perotti model (2006), and the DVEP model begin to deteriorate. However, as explained in Chapter 6, these discrepancies are likely due to the development of increased expansion variations that are shown to occur after the yielding of reinforcement in all directions.

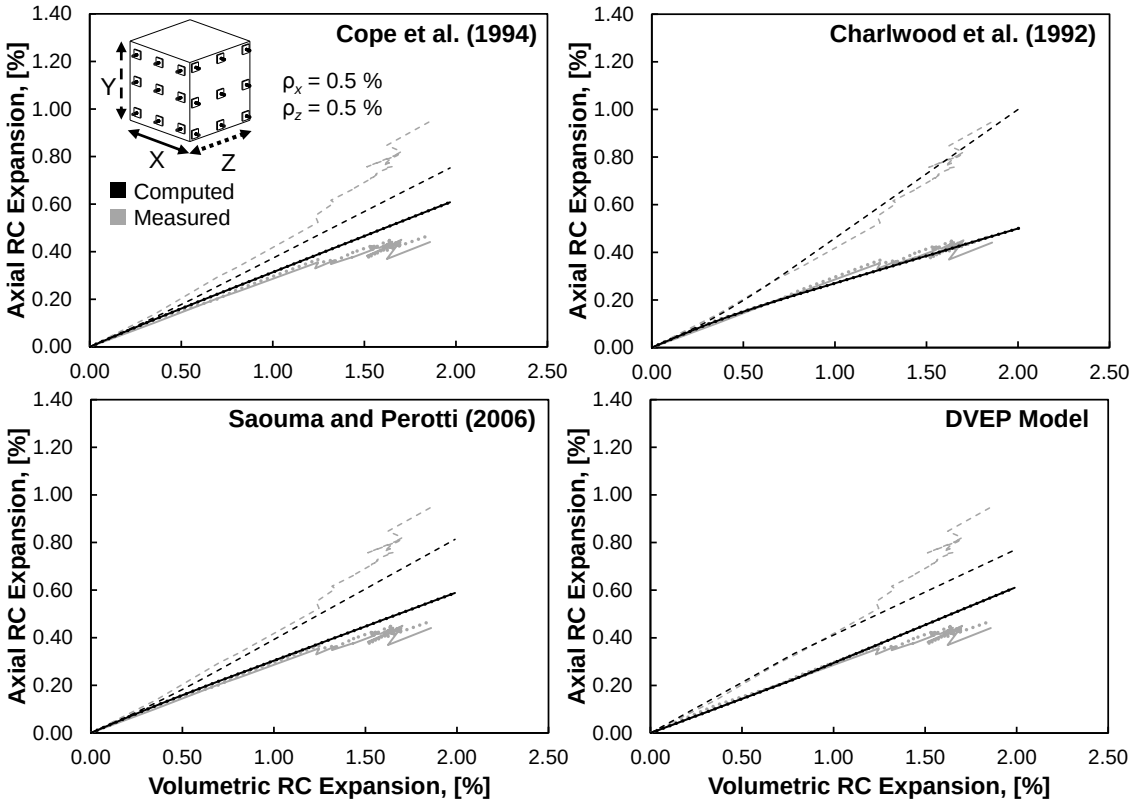

Figure 7-5: Comparison of modeling results for equal biaxially reinforced cube A1-101

Results shown in Figure 7-6 are for the equal biaxially reinforced cube A1-303 from Example 5 in Chapter 6 with 1.5 % reinforcement in two directions. For the same reasons described in the discussion of the uniaxially reinforced cube with a higher reinforcement ratio, the incremental models generate poorer expansion response estimates as compared to the DVEP model and relative to their success in estimating behavior with only 0.5 % reinforcement.

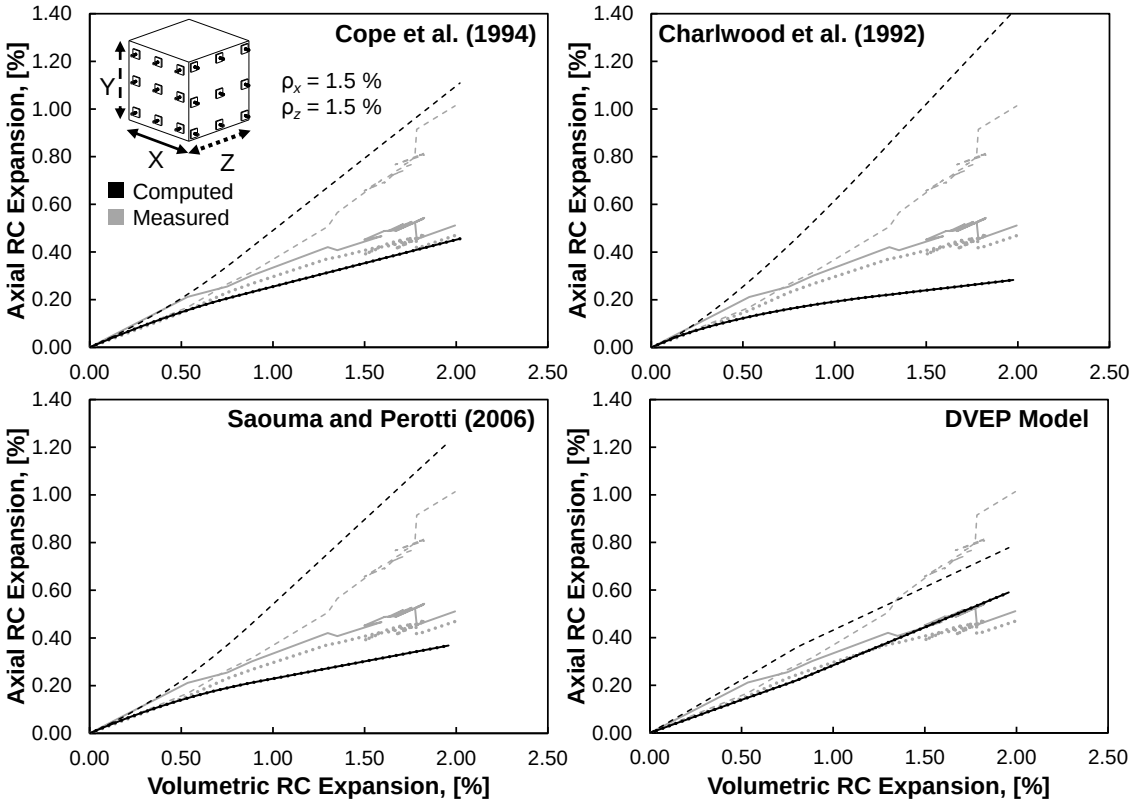

Figure 7-6: Comparison of modeling results for equal biaxially reinforced cube A1-303

Results shown in Figure 7-7 are for the unequal biaxially reinforced cube A1-102a from Example 2 in Chapter 6 with 0.5 % and 1.1 % reinforcement in two directions. The accuracy of the different models tends to vary. Each model correctly captures that expansions are less in the more highly reinforced direction. The model by Saouma and Perotti (2006) produces the best results. Meanwhile, the DVEP model and the model by Cope et al. (1994) perform well until 1.25 % volumetric expansion, beyond which there are discrepancies between the computed and measured results likely as a function of the aforementioned post-yield variability.

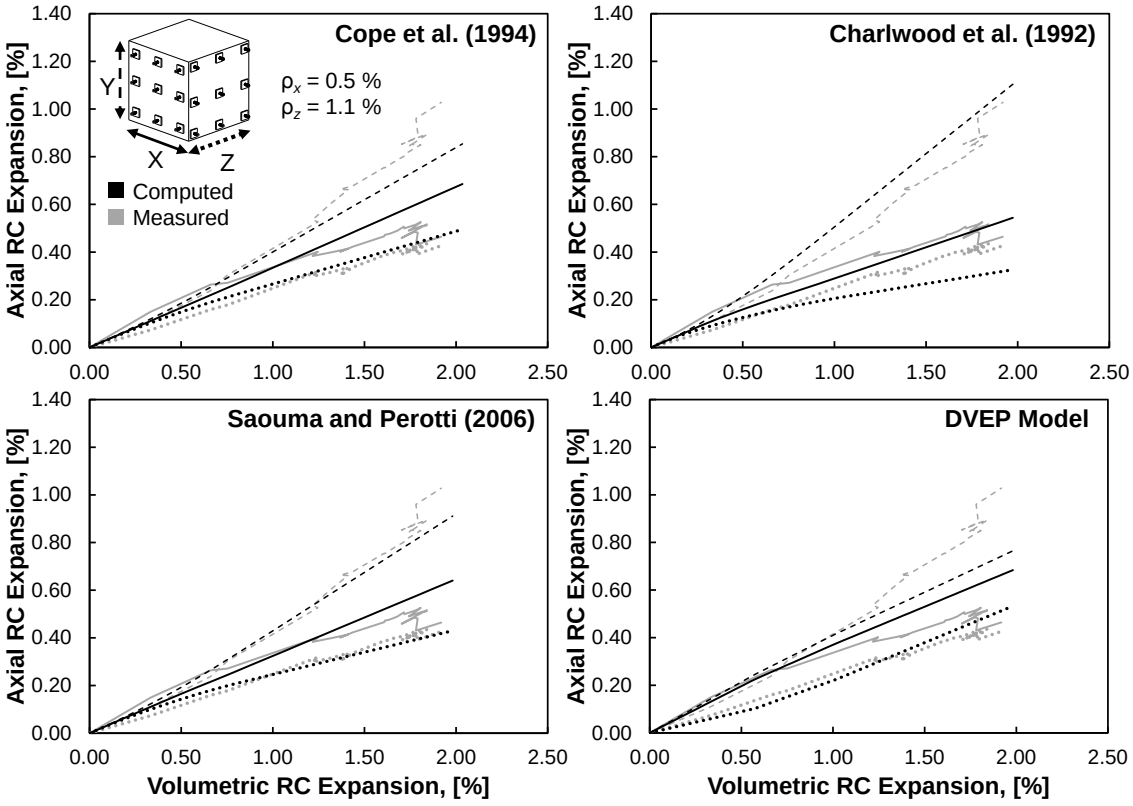

Figure 7-7: Comparison of modeling results for unequal biaxially reinforced cube A1-102a

Results shown in Figure 7-8 are for the biaxially reinforced beam (in Zone A) from Example 1 in Chapter 6 with 1.1 % and 0.7 % reinforcement in two directions. Unlike the DVEP model, which estimates expansions with high accuracy, in part due to the fact that this specimen was considered in the calibration of the model, the incremental models perform poorly. The DVEP model captures behavior well as it directly accounts for bar spacings and pre-yield plateauing of expansions. It is likely that high fidelity finite element modeling with discrete reinforcement may be required to improve the results obtained using the other modeling procedures.

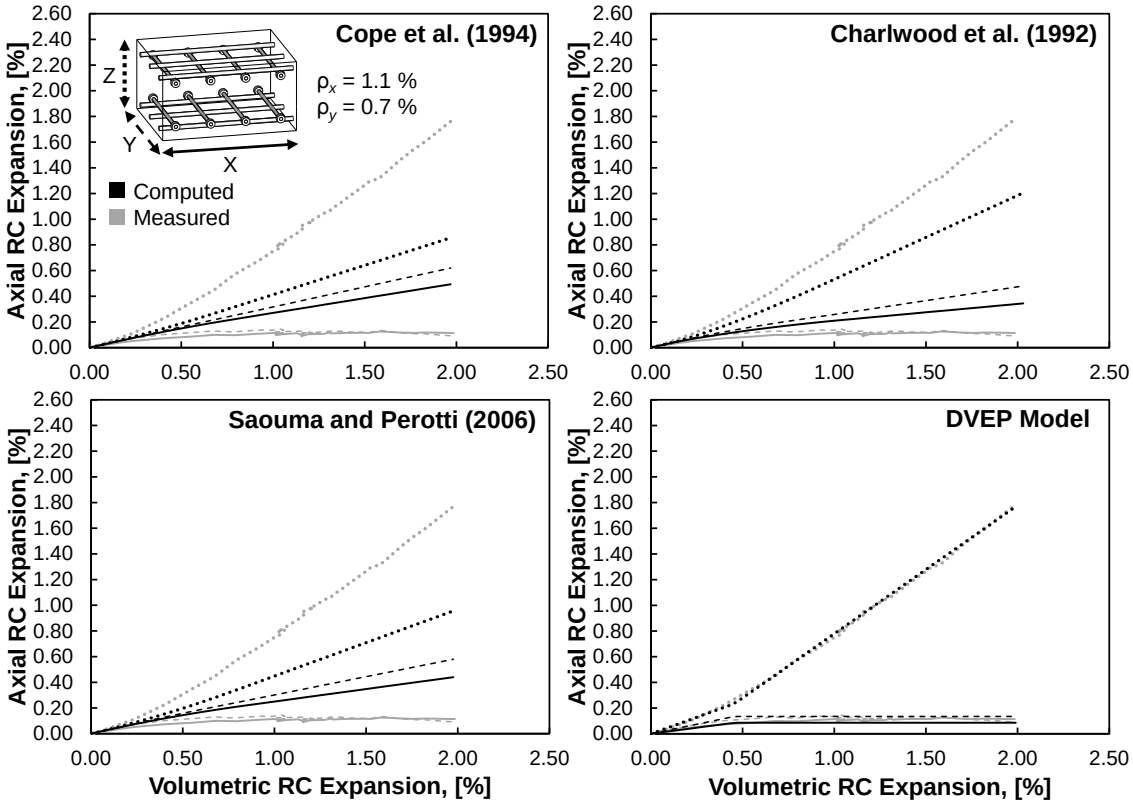

Figure 7-8: Comparison of modeling results for Zone A of biaxially reinforced beam from Wald et al. (2017a)

Results shown in Figure 7-9 are for the triaxially reinforced beam LSC4 from Example 9 in Chapter 6 with 1.6, 0.22, and 0.11 % reinforcement in the directions along with 3.45 MPa of applied axial compression. Again, the DVEP model performs very well for this case while the incremental models tend to generate results providing limited agreement with the measured response. In particular, the incremental models do not capture the large, immediate divergence of expansions in the three directions at the onset of ASR. As in the previous case, full finite element modeling may lead to improved results when using the incremental models.

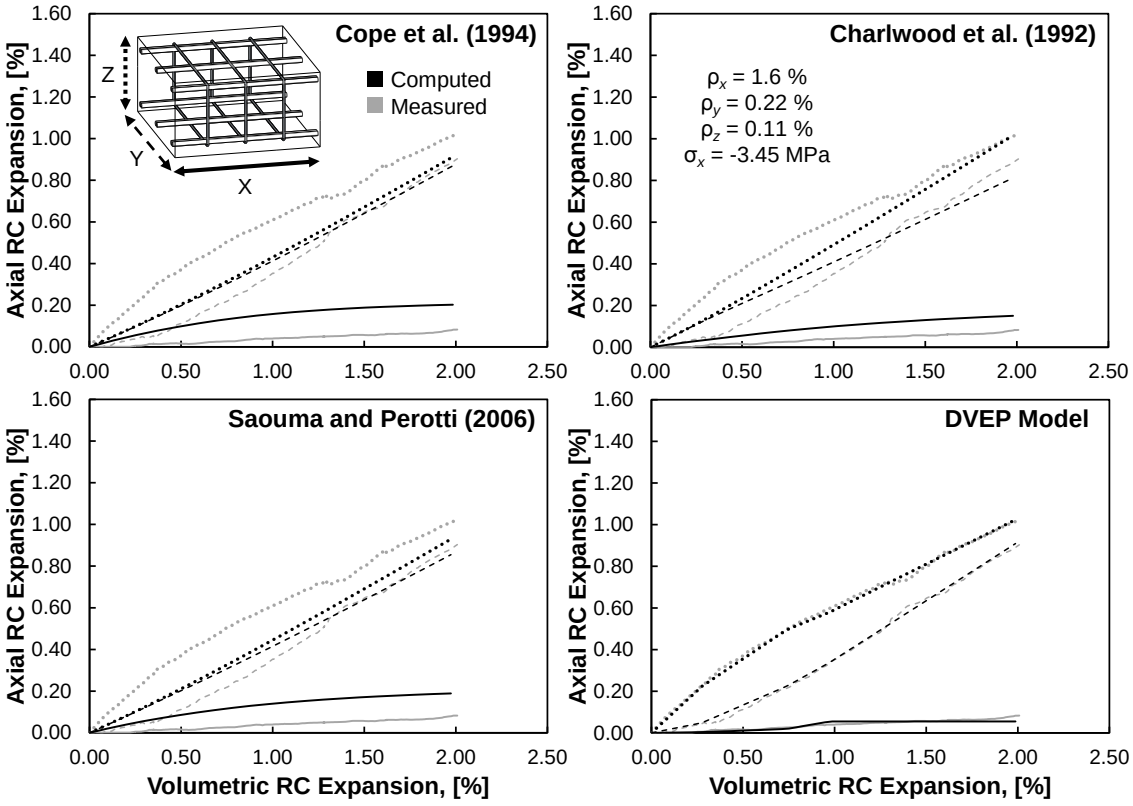

Figure 7-9: Comparison of modeling results for triaxially reinforced beam LSC4 from Bracci et al. (2012)

7.4.1 Conclusions from Comparison of Model Results

Based on the comparison of results for the four expansion distribution models discussed, the following conclusions about the models' successfulness are drawn:

- The DVEP model was able to capture expansion behavior well in all cases when modeling specimens as singular elements with smeared reinforcement due to its direct consideration of bar spacing effects.
- The incremental models often generated good approximations of expansion behavior in cube elements with well-distributed reinforcement. A more uniform reinforcement layout more closely matches a smeared condition, enabling the use of a single, smeared RC element to model behavior.
- The incremental models could not correctly capture apparently similar expansion behaviors for elements with a like number of reinforced directions but containing

different reinforcement ratios. This would imply that these models' reliance upon any concrete stresses (in this case passively induced) as the controlling factor dictating restraint may not be adequate for reinforced concrete as it is for plain concrete under conditions of applied stress.

- The incremental models poorly estimated expansion behavior in beam-type members modeled as singular elements as they could not, as intended, account for nonuniform stress conditions generated in the presence of nonuniformly distributed reinforcement layouts.

7.5 REVIEW OF ADVANTAGES OF DVEP MODEL OVER OTHER MODELS

As suggested throughout Chapters 5 and 6, and given the preceding information presented in this chapter, the DVEP model offers a unique set of advantages compared to other expansion distribution models:

- Calculations can be performed by hand, or with a simple spreadsheet program, without the need to implement the model in a finite element or RC behavior computer program.
- The model was formulated specifically for use with a secant stiffness methodology.
- Overall expansion distribution patterns at threshold levels of volumetric expansions can be determined without any dependency on time or environmental conditioning factors.
- Overall expansion behavior may be found without extensive finite element modeling. As an example, only the DVEP model was found to successfully capture the behavior of ASR-affected beams via single-element analyses.
- The model's formulation reduces computation time and the level of subjectivity associated with model application, namely due to the use of a non-incremental analysis approach and ability to idealize components as single elements.

7.6 SUMMARY

The DVEP model serves as a robust alternative to incremental, single-phase, macroscopic models for estimating ASR expansion behavior. Global expansion patterns can be readily identified using mechanics-based equations, direct formulaic inputs of structural detailing parameters, and distinct considerations of applied loading and passive restraint provided by reinforcement. While all models can, and have been, introduced within the framework of nonlinear finite element analysis software employing a total load, secant stiffness solution methodology, the DVEP model was specifically designed to work hand-in-hand with the secant stiffness approach. Other expansion models necessitate incremental analysis procedures via multiple load stages in finite element analyses. Because of this, their application can be somewhat subjective, and the computational results generated from these models may require additional validation. In contrast, the DVEP model can be used to identify the multi-directional distribution of ASR-induced expansions at any given level of volumetric expansion with a single load stage without consideration of prior behavior. Structural components can very often be successfully modeled as singular RC elements with smeared properties for rapid and still-accurate assessment, regardless of element size and reinforcement layout. Alternatively, guidance exists for how to more objectively divide a modeled component into multiple analysis regions or finite elements.

CHAPTER 8: INFLUENCE OF ASR EXPANSIONS ON STRUCTURAL RESPONSE

8.1 OVERVIEW

This chapter includes the presentation of a brief analytical exploration of the influence of ASR-induced expansions on the mechanical behavior of RC under load. The influences of expansion-induced prestressing, multi-axial confinement, reinforcement yielding, and material property degradation on the strength, stiffness, and deformation capacity of idealized RC elements subjected to simple loading configurations are addressed. The concepts and findings from this chapter are aimed toward gaining insight as to how ASR expansions may alter structural performance along with added impetus for further investigations in the future.

8.2 SINGLE ELEMENT MECHANICAL BEHAVIOR

Using the three-dimensional, solid element modeling capabilities of the VecTor Suite of RC finite element analysis programs (Wong et al. (2013)), the load-deformation behavior of individual RC elements under unidirectional compression, unidirectional tension, and planar shear were evaluated. Cracked concrete material modeling was evaluated using the Modified Compression Field Theory (Vecchio and Collins 1986). Elements were modeled with 1 % smeared and perfectly bonded reinforcement in up to three orthogonal directions, with reinforcement provided, at a minimum, in the direction of axial loading or two directions of a shear plane. The concrete was assigned a compressive strength of 30 MPa with a strain of 2.0 mε corresponding to the peak stress, while the reinforcement was assigned a yield strength of 400 MPa with a yield strain, ε_y, of 2.0 mε. Reinforcement was treated as elastic-perfectly plastic in both tension and compression. In all cases, structural loading was applied after ASR generation. ASR-induced concrete material expansions were evaluated using the DVEP model and then

applied as constant concrete material prestrains under subsequent loading scenarios. Load-deformation behavior was identified for input volumetric concrete material expansions of 0, 0.25, 0.50, and 1.0 %. The directional distributions of expansions were computed assuming a bar spacing consistent with a reinforcement influence factor, λ_ρ, of 0.875 and a bar spacing density below 0.5 to ensure that reinforcement could yield without pre-yield plateauing of expansions. Table 8-1 lists all expansion distribution patterns considered in the analyses.

Table 8-1: Input DVEP model expansions for structural response analyses

			Directional Expansion in Concrete Material, ε_i^{ASR} (%)			
	Volumetric Expansion (%)		0	0.25	0.50	1.0
Reinforcement Layout*	*Uniaxial*	R	0	0.073	0.146	0.295
		U	0	0.089	0.177	0.352
	Biaxial	R	0	0.073	0.146	0.299
		U	0	0.104	0.208	0.402
	Triaxial	R	0	0.083	0.167	0.333
		U	---	---	---	---

*Direction with 1 % reinforcement (R) or without reinforcement (U)

Discussions of the results obtained from these analyses focus primarily on qualitative assessments of how and why ASR may alter the strength, stiffness, and deformation capacity of RC elements. It is understood that quantitative results are subject to change depending on which ASR expansion model or other materials models are used. The concrete and steel are assumed to be perfectly bonded, although in reality, bond degradation may occur due to ASR. Material property degradation is considered, though much uncertainty on this topic remains. The relevant material models employed for these analyses, which are described in more detail in Wong et al. (2013), are outlined in Table 8-2.

Table 8-2: Materials models used for VecTor analyses

	Model Type	VecTor Model
	Analysis Approach	Modified Compression Field Theory
Concrete	Compression Stress-Strain Response	Hognestad (Parabola)
	Tension Stiffening	Modified Bentz 2003
	Tension Softening	Vecchio 1992-A
	Dilation (Poisson Effects)	Variable – Kupfer
	Confinement	Kupfer/Richart
Steel	Hysteretic Stress-Strain Response	Elastic-Plastic (Bilinear)
	Concrete-Steel Bond	Perfect Bond
ASR	ASR Expansion	DVEP Model
	ASR Degradation	ISE 1992

Note that the presented plots of load-deformation response depict applied compressive, tensile, or shear stresses [(-)σ, (+)σ, and τ, respectively] versus the corresponding total element strains that develop only after the generation of ASR. The axial and shear strains are denoted as ε* and γ*, respectively, to differentiate them from the total element strains, ε and γ, which develop relative to a pre-ASR-affected, undeformed state.

8.2.1 Uniaxial Compression

Load-deformation behavior was evaluated for ASR-affected RC elements under pure compression loading with reinforcement provided in the direction of loading and, in some cases, with additional reinforcement also provided in one or two transverse directions. For these analyses, potential buckling of reinforcement was not considered. Compressive failure occurred in all cases upon crushing of the concrete with reinforcement either yielding in compression beforehand, simultaneously with crushing,

or not at all. Points of reinforcement yielding in compression are denoted in plots with a circle marker.

8.2.1.1 Uniaxially Reinforced Elements without Material Property Degradation

Figure 8-1 shows the compressive load-deformation behavior for an element containing reinforcement only in the direction of loading. An element not affected by ASR fails by simultaneous crushing of concrete and yielding of reinforcement at an applied compressive strain of 2.0 mε (i.e., the peak strain of concrete and yield strain of steel). The full plastic capacity of the element ($f_c^{'}$ + ρf_y= 34.5 MPa) is achieved. Meanwhile, in the presence of ASR, the peak compressive capacity and deformation drop, and the initial stiffness of the element is slightly reduced, with greater reductions seen for increasing levels of ASR. In all cases with ASR, the concrete crushes before yielding of reinforcement in compression.

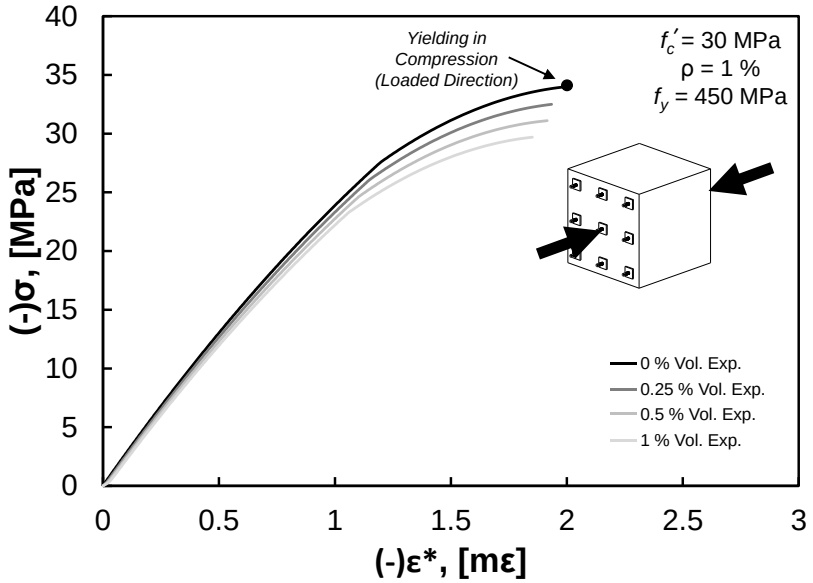

Figure 8-1: Compressive load-deformation response for ASR-affected RC elements with reinforcement in one direction and no material property degradation

Given ASR expansions, reinforcement is stressed/strained in tension and concrete is stressed/strained in compression. As reinforcement is strained further in tension with

increasing levels of ASR, more compressive strain must be applied during a load reversal to be able to fully engage the steel's compressive capacity (i.e., yield in compression). Without ASR, the steel need only be strained in compression by ε_y in order to yield. With ASR, the steel must be strained in compression by anywhere between ε_y to $2\varepsilon_y$ in order to yield. Note that a compressive strain of $2\varepsilon_y$ must be applied if the reinforcement yields in tension during ASR generation. Unless the perfectly bonded concrete can be strained in compression by an additional ε_y to $2\varepsilon_y$ during loading, the concrete will crush before the steel can yield. As more of the concrete's compressive strain capacity is pre-engaged during ASR generation and the peak strain in concrete remains constant, the element's deformation capacity reduces, less of the steel's compressive capacity is engaged, and the overall compressive capacity of the element suffers. Further, due to the nonlinearity of concrete and an initial precompression in the concrete which increases with greater expansions, the concrete responds to load beginning at a softer portion of the material's stress-strain curve. This leads to a reduction in overall element stiffness in response to the applied compression.

Figure 8-1 also indicates that, at the extreme when reinforcement yields in tension during ASR generation (as is the case for 1 % volumetric expansion), the compressive capacity of an RC element (29.7 MPa) is essentially equal to the compressive capacity of a plain concrete element (30 MPa). Compared to a non-ASR-affected element, the drop in capacity is nearly equal to the precompression induced in the concrete (ρf_y = 4.5 MPa). In general, at any level of ASR, the drop in compression capacity relative to that for a non-ASR-affected element is approximately equal to the existing precompression.

8.2.1.2 Biaxially Reinforced Elements without Material Property Degradation

Figure 8-2 shows the compressive load-deformation behavior for elements containing reinforcement in the direction of loading and in one transverse direction. An element not affected by ASR is estimated to fail at a higher peak stress and strain than a uniaxially reinforced element due to influences associated with passive confinement

provided by transverse reinforcement that is engaged by laterally expanding concrete. The peak stress and strain of the concrete are elevated in the presence of a confining stress, which allows the steel to yield prior to crushing of the concrete. ASR-affected elements not only benefit from load-induced confining effects, but also from confinement introduced via the ASR-induced prestressing in the transverse direction. By the time 0.25 % volumetric expansion is applied, an element fails under a maximum confinement condition where the transverse reinforcement has yielded. In addition to a baseline increase in peak stress and strain of concrete, an improved deformation capacity for the element prior to crushing enables more of a reinforcement's compressive capacity to be engaged.

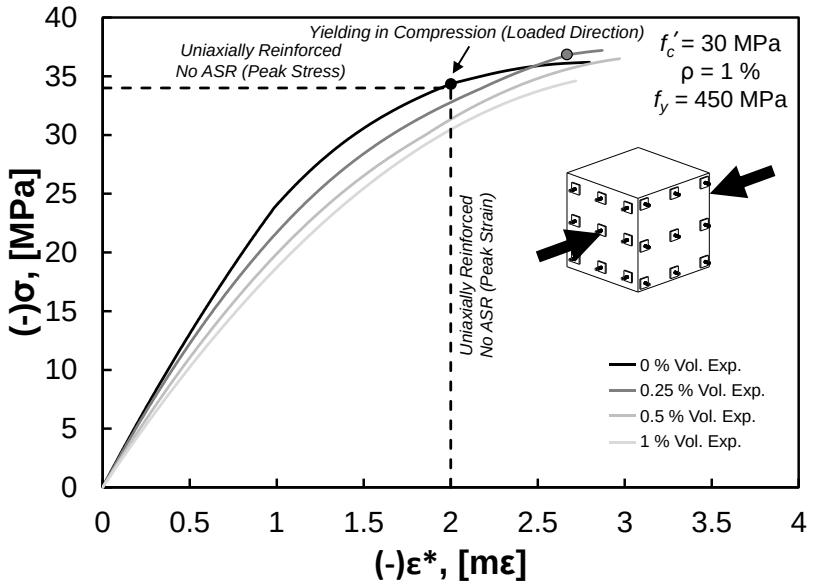

Figure 8-2: Compressive load-deformation response for ASR-affected RC elements with reinforcement in two directions and no material property degradation

The potential benefits of confinement offset with the baseline disadvantages of increasing levels of ASR described in Section 8.2.1.1 (i.e., reduced capacity, applied deformation, and stiffness) were estimated to generate the following results:

- At 0.25 % volumetric expansion, the peak strength and deformation capacity for the element increase compared to that for a non-ASR-affected element. This is

due to the benefits of higher confinement achieved through ASR-induced prestressing in the transverse direction.

- For subsequent increases in volumetric expansion, the peak capacity for an element decreases while confinement is maximized (due to tensile yielding of transverse reinforcement) and the baseline capacity reduction phenomenon dominates response given that the concrete crushes prior to compressive yielding of the loading direction reinforcement. At the same time, element stiffness decreases while peak strain slightly increases.

8.2.1.3 Triaxially Reinforced Elements without Material Property Degradation

Figure 8-3 shows the compressive load-deformation behavior for an element containing reinforcement in three orthogonal directions. Overall load-deformation response is controlled by the same competing factors discussed in Section 8.2.1.2; however, the benefits of confinement in boosting concrete (and thus element) peak stress and strain and facilitating more engagement of steel compressive capacity are significantly improved. Triaxial confinement is estimated to result in a 50-60 % increase in element capacity and more than 200 % increase in peak deformation that can be achieved compared to an unconfined element. These benefits far outweigh any of the baseline reductions to capacity or deformation that might be seen when increasing ASR. At all levels of ASR expansion shown, reinforcement in the loaded direction yields in compression prior to crushing of concrete, and transverse reinforcement yields in tension to generate maximum confinement. Consequently, the capacity of each element is the same and at a maximum. The most significant difference between these elements is that the increased presence of ASR is estimated to produce increased reduction in the initial stiffness of an element.

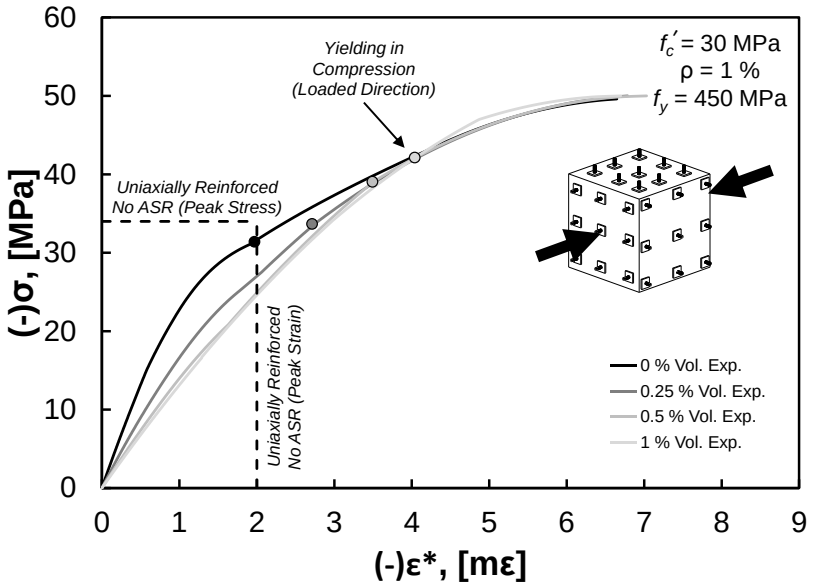

Figure 8-3: Compressive load-deformation response for ASR-affected RC elements with reinforcement in three directions and no material property degradation

8.2.1.4 Influence of Material Property Degradation

Figures 8-4 to 8-6 show the compressive load-deformation behaviors for uniaxially, biaxially, and triaxially reinforced elements with material property degradation considered. The compressive strength and modulus of elasticity of concrete were reduced according to ISE Guidelines (1992), described in Chapter 2. These reductions were evaluated as a function of the restrained, concrete material expansions due to ASR and not free expansions. As such, anisotropic material property reductions were employed. To apply these property reductions, the base compressive stress-strain curve for concrete – in this case, Hognestad's parabola – was modified. The peak stress was simply reduced while the peak strain was assumed to increase to generate the appropriate, reduced elastic modulus. Given that the modulus of elasticity degrades faster than the compressive strength, the peak strain increases with increasing levels of ASR. Such an increase in peak strain can facilitate more engagement of the compressive capacity of reinforcement. Ultimately, the net result of the given material property degradation, the aforementioned baseline disadvantages of increasing ASR, and the

aforementioned advantages of confinement result in a reduction of element strength and stiffness and an increase in total deformation capacity with increasing expansions.

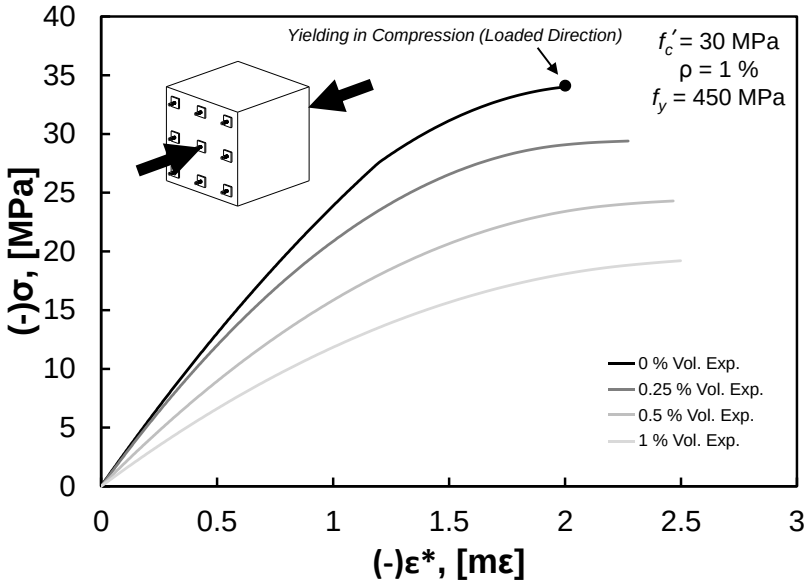

Figure 8-4: Compressive load-deformation response for ASR-affected RC elements with reinforcement in one direction and material property degradation

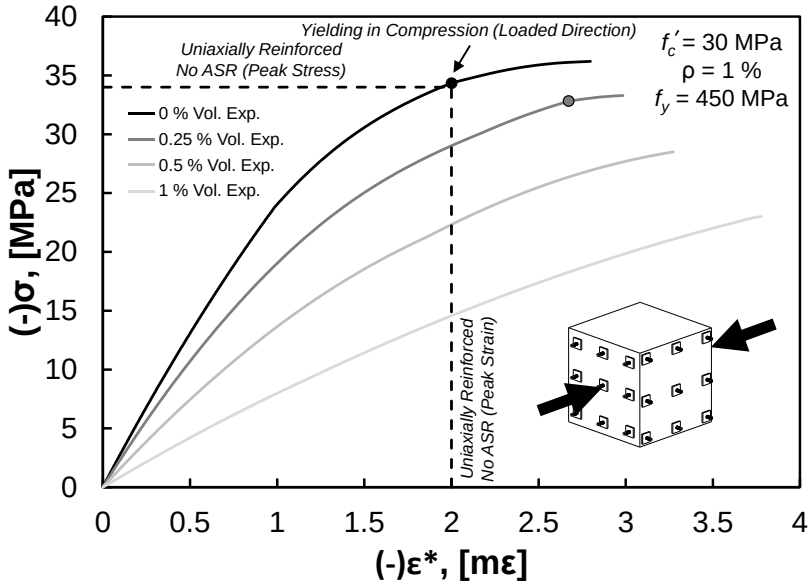

Figure 8-5: Compressive load-deformation response for ASR-affected RC elements with reinforcement in two directions and material property degradation

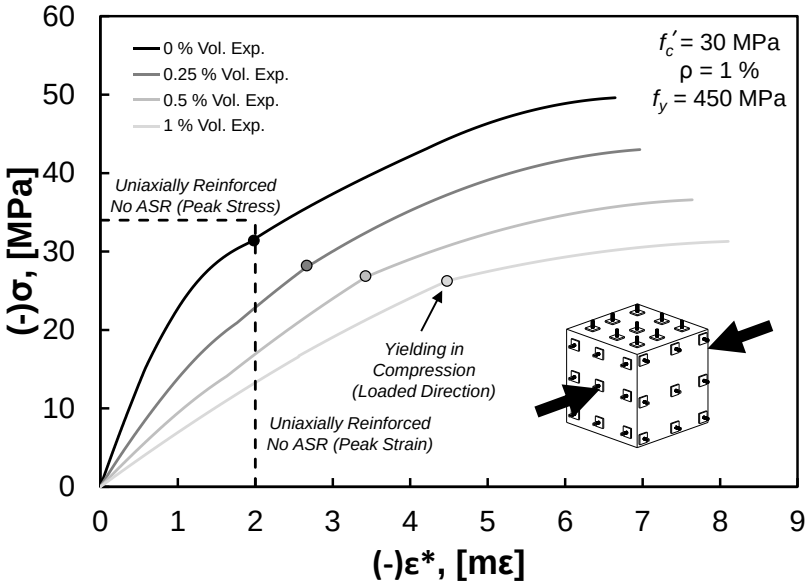

Figure 8-6: Compressive load-deformation response for ASR-affected RC elements with reinforcement in three directions and material property degradation

8.2.2 Uniaxial Tension

Load-deformation behavior was evaluated for ASR-affected RC elements under pure tension with reinforcement in the direction of loading. Given a uniaxial compressive strength of 30 MPa and modulus of elasticity of 30,000 MPa, the tensile strength and cracking strain for the concrete were approximated as 1.81 MPa and 0.06 mε, respectively, on the basis of the assumption that the direct tensile concrete strength can be taken as $0.33\sqrt{f_c'}$ (in MPa).

Tensile load-deformation behavior for RC is generally explained as follows. Prior to cracking, concrete resists almost the entirety of the applied tension. After cracking, the tensile resistance capacity of the concrete drops and the steel begins to resist the bulk of the applied tensile load. Where the load is held constant upon cracking, as in a load-controlled analysis, the load-deformation curve exhibits an abrupt shift in element deformation (i.e., a horizontal shift on the load-deformation curve) with a spike in average steel stress and local steel stress at a crack. As long as the reinforcement does not

yield at this time, the concrete is estimated to resist some tension due to the tension stiffening phenomenon (Scanlon 1971). The element will exhibit a much softer response in the post-cracking state. Eventually, a peak stress will be reached when steel yields and the tension stiffening effect is lost or when the combination of an increase in steel stress and decrease in concrete stress cannot equilibrate any additional applied tension.

Figure 8-7 shows tensile load-deformation behavior for ASR-affected elements without material property degradation considered. Points where concrete cracks are denoted with diamond markers. The presence of ASR in increasing amounts results in an increase in cracking load, a decrease in deformation capacity, and an estimated increase in ultimate load-carrying capacity for some cases. As the amount of ASR expansion increases and the level of precompression in the concrete rises, up until yielding of the reinforcement, the concrete can resist more applied tension until the net tensile stress in the material reaches the cracking stress. This is the same phenomenon that is taken advantage of in typical prestressing design applications. At 0.25 % volumetric expansion, an element is able to carry load beyond cracking and maintains a similar capacity as a non-ASR-affected element, but this element fails at an earlier deformation upon yielding of reinforcement locally at a crack. At higher levels of volumetric expansions, elements have higher overall capacities due to the significant boost in cracking loads, but these elements fail upon cracking and thus have very little deformation capacity. At 0.50 % volumetric expansion, reinforcement yields as load is being transferred from cracked concrete to the steel. At 1.0 % volumetric expansion, the reinforcement has already yielded due to ASR, prior to cracking.

Figure 8-8 illustrates the effects of material property degradation on tensile load-deformation behavior. As the level of ASR increases, the tensile strength of concrete reduces, resulting in an increased reduction in cracking load, softer pre-cracking response, and a slight increase in post-cracking deformation capacity compared to that for a comparable element without material property degradation. Notably, at the highest volumetric expansion, the pre-cracking stiffness of the element is significantly reduced

since the reinforcement is pre-yielded and does not contribute to the overall element stiffness.

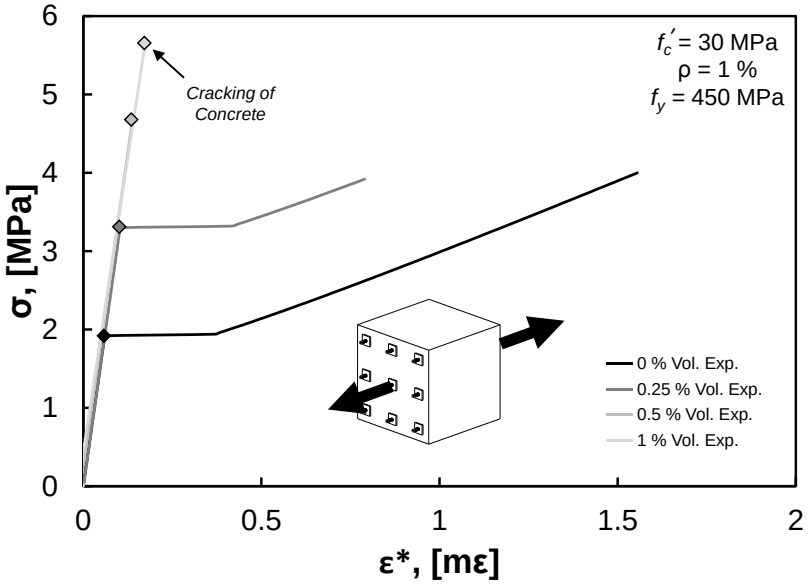

Figure 8-7: Tensile load-deformation response for ASR-affected RC elements with no material property degradation

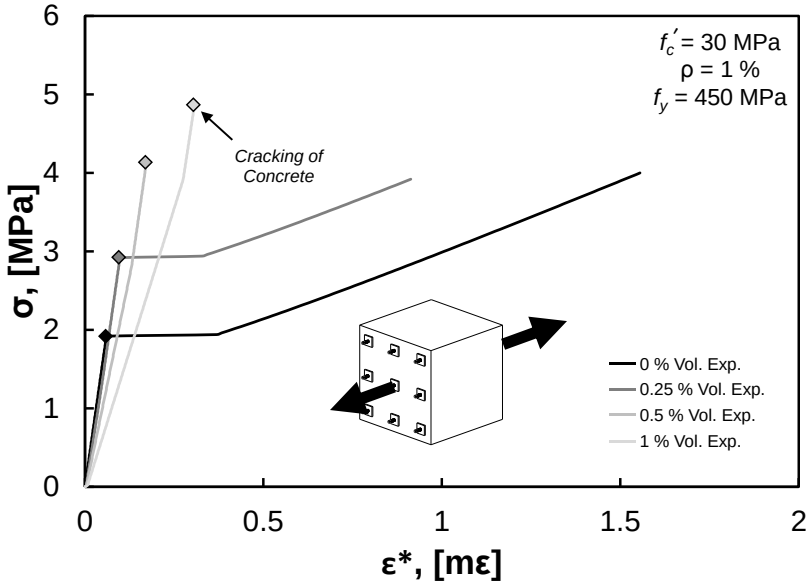

Figure 8-8: Tensile load-deformation response for ASR-affected RC elements with material property degradation

8.2.3 Pure Planar Shear

Figures 8-9 and 8-10 show the load-deformation behavior evaluated for ASR-affected RC elements under pure shear in one plane and containing reinforcement in both planar directions. Material property degradation was only considered for the analyses presented in Figure 8-10. Points where concrete cracks are denoted with diamond markers. For the elements analyzed, the load-deformation response in shear is the same as the load-deformation response of elements in tension. Increasing ASR results in an increase in shear-cracking loads (and ultimate capacity at higher expansion levels) due to precompression and a reduction in deformation capacity due to earlier yielding of reinforcement. Meanwhile, material property degradation counteracts the rise in cracking loads while slightly softening response. These behaviors are evidenced because the elements analyzed exhibit a response dominated by shear-tension. It is probable that elements with different reinforcement configurations and controlled by shear-compression response would display similar characteristics as the load-deformation response of elements under pure compression.

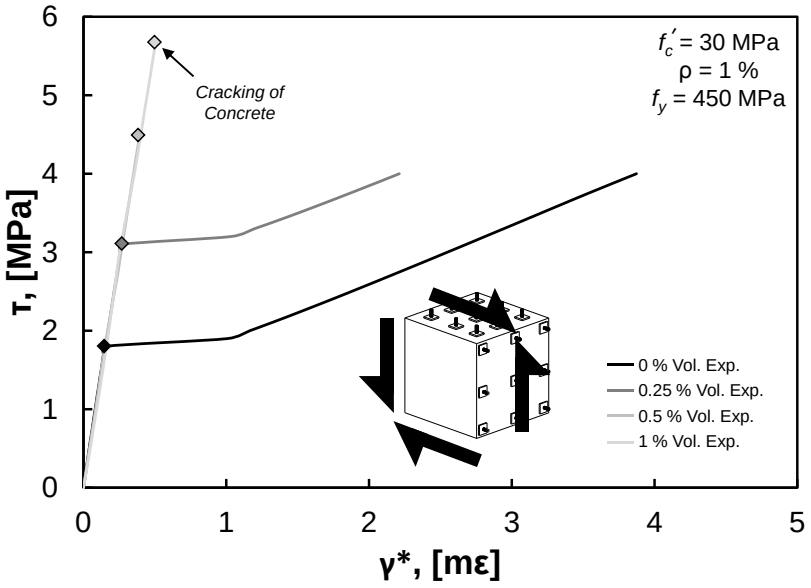

Figure 8-9: Shear load-deformation response for ASR-affected RC elements with no material property degradation

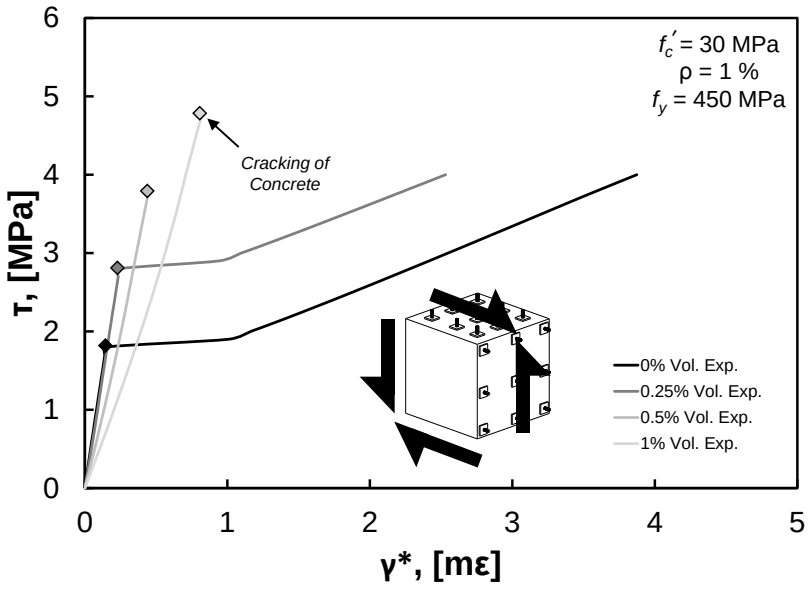

Figure 8-10: Shear load-deformation response for ASR-affected RC elements with material property degradation

8.3 SUMMARY

As evidenced from analyses conducted on individual RC elements, ASR-induced expansions are estimated alter the load-deformation response of RC structures subjected to compression, tension, or shear. Changes in structural performance depend on the level and distribution of ASR-induced expansions and the amounts of associated chemical prestressing and material property degradation that may result.

In RC, the precompression of concrete due to ASR reduces the initial stiffness of elements under compression but can significantly enhance cracking loads in tension. Given multiple directions of reinforcement, the concrete can be subjected to multi-axial states of confinement, significantly boosting compressive capacity and deformation capacity. At the same time, the pretensioning of reinforcement can prevent an element from fully utilizing the compressive capacity of the steel and limit post-cracking deformation capacity in tension through expedited yielding and a loss of tension stiffening. Ultimately, these beneficial and detrimental consequences of ASR-induced expansions, along with material property degradation, should be modeled appropriately in an effort to capture the structural response accurately.

CHAPTER 9: SUMMARY, CONCLUSIONS, AND FUTURE WORK

9.1 DISSERTATION SUMMARY

As RC infrastructure ages, the need to conduct evaluation on structures increases for a multitude of reasons ranging from ensuring continued operational safety to accommodating new purposes for old structures. Alkali-silica reaction represents one of the most complicated and controversial, long-term phenomenological behaviors in concrete that must be accounted for. The controversy stems from the disconnect between the behavior observed for plain, ASR-affected concrete and ASR-affected RC. That is to say, while ASR impacts mechanical properties of plain concrete greatly, its influence on the structural response of RC may not be as severely detrimental for many behavioral modes.

ASR may pose a potential threat to the long-term durability, functionality, and integrity of RC structures. Of special consideration is that the deleterious expansion and cracking behavior which results may alter the manner in which a structure carries loads. Up until now, ASR has commonly been viewed as more of a materials science problem, with an extensive amount of research having been conducted on the mechanisms of expansion and cracking in plain concrete. ASR-affected RC, however, behaves differently from ASR-affected plain concrete. The presence of reinforcement and applied loads changes the nature of ASR-affected concrete, resulting in variations in the amounts, time-development, and multi-directional distribution patterns of expansions. Cracking consistent with ASR-induced expansions can be detrimental to concrete-steel bond, load transfer, and the strength and stiffness response of concrete. Further, the mechanical interaction of expanding concrete and restraining reinforcement transforms RC into an unanticipated form of prestressed concrete. Ultimately, ASR should be viewed just as much so as a structural engineering problem.

The research described in this dissertation was conducted in an effort to comprehensively present the problem of ASR from a structural engineer's perspective,

moving the discussion toward practical application of information valuable for performance-based assessments of affected RC structures and away from exclusive focus on the behavior of plain ASR-affected concrete, which carries little value in structural applications. Specifically, focus was placed on understanding the development, quantification, and implications of ASR-induced expansion behavior as influenced by structural details (e.g., reinforcement amounts and layouts and loading conditions). These goals were achieved through a combination of large-scale experimentation and numerical modeling development and application, tasks which are summarized as follows:

- Task 1: Experimentation – The time development and multi-axial distribution patterns of ASR-induced expansions in large-scale RC elements were monitored in two experimental studies. The research was intended to expand a limited database of existing information, often collected on small-scale and lightly monitored specimens, to better comprehend RC expansion behavior and provide the research community with data for the development and validation of new and existing analytical tools. The multi-directional influences of reinforcement ratios and layouts on expansion behavior were evaluated with respect to time and volumetric expansion development while also considering the roles of differing ASR-affected concrete mixture reactivities and environmental exposure conditions – the main variables in experimentation on ASR-affected plain concrete.
- Task 2: Numerical Modeling – A new analytical tool (the DVEP model) was developed for use in quickly and reliably estimating the multi-directional distribution of ASR-induced expansions in RC elements under any defined combination of multi-directional reinforcement and applied loading scheme. The model was derived from first principles of mechanics with limited calibration against experimentation and validated against experimental data obtained from new studies and that found in the literature. The model was compared to existing analytical techniques and used to help introduce how load-deformation behavior

of ASR-affected elements under various loading conditions may be influenced by concrete material expansions.

9.2 CONCLUSIONS

Principal findings and conclusions drawn from the new experimental and analytical work on ASR expansion behavior in RC described in this dissertation are summarized in the following sections.

9.2.1 Experimentation

- ASR expansion behavior in RC elements was seen to be a multi-directional phenomenon, and the expansions in element directions did not appear to be independent of one another. It is thus critical to monitor expansions in all three directions of experimental test specimens to obtain a reliable and complete set of results.
- Perturbations in local expansion behavior can exist due to a variety of factors including local reactivity of concrete constituents, leaching of alkalis, direct environmental exposure, and concrete permeability. However, for the purposes of structural engineering, and for the fact that quantification of such expansion variations in field structures is not possible, focus should be kept on gross expansion behavior and the structural details (e.g., reinforcement quantity and detailing, applied loading, and casting direction) which influence such overall behavior. Of note, while casting direction was previously reported to be an important consideration, expansions for the specimens monitored were not found to have been influenced heavily by casting direction, suggesting that reinforcement may play a more prominent role in affecting overall expansion behavior.
- The multi-directional distribution of ASR-induced volumetric expansions in RC elements was found to depend on the number of reinforced directions, amounts of reinforcement, and layouts of reinforcement present in those elements.

- The influence of reinforcement in restraining expansions appeared to be distinct from that of applied loading. There was no prominent decline in expansion rates with increasing passively induced stresses, and, in the event of expansions plateauing prior to yielding of reinforcement, expansions stopped given lower concrete stress levels than have been derived from experiments on actively restrained elements affected by ASR.
- Concrete mixture reactivity and environmental exposure conditions were found to influence the time-development but not the multi-directional distribution of volumetric expansions.
- ASR expansion behavior was found to be easier to examine for specimens from a single study or between multiple studies by plotting directional expansions against volumetric expansions, thus filtering out the influence of time, chemical reactivity, temperature, and humidity.
- Expansion development in a direction was seen to restricted by the presence of reinforcement such that a reinforced direction will expand less than an unreinforced direction; however, unrestrained expansions may be influenced by reinforcement in other directions and are not the same as free expansions of plain concrete.
- Within an individual element, a highly reinforced direction expanded less than a lightly reinforced direction, but amongst different elements with similar reinforcement layouts, a greater amount of reinforcement did not necessarily equate to less directional or volumetric expansions.
- An increasing number of reinforced directions for an element resulted in a reduction in volumetric expansion development with time.
- The layout of reinforcement in a given element direction influenced the uniformity of expansions and influenced the propensity for the reinforcement to yield or for expansions to plateau prior to the reinforcement yielding.
- There may exist a practical distance-related zone of influence for reinforcing bars in restraining expansions which may factor in when trying to compare and

contrast expansion behavior in core and cover concretes or between portions of a structure reinforced differently.

9.2.2 Numerical Modeling

- The multi-directional distributions of ASR-induced volumetric expansions in RC elements were able to be well-estimated with a new single-phase, macroscopic modeling approach eschewing classic dependencies on expansion development with time and environmental conditions, concrete reactivity, incrementation, and complex finite element modeling.
- The use of a constitutive formulation derived from simple principles of mechanics and a distinction made between the influence of active and passive restraint conditions provided a rational basis for empirically observed behavior.
- Direct consideration of material stiffnesses, reinforcement ratios and layouts (e.g., bar spacings and degree of uniformity), and applied loading through formulation and well-defined rules of model application permitted the evaluation of expansion behavior in large structural components with very limited subjective analysis using hand calculations and/or, in many cases, with singular finite elements.
- Extensive validation of the modeling approach achieved through comparison of computed and experimentally measured results from in-house and external studies illustrated high levels of robustness and accuracy.
- Compared to existing modeling approaches, the new approach offered a faster, less subjective, and more direct solution methodology with improved consideration of the effects of reinforcement and abrupt changes in expansion behavior caused by reinforcement yielding or plateauing expansions given various reinforcement layouts.
- ASR-induced expansions that can be estimated with an ASR expansion distribution model may alter the load-deformation behavior of an RC structure under compression, tension, or shear due to chemically-induced prestressing and the degradation of concrete material properties in one or more directions.

Potential benefits of expansion include increased cracking loads and confinement provided by multi-directional precompression induced in concrete. Potential detriments of expansion include a limitation on the efficacy of reinforcement in compression due to ASR-induced pretensioning, a loss of post-cracking deformation capacity, and an overall reduction in element strength and stiffness due to concrete material property degradation.

9.3 RECOMMENDATIONS AND FUTURE WORK

Despite the considerable amount of research that has been conducted on the topic of ASR, a shift in focus toward ASR behavior in RC structures and bridging the gap between materials science and practical structural engineering applications is in its infancy. The research presented in this dissertation was aimed at expanding the database of information and fundamental knowledge of ASR expansion behavior in RC and introduced a new analysis tool to aid structural engineers evaluate current and future performance of ASR-affected RC structures. As the scientific community continues to pursue a holistic understanding of ASR behavior and better engage structural engineers in addressing durability-related distress mechanisms, the following future research ideas may prove to be useful:

- Attempts should be made to achieve more consistency amongst different ASR expansion studies focusing on the influences of reinforcement and/or applied loads in order to better compare experimental results and draw meaningful conclusions. Although concrete mixture reactivity, environmental conditioning, and specimen size, amongst other factors, play important roles in influencing expansion behavior, significant variations in experimental programs make it extremely difficult to isolate the independent role of restraint. Further, potential differences between the two types of restraint to expansions (active and passive) should be explored in greater detail. More experimental data is needed to assess the influence of applied loading, notably in larger specimens, on volumetric and multi-directional expansion behavior (i.e., not only in the direction of loading).

More data is needed on expansion behavior for elements subjected to multi-axial states of loading, sustained shear, and a combination of active and passive restraint.

- Expansions of experimentally monitored specimens, and ideally any field-monitored structures, need to be recorded in three, not only one or two, orthogonal directions. As indicated in this dissertation, ASR expansion behavior is a volumetric phenomenon with interactions between multiple expanding directions which can only be captured if a full set of expansions are measured. Further, attempts to better standardize expansion measurement techniques would be advantageous.
- Formulaic methods to assess structural performance of ASR-affected structures given information about expansion behavior – that obtained experimentally or through numerical modeling – should be developed. This may include development of new equations or the modification/adaptation of existing design code equations.
- Material property degradation in large-scale and restrained RC structures needs to be better addressed. The discrepancies between the load-carrying response of plain concrete materials samples and real structures must be reconciled. Full compressive and tensile stress-strain response at varying levels of ASR-induced expansion should be obtained.
- The potential for the degradation of concrete-steel bond should be explored further through experimentation and accounted for in numerical modeling. The formulation of the DVEP model may require updating to account for the role which bond degradation may play in counteracting the prestressing effect due to ASR.
- For the performance-based assessment of existing structures affected by ASR, the DVEP model may be of greatest value for engineers in estimating expansion behavior given only a few select volumetric expansions without the need for incremental analyses or the identification of expansion distribution patterns for all

possible levels of distress. Identification of individual or ranged values of critical, or threshold, levels of volumetric expansion for which an ASR-affected structure should be analyzed is an important task for the future. An upper-bound of volumetric expansion expected to be reached by a structure during its service life may be estimated from experimental or field observations. For reference, some specimens monitored in the studies described in this dissertation reached as high as 2-2.5% volumetric expansion by the conclusion of the monitoring periods.

- More research should be performed to identify the structural performance of large-scale ASR-affected members. The shear, flexural, and anchorage behaviors of RC members should be explored to a greater degree through experimentation and numerical modeling. Particularly, emphasis should be placed on identifying how load-carrying response is affected in ASR-affected structures given a wide array of possible structural designs and details.

APPENDIX A: CHAPTER 6 DVEP MODEL EXAMPLE CALCULATIONS*

This appendix consists of Tables A-1 through A-14 which document, for Examples 2-9 in Chapter 6, all pertinent computed values and parameters related to ASR stage and critical event behavior determined in Phase I using the DVEP model. The information contained within each table is the same as that in Table 6-1 for Example 1.

* Portions of this appendix have been extracted directly from the following prospective publication (unpublished at time of dissertation submission) written by the author of this dissertation, with tables reformatted for use in this dissertation:

Wald, D. M., Hrynyk, T. D., and Bayrak, O. (2017). "The Distributed Volumetric Expansion Pressure Model for ASR Expansion Behavior in Reinforced Concrete Elements – Part 2: Implementation and Validation." (submitted to *ASCE Journal of Structural Engineering*)

- Dissertator contribution: Primary author and lead researcher

Table A-1: Example 2 calculations

		X	Y	Z			X	Y	Z
	$\lambda_{\sigma i}$	1.0	1.0	1.0		$\lambda_{\rho i}$	0.875	1.0	0.875
Stage 1	Eqn. 5-	---	---	---	**CEV#1**	CEV	---	NEPR	---
	λ_{1i}	0.292	0.333	0.292		σ_{vol}^{exp} (MPa)		--- 0 ---	
	γ_1		--- 0.083 ---			$\Delta\sigma_{vol,1}^{exp}$ (MPa)		--- 0 ---	
	RSTC	2	1	2		$\Delta\sigma_{i,1}^{exp}$ (MPa)	0	0	0
	$\gamma_{1,dist,i}$	0	0.083	0		σ_i^{exp} (MPa)	0	0	0
	κ_{1i}	0.292	0.417	0.292		$\Delta\varepsilon_{i,1}^{ASR}$ (%)	0	0	0
						ε_i^{ASR} (%)	0	0	0
						ε_{vol}^{ASR} (%)		--- 0 ---	
Stage 2	Eqn. 5-	9	5,10	9	**CEV#2**	CEV	Y	---	---
	λ_{2i}	0.292	0.333	0.292		σ_{vol}^{exp} (MPa)		--- 7.71 ---	
	γ_2		--- 0.083 ---			$\Delta\sigma_{vol,2}^{exp}$ (MPa)		--- 7.71 ---	
	RSTC	2	1	2		$\Delta\sigma_{i,2}^{exp}$ (MPa)	2.25	3.21	2.25
	$\gamma_{2,dist,i}$	0	0.083	0		σ_i^{exp} (MPa)	2.25	3.21	2.25
	κ_{2i}	0.292	0.417	0.292		$\Delta\varepsilon_{i,2}^{ASR}$ (%)	0.231	0.243	0.109
						ε_i^{ASR} (%)	0.231	0.243	0.109
						ε_{vol}^{ASR} (%)		--- 0.583 ---	
Stage 3	Eqn. 5-	5,10	5,10	9	**CEV#3**	CEV	---	---	Y
	λ_{3i}	0.292	0.333	0.292		σ_{vol}^{exp} (MPa)		--- 16.97 ---	
	γ_3		--- 0.083 ---			$\Delta\sigma_{vol,3}^{exp}$ (MPa)		--- 9.26 ---	
	RSTC	1	1	2		$\Delta\sigma_{i,3}^{exp}$ (MPa)	3.09	3.47	2.70
	$\gamma_{3,dist,i}$	0.041	0.041	0		σ_i^{exp} (MPa)	5.34	6.69	4.95
	κ_{3i}	0.333	0.375	0.292		$\Delta\varepsilon_{i,3}^{ASR}$ (%)	0.149	0.168	0.130
						ε_i^{ASR} (%)	0.380	0.410	0.239
						ε_{vol}^{ASR} (%)		--- 1.029 ---	
Stage 4	Eqn. 5-	5,10	5,10	5,10					
	λ_{4i}	0.292	0.333	0.292					
	γ_4		--- 0.083 ---						
	RSTC	1	1	1					
	$\gamma_{4,dist,i}$	0.028	0.028	0.028					
	κ_{4i}	0.319	0.361	0.319					

Note: CEV Types - NEPR = no EPR; Y = yielding of reinforcement; MAX = max expansion reached

Table A-2: Example 3 calculations – A1-001b

		X	Y	Z			X	Y	Z
	$\lambda_{\sigma i}$	1.0	1.0	1.0		$\lambda_{\rho i}$	0.875	1.0	1.0
Stage 1	Eqn. 5-	---	---	---	**CEV#1**	CEV	---	NEPR	---
	λ_{1i}	0.292	0.333	0.333		σ_{vol}^{exp} (MPa)		--- 0 ---	
	γ_1		--- 0.042 ---			$\Delta\sigma_{vol,1}^{exp}$ (MPa)		--- 0 ---	
	RSTC	2	1	1		$\Delta\sigma_{i,1}^{exp}$ (MPa)	0	0	0
	$\gamma_{1,dist,i}$	0	0.021	0.021		σ_i^{exp} (MPa)	0	0	0
	κ_{1i}	0.292	0.354	0.354		$\Delta\varepsilon_{i,1}^{ASR}$ (%)	0	0	0
						ε_i^{ASR} (%)	0	0	0
						ε_{vol}^{ASR} (%)		--- 0 ---	
Stage 2	Eqn. 5-	---	---	---	**CEV#2**	CEV	---	---	NEPR
	λ_{2i}	0.292	0.333	0.333		σ_{vol}^{exp} (MPa)		--- 0 ---	
	γ_2		--- 0.042 ---			$\Delta\sigma_{vol,2}^{exp}$ (MPa)		--- 0 ---	
	RSTC	2	1	1		$\Delta\sigma_{i,2}^{exp}$ (MPa)	0	0	0
	$\gamma_{2,dist,i}$	0	0.021	0.021		σ_i^{exp} (MPa)	0	0	0
	κ_{2i}	0.292	0.354	0.354		$\Delta\varepsilon_{i,2}^{ASR}$ (%)	0	0	0
						ε_i^{ASR} (%)	0	0	0
						ε_{vol}^{ASR} (%)		--- 0 ---	
Stage 3	Eqn. 5-	9	5,10	5,10	**CEV#3**	CEV	Y	---	---
	λ_{3i}	0.292	0.333	0.333		σ_{vol}^{exp} (MPa)		--- 7.71 ---	
	γ_3		--- 0.042 ---			$\Delta\sigma_{vol,3}^{exp}$ (MPa)		--- 7.71 ---	
	RSTC	2	1	1		$\Delta\sigma_{i,3}^{exp}$ (MPa)	2.25	2.73	2.73
	$\gamma_{3,dist,i}$	0	0.021	0.021		σ_i^{exp} (MPa)	2.25	2.73	2.73
	κ_{3i}	0.292	0.354	0.354		$\Delta\varepsilon_{i,3}^{ASR}$ (%)	0.231	0.281	0.281
						ε_i^{ASR} (%)	0.231	0.281	0.281
						ε_{vol}^{ASR} (%)		--- 0.793 ---	
Stage 4	Eqn. 5-	5,10	5,10	5,10					
	λ_{4i}	0.292	0.333	0.333					
	γ_4		--- 0.042 ---						
	RSTC	1	1	1					
	$\gamma_{4,dist,i}$	0.014	0.014	0.014					
	κ_{4i}	0.306	0.347	0.347					

Note: CEV Types - NEPR = no EPR; Y = yielding of reinforcement; MAX = max expansion reached

Table A-3: Example 3 calculations – A1-003

		X	Y	Z			X	Y	Z
	$\lambda_{\sigma i}$	1.0	1.0	1.0		$\lambda_{\rho i}$	0.875	1.0	1.0
Stage 1	Eqn. 5-	---	---	---	**CEV#1**	CEV	---	NEPR	---
	λ_{1i}	0.292	0.333	0.333		σ_{vol}^{exp} (MPa)		--- 0 ---	
	γ_1		--- 0.042 ---			$\Delta\sigma_{vol,1}^{exp}$ (MPa)		--- 0 ---	
	RSTC	2	1	1		$\Delta\sigma_{i,1}^{exp}$ (MPa)	0	0	0
	$\gamma_{1,dist,i}$	0	0.021	0.021		σ_i^{exp} (MPa)	0	0	0
	κ_{1i}	0.292	0.354	0.354		$\Delta\varepsilon_{i,1}^{ASR}$ (%)	0	0	0
						ε_i^{ASR} (%)	0	0	0
						ε_{vol}^{ASR} (%)		--- 0 ---	
Stage 2	Eqn. 5-	---	---	---	**CEV#2**	CEV	---	---	NEPR
	λ_{2i}	0.292	0.333	0.333		σ_{vol}^{exp} (MPa)		--- 0 ---	
	γ_2		--- 0.042 ---			$\Delta\sigma_{vol,2}^{exp}$ (MPa)		--- 0 ---	
	RSTC	2	1	1		$\Delta\sigma_{i,2}^{exp}$ (MPa)	0	0	0
	$\gamma_{2,dist,i}$	0	0.021	0.021		σ_i^{exp} (MPa)	0	0	0
	κ_{2i}	0.292	0.354	0.354		$\Delta\varepsilon_{i,2}^{ASR}$ (%)	0	0	0
						ε_i^{ASR} (%)	0	0	0
						ε_{vol}^{ASR} (%)		--- 0 ---	
Stage 3	Eqn. 5-	9	5,10	5,10	**CEV#3**	CEV	Y	---	---
	λ_{3i}	0.292	0.333	0.333		σ_{vol}^{exp} (MPa)		--- 23.14 ---	
	γ_3		--- 0.042 ---			$\Delta\sigma_{vol,3}^{exp}$ (MPa)		--- 23.14 ---	
	RSTC	2	1	1		$\Delta\sigma_{i,3}^{exp}$ (MPa)	6.75	8.20	8.20
	$\gamma_{3,dist,i}$	0	0.021	0.021		σ_i^{exp} (MPa)	6.75	8.20	8.20
	κ_{3i}	0.292	0.354	0.354		$\Delta\varepsilon_{i,3}^{ASR}$ (%)	0.244	0.296	0.296
						ε_i^{ASR} (%)	0.244	0.296	0.296
						ε_{vol}^{ASR} (%)		--- 0.836 ---	
Stage 4	Eqn. 5-	5,10	5,10	5,10					
	λ_{4i}	0.292	0.333	0.333					
	γ_4		--- 0.042 ---						
	RSTC	1	1	1					
	$\gamma_{4,dist,i}$	0.014	0.014	0.014					
	κ_{4i}	0.306	0.347	0.347					

Note: CEV Types - NEPR = no EPR; Y = yielding of reinforcement; MAX = max expansion reached

Table A-4: Example 4 calculations – Blocks 2 and 8

		X	Y	Z			X	Y	Z
	$\lambda_{\sigma i}$	1.0	1.0	1.0		$\lambda_{\rho i}$	0.875	1.0	1.0
Stage 1	Eqn. 5-	---	---	---	**CEV#1**	CEV	---	NEPR	---
	λ_{1i}	0.292	0.333	0.333		σ_{vol}^{exp} (MPa)		--- 0 ---	
	γ_1		--- 0.042 ---			$\Delta\sigma_{vol,1}^{exp}$ (MPa)		--- 0 ---	
	RSTC	2	1	1		$\Delta\sigma_{i,1}^{exp}$ (MPa)	0	0	0
	$\gamma_{1,dist,i}$	0	0.021	0.021		σ_i^{exp} (MPa)	0	0	0
	κ_{1i}	0.292	0.354	0.354		$\Delta\varepsilon_{i,1}^{ASR}$ (%)	0	0	0
						ε_i^{ASR} (%)	0	0	0
						ε_{vol}^{ASR} (%)		--- 0 ---	
Stage 2	Eqn. 5-	---	---	---	**CEV#2**	CEV	---	---	NEPR
	λ_{2i}	0.292	0.333	0.333		σ_{vol}^{exp} (MPa)		--- 0 ---	
	γ_2		--- 0.042 ---			$\Delta\sigma_{vol,2}^{exp}$ (MPa)		--- 0 ---	
	RSTC	2	1	1		$\Delta\sigma_{i,2}^{exp}$ (MPa)	0	0	0
	$\gamma_{2,dist,i}$	0	0.021	0.021		σ_i^{exp} (MPa)	0	0	0
	κ_{2i}	0.292	0.354	0.354		$\Delta\varepsilon_{i,2}^{ASR}$ (%)	0	0	0
						ε_i^{ASR} (%)	0	0	0
						ε_{vol}^{ASR} (%)		--- 0 ---	
Stage 3	Eqn. 5-	9	5,10	5,10	**CEV#3**	CEV	Y	---	---
	λ_{3i}	0.292	0.333	0.333		σ_{vol}^{exp} (MPa)		--- 5.86 ---	
	γ_3		--- 0.042 ---			$\Delta\sigma_{vol,3}^{exp}$ (MPa)		--- 5.86 ---	
	RSTC	2	1	1		$\Delta\sigma_{i,3}^{exp}$ (MPa)	1.71	2.08	2.08
	$\gamma_{3,dist,i}$	0	0.021	0.021		σ_i^{exp} (MPa)	1.71	2.08	2.08
	κ_{3i}	0.292	0.354	0.354		$\Delta\varepsilon_{i,3}^{ASR}$ (%)	0.229	0.278	0.278
						ε_i^{ASR} (%)	0.229	0.278	0.278
						ε_{vol}^{ASR} (%)		--- 0.786 ---	
Stage 4	Eqn. 5-	5,10	5,10	5,10					
	λ_{4i}	0.292	0.333	0.333					
	γ_4		--- 0.042 ---						
	RSTC	1	1	1					
	$\gamma_{4,dist,i}$	0.014	0.014	0.014					
	κ_{4i}	0.306	0.347	0.347					

Note: CEV Types - NEPR = no EPR; Y = yielding of reinforcement; MAX = max expansion reached

Table A-5: Example 4 calculations – Blocks 3 and 9

		X	Y	Z			X	Y	Z
	$\lambda_{\sigma i}$	1.0	1.0	1.0		$\lambda_{\rho i}$	0.875	1.0	1.0
Stage 1	Eqn. 5-	---	---	---	**CEV#1**	CEV	---	NEPR	---
	λ_{1i}	0.292	0.333	0.333		σ_{vol}^{exp} (MPa)		--- 0 ---	
	γ_1		--- 0.042 ---			$\Delta\sigma_{vol,1}^{exp}$ (MPa)		--- 0 ---	
	RSTC	2	1	1		$\Delta\sigma_{i,1}^{exp}$ (MPa)	0	0	0
	$\gamma_{1,dist,i}$	0	0.021	0.021		σ_i^{exp} (MPa)	0	0	0
	κ_{1i}	0.292	0.354	0.354		$\Delta\varepsilon_{i,1}^{ASR}$ (%)	0	0	0
						ε_i^{ASR} (%)	0	0	0
						ε_{vol}^{ASR} (%)		--- 0 ---	
Stage 2	Eqn. 5-	---	---	---	**CEV#2**	CEV	---	---	NEPR
	λ_{2i}	0.292	0.333	0.333		σ_{vol}^{exp} (MPa)		--- 0 ---	
	γ_2		--- 0.042 ---			$\Delta\sigma_{vol,2}^{exp}$ (MPa)		--- 0 ---	
	RSTC	2	1	1		$\Delta\sigma_{i,2}^{exp}$ (MPa)	0	0	0
	$\gamma_{2,dist,i}$	0	0.021	0.021		σ_i^{exp} (MPa)	0	0	0
	κ_{2i}	0.292	0.354	0.354		$\Delta\varepsilon_{i,2}^{ASR}$ (%)	0	0	0
						ε_i^{ASR} (%)	0	0	0
						ε_{vol}^{ASR} (%)		--- 0 ---	
Stage 3	Eqn. 5-	9	5,10	5,10	**CEV#3**	CEV	MAX	---	---
	λ_{3i}	0.292	0.333	0.333		σ_{vol}^{exp} (MPa)		--- 7.16 ---	
	γ_3		--- 0.042 ---			$\Delta\sigma_{vol,3}^{exp}$ (MPa)		--- 7.16 ---	
	RSTC	2	1	1		$\Delta\sigma_{i,3}^{exp}$ (MPa)	2.09	2.53	2.53
	$\gamma_{3,dist,i}$	0	0.021	0.021		σ_i^{exp} (MPa)	2.09	2.53	2.53
	κ_{3i}	0.292	0.354	0.354		$\Delta\varepsilon_{i,3}^{ASR}$ (%)	0.141	0.171	0.171
						ε_i^{ASR} (%)	0.141	0.171	0.171
						ε_{vol}^{ASR} (%)		--- 0.483 ---	
Stage 4	Eqn. 5-	9	5,10	5,10					
	λ_{4i}	0	0.333	0.333					
	γ_4		--- 0.333 ---						
	RSTC	9	1	1					
	$\gamma_{4,dist,i}$	0	0.167	0.167					
	κ_{4i}	0	0.5	0.5					

Note: CEV Types - NEPR = no EPR; Y = yielding of reinforcement; MAX = max expansion reached

Table A-6: Example 4 calculations – Blocks 4 and 11

		X	Y	Z			X	Y	Z
	$\lambda_{\sigma i}$	1.0	1.0	1.0		$\lambda_{\rho i}$	0.875	1.0	1.0
Stage 1	Eqn. 5-	---	---	---	**CEV#1**	CEV	---	NEPR	---
	λ_{1i}	0.292	0.333	0.333		σ_{vol}^{exp} (MPa)		--- 0 ---	
	γ_1		--- 0.042 ---			$\Delta\sigma_{vol,1}^{exp}$ (MPa)		--- 0 ---	
	RSTC	2	1	1		$\Delta\sigma_{i,1}^{exp}$ (MPa)	0	0	0
	$\gamma_{1,dist,i}$	0	0.021	0.021		σ_i^{exp} (MPa)	0	0	0
	κ_{1i}	0.292	0.354	0.354		$\Delta\varepsilon_{i,1}^{ASR}$ (%)	0	0	0
						ε_i^{ASR} (%)	0	0	0
						ε_{vol}^{ASR} (%)		--- 0 ---	
Stage 2	Eqn. 5-	---	---	---	**CEV#2**	CEV	---	---	NEPR
	λ_{2i}	0.292	0.333	0.333		σ_{vol}^{exp} (MPa)		--- 0 ---	
	γ_2		--- 0.042 ---			$\Delta\sigma_{vol,2}^{exp}$ (MPa)		--- 0 ---	
	RSTC	2	1	1		$\Delta\sigma_{i,2}^{exp}$ (MPa)	0	0	0
	$\gamma_{2,dist,i}$	0	0.021	0.021		σ_i^{exp} (MPa)	0	0	0
	κ_{2i}	0.292	0.354	0.354		$\Delta\varepsilon_{i,2}^{ASR}$ (%)	0	0	0
						ε_i^{ASR} (%)	0	0	0
						ε_{vol}^{ASR} (%)		--- 0 ---	
Stage 3	Eqn. 5-	9	5,10	5,10	**CEV#3**	CEV	MAX	---	---
	λ_{3i}	0.292	0.333	0.333		σ_{vol}^{exp} (MPa)		--- 7.16 ---	
	γ_3		--- 0.042 ---			$\Delta\sigma_{vol,3}^{exp}$ (MPa)		--- 7.16 ---	
	RSTC	2	1	1		$\Delta\sigma_{i,3}^{exp}$ (MPa)	2.09	2.53	2.53
	$\gamma_{3,dist,i}$	0	0.021	0.021		σ_i^{exp} (MPa)	2.09	2.53	2.53
	κ_{3i}	0.292	0.354	0.354		$\Delta\varepsilon_{i,3}^{ASR}$ (%)	0.073	0.089	0.089
						ε_i^{ASR} (%)	0.073	0.089	0.089
						ε_{vol}^{ASR} (%)		--- 0.252 ---	
Stage 4	Eqn. 5-	9	5,10	5,10					
	λ_{4i}	0	0.333	0.333					
	γ_4		--- 0.333 ---						
	RSTC	9	1	1					
	$\gamma_{4,dist,i}$	0	0.167	0.167					
	κ_{4i}	0	0.5	0.5					

Note: CEV Types - NEPR = no EPR; Y = yielding of reinforcement; MAX = max expansion reached

Table A-7: Example 5 calculations – A1-101b

		X	Y	Z			X	Y	Z
	$\lambda_{\sigma i}$	1.0	1.0	1.0		$\lambda_{\rho i}$	0.875	1.0	0.875
Stage 1	Eqn. 5-	---	---	---	**CEV#1**	CEV	---	NEPR	---
	λ_{1i}	0.292	0.333	0.292		σ_{vol}^{exp} (MPa)		--- 0 ---	
	γ_1		--- 0.083 ---			$\Delta\sigma_{vol,1}^{exp}$ (MPa)		--- 0 ---	
	RSTC	2	1	2		$\Delta\sigma_{i,1}^{exp}$ (MPa)	0	0	0
	$\gamma_{1,dist,i}$	0	0.083	0		σ_i^{exp} (MPa)	0	0	0
	κ_{1i}	0.292	0.417	0.292		$\Delta\varepsilon_{i,1}^{ASR}$ (%)	0	0	0
						ε_i^{ASR} (%)	0	0	0
						ε_{vol}^{ASR} (%)		--- 0 ---	
Stage 2	Eqn. 5-	9	5,10	9	**CEV#2**	CEV	Y	---	---
	λ_{2i}	0.292	0.333	0.292		σ_{vol}^{exp} (MPa)		--- 7.71 ---	
	γ_2		--- 0.083 ---			$\Delta\sigma_{vol,2}^{exp}$ (MPa)		--- 7.71 ---	
	RSTC	2	1	2		$\Delta\sigma_{i,2}^{exp}$ (MPa)	2.25	3.21	2.25
	$\gamma_{2,dist,i}$	0	0.083	0		σ_i^{exp} (MPa)	2.25	3.21	2.25
	κ_{2i}	0.292	0.417	0.292		$\Delta\varepsilon_{i,2}^{ASR}$ (%)	0.231	0.330	0.231
						ε_i^{ASR} (%)	0.231	0.330	0.231
						ε_{vol}^{ASR} (%)		--- 0.793 ---	
Stage 3	Eqn. 5-	5,10	5,10	9	**CEV#3**	CEV	---	---	Y
	λ_{3i}	0.292	0.333	0.292		σ_{vol}^{exp} (MPa)		--- 7.71 ---	
	γ_3		--- 0.083 ---			$\Delta\sigma_{vol,3}^{exp}$ (MPa)		--- 0 ---	
	RSTC	1	1	2		$\Delta\sigma_{i,3}^{exp}$ (MPa)	0	0	0
	$\gamma_{3,dist,i}$	0.042	0.042	0		σ_i^{exp} (MPa)	2.25	3.21	2.25
	κ_{3i}	0.333	0.375	0.292		$\Delta\varepsilon_{i,3}^{ASR}$ (%)	0	0	0
						ε_i^{ASR} (%)	0.231	0.330	0.231
						ε_{vol}^{ASR} (%)		--- 0.793 ---	
Stage 4	Eqn. 5-	5,10	5,10	5,10					
	λ_{4i}	0.292	0.333	0.292					
	γ_4		--- 0.083 ---						
	RSTC	1	1	1					
	$\gamma_{4,dist,i}$	0.028	0.028	0.028					
	κ_{4i}	0.319	0.361	0.319					

Note: CEV Types - NEPR = no EPR; Y = yielding of reinforcement; MAX = max expansion reached

Table A-8: Example 5 calculations – A1-303

		X	Y	Z			X	Y	Z
	$\lambda_{\sigma i}$	1.0	1.0	1.0		$\lambda_{\rho i}$	0.875	1.0	0.875
Stage 1	Eqn. 5-	---	---	---	**CEV#1**	CEV	---	NEPR	---
	λ_{1i}	0.292	0.333	0.292		σ_{vol}^{exp} (MPa)		--- 0 ---	
	γ_1		--- 0.083 ---			$\Delta\sigma_{vol,1}^{exp}$ (MPa)		--- 0 ---	
	RSTC	2	1	2		$\Delta\sigma_{i,1}^{exp}$ (MPa)	0	0	0
	$\gamma_{1,dist,i}$	0	0.083	0		σ_i^{exp} (MPa)	0	0	0
	κ_{1i}	0.292	0.417	0.292		$\Delta\varepsilon_{i,1}^{ASR}$ (%)	0	0	0
						ε_i^{ASR} (%)	0	0	0
						ε_{vol}^{ASR} (%)		--- 0 ---	
Stage 2	Eqn. 5-	9	5,10	9	**CEV#2**	CEV	Y	---	---
	λ_{2i}	0.292	0.333	0.292		σ_{vol}^{exp} (MPa)		--- 23.14 ---	
	γ_2		--- 0.083 ---			$\Delta\sigma_{vol,2}^{exp}$ (MPa)		--- 23.14 ---	
	RSTC	2	1	2		$\Delta\sigma_{i,2}^{exp}$ (MPa)	6.75	9.64	6.75
	$\gamma_{2,dist,i}$	0	0.083	0		σ_i^{exp} (MPa)	6.75	9.64	6.75
	κ_{2i}	0.292	0.417	0.292		$\Delta\varepsilon_{i,2}^{ASR}$ (%)	0.244	0.349	0.244
						ε_i^{ASR} (%)	0.244	0.349	0.244
						ε_{vol}^{ASR} (%)		--- 0.836 ---	
Stage 3	Eqn. 5-	5,10	5,10	9	**CEV#3**	CEV	---	---	Y
	λ_{3i}	0.292	0.333	0.292		σ_{vol}^{exp} (MPa)		--- 23.14 ---	
	γ_3		--- 0.083 ---			$\Delta\sigma_{vol,3}^{exp}$ (MPa)		--- 0 ---	
	RSTC	1	1	2		$\Delta\sigma_{i,3}^{exp}$ (MPa)	0	0	0
	$\gamma_{3,dist,i}$	0.042	0.042	0		σ_i^{exp} (MPa)	6.75	9.64	6.75
	κ_{3i}	0.333	0.375	0.292		$\Delta\varepsilon_{i,3}^{ASR}$ (%)	0	0	0
						ε_i^{ASR} (%)	0.244	0.349	0.244
						ε_{vol}^{ASR} (%)		--- 0.836 ---	
Stage 4	Eqn. 5-	5,10	5,10	5,10					
	λ_{4i}	0.292	0.333	0.292					
	γ_4		--- 0.083 ---						
	RSTC	1	1	1					
	$\gamma_{4,dist,i}$	0.028	0.028	0.028					
	κ_{4i}	0.319	0.361	0.319					

Note: CEV Types - NEPR = no EPR; Y = yielding of reinforcement; MAX = max expansion reached

Table A-9: Example 6 calculations – 5 MPa load

		X	Y	Z			X	Y	Z
	$\lambda_{\sigma i}$	0.5	1.0	1.0		$\lambda_{\rho i}$	1.0	1.0	1.0
Stage 1	Eqn. 5-	---	---	---	**CEV#1**	CEV	NEPR	---	---
	λ_{1i}	0.167	0.333	0.333		σ_{vol}^{exp} (MPa)		--- 0 ---	
	γ_1		--- 0.167 ---			$\Delta\sigma_{vol,1}^{exp}$ (MPa)		--- 0 ---	
	RSTC	5	1	1		$\Delta\sigma_{i,1}^{exp}$ (MPa)	0	0	0
	$\gamma_{1,dist,i}$	0	0.083	0.083		σ_i^{exp} (MPa)	0	0	0
	κ_{1i}	0.167	0.417	0.417		$\Delta\varepsilon_{i,1}^{ASR}$ (%)	0	0	0
						ε_i^{ASR} (%)	0	0	0
						ε_{vol}^{ASR} (%)		--- 0 ---	
Stage 2	Eqn. 5-	---	---	---	**CEV#2**	CEV	---	NEPR	---
	λ_{2i}	0.167	0.333	0.333		σ_{vol}^{exp} (MPa)		--- 0 ---	
	γ_2		--- 0.167 ---			$\Delta\sigma_{vol,2}^{exp}$ (MPa)		--- 0 ---	
	RSTC	5	1	1		$\Delta\sigma_{i,2}^{exp}$ (MPa)	0	0	0
	$\gamma_{2,dist,i}$	0	0.083	0.083		σ_i^{exp} (MPa)	0	0	0
	κ_{2i}	0.167	0.417	0.417		$\Delta\varepsilon_{i,2}^{ASR}$ (%)	0	0	0
						ε_i^{ASR} (%)	0	0	0
						ε_{vol}^{ASR} (%)		--- 0 ---	
Stage 3	Eqn. 5-	---	---	---	**CEV#3**	CEV	---	---	NEPR
	λ_{3i}	0.167	0.333	0.333		σ_{vol}^{exp} (MPa)		--- 0 ---	
	γ_3		--- 0.167 ---			$\Delta\sigma_{vol,3}^{exp}$ (MPa)		--- 0 ---	
	RSTC	5	1	1		$\Delta\sigma_{i,3}^{exp}$ (MPa)	0	0	0
	$\gamma_{3,dist,i}$	0	0.083	0.083		σ_i^{exp} (MPa)	0	0	0
	κ_{3i}	0.167	0.417	0.417		$\Delta\varepsilon_{i,3}^{ASR}$ (%)	0	0	0
						ε_i^{ASR} (%)	0	0	0
						ε_{vol}^{ASR} (%)		--- 0 ---	
Stage 4	Eqn. 5-	5,10	5,10	5,10					
	λ_{4i}	0.167	0.333	0.333					
	γ_4		--- 0.167 ---						
	RSTC	5	1	1					
	$\gamma_{4,dist,i}$	0	0.083	0.083					
	κ_{4i}	0.167	0.417	0.417					

Note: CEV Types - NEPR = no EPR; Y = yielding of reinforcement; MAX = max expansion reached

Table A-10: Example 6 calculations – 10 MPa load

		X	Y	Z			X	Y	Z
	$\lambda_{\sigma i}$	0	1.0	1.0		$\lambda_{\rho i}$	1.0	1.0	1.0
Stage 1	Eqn. 5-	---	---	---	**CEV#1**	CEV	NEPR	---	---
	λ_{1i}	0	0.333	0.333		σ_{vol}^{exp} (MPa)		--- 0 ---	
	γ_1		--- 0.333 ---			$\Delta\sigma_{vol,1}^{exp}$ (MPa)		--- 0 ---	
	RSTC	9	1	1		$\Delta\sigma_{i,1}^{exp}$ (MPa)	0	0	0
	$\gamma_{1,dist,i}$	0	0.167	0.167		σ_i^{exp} (MPa)	0	0	0
	κ_{1i}	0	0.5	0.5		$\Delta\varepsilon_{i,1}^{ASR}$ (%)	0	0	0
						ε_i^{ASR} (%)	0	0	0
						ε_{vol}^{ASR} (%)		--- 0 ---	
Stage 2	Eqn. 5-	---	---	---	**CEV#2**	CEV	---	NEPR	---
	λ_{2i}	0	0.333	0.333		σ_{vol}^{exp} (MPa)		--- 0 ---	
	γ_2		--- 0.333 ---			$\Delta\sigma_{vol,2}^{exp}$ (MPa)		--- 0 ---	
	RSTC	9	1	1		$\Delta\sigma_{i,2}^{exp}$ (MPa)	0	0	0
	$\gamma_{2,dist,i}$	0	0.167	0.167		σ_i^{exp} (MPa)	0	0	0
	κ_{2i}	0	0.5	0.5		$\Delta\varepsilon_{i,2}^{ASR}$ (%)	0	0	0
						ε_i^{ASR} (%)	0	0	0
						ε_{vol}^{ASR} (%)		--- 0 ---	
Stage 3	Eqn. 5-	---	---	---	**CEV#3**	CEV	---	---	NEPR
	λ_{3i}	0	0.333	0.333		σ_{vol}^{exp} (MPa)		--- 0 ---	
	γ_3		--- 0.333 ---			$\Delta\sigma_{vol,3}^{exp}$ (MPa)		--- 0 ---	
	RSTC	9	1	1		$\Delta\sigma_{i,3}^{exp}$ (MPa)	0	0	0
	$\gamma_{3,dist,i}$	0	0.167	0.167		σ_i^{exp} (MPa)	0	0	0
	κ_{3i}	0	0.5	0.5		$\Delta\varepsilon_{i,3}^{ASR}$ (%)	0	0	0
						ε_i^{ASR} (%)	0	0	0
						ε_{vol}^{ASR} (%)		--- 0 ---	
Stage 4	Eqn. 5-	5,10	5,10	5,10					
	λ_{4i}	0	0.333	0.333					
	γ_4		--- 0.333 ---						
	RSTC	9	1	1					
	$\gamma_{4,dist,i}$	0	0.167	0.167					
	κ_{4i}	0	0.5	0.5					

Note: CEV Types - NEPR = no EPR; Y = yielding of reinforcement; MAX = max expansion reached

Table A-11: Example 7 calculations

		X	Y	Z			X	Y	Z
	$\lambda_{\sigma i}$	0.61	0.61	1.0		$\lambda_{\rho i}$	0.875	0.875	1.0
Stage 1	Eqn. 5-	---	---	---	**CEV#1**	CEV	---	---	NEPR
	λ_{1i}	0.178	0.178	0.333		σ_{vol}^{exp} (MPa)		--- 0 ---	
	γ_1		--- 0.311 ---			$\Delta\sigma_{vol,1}^{exp}$ (MPa)		--- 0 ---	
	RSTC	6	6	1		$\Delta\sigma_{i,1}^{exp}$ (MPa)	0	0	0
	$\gamma_{1,dist,i}$	0	0	0.311		σ_i^{exp} (MPa)	0	0	0
	κ_{1i}	0.178	0.178	0.644		$\Delta\varepsilon_{i,1}^{ASR}$ (%)	0	0	0
						ε_i^{ASR} (%)	0	0	0
						ε_{vol}^{ASR} (%)		--- 0 ---	
Stage 2	Eqn. 5-	9	9	5,10	**CEV#2**	CEV	MAX	---	---
	λ_{2i}	0.178	0.178	0.333		σ_{vol}^{exp} (MPa)		--- 12.46 ---	
	γ_2		--- 0.311 ---			$\Delta\sigma_{vol,2}^{exp}$ (MPa)		--- 12.46 ---	
	RSTC	6	6	1		$\Delta\sigma_{i,2}^{exp}$ (MPa)	2.22	2.22	8.02
	$\gamma_{2,dist,i}$	0	0	0.311		σ_i^{exp} (MPa)	2.22	2.22	8.02
	κ_{2i}	0.178	0.178	0.644		$\Delta\varepsilon_{i,2}^{ASR}$ (%)	0.143	0.143	0.519
						ε_i^{ASR} (%)	0.143	0.143	0.519
						ε_{vol}^{ASR} (%)		--- 0.806 ---	
Stage 3	Eqn. 5-	9	9	5,10	**CEV#3**	CEV	---	MAX	---
	λ_{3i}	0	0.178	0.333		σ_{vol}^{exp} (MPa)		--- 12.46 ---	
	γ_3		--- 0.489 ---			$\Delta\sigma_{vol,3}^{exp}$ (MPa)		--- 0 ---	
	RSTC	9	6	1		$\Delta\sigma_{i,3}^{exp}$ (MPa)	0	0	0
	$\gamma_{3,dist,i}$	0	0	0.489		σ_i^{exp} (MPa)	2.22	2.22	8.02
	κ_{3i}	0	0.178	0.822		$\Delta\varepsilon_{i,3}^{ASR}$ (%)	0	0	0
						ε_i^{ASR} (%)	0.143	0.143	0.519
						ε_{vol}^{ASR} (%)		--- 0.806 ---	
Stage 4	Eqn. 5-	9	9	5,10					
	λ_{4i}	0	0	0.333					
	γ_4		--- 0.667 ---						
	RSTC	9	9	1					
	$\gamma_{4,dist,i}$	0	0	0.667					
	κ_{4i}	0	0	1.0					

Note: CEV Types - NEPR = no EPR; Y = yielding of reinforcement; MAX = max expansion reached

Table A-12: Example 8 calculations – biaxially reinforced analysis zone

		X	Y	Z			X	Y	Z
	$\lambda_{\sigma i}$	1.0	1.0	1.0		$\lambda_{\rho i}$	0.75	1.0	0.75
Stage 1	Eqn. 5-	---	---	---	**CEV#1**	CEV	---	NEPR	---
	λ_{1i}	0.25	0.333	0.25		σ_{vol}^{exp} (MPa)		--- 0 ---	
	γ_1		--- 0.167 ---			$\Delta\sigma_{vol,1}^{exp}$ (MPa)		--- 0 ---	
	RSTC	2	1	2		$\Delta\sigma_{i,1}^{exp}$ (MPa)	0	0	0
	$\gamma_{1,dist,i}$	0	0.167	0		σ_i^{exp} (MPa)	0	0	0
	κ_{1i}	0.25	0.5	0.25		$\Delta\varepsilon_{i,1}^{ASR}$ (%)	0	0	0
						ε_i^{ASR} (%)	0	0	0
						ε_{vol}^{ASR} (%)		--- 0 ---	
Stage 2	Eqn. 5-	9	5,10	9	**CEV#2**	CEV	MAX	---	---
	λ_{2i}	0.25	0.333	0.25		σ_{vol}^{exp} (MPa)		--- 7.47 ---	
	γ_2		--- 0.167 ---			$\Delta\sigma_{vol,2}^{exp}$ (MPa)		--- 7.47 ---	
	RSTC	2	1	2		$\Delta\sigma_{i,2}^{exp}$ (MPa)	1.87	3.73	1.87
	$\gamma_{2,dist,i}$	0	0.167	0		σ_i^{exp} (MPa)	1.87	3.73	1.87
	κ_{2i}	0.25	0.5	0.25		$\Delta\varepsilon_{i,2}^{ASR}$ (%)	0.193	0.283	0.091
						ε_i^{ASR} (%)	0.193	0.283	0.091
						ε_{vol}^{ASR} (%)		--- 0.566 ---	
Stage 3	Eqn. 5-	9	5,10	9	**CEV#3**	CEV	---	---	MAX
	λ_{3i}	0	0.333	0.25		σ_{vol}^{exp} (MPa)		--- 7.47 ---	
	γ_3		--- 0.417 ---			$\Delta\sigma_{vol,3}^{exp}$ (MPa)		--- 0 ---	
	RSTC	9	1	2		$\Delta\sigma_{i,3}^{exp}$ (MPa)	0	0	0
	$\gamma_{3,dist,i}$	0	0.417	0		σ_i^{exp} (MPa)	1.87	3.73	1.87
	κ_{3i}	0	0.75	0.25		$\Delta\varepsilon_{i,3}^{ASR}$ (%)	0	0	0
						ε_i^{ASR} (%)	0.193	0.283	0.091
						ε_{vol}^{ASR} (%)		--- 0.566 ---	
Stage 4	Eqn. 5-	9	5,10	9					
	λ_{4i}	0	0.333	0					
	γ_4		--- 0.667 ---						
	RSTC	9	1	9					
	$\gamma_{4,dist,i}$	0	0.667	0					
	κ_{4i}	0	1.0	0					

Note: CEV Types - NEPR = no EPR; Y = yielding of reinforcement; MAX = max expansion reached

Table A-13: Example 8 calculations – unreinforced analysis zone

		X	Y	Z			X	Y	Z
	$\lambda_{\sigma i}$	1.0	1.0	1.0		$\lambda_{\rho i}$	0.75	1.0	0.75
Stage 1	Eqn. 5-	---	---	---	**CEV#1**	CEV	NEPR	---	---
	λ_{1i}	0.25	0.333	0.25		σ_{vol}^{exp} (MPa)		--- 0 ---	
	γ_1		--- 0.167 ---			$\Delta\sigma_{vol,1}^{exp}$ (MPa)		--- 0 ---	
	RSTC	2	1	2		$\Delta\sigma_{i,1}^{exp}$ (MPa)	0	0	0
	$\gamma_{1,dist,i}$	0	0.167	0		σ_i^{exp} (MPa)	0	0	0
	κ_{1i}	0.25	0.5	0.25		$\Delta\varepsilon_{i,1}^{ASR}$ (%)	0	0	0
						ε_i^{ASR} (%)	0	0	0
						ε_{vol}^{ASR} (%)		--- 0 ---	
Stage 2	Eqn. 5-	---	---	---	**CEV#2**	CEV	---	NEPR	---
	λ_{2i}	0.25	0.333	0.25		σ_{vol}^{exp} (MPa)		--- 0 ---	
	γ_2		--- 0.167 ---			$\Delta\sigma_{vol,2}^{exp}$ (MPa)		--- 0 ---	
	RSTC	2	1	2		$\Delta\sigma_{i,2}^{exp}$ (MPa)	0	0	0
	$\gamma_{2,dist,i}$	0	0.167	0		σ_i^{exp} (MPa)	0	0	0
	κ_{2i}	0.25	0.5	0.25		$\Delta\varepsilon_{i,2}^{ASR}$ (%)	0	0	0
						ε_i^{ASR} (%)	0	0	0
						ε_{vol}^{ASR} (%)		--- 0 ---	
Stage 3	Eqn. 5-	---	---	---	**CEV#3**	CEV	---	---	NEPR
	λ_{3i}	0.25	0.333	0.25		σ_{vol}^{exp} (MPa)		--- 0 ---	
	γ_3		--- 0.167 ---			$\Delta\sigma_{vol,3}^{exp}$ (MPa)		--- 0 ---	
	RSTC	2	1	2		$\Delta\sigma_{i,3}^{exp}$ (MPa)	0	0	0
	$\gamma_{3,dist,i}$	0	0.167	0		σ_i^{exp} (MPa)	0	0	0
	κ_{3i}	0.25	0.5	0.25		$\Delta\varepsilon_{i,3}^{ASR}$ (%)	0	0	0
						ε_i^{ASR} (%)	0	0	0
						ε_{vol}^{ASR} (%)		--- 0 ---	
Stage 4	Eqn. 5-	5,10	5,10	5,10					
	λ_{4i}	0.25	0.333	0.25					
	γ_4		--- 0.167 ---						
	RSTC	2	1	2					
	$\gamma_{4,dist,i}$	0	0.167	0					
	κ_{4i}	0.25	0.5	0.25					

Note: CEV Types - NEPR = no EPR; Y = yielding of reinforcement; MAX = max expansion reached

Table A-14: Example 9 calculations

		X	Y	Z			X	Y	Z
	$\lambda_{\sigma i}$	0.687	1.0	1.0		$\lambda_{\rho i}$	0.75	0.75	0.375
Stage 1	Eqn. 5-	9	9	9	**CEV#1**	CEV	---	---	Y
	λ_{1i}	0.172	0.25	0.125		σ_{vol}^{exp} (MPa)	--- 0.86 ---		
	γ_1	--- 0.453 ---				$\Delta\sigma_{vol,1}^{exp}$ (MPa)	--- 0.86 ---		
	RSTC	6	3	2		$\Delta\sigma_{i,1}^{exp}$ (MPa)	0.15	0.21	0.50
	$\gamma_{1,dist,i}$	0	0	0.453		σ_i^{exp} (MPa)	0.15	0.21	0.50
	κ_{1i}	0.172	0.25	0.578		$\Delta\varepsilon_{i,1}^{ASR}$ (%)	0.005	0.049	0.227
						ε_i^{ASR} (%)	0.005	0.049	0.227
						ε_{vol}^{ASR} (%)	--- 0.281 ---		
Stage 2	Eqn. 5-	9	9	5,10	**CEV#2**	CEV	---	Y	---
	λ_{2i}	0.172	0.25	0.125		σ_{vol}^{exp} (MPa)	--- 3.96 ---		
	γ_2	--- 0.453 ---				$\Delta\sigma_{vol,2}^{exp}$ (MPa)	--- 3.10 ---		
	RSTC	6	3	1		$\Delta\sigma_{i,2}^{exp}$ (MPa)	0.53	0.78	1.80
	$\gamma_{2,dist,i}$	0	0	0.453		σ_i^{exp} (MPa)	0.68	0.99	2.29
	κ_{2i}	0.172	0.25	0.578		$\Delta\varepsilon_{i,2}^{ASR}$ (%)	0.018	0.179	0.270
						ε_i^{ASR} (%)	0.023	0.228	0.497
						ε_{vol}^{ASR} (%)	--- 0.748 ---		
Stage 3	Eqn. 5-	9	5,10	5,10	**CEV#3**	CEV	MAX	---	---
	λ_{3i}	0.172	0.25	0.125		σ_{vol}^{exp} (MPa)	--- 10.87 ---		
	γ_3	--- 0.453 ---				$\Delta\sigma_{vol,3}^{exp}$ (MPa)	--- 6.91 ---		
	RSTC	2	1	1		$\Delta\sigma_{i,3}^{exp}$ (MPa)	1.19	3.29	2.43
	$\gamma_{3,dist,i}$	0	0.227	0.227		σ_i^{exp} (MPa)	1.87	4.28	4.72
	κ_{3i}	0.172	0.477	0.352		$\Delta\varepsilon_{i,3}^{ASR}$ (%)	0.041	0.113	0.083
						ε_i^{ASR} (%)	0.064	0.341	0.580
						ε_{vol}^{ASR} (%)	--- 0.986 ---		
Stage 4	Eqn. 5-	5,10	5,10	5,10					
	λ_{4i}	0	0.25	0.125					
	γ_4	--- 0.625 ---							
	RSTC	9	1	1					
	$\gamma_{4,dist,i}$	0	0.313	0.313					
	κ_{4i}	0	0.563	0.438					

Note: CEV Types - NEPR = no EPR; Y = yielding of reinforcement; MAX = max expansion reached

REFERENCES

AASHTO. AAHSTO LRFD Bridge Design Specifications: Customary U.S. Units, 7th Edition. *American Association of State Highway and Transportation Officials*, Washington, DC.

ACI Committee 318. Building Code Requirements for Structural Concrete and Commentary. *American Concrete Institute*, Farmington Hills, MI, 2014.

Allford, M. T. Expansion Behavior of Reinforced Concrete Elements Due to Alkali-Silica Reaction. *Master's thesis*, The University of Texas at Austin, Austin, TX, 2016, 163 pp.

ASTM A615/A615M: Standard Specification for Deformed and Plain Carbon-Steel Bars for Concrete Reinforcement. *ASTM International*, West Conshohocken, PA, 2016, 8 pp.

ASTM C 1293: Standard Test Method for Determination of Length Change of Concrete Due to Alkali-Silica Reaction. *ASTM International*, West Conshohocken, PA, 2008, 7 pp.

ASTM C 469: Standard Test Method for Static Modulus of Elasticity and Poisson's Ratio of Concrete in Compression. *ASTM International*, West Conshohocken, PA, 2010, 5 pp.

Ballivy, G. and Khayat, K.: Influence of Reinforcement Steel on the Expansion of Concrete Affected by AAR. *Proceedings of 11th International Conference on Alkali-Aggregate Reaction in Concrete*, Québec, Canada, 2000, pp. 919-928.

Barbosa, R. A. and Hansen, K. K. The influence of alkali-silica reaction and crack orientation on the mechanical properties of concrete. *Proceedings of the 10th fib International PhD Symposium in Civil Engineering*, Québec, Canada, 2014, pp. 111-116.

Bauer, S., Cornell, B., Figurski, D., Ley, T. Miralles, J., and Folliard, K. Alkali-Silica Reaction and Delayed Ettringite Formation in Concrete: A Literature Review. *Technical Report No. FHWA/TX-06/0-4085-1*, Center for Transportation Research, Austin, TX, February 2006, 73 pp.

Bažant, Z. P. and Steffens, A. Mathematical model for kinetics of alkali-silica reaction in concrete. *Cement and Concrete Research*, V. 30, No. 3, 2000, pp. 419-428.

Bracci, J. M., Gardoni, P., Eck, M. K., and Trejo, D. Performance of Lap Splices in Large-Scale Column Specimens Affected by ASR and/or DEF. *Technical Report No. FHWA/TX-12/0-5722-1*, Texas Transportation Institute, College Station, TX, June 2012, 380 pp.

Chana P. S. Bond strength of reinforcement in concrete affected by alkali silica reaction. *Contractor Report 141*, Transport and Road Research Laboratory, Department of Transport, Crowthorne, U. K., 1989, 58 pp.

Chana, P. S. and Korobokis, G. A. Structural Performance of Reinforced Concrete Affected by ASR: Phase 1. *Contractor Report 267*, Transport and Road Research Laboratory, Department of Transport, Crowthorne, U. K., 1991, 77 pp.

Charlwood, R. G., Solymar, S. V., and Curtis, D. D. A Review of Alkali Aggregate Reactions in Hydroelectric Plants and Dams. *Proceedings of the International Conference of Alkali-Aggregate Reactions in Hydroelectric Plants and Dams*, Fredericton, Canada, September-October 1992, 129 pp.

Chrisp, T. M., Waldron, P., and Wood, J. G. M. Development of a non-destructive test to quantify damage in deteriorated concrete. Magazine of Concrete Research, V. 45, No. 165, 1993, pp. 247-256.

Cope, R. J., Wen, H. X., and May, I. M. Prediction of stress distributions in reinforced concrete members affected by alkali aggregate reaction. *Project Report 44*, Transport Research Laboratory, Crowthorne, U.K., 1994, 66 pp.

Courtier, R. H. The Assessment of ASR-Affected Structures. *Cement & Concrete Composites*, V. 12, 1990, pp. 191-201.

Curtis, D. D. Analysis and Structure Response to Recent Slot Cutting at Mactaquac Generating Station. *Proceedings of the 11th International Conference on Alkali-Aggregate Reaction in Concrete*, Quebec, Canada, 2000.

Deschenes, D. J., Bayrak, O., and Folliard, K. J. ASR/DEF-Damaged Bent Caps: Shear Tests and Field Implications. *Technical Report No. 12-8XXIA006*, The University of Texas at Austin, Austin, TX, August 2009, 271 pp.

Dunant, C. F. and Scrivener, K. L. Micro-mechanical modelling of alkali-silica-reaction-induced degradation using the AMIE framework. *Cement and Concrete Research*, V. 40, No. 4, 2010, pp. 517-525.

Dunant, C. F. and Scrivener, K. L. Effects of uniaxial stress on alkali-silica reaction induced expansion of concrete. *Cement and Concrete Research*, V. 42, No. 3, 2012, pp. 567-576.

Farny, J. A. and Kerkhoff, B. Diagnosis and Control of Alkali-Aggregate Reactions in Concrete. *Concrete Technology*, Portland Cement Association, Stokie, IL, 2007.

Fournier, B. and Bérubé, M. Alkali-aggregate reaction in concrete: a review of basic concepts and engineering implications. *Canadian Journal of Civil Engineering*, V. 27, 2000, pp 167-191.

Fournier, B., Bérubé, M., Folliard, K. J., and Thomas, M. Report on the Diagnosis, Prognosis, and Mitigation of Alkali-Silica Reaction (ASR) in Transportation Structures. *Technical Report No. FHWA-HIF-09-004*, Federal Highway Administration, January 2010, 154 pp.

Gautam, B. P., Panesar, D. K., Sheikh, S. A., and Vecchio, F. J. Multiaxial Expansion-Stress Relationship for Alkali Silica Reaction-Affected Concrete. *ACI Materials Journal*, V. 114, No. 1, January-February 2017, pp. 171-183.

Gautam, B. P., Panesar, D. K., Sheikh, S. A., Vecchio, F. J., and Orbovic, N. Alkali Aggregate Reaction in Nuclear Concrete Structures: Part 2: Concrete Materials Aspects. *Transactions of 23rd Conference on Structural Mechanics in Reactor Technology*, Manchester, U.K., August 2015, 9 pp.

Giannini E. and Folliard, K. J. Stiffness Damage and Mechanical Testing of Core Specimens for the Evaluation of Structures Affected by ASR. *Proceedings of the 14th International Conference on Alkali-Aggregate Reaction*, Austin, TX, 2012, 11 pp.

Grattan-Bellew, P. E. and Danay, A. Comparison of laboratory and field evaluation of AAR in large dams. *Proceedings of the International Conference on Concrete Alkali-Aggregate Reactions in Hydroelectric Plants and Dams*, Fredericton, Canada, September-October 1992.

Huang, M. and Pietruszczak, S. Modeling of Thermomechanical Effects of Alkali-Silica Reaction. *Journal of Engineering Mechanics*, April 1999, pp. 476-485.

Inoue, S., Fujii, M., Kobayashi, K., and Nakano, K. Structural behaviors of reinforced concrete beams affected by alkali–silica reaction. *Proceedings of 8th International Conference on Alkali-Aggregate Reaction in Concrete*, Kyoto, Japan, 1989, pp. 727-732.

Jones, A. E. K. and Clark, L. A. The practicalities and theory of using crack width summation to estimate ASR expansion. *Proceedings of the Institution of Civil Engineers – Structures & Buildings*, May 1994, pp. 183-192.

Jones, A. E. K. and Clark, L.A. The effects of restraint on ASR expansion of reinforced concrete. *Magazine of Concrete Research*, V. 48, No. 174, March 1996, pp. 1-13.

Jones, A. E. K. Cracking, Expansion and Strength of Concrete Subjected to Restrained Alkali Silica Reaction. *PhD Thesis*, University of Birmingham, Birmingham, U. K. 1994, 350 pp.

Jurcut, A. Modelling of Alkali-Aggregate Reaction Effects in Reinforced Concrete Structures. *Master's thesis*, University of Toronto, Toronto, Canada, 2015, 136 pp.

Kobayashi, K., Kawano, H., and Tsujiko, M. A study on the testing method to determine expansion due to AAR from cracks. Rev. 31st General Meeting – Technical Session, Cement Association of Japan, 1987.

Koyanagi, W., Rokugo, K., and Uchida, Y. Mechanical Properties of Concrete Deteriorated by Alkali Aggregate Reaction under Various Reinforcement Ratios. *Proceedings of 9th International Conference on Alkali-Aggregate Reaction in Concrete*, London, U. K., 1992, pp. 556-563.

Kreitman, K. L. Nondestructive Evaluation of Reinforced Concrete Structures Affected by Alkali-Silica Reaction and Delayed Ettringite Formation. *Master's thesis*, The University of Texas at Austin, Austin, TX, 2011, 147 pp.

Larive, C. Apports Combinés de l'Expérimentation et de la Modélisation à la Compréhension de l'Alcali-Réaction et de ses Effets Mécaniques. *PhD thesis*, École Nationale des Ponts et Chaussées, Paris, France, 1997, 335 pp. (in French)

Le Roux, A., Massieu, E., and Godart, B. Evolution Under Stress of a Concrete Affected By A.A.R. – Application to the Feasibility of Strengthening a Bridge by Prestressing. *Proceedings of the 9th International Conference on Alkali-Aggregate Reaction in Concrete*, London, U.K., 1992, pp. 599-606.

Léger, P., Côté, P., and Tinawi, R. Finite Element Analysis of Concrete Swelling Due to Alkali-Aggregate Reactions in Dams. *Computers & Structures*, V. 60, No. 4, 1996, pp. 601-611.

McGowan, J. K. and Vivian, H. E. Studies in cement aggregate reaction: The correlation between crack development and expansion of mortar. *Australian Journal of Applied Science*, V. 3, No. 3, 1952, pp. 228-232.

Miyagawa, T., Seto, K., Sasaki, K., Mikata, Y., Kuzume, K., and Minami, T. Fracture of Reinforcing Steels in Concrete Structural Damaged by Alkali-Silica Reaction –

Field Survey, Mechanism, and Maintenance. *Journal of Advanced Concrete Technology*, V. 4, No. 3, 2006, pp. 339-355.

Mohammed, T. U., Hamada, H., and Yamaji, T. Alkali-Silica Reaction-Induced Strains over Concrete Surface and Steel Bars in Concrete. *ACI Materials Journal*, V. 100, No. 2, March-April 2003, pp. 133-142.

Multon, S. and Toutlemonde, F. Effect of applied stresses on alkali-silica reaction-induced expansions. *Cement and Concrete Research*, V. 36, 2006, pp. 912-920.

Ng, K. E. and Clark, L. A. Punching tests on slabs with alkali-silica reaction. *The Structural Engineer*, V. 70, No. 14, 1992, pp. 245-252.

Ng, K. E. Effect of alkali silica reaction on the punching shear capacity of reinforced concrete slabs. *PhD Thesis*. University of Birmingham, Birmingham, U.K., 1991.

Nishibayashi, S., Yamura, K., and Sakata, K. Evaluation of cracking of concrete due to alkali aggregate reaction. *Proceedings of the 8th International Conference on Alkali-Aggregate Reaction in Concrete*, Kyoto, Japan, 1989, pp. 759-764.

Pan, J. W., Feng, Y. T., Wang, J. T., Sun, Q. C., Zhang, C. H., and Owen, D. R. J. Modeling of alkali-silica reaction in concrete: a review. *Frontiers of Structural and Civil Engineering*, V. 6, No. 1, 2012, 18 pp.

Puatatsananon, W. and Saouma, V. Chemo-Mechanical Micromodel for Alkali-Silica Reaction. ACI Materials Journal, V. 110, No. 1, January-February 2013, pp. 67-77.

Popovics, S. A Numerical Approach to the Complete Stress-Strain Curve of Concrete. *Cement and Concrete Research*, V. 3, No. 5, 1973, pp. 583-599.

Saouma, V. and Perotti, L. Constitutive Model for Alkali-Aggregate Reactions. *ACI Materials Journal*, V. 103, No. 3, May-June 2006, pp. 194-202.

Saouma, V. Numerical Modeling of ASR. *CRC Press Taylor & Francis Group*, Boca Raton, FL, 2014.

Scanlon, A. Time Dependent Deflections of Reinforced Concrete Slabs. *PhD Thesis*. University of Alberta, Edmonton, Canada, 1971.

Schlangen, E. and Garboczi, E. J. Fracture simulations of concrete using computational aspects. *Engineering Fracture Mechanics*, V. 57, No. 2, 1997, pp. 319-332.

Smaoui, N., Bérubé, M. A., Fournier, B., Bissonnette, B., and Durand, B. Evaluation of the expansion attained to date by concrete affected by alkali-silica reaction – Part

I: Experimental study. *Canadian Journal of Civil Engineering*, V. 31, 2004, pp 826-845.

Smaoui, N., Bissonnette, B., Bérubé, M. A., and Fournier, B. Stresses induced by alkali-silica reactivity in prototypes of reinforced concrete columns incorporating various types of reactive aggregates. *Canadian Journal of Civil Engineering*, V. 34, No. 12, 2007, pp. 1554-1566.

Smaoui, N., Bissonnette, B., Bérubé, M. A., Fournier, B., and Durand, B. Mechanical properties of ASR-affected concrete containing fine or coarse reactive aggregates. *Journal of ASTM International*, V. 3, No. 3, 2006, 16 pp.

Struble, L. J. and Diamond, S. Swelling Properties of Synthetic Alkali Silica Gels. *Journal of the American Ceramic Society*, V. 64, No. 11, 1981, pp. 652-655.

Swamy, R. N. and Al-Asali, M. M. Engineering Properties of Concrete Affected by Alkali-Silica Reaction. *ACI Materials Journal*, V. 85, No. 5, 1988, pp. 367-374.

The Institution of Structural Engineers (ISE). Structural effects of alkali-silica reaction. London, U.K., 1992, 43 pp.

Ulm, F., Coussy, O., Kefei, L., Larive, C. Thermo-Chemo-Mechanics of ASR Expansion in Concrete Structures. *Journal of Engineering Mechanics*, V. 126, No. 3, 2000, pp. 233-242.

Vecchio, F. J. and Collins, M. P. The Modified Compression Field Theory for Reinforced Concrete. *ACI Journal*, V. 83, No. 2, 1986, pp. 219-231.

Wald, D., Arrieta Martinez, G., and Bayrak, O. (2017). "Expansion Behavior of a Biaxially Reinforced Concrete Member Affected by Alkali-Silica Reaction." *Structural Concrete*, 11 pp. https://doi.org/10.1002/suco.201600143

Wald, D. M., Allford, M. T., Bayrak, O., and Hrynyk, T. D. (2017). "Development and Multi-Axial Distribution of Expansions in Multi-Directionally Reinforced Concrete Elements Affected by Alkali-Silica Reaction." *Structural Concrete*, 15 pp. https://doi.org/10.1002/suco.201600220

Wald, D. M., Hrynyk, T. D., and Bayrak, O. (2017). "The Distributed Volumetric Expansion Pressure Model for ASR Expansion Behavior in Reinforced Concrete Elements – Part 1: Background and Development." *ASCE Journal of Structural Engineering*. (unpublished)

Wald, D. M., Hrynyk, T. D., and Bayrak, O. (2017). "The Distributed Volumetric Expansion Pressure Model for ASR Expansion Behavior in Reinforced Concrete

Elements – Part 2: Implementation and Validation." *ASCE Journal of Structural Engineering*. (unpublished)

Wigum, B. J., Pedersen, L. T., Grelk, B., and Lindgard, J. State-of-the art report: Key parameters influencing alkali aggregate reaction. *Report 2.1*, SINTEF Building and Infrastructure, October 2006, 58 pp.

VITA

David Michael Wald was born in Houston, Texas. He graduated from J. Frank Dobie High School in Houston, Texas in 2006. He then went on to receive his Bachelor of Science in Architectural Engineering with Highest Honors and his Master of Science in Engineering from the University of Texas at Austin in May, 2010 and December, 2012, respectively. He served as a Graduate Research Assistant at the Phil M. Ferguson Structural Engineering Laboratory, completing his PhD in August, 2017.

Permanent email address: d.wald@utexas.edu

This dissertation was typed by the author.